

Geoscience BC

Minerals

SUMMARY OF ACTIVITIES

2020



GEOSCIENCE BC

SUMMARY OF ACTIVITIES 2020:

MINERALS

Geoscience BC Report 2021-01

© 2021 by Geoscience BC.

All rights reserved. Electronic edition published 2021.

This publication is also available, free of charge, as colour digital files in Adobe Acrobat® PDF format from the Geoscience BC website: <http://www.geosciencebc.com/updates/summary-of-activities/>.

Every reasonable effort is made to ensure the accuracy of the information contained in this report, but Geoscience BC does not assume any liability for errors that may occur. Source references are included in the report and the user should verify critical information.

When using information from this publication in other publications or presentations, due acknowledgment should be given to Geoscience BC. The recommended reference is included on the title page of each paper. The complete volume should be referenced as follows:

Geoscience BC (2021): Geoscience BC Summary of Activities 2020: Minerals; Geoscience BC, Report 2021-01, 146 p.

Summary of Activities: Minerals (Geoscience BC)
Annual publication

ISSN 2562-8623 (Print)
ISSN 2562-8631 (Online)

Geoscience BC
1101–750 West Pender Street
Vancouver, British Columbia V6C 2T7
Canada

Front cover photo and credit: Crew member B. Elder sampling till as part of the Central Interior Copper-Gold Research Projects: surficial exploration program (H. Bains, 2020).

Foreword

Geoscience BC is pleased to once again present results from our ongoing projects and scholarship recipients in our annual *Summary of Activities* publication. Papers are published in two separate volumes: *Energy and Water*, and this volume, *Minerals*. Both volumes are available in print and online via www.geosciencebc.com.

Summary of Activities 2020: Minerals

This volume, *Summary of Activities 2020: Minerals*, contains 15 papers from Geoscience BC–funded projects or scholarship recipients that are within Geoscience BC’s strategic focus area of minerals. The papers are divided into two sections, based on Geoscience BC’s strategic objectives of

- 1) Identifying New Natural Resource Opportunities, and
- 2) Advancing Science and Innovative Geoscience Technologies.

The first two papers in the ‘Identifying New Natural Resource Opportunities’ section focus on the Central Interior Copper-Gold Research series of projects, which are aimed at increasing our knowledge of the highly prospective Quesnel terrane where it is obscured by extensive glacial-till cover. Sacco et al. provide an update on the development of till-sampling–suitability maps and reanalysis of archived till samples, and describe fieldwork undertaken in 2020 to collect new till geochemical samples. Mitchinson et al. aim to look below the surficial material by using geology and 3-D geophysics to model the thickness of the glacial cover and resolve geophysical anomalies that may indicate prospective hostrocks.

Two papers highlight ongoing research in BC’s Golden Triangle area. Pellett et al. give an update on Geoscience BC’s initiative to purchase industry geophysical data and compile it with existing publicly available data to create new geophysical products. Peddle and Johnston describe structural-geology investigations at the Brucejack deposit, which is the focus of the lead author’s M.Sc. thesis.

Chapman et al. discuss progress over the last year in their establishment of a database containing microchemical characterization of gold particles in different styles of mineralization from across the province, and the identification of gold signatures using exploratory data analysis.

The final three papers in this section focus on southern BC. Morris and Canil describe ongoing geochemical investigations at the Merry Widow deposit on Vancouver Island, and Höy et al. detail new geochronological analyses and mapping investigations conducted last summer in the Penticton map area. Kuppusamy and Holuszko describe ongoing work to investigate the rare-earth element (REE) content of southern BC coal deposits and the potential to extract REEs from them.

The ‘Advancing Science and Innovative Geoscience Technologies’ section starts off with Ledoux and Hart presenting continuing research into porphyry-indicator minerals, particularly the use of zircon to potentially distinguish variability in magmatic-porphyry fertility in southern BC’s Quesnel terrane. The following two papers turn their attention to the Toodoggone district in northern BC. Bouzari et al. detail ongoing research into using mineralogy and geochemistry to vector toward deposits within advanced argillic-altered rocks, and Jones et al. present new zircon geochemistry that will help characterize the magmatic evolution and mineral potential of northern Hogem batholith.

Switching from papers with a mineral-exploration theme to work that supports responsible natural-resource development, Doucet et al. describe research into potential methods to measure CO₂ fluxes between the atmosphere and mine tailings containing ultramafic minerals. Two papers describe ongoing research at Thompson Rivers University focused on biological studies to support improved mine reclamation in southern BC. Gervan et al. focus on the response of invertebrates as a measure of examining reclamation success, and Fischer et al. consider changes in geochemical and microbial properties as they relate to depth in topsoil stockpiles.

Finally, Ledwon and Ogrzylo provide an update on improvements to Smithers Exploration Group’s Rock Room and getting their message out during the COVID-19 pandemic.

Geoscience BC Minerals Publications 2020

In addition to the two *Summary of Activities* volumes, Geoscience BC releases interim and final Geoscience BC reports and maps. The following ten ‘Minerals’ reports were published in 2020:

- Twenty technical papers in the **Geoscience BC Summary of Activities 2019: Minerals** volume (Geoscience BC Report 2020-01)
- **Microbial-Community Fingerprints as Indicators for Buried Mineralization in British Columbia**, by R.L. Simister, B.P. Iulianella Phillips, P.A. Winterburn and S.A. Crowe (Geoscience BC Report 2020-03 / MDRU Publication 446)
- **A Geochemical Investigation of Halogens in Spruce Treetops and Integration with Existing Multi-Element Data – Blackwater/TREK Regions, Central British Columbia (NTS 093C, 093F)**, by C.E. Dunn and D.R. Heberlein (Geoscience BC Report 2020-04)
- **Vancouver Island North Regional Project – Airborne Magnetic and Radiometric Survey**, by Precision GeoSurveys Inc. (Geoscience BC Report 2020-05)
- **Mineral-Resource Prediction Using Advanced Data Analysis and Machine Learning of the QUEST-South Stream-Sediment Geochemical Data, Southwestern British Columbia (Parts of NTS 082, 092)**, by E.C. Grunsky and D.C. Arne (Geoscience BC Report 2020-06)
- **Real-Time Analysis of Soil Gas for Carbon Dioxide and Oxygen to Identify Bedrock Mineralization and Geological Faults Beneath Glacial Deposits in Central British Columbia**, by R.E. Lett, D.A. Sacco, B. Elder and W. Jackaman (Geoscience BC Report 2020-07)
- **Assessing Porphyry Copper Deposit Fertility in British Columbia Batholiths using Zircons**, by F. Bouzari, C.J.R. Hart and T. Bissig (Geoscience BC Report 2020-08 / MDRU Publication 450)
- **Producing Clean Coal Samples from Western Canadian Coalfields Using the Water-Based Roben Jig Process: Application to an Industrial Setting**, by M. Mackay, L. Giroux, R. Leeder, H. Dexter, J. Halko, M. Holuszko and D. Thomas (Geoscience BC Report 2020-10)
- **Digitizing British Columbia’s Geological Heritage: Geoscience BC Final Report**, by J. Moffatt, A. Whistler, J. Sly, A. Randell and L. Connor (Geoscience BC Report 2020-11)
- **The Carbon Mineralization Potential of Ultramafic Rocks in British Columbia: A Preliminary Assessment**, by D. Mitchinson, J. Cutts, D. Fournier, A. Naylor, G. Dipple, C.J.R. Hart, C. Turvey, M. Rahimi and D. Milidragovic (Geoscience BC Report 2020-15 / MDRU Publication 452)

All releases of Geoscience BC reports, maps and data are published on our website and are announced through our website and e-mail updates. Most final reports and data can also be viewed or accessed through our Earth Science Viewer at <https://gis.geosciencebc.com/esv/?viewer=esv>.

Acknowledgments

Geoscience BC would like to thank all authors and reviewers of the *Summary of Activities* for their contributions to this volume. COVID-19 has made this a challenging year for both field programs and laboratory research, and Geoscience BC is grateful for the perseverance of our researchers and scholarship recipients in continuing their projects during the past nine months.

RnD Technical is also acknowledged for its work in editing and assembling both volumes. As well, Geoscience BC would like to acknowledge the Province of British Columbia and our project funding partners for their ongoing support of public geoscience, and express our appreciation for the leaders and volunteers in British Columbia’s mineral exploration, mining and energy sectors who support our organization through their guidance, use and recognition of the data and information that we collect and distribute.

Christa Pellett
Vice President, Minerals
Geoscience BC
www.geosciencebc.com

Contents

Identifying New Natural Resource Opportunities

D.A. Sacco, W. Jackaman and C. Knox: Proven approach to mineral exploration in thick surficial deposits applied to the Central Interior Copper-Gold Research projects area, central British Columbia.	1
D.E. Mitchinson, C.J.R. Hart and D. Fournier: Uncovering porphyry-deposit potential in the Quesnel terrane of central British Columbia using geology and 3-D geophysics	11
C.L. Pellett, T.A. Ballantyne and B.K. Clift: Geophysical data compilation project in British Columbia's Golden Triangle area	25
C. Peddle and S.T. Johnston: Review of the structural geology of the Brucejack intermediate-sulphidation epithermal deposit, northwestern British Columbia	29
R.J. Chapman, R.J. Murphy, J.K. Mortensen, B. Bluemel and D.A. Banks: British Columbia gold composition atlas update 2020: developing a new tool for the exploration community	41
R. Morris and D. Canil: Cryptic magmatic skarn of the Merry Widow deposit, Vancouver Island	47
T. Höy, R. Friedman and J. Gabites: Paleogene Penticton Group, Boundary area, southern British Columbia: geochronology and implications for precious metal mineralization	55
V.K. Kuppusamy and M.E. Holuszko: Development of rare-earth elements database for the East Kootenay coalfield of southeastern British Columbia using field collected samples: preliminary results	67

Advancing Science and Innovative Geoscience Technologies

T.J. Ledoux and C.J.R. Hart: Evolution of the southern Quesnel arc: potential to distinguish variability in magmatic porphyry fertility, south-central British Columbia.	75
F. Bouzari, R.G. Lee, C.J.R. Hart and B.I. van Straaten: Mineralogical and geochemical vectors within advanced argillic-altered rocks of north-central British Columbia	91
G.O. Jones, D.G. Pearson, A. Vezinet, Y. Luo, R.A. Stern, D. Milidragovic and L. Ootes: Preliminary zircon geochemistry of northern Hogem batholith, Quesnel terrane, north-central British Columbia.	105
A.-M. Doucet, F.A. Jones, G.M. Dipple and K.U. Mayer: Pilot study comparing eddy covariance and dynamic closed-chamber methods for measuring CO ₂ fluxes above the hydromagnesite-magnesite playas near Atlin, northwestern British Columbia	121
C.A. Gervan, W.C. Gardner, E.M. Bottos, J.D. Van Hamme, R.J. Higgins and L.H. Fraser: Invertebrate response to mine reclamation in south-central British Columbia: effects of reclamation age on arthropod assemblages at the Highland Valley Copper and New Afton mines	129
A.M. Fischer, J.D. Van Hamme, E.M. Bottos, W.C. Gardner and L.H. Fraser: Post-mining restoration in south-central British Columbia: modelling microbial and geochemical changes in topsoil stockpiles	137
A. Ledwon and C. Ogryzlo: Progress report on Smithers Exploration Group's Rock Room and getting creative during COVID (northwestern British Columbia)	143

Proven Approach to Mineral Exploration in Thick Surficial Deposits Applied to the Central Interior Copper-Gold Research Projects Area, Central British Columbia (Parts of NTS 093A, B, G, J, K, O)

D.A. Sacco, Palmer, Vancouver, British Columbia, dave.sacco@pecg.ca

W. Jackaman, Noble Exploration Services Ltd., Jordan River, British Columbia

C. Knox, Palmer, Vancouver, British Columbia

Sacco, D.A., Jackaman, W. and Knox, C. (2021): Proven approach to mineral exploration in thick surficial deposits applied to the Central Interior Copper-Gold Research projects area, central British Columbia (parts of NTS 093A, B, G, J, K, O); *in* Geoscience BC Summary of Activities 2020: Minerals, Geoscience BC, Report 2021-01, p. 1–10.

Introduction

Geoscience BC is undertaking a series of projects in the Central Interior Copper-Gold Research (CICGR) projects area, which occupies a large region in central British Columbia (BC) between the communities of Mackenzie and Williams Lake (Figure 1a). This region has significant mineral potential; however, exploration is hindered by extensive Quaternary sediment units that obscure bedrock. The objective of the CICGR projects is to investigate the potential for undiscovered mineral deposits buried beneath thick glacial sediments.

Drift prospecting using a comprehensive understanding of the surficial geology has been proven to reveal exploration targets where thick glacial sediments occur (e.g., Levson et al., 1994; Levson, 2001; Plouffe et al., 2001; Sacco et al., 2018). This paper contains a summary of the progress of a multiyear surficial exploration program targeting specific areas (surficial study areas; Figure 1a, b) within the larger CICGR projects area. The program is modelled after Geoscience BC's highly successful Targeting Resources through Exploration and Knowledge (TREK; e.g., Jackaman and Sacco, 2014; Jackaman et al., 2014, 2015; Sacco and Jackaman, 2015; Sacco et al., 2018) and Quesnelia Exploration Strategy (QUEST; e.g., Sacco et al., 2010; Ward et al., 2011, 2012, 2013) surficial exploration programs (Figure 1). The CICGR projects are generating high-quality baseline data integral to promoting and supporting successful mineral exploration in this challenging setting. Combined with data from the TREK (Jackaman et al., 2015) and QUEST (Ward et al., 2013) projects, the results of this study extend the coverage of directly comparable geochemical and mineralogical data and 1:50 000 scale surficial mapping to a large nearly continuous portion of central BC.

The proven methodology applied in this program is designed to generate a geochemical and mineralogical database, and an understanding of the surficial geology necessary to collect and interpret these data, such that they can be integrated into and guide private-sector exploration. The scope of the program defines three objectives:

- 1) 1:50 000 scale surficial geology mapping;
- 2) comprehensive compilation of historical data and reanalysis of archived till survey samples; and
- 3) new and infill till geochemical and mineralogical surveys.

The surficial geology mapping provides an understanding of the drift composition, allowing optimal exploration methods to be selected. Interpretations of surficial geology were used to derive till sampling suitability (TSS) and drift thickness maps. The TSS maps identify areas well- and poorly suited to till sampling. The drift thickness maps provide depth to bedrock estimations that help guide bedrock mapping and prospecting programs, and identify areas where drill-supported sediment and/or bedrock sampling could be beneficial. Areas that are poorly suited to till sampling but have thick drift are good candidates for drill-supported sampling.

Archived samples with incomplete or outdated analytical information were reanalyzed as part of objective 2 and provide results that are compatible and comparable to the current provincial database. The results of the surficial mapping and data reconciliation were used to support the design and execution of subglacial till geochemistry and mineralogy sampling programs as part of objective 3. New data resulting from these programs will be combined with the reanalyzed sample data, significantly improving sample site densities across the project area, and reducing the analytical and genetic variability in the dataset, allowing for the generation of lower risk exploration targets.

This publication is also available, free of charge, as colour digital files in Adobe Acrobat® PDF format from the Geoscience BC website: <http://geosciencebc.com/updates/summary-of-activities/>.

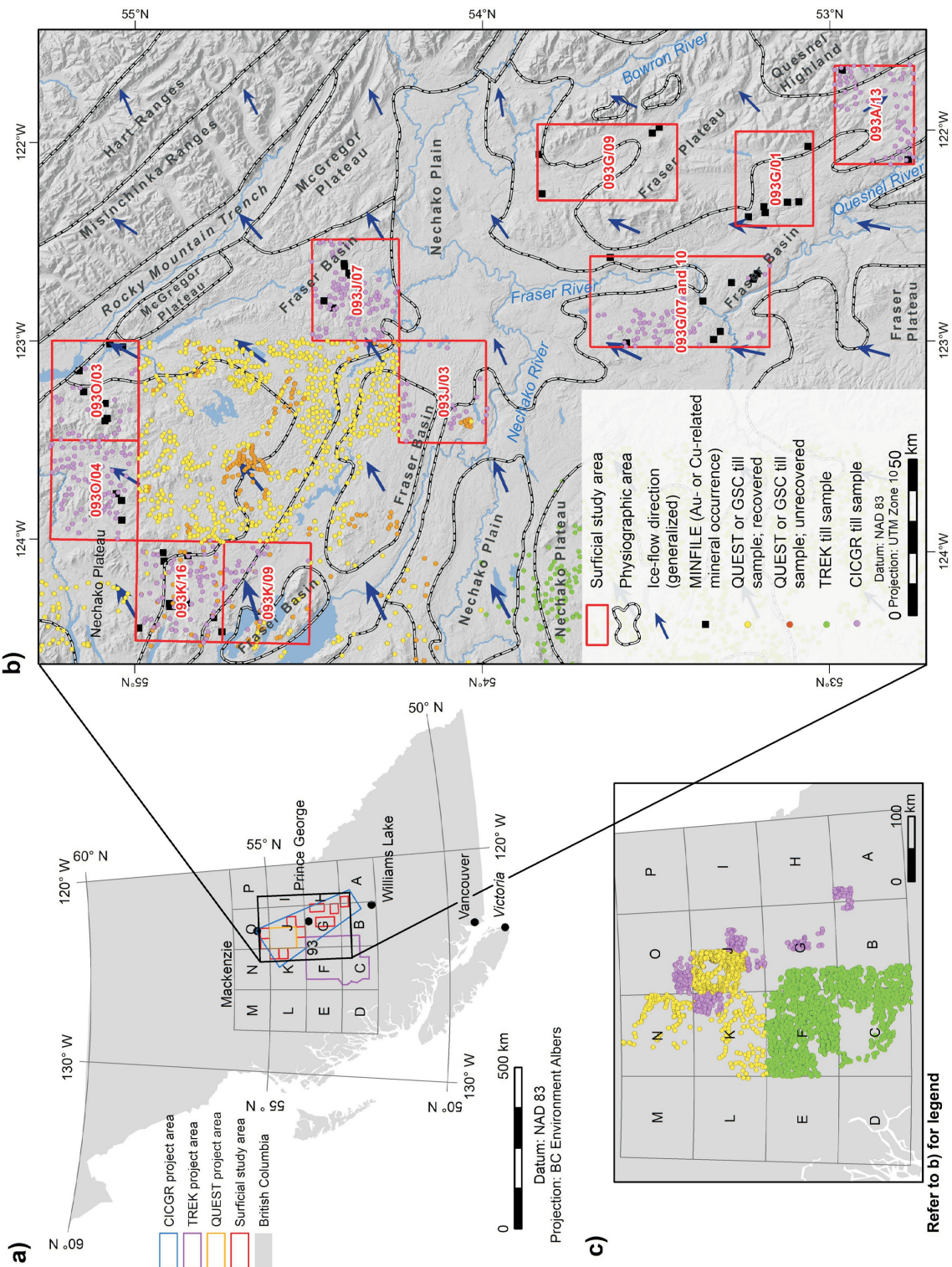


Figure 1. a) Location of Central Interior Copper-Gold Research (CICGR), Targeting Resources through Exploration and Knowledge (TREK) and Quesnelia Exploration Strategy (QUEST) projects areas. b) Surficial study areas; physiographic areas; locations of historical surface sediment samples proposed for reanalysis from QUEST (Ward et al., 2013) and Geological Survey of Canada (GSC) programs (Plouffe and Ballantyne, 1993; Plouffe, 1995; Plouffe and Williams, 1998); TREK till sample locations (Jackaman et al., 2015); and till samples collected during this study. c) Distribution of recovered historical till samples (yellow symbols) in central British Columbia, which will be reanalyzed to produce data comparable to existing data from the TREK project (green symbols) and this study (purple symbols).

Projects Area and Previous Work

The CICGR projects area occupies a large region in central BC between Mackenzie and Williams Lake. Within the CICGR projects area, the surficial exploration study areas include parts of NTS 093A, B, G, J, K and O and cover approximately 9700 km² (Figure 1). During the second year of the project, the area of the surficial exploration study was increased from 8600 to 9700 km², with the addition of 1100 km² dominantly in the NTS 093G/09 map area. There are 52 MINFILE mineral occurrences related to Au or Cu mineralization within the surficial study areas (BC Geological Survey, 2020), although significantly more occur within the larger CICGR projects area. The surficial study areas were determined based on three main criteria: 1) prospective geology; 2) avoidance of private land; and 3) applicability of till sampling. Surficial study area boundaries are based on the NTS map area boundaries, but some boundaries were adjusted to accommodate these criteria. For continuity of the till database, the compilation of historical till data and reanalysis of archived samples extends beyond the CICGR projects area to include the full extent of previous surveys (Figure 1).

The surficial study areas are within the Interior Plateau physiographic region and consist of parts of the Fraser Basin, Fraser Plateau, Nechako Plain, Nechako Plateau, Rocky Mountain Trench and Quesnel Highland (Holland, 1976; Mathews, 1986; Figure 1b). Bedrock exposures are commonly obscured by thick surficial deposits, composed dominantly of till, glaciolacustrine and glaciofluvial sediments. Surficial geology mapping has been conducted at various scales throughout the project area, providing an important regional context for the current, higher resolution interpretations. See Sacco et al. (2020) for a complete list of existing surficial geology mapping within the study areas.

The coalescence and subsequent divergence of glaciers in and around the northern part of the CICGR area during the last (Fraser) glaciation resulted in a complex surficial setting that has hindered exploration efforts. During the onset of the last glaciation, ice advancing from source areas north, south and west of the CICGR projects area coalesced, causing significant variations in ice flow and sediment transport and altered drainage systems resulting in the development of extensive glacial lakes (Clague, 1988; Plouffe, 1997; Sacco et al., 2017). Till was deposited in most areas during this glaciation; transport directions varied as the morphology of the ice sheet changed in relation to advance, climax and deglaciation. During deglaciation, ice retreated to the source areas leaving behind ablating ice masses in topographic lows. The retreating and stagnating ice altered drainage resulting in the deposition of large outwash deposits and the development of glacial Lake Fraser, a dynamic, time-transgressive body of water in which significant amounts of sediment accumulated. These thick

sediment units obscure the underlying bedrock and till, which typically provide a basis for exploration, hindering the collection of high-quality surface sediment data. As a result, the CICGR area is underexplored and its mineral resources are largely unknown. Previous till sampling programs have been conducted in the northwestern part of the project area (Figure 1) and a description of past sampling programs relevant to the project is provided in Sacco et al. (2020).

Methods

The methodology for this program was adopted and improved from the previously completed TREK and QUEST projects. Surficial geology mapping was used to inform the reanalysis and genetic assessment of existing surface sediment samples and the planning and execution of the subsequent till sampling program. The till sampling program includes infill sampling in areas where the current density is insufficient and new sampling where no previous sampling has occurred. The new till sampling, combined with the reanalysis of archived samples, will culminate in a directly comparable till geochemical and mineralogical dataset for the surficial study areas.

Objective 1: Surficial Mapping and Till Sampling Suitability

Surficial geology mapping provides a basis for the collection and interpretation of surface sediment data. For this project, it identifies areas where subglacial till, the optimal surface sediment sample media for exploration, occurs at surface and provides the necessary framework to evaluate analytical results from historical and new surface sediment data. The surficial geology was interpreted at a scale of 1:50 000 from 1.5 m resolution satellite imagery converted into pseudo-stereo based on a digital elevation model (Natural Resources Canada, 2015). The stereo imagery enables the distinction of subtle patterns in topography and ground vegetation, which are diagnostic in interpreting the thicknesses and types of material and types of landforms in the shallow subsurface, and geomorphological processes that have affected the region.

The Geological Survey of Canada (GSC) mapping protocols (Deblonde et al., 2018) were chosen to maintain consistency with existing regional mapping by the GSC and similar scale mapping conducted by the BC Geological Survey (BCGS). Minor refinements were made to the mapping protocols to improve the accuracy of the TSS and drift thickness map products. Polygons were delineated based on surface material and expression, with an emphasis on identifying features that affect till sampling programs such as facies discrimination (e.g., subglacial till versus ablation till), geomorphological processes and important linear and point features (e.g., ice-flow indicators).

The TSS and drift thickness map products were derived from the surficial geology mapping (Figure 2). A multiclass TSS index, used to attribute each polygon, was based on the occurrence of subglacial till with consideration for any geomorphological processes that may have affected the material (e.g., reworking by meltwater, slope processes, etc.). The TSS is ultimately based on the proportion of subglacial till at the surface that is suitable for sampling. The drift thickness maps were derived using the expression and stratigraphic relationships of surficial map units, with a multiclass thickness index being used to symbolize mapped polygons following a similar approach as the TSS maps.

Objective 2: Compilation of Historical Data and Reanalysis of Archive Samples

The reanalysis of till samples archived from previous regional geochemical surveys is a cost-effective method of significantly upgrading the utility of the associated geochemical datasets. Maintaining the integrity and function of a regional geochemical database is a challenge when the analytical information being compiled is acquired from surveys conducted in different years. Many of these historic projects were completed in the 1990s when sampling protocols were less strict, and a considerable amount of the original results were generated using analytical methods that are now outdated.

Each of the archived samples is attributed with a genetic category based primarily on the original sample notes, where available, or the new surficial interpretations and observations made during fieldwork. A genetic category for each sample will be included in the final data compilation. Archive sample material was sent to Bureau Veritas Minerals (Vancouver, BC) for analysis of the silt plus clay-size ($<0.063\text{ mm}$) fraction to elevate these datasets to current standards. Analytical packages include an ultra-trace analysis by inductively coupled plasma–mass spectrometry (ICP-MS) for 53 elements following aqua-regia digestion, and major and minor elements by inductively coupled plasma–emission spectrometry (ICP-ES) following lithium metaborate-tetraborate fusion and dilute acid digestion. Prior to analysis by the laboratory, analytical duplicate and control reference samples were inserted into the sample sequence to monitor and assess the accuracy and precision of the new analytical results. The reanalysis by modern laboratory techniques combined with the genetic interpretations of these samples create a high-quality dataset that is comprehensive and directly comparable to the standard of current provincial datasets used to support exploration and environmental assessments.

Objective 3: Till Geochemical and Mineralogical Survey

The till geochemical and mineralogical survey began during year two of the program. Subglacial till is the primary

target because it is a first derivative of bedrock (Schilts, 1993), is predictably transported in the direction of ice flow and provides a larger anomaly than the original bedrock source (Levson, 2001). Target sample media must be correctly identified to limit variability within the dataset and ensure contrasts in the dataset (i.e., anomalies) are related to mineralization rather than material genesis. The surficial geology and TSS mapping provided the foundation to plan and collect suitable subglacial till samples at $\sim 2\text{ km}$ spacing. The survey was conducted to established standards to produce high-quality field and analytical results that are consistent with and comparable to the existing provincial till geochemical database.

At each sample site, two $1\text{--}2\text{ kg}$ subglacial till samples were collected from the C horizon for geochemical analysis and 50 clasts of large pebble- to small cobble-size were collected for lithological analysis. At approximately every other site, a $10\text{--}12\text{ kg}$ bulk subglacial till sample was collected for mineralogical analysis. Sacco et al. (2020) detail the field sampling protocols used in the till geochemical and mineralogical survey.

The subglacial till samples for geochemical analysis were shipped to Bureau Veritas Minerals, where they will be dried, have an archive generated, and processed to produce clay-size (0.002 mm) and silt plus clay-size ($<0.063\text{ mm}$) fraction splits. Both fractions will be analyzed for minor and trace elements by an ultra-trace aqua-regia digestion (0.5 g) ICP-MS package for 53 elements and by instrumental neutron activation analysis (INAA) for total gold plus 34 elements. Major and minor elements will be determined by ICP-ES following a lithium metaborate-tetraborate fusion and dilute acid digestion. This analytical package will include loss-on-ignition by weight difference after ignition at 1000°C , plus total carbon and sulphur by LECO analysis. The LECO analysis converts carbon and sulphur forms in a sample into CO_2 and SO_2 by combustion in an induction furnace. The concentrations of CO_2 and SO_2 are measured by infrared absorption and thermal conductivity to determine total concentrations of carbon and sulphur. Quality control for analytical determinations will include the use of field duplicates, analytical duplicates, reference standards and blanks, based on established protocols (Spirito et al., 2011).

Clast lithologies will be grouped into broad categories that reflect the main lithologies of local bedrock to provide insight on the direction and distance of glacial transport. The bulk till samples were sent to Overburden Drilling Management Limited (Ottawa, Ontario) and processed for gold grain concentrates ($<2.0\text{ mm}$) and heavy and medium mineral concentrates ($0.25\text{--}2.0\text{ mm}$) using a combination of gravity tables and heavy liquids. Concentrates will be visually picked for gold and porphyry-copper-indicator minerals.

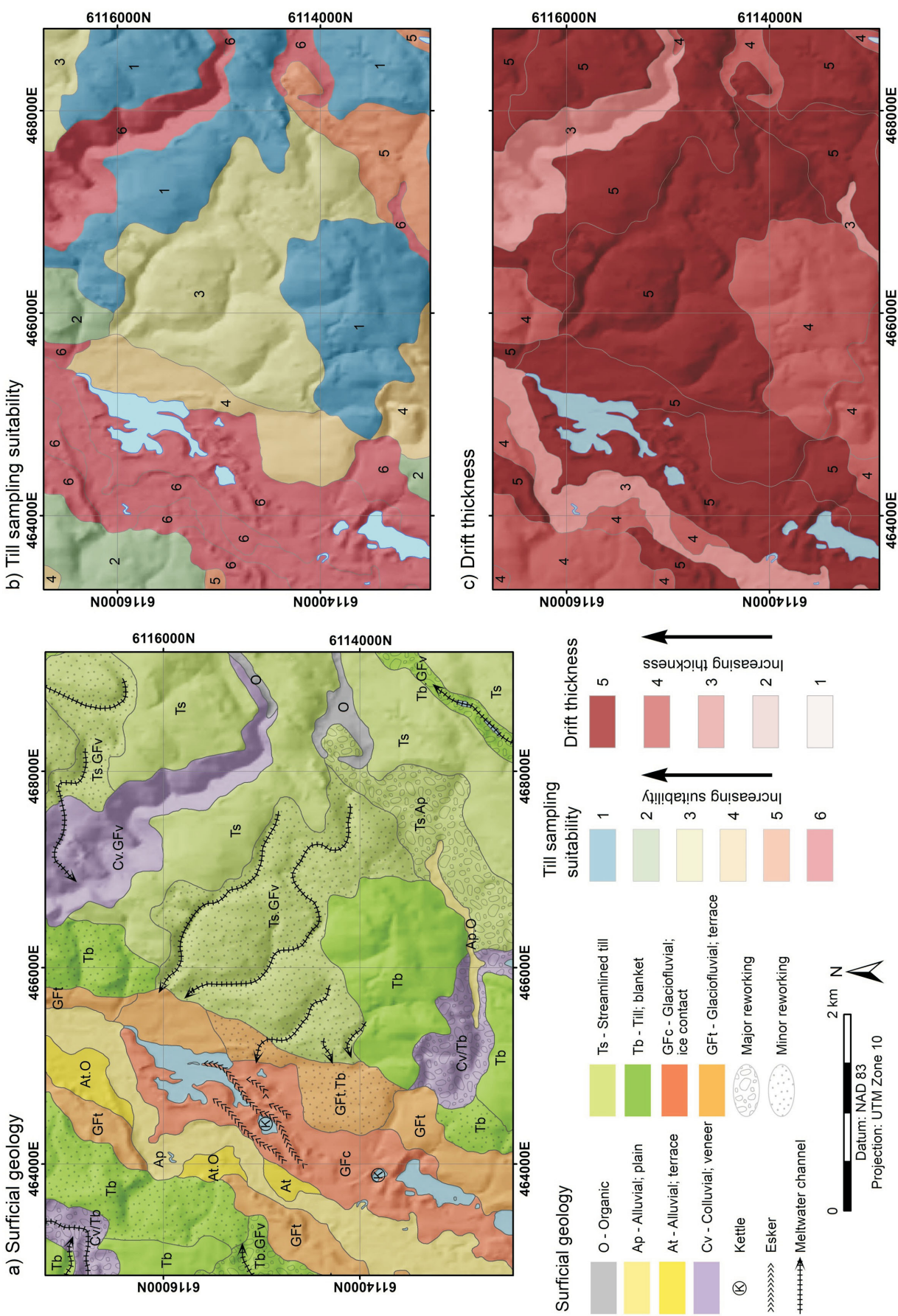


Figure 2. Examples of a) surficial geology, b) derived till sampling suitability and c) drift thickness mapping in the Central Interior Copper-Gold Research surficial study areas.

Progress and Future Work

Approximately 700 till samples that were collected in the 1990s as part of a GSC regional till sampling program (Plouffe and Ballantyne, 1993; Plouffe, 1995; Plouffe and Williams, 1998) and 825 samples collected in the late 2000s as part of Geoscience BC's QUEST project (Ward et al., 2013) have been proposed for reanalysis. In co-operation with the GSC, 288 representative 2 g splits of the silt plus clay-size (<0.063 mm) fraction of archive sample material and 672 original unprocessed character splits were retrieved from the storage facilities in Ottawa. The reanalysis of these 960 historic samples using modern laboratory techniques has been completed, creating an updated, higher quality dataset. Upon finalization of the surficial geology mapping, genetic attributions for the analyzed samples will be added to the database. Table 1 and Figure 1 indicate the historical sample sources and their recovery status. Recovery of the remaining archived samples proposed for reanalysis will be attempted during year three of this multiyear project; however, the current reanalysis results may be released sooner.

The 2020 field program focused on till sample collection and field verification of the surficial geology mapping, however, progress was slowed due to the effects of the COVID-19 pandemic. Adhering to WorkSafeBC safety guidelines created logistical challenges that extended beyond normal field program issues related to weather and mechanical breakdowns. Most notably, maintaining small working group bubbles was required to reduce the risk of crew exposure and community spread of COVID-19. The limited availability of basic services such as appropriate lodging and air travel were restricted, which limited accommodation and travel options, subsequently increasing the time required to move field crews. In addition, a decision was made to prioritize sample collection over field verification of the surficial interpretations. As a result, sample collection rates were slightly lower than anticipated but field verification was significantly curtailed.

To date, 456 new till samples have been collected in the CICGR project area (Figure 1). Adequate sample density

has been attained within NTS map areas 093J/03 and 07, 093K/09 and 16, and 093O/03 and 04. The study areas that are mostly within 093A/13 and 093G/07 and 10 were partially sampled but require additional sampling to attain the ideal sampling density and distribution. Future sampling will address undersampled areas in 093A/13 and 093G/07 and 10, and in 093G/01 and 09, which have not been sampled yet.

The 2020 samples have been sent to Bureau Veritas Minerals and Overburden Drilling Management Limited for geochemical and mineralogical analysis, respectively. The geochemical, mineralogical and pebble data from the new samples will be evaluated and compiled before they are released as digital databases, which will include all analytical results, quality control data, and results from the reanalyzed historic samples.

Surficial geology mapping was finalized for NTS map areas 093J/07 and 03, 093K/09 and 16 and 093O/03 and 04, during the second year of the program. Preliminary surficial geology interpretations have also been completed for the remaining study areas. These preliminary interpretations will be finalized using field observations collected during the 2021 sampling program.

Till sampling suitability (Table 2) and drift thickness categories (Table 3) were finalized and attributed to the surficial geology polygons. In the CICGR area, TSS is most heavily influenced by the distribution of glacial lake sediments and ablation till. These glacial lake and stagnating ice deposits are also generally associated with thicker drift as they tend to accumulate in large depressions (i.e., Fraser Basin around Prince George) and within valley fill sequences. As a result, the areas that are poorly suited to surface till sampling due to overlying glaciolacustrine and ablation till deposits are well-suited to subsurface drill-supported sampling. Drill-supported sampling has the potential to provide till and bedrock samples, and stratigraphic information, which can inform the evaluation of surface sediment exploration data and provide information about groundwater and sediment aquifer potential.

Table 1. Sources and status of archive sample compilation for the Central Interior Copper-Gold Research projects area, northeastern British Columbia.

Report	Year	Recovered (n)	Pending recovery (n)	Archived fraction	NTS map area
Geoscience BC Report 2013-15 (Ward et al., 2013)	2013	672	153	Unprocessed	093J/03, 05, 06, 10-14
GSC Open File 2593 (Plouffe and Ballantyne, 1993)	1990, 1991	225	63	0.063 mm	093K/01-08, 10-12, 15, 16; 093N/01, 02, 06-11
GSC Open File 3194 (Plouffe, 1995)	1992, 1993, 1994	53	353	0.063 mm/ unprocessed	093K/01-10, 12, 14-16; 093L/01, 08; 093N/02-12, 14-16; 093O/05, 12
GSC Open File 3687 (Plouffe and Williams, 1998)	1997	2	0	0.063 mm	093K/04
Unpublished	1997, 1999	8	2	0.063 mm	093K/09, 15; 093N/02, 03, 06, 11

Abbreviation: GSC, Geological Survey of Canada

Table 2. Till sampling suitability classifications for the Central Interior Copper-Gold Research projects area.

Till sampling suitability class	Description	Implications for exploration
1	All subglacial till	Most surface sediment is composed of till and suitable for sampling; minor amounts of other materials may occur even where not indicated in map unit.
2	Dominantly subglacial till or all subglacial till with minor reworking	Till is the dominant surficial material, or greater than half of the map unit is in situ subglacial till. Most of the map unit is suitable for surface till sampling.
3	Lesser amounts of subglacial till or dominantly subglacial till with minor reworking	In situ subglacial till comprises less than half of the map unit. Focus on high ground and down-ice from bedrock outcrops to increase the probability of finding till suitable for sampling at surface.
4	Lesser amounts of till with minor reworking or all till with major reworking	Suitable till for sampling likely occurs at surface in a small proportion of map unit. Focus on high ground and down-ice from bedrock outcrops to increase the probability of finding till suitable for sampling at surface; machine-supported sampling may be beneficial.
5	Till is dominant material with major reworking	Map unit dominantly composed of reworked till at surface, which is not suitable for sampling, and other materials. Till suitable for sampling is most likely to occur on high ground, but will be very limited in extent; machine-supported sampling is recommended.
6	Minor till with major reworking or no till	Unlikely to locate suitable till for sampling at surface within map unit; machine-supported sampling is recommended.

Table 3. Drift thickness classifications for the Central Interior Copper-Gold Research projects area.

Drift thickness class	Description	Implications for exploration
1	Bedrock is the dominant material exposed at surface; majority of overlying sediment is interpreted to be less than 2 m thick.	Bedrock occurs at surface or can be accessed with hand tools in most areas; optimal target for bedrock mapping and sampling; till in these units is commonly weathered and may not be suitable for mineral exploration samples.
2	Bedrock is the secondary surficial material; more than 50% of unit is interpreted to be overlain by sediment up to 2 m thick.	Bedrock is exposed at surface on topographic highs and can be accessed in hand-dug pits in most areas; good target for bedrock mapping and sampling; weathered till is common; composition of in situ till reflective of local bedrock.
3	Veneer is identified as the dominant surface expression with minimal bedrock outcrop; most bedrock in this unit is overlain by up to 2 m of sediment.	Bedrock outcrop is limited, but may be accessible with hand tools on topographic highs, along steep slopes, and where meltwater has removed sediment; bedrock likely accessible with an excavator; till composition typically reflects local bedrock.
4	Blankets greater than 2 m thick are dominant; sediment generally forms mantles that follow bedrock topography and thin on topographic highs.	Bedrock outcrop is rare and will likely only occur on topographic highs; bedrock may be accessible using excavator; till composition reflective of more distal bedrock sources.
5	Ablation till and large constructional glaciofluvial landforms that typically overlie subglacial till blankets.	Drill likely needed to access bedrock; underlying till is likely representative of more distal bedrock sources.
6	Thick glaciolacustrine or glaciofluvial deposits that form the upper surface of valley fill sequences or infill large depressions; commonly underlain by till and/or advance-stage glacial sediments.	Drill needed to access bedrock; potential for complex stratigraphy must be considered during drill-supported sediment sampling.

The finalized surficial mapping products and reanalysis results are planned for release in early 2021. The mapping release will include georeferenced PDF map sets of surficial geology, TSS and drift thickness. All mapping files will be provided in Esri geodatabase and shapefile format, embed-

ded with appropriate GSC symbology codes such that users can easily import and symbolize these data to assist with their own exploration activities. The data release will include the analytical results from the archive samples and all quality assurance-quality control material.

Conclusions

The integration of surficial mapping and results of surface sediment sample analyses into a comprehensive dataset contributes to the ongoing development of a province-wide, regional exploration database. Survey methods conform to strict specifications; compiled information is comprehensive, compatible and reproducible; and the package complements a wide range of other ongoing geoscience initiatives and exploration activities. The project results, combined with data from the earlier Targeting Resources through Exploration and Knowledge (TREK) and QUEST projects, extend the coverage of comprehensive geochemical and mineralogical data to a larger portion of central British Columbia, and will promote increased awareness in a highly prospective region, assist in the identification of new exploration targets and support follow-up activities. In addition, these results will highlight specific areas where till sampling with hand tools cannot be used to determine mineral potential and different exploration techniques may be required.

Acknowledgments

This program was funded by Geoscience BC. The authors would like to thank A. Plouffe from the Geological Survey of Canada for his heroic efforts to recover archive samples from storage in Ottawa and his support in the development of this project. Assistance in archive sample recovery was also provided by R. Lett, B. Ward and T. Ferbey. Additional field support was provided by H. Bains, B. Elder, J. Constantine and B. Janzen and their willingness to dig ‘just a bit deeper’ helped ensure high-quality samples were collected. A special thank you to D. Turner for his thorough review and thoughtful comments that improved the quality of this paper.

References

- BC Geological Survey (2020): MINFILE BC mineral deposits database; BC Ministry of Energy, Mines and Low Carbon Innovation, BC Geological Survey, URL <<http://minfile.ca>> [October 2020].
- Clague, J.J. (1988): Quaternary stratigraphy and history, Quesnel, British Columbia; Géographie physique et Quaternaire, v. 42, p. 279–288.
- Deblonde, C., Cocking, R.B., Kerr, D.E., Campbell, J.E., Eagles, S., Everett, D., Huntley, D.H., Inglis, E., Parent, M., Plouffe, A., Robertson, L., Smith, I.R. and Weatherston, A. (2018): Surficial data model: the science language of the integrated Geological Survey of Canada data model for surficial geology maps (ed. ver. 2.3.14); Geological Survey of Canada, Open File 8236, 50 p.
- Holland, S.S. (1976): Landforms of British Columbia: a physiographic outline (second edition); BC Ministry of Energy, Mines and Low Carbon Innovation, Bulletin 48, 138 p.
- Jackaman, W. and Sacco, D. (2014): Geochemical and mineralogical data, TREK project, Interior Plateau, British Columbia; Geoscience BC, Report 2014-10, 13 p., URL <<http://www.geosciencebc.com/reports/gbcr-2014-10/>> [October 2020].
- Jackaman, W., Sacco, D. and Lett, R.E. (2014): Geochemical reanalysis of archived till samples, TREK project, Interior Plateau, central BC (parts of NTS 093C, 093B, 093F & 093K); Geoscience BC, Report 2015-09, 5 p., URL <<http://www.geosciencebc.com/reports/gbcr-2015-09/>> [October 2020].
- Jackaman, W., Sacco, D.A. and Lett, R.E. (2015): Regional geochemical and mineralogical data, TREK project – year 2, Interior Plateau, British Columbia; Geoscience BC, Report 2015-12, 13 p., URL <<http://www.geosciencebc.com/reports/gbcr-2015-12/>> [October 2020].
- Levson, V.M. (2001): Regional till geochemical surveys in the Canadian Cordillera: sample media, methods, and anomaly evaluation; in Drift Exploration in Glaciated Terrain, M.B. McClenaghan, P.T. Bobrowsky, G.E.M. Hall and S.J. Cook (ed.), Geological Society, Special Publication No. 185, p. 45–68.
- Levson, V.M., Giles, T.R., Cook, S.J. and Jackaman, W. (1994): Till geochemistry of the Fawnie Creek area (93F/03); BC Ministry of Energy, Mines and Low Carbon Innovation, BC Geological Survey, Open File 1994-18, 40 p., URL <<https://www2.gov.bc.ca/gov/content/industry/mineral-exploration-mining/british-columbia-geological-survey/publications/openfiles-1999-1990#1994>> [October 2020].
- Mathews, W.H. (1986): Physiographic map of the Canadian Cordillera; Geological Survey of Canada, “A” Series Map 1710A, scale 1:5 000 000.
- Natural Resources Canada (2015): Canadian Digital Elevation Model; Natural Resources Canada, URL <<https://open.canada.ca/data/en/dataset/7f245e4d-76c2-4caa-951a-45d1d2051333>> [October 2020].
- Plouffe, A. (1995): Geochemistry, lithology, mineralogy and visible gold grain content of till in the Manson River and Fort Fraser map areas, central British Columbia (NTS 093K, N); Geological Survey of Canada, Open File 3194, 119 p.
- Plouffe, A. (1997): Ice-flow and late-glacial lakes of the Fraser glaciation, central British Columbia; in Current Research 1997-A/B, Geological Survey of Canada, p. 133–143.
- Plouffe, A. and Ballantyne, S.B. (1993): Regional till geochemistry, Manson River and Fort Fraser area, British Columbia (NTS 093K, N), silt plus clay and clay size fractions; Geological Survey of Canada, Open File 2593, 224 p.
- Plouffe, A. and Williams, S.P. (1998): Regional till geochemistry of the northern sector of Nechako River map area, British Columbia (NTS 093F); Geological Survey of Canada, Open File 3687, scale 1:400 000.
- Plouffe, A., Levson, V.M. and Mate, D.J. (2001): Till geochemistry of the Nechako River map area (NTS 93F), central British Columbia; Geological Survey of Canada, Open File 4166, 66 p.
- Sacco, D.A. and Jackaman, W. (2015): Targeted geochemical and mineralogical surveys in the TREK project area, central British Columbia (parts of NTS 093B, C, F, G): year two; in Geoscience BC Summary of Activities 2014, Geoscience BC, Report 2015-01, p. 1–12, URL <http://cdn.geosciencebc.com/pdf/SummaryofActivities2014/SoA-2014_Sacco.pdf> [October 2020].
- Sacco, D.A., Jackaman, W. and McGregor, C. (2020): Mineral exploration in central British Columbia’s thick surficial deposits: surficial mapping to inform surface sediment data

- compilation and till sample reanalysis and collection in the Central Interior Copper-Gold Research project area (parts of NTS 093A, B, G, J, K, O); *in* Geoscience BC Summary of Activities 2019: Minerals, Geoscience BC, Report 2020-01, p. 83–92, URL <http://www.geosciencebc.com/i/pdf/SummaryofActivities2019/Minerals/Project%202018-050_Minerals_SOA2019.pdf> [October 2020].
- Sacco, D.A., Lett, R., Jackaman, W. and Elder, B. (2018): Advanced processing of the TREK project geochemical data: identifying and enhancing geochemical anomalies in the TREK project area using sediment transport modeling combined with multimedia and multivariate analysis; Geoscience BC, Report 2018-07, 56 p., URL <http://www.geosciencebc.com/i/project_data/GBCReport2018-07/GBCReport2018-07.pdf> [October 2020].
- Sacco, D.A., Ward, B.C., Lian, O.B., Maynard, D.E. and Geertsema, M. (2017): Quaternary geology of part of the McLeod Lake map area (NTS 093J), central British Columbia: lithostratigraphy, glacial history, and chronology; Canadian Journal of Earth Sciences, v. 54, no. 10, p. 1063–1084.
- Sacco, D.A., Ward, B.C., Maynard, D., Geertsema, M. and Reichheld, S. (2010): Terrain mapping, glacial history and drift prospecting in the north west corner of McLeod Lake map area (part of NTS 093J), central British Columbia; *in* Geoscience BC Summary of Activities 2009, Geoscience BC, Report 2010-01, p. 33–42, URL <http://cdn.geosciencebc.com/pdf/SummaryofActivities2009/SoA-2009_Sacco.pdf> [October 2020].
- Shilts, W. (1993): Geological Survey of Canada's contributions to understanding the composition of glacial sediments; Canadian Journal of Earth Sciences, v. 30, p. 333–353.
- Spirito, W.A., McClenaghan, M.B., Plouffe, A., McMartin, I., Campbell, J.E., Paulen, R.C. and Hall, G.E.M. (2011): Till sampling and analytical protocols for GEM projects: from field to archive; Geological Survey of Canada, Open File 6850, 83 p.
- Ward, B.C., Leybourne, M.I. and Sacco, D.A. (2011): Drift prospecting within the QUEST project area, central British Columbia (NTS 093J): potential for porphyry copper-gold, volcanogenic massive sulphide mineralization and gold-copper veins; *in* Geoscience BC Summary of Activities 2010, Geoscience BC, Report 2011-01, p. 73–96, URL <http://cdn.geosciencebc.com/pdf/SummaryofActivities-2010/SoA2010_Ward_et.al.pdf> [October 2020].
- Ward, B.C., Leybourne, M.I. and Sacco, D.A. (2012): Heavy mineral analysis of till samples within the QUEST project area, central British Columbia (NTS 093J); *in* Geoscience BC Summary of Activities 2011, Geoscience BC, Report 2012-01, p. 59–68, URL <http://cdn.geosciencebc.com/pdf/SummaryofActivities2011/SoA2011_Ward.pdf> [October 2020].
- Ward, B.C., Leybourne, M.I., Sacco, D.A., Lett, R.E. and Struik, L.C. (2013): Drift prospecting for porphyry copper-gold, volcanogenic massive sulphide mineralization and precious and base metal veins within the QUEST project area, central British Columbia (NTS 093J); Geoscience BC, Report 2013-15, 59 p., URL <<http://www.geosciencebc.com/reports/gbcr-2013-15/>> [October 2020].

Uncovering Porphyry-Deposit Potential in the Quesnel Terrane of Central British Columbia Using Geology and 3-D Geophysics (Parts of NTS 093A, B, G, H, J, K, O)

D.E. Mitchinson, MDRU – Mineral Deposit Research Unit, The University of British Columbia, Vancouver, British Columbia, dmitch@eoas.ubc.ca

C.J.R. Hart, MDRU – Mineral Deposit Research Unit, The University of British Columbia, Vancouver, British Columbia

D. Fournier, Mira Geoscience Ltd., Vancouver, British Columbia

Mitchinson, D.E., Hart, C.J.R. and Fournier, D. (2021): Uncovering porphyry-deposit potential in the Quesnel terrane of central British Columbia using geology and 3-D geophysics (parts of NTS 093A, B, G, H, J, K, O); *in* Geoscience BC Summary of Activities 2020: Minerals, Geoscience BC, Report 2021-01, p. 11–24.

Introduction

The Quesnel terrane of British Columbia (BC) is well known in the mineral exploration community as a terrane that is well endowed in porphyry Cu-Au mineralization. Past-producing, currently producing and developed porphyry deposits are aligned the length of the Quesnel terrane, with an obvious, approximately 300 km gap in occurrences between the currently producing Mount Milligan and Mount Polley porphyry Cu-Au deposits (Figure 1). The overall high porphyry prospectivity to the north and south of this region suggests that new porphyry deposits are yet to be discovered within this gap. The reason for the lack of exploration and discovery in this area is the extensive Quaternary cover, which limits geological knowledge and discourages exploratory drilling.

A significant amount of geophysical data exists across this region, much of which has been collected and generated through previous Geoscience BC endeavours. The Geoscience BC QUEST project, in particular, led to the collection of valuable electromagnetic (EM) and gravity data (Barnett and Kowalczyk, 2008; Geotech Ltd., 2008; Sander Geophysics Ltd., 2008). Along with the existing country-wide Natural Resources Canada (NRCan) magnetic datasets (Natural Resources Canada, 2020), the available geophysical knowledge has the potential to provide insight into the geology of the drift-covered central Quesnel terrane. Geophysical data have been employed to various extents in past work to advance knowledge of geology and structure in central BC (Mira Geoscience Ltd., 2009; Siddorn, 2011; Sanchez et al., 2015). However, the value of the existing data and 3-D geophysical inversion models derived from these data has yet to be fully realized, with op-

portunities for more co-operative interpretation, integrating existing geological knowledge, still available.

This project, titled ‘Identification of New Porphyry Potential Under Cover in Central British Columbia’ and part of Geoscience BC’s Central Interior Copper-Gold Research series, has an area of interest that overlaps that of Geoscience BC’s former QUEST project but focuses specifically on the areas of more extensive overburden. Existing data from previous Geoscience BC projects and from NRCan are used to 1) model the overburden thickness through the most heavily covered portions of the Quesnel terrane; and 2) attempt to characterize and resolve a suite of geophysical anomalies that is consistent with hostrocks of porphyry deposits. Consolidating knowledge of overburden thickness and buried geology will help explorers know where to focus efforts and gain insight for future exploration, geophysical and geochemical survey design, and mine development.

Project Strategy

Gold-rich alkalic-porphyry deposits are a feature of BC geology (Lang et al., 1995; Chamberlain et al., 2007) and are genetically associated with oxidized magmas. Thus, the magmas contain abundant magnetite. In addition, alteration-mineral assemblages, notably those characterizing the potassic-alteration phases related to the hot, metal-rich fluids from the core of these porphyry systems, typically also contain magnetite (Chamberlain et al., 2007). These are positive features for geophysics-based porphyry exploration, since magnetic highs will be associated with alkalic-porphyry intrusions and their alteration haloes.

Logan and Schiarizza (2011) outlined two belts of alkalic intrusions in the southern Quesnel terrane. These alkalic intrusions, many of which have associated porphyry mineral occurrences and deposits, are strongly correlated with magnetic anomalies (Figure 2). Based on this observation, a suite of similar magnetic targets within the ‘gap’ between

This publication is also available, free of charge, as colour digital files in Adobe Acrobat® PDF format from the Geoscience BC website: <http://geosciencebc.com/updates/summary-of-activities/>.

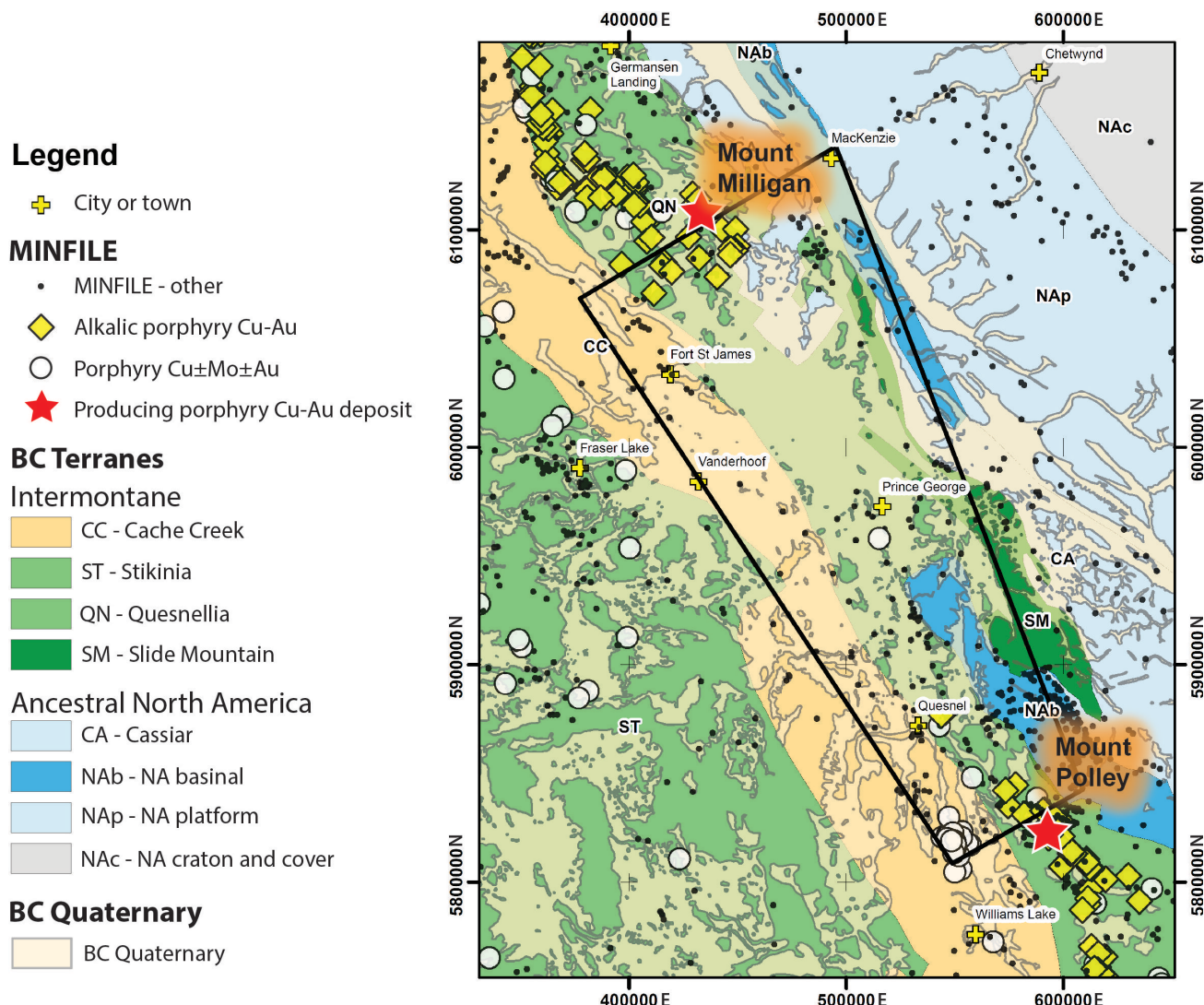


Figure 1. Project area overlain on the northern Cordilleran geological terrane map (Colpron and Nelson, 2011). Surficial geology indicating Quaternary overburden distribution through the region shown in pale transparent yellow (Cui et al., 2017). Locations of MINFILE BC (BC Geological Survey, 2020) porphyry occurrences shown as yellow diamonds (alkalic-porphyry Cu-Au occurrences) and white circles (porphyry Cu-Mo-Au occurrences). Project area outlined in black. Map co-ordinates in UTM Zone 10, NAD 83.

the Mount Milligan and the Mount Polley deposits was selected. These interpreted intrusive targets are the focus of this project, and their prospectivity as porphyry hosts or sources is followed up with consideration of regional overburden thickness and other geophysical and geological characteristics.

A new overburden-thickness model for the central Quesnel terrane is developed as part of this project. Surficial-geology maps, as well as drift-thickness models, have previously been completed in this region (Andrews and Russell, 2008; Maynard et al., 2010). These are based primarily on mapping and on existing BC groundwater-well databases. In the surficial maps, whose primary purpose is to map different types of surficial material, thicknesses are provided as broadly estimated ranges. Helicopter-borne Versatile Time-Domain Electromagnetic (VTEM™) data from

Geoscience BC's QUEST project, and information from associated inversion models, have not been previously incorporated into these maps or models of overburden thickness. The inverted VTEM data provide the key control in developing an improved thickness model. The VTEM data significantly increase the regional coverage beyond populated regions where water wells are focused and into more heavily covered areas where thickness estimates from surficial mapping are less well constrained.

This paper focuses on preliminary selection of intrusive targets and modelling of overburden thickness using VTEM. The advances reported herein are steps toward a more in-depth investigation and final report on prospective porphyry environments in the Quesnel terrane, which will be released in 2021.

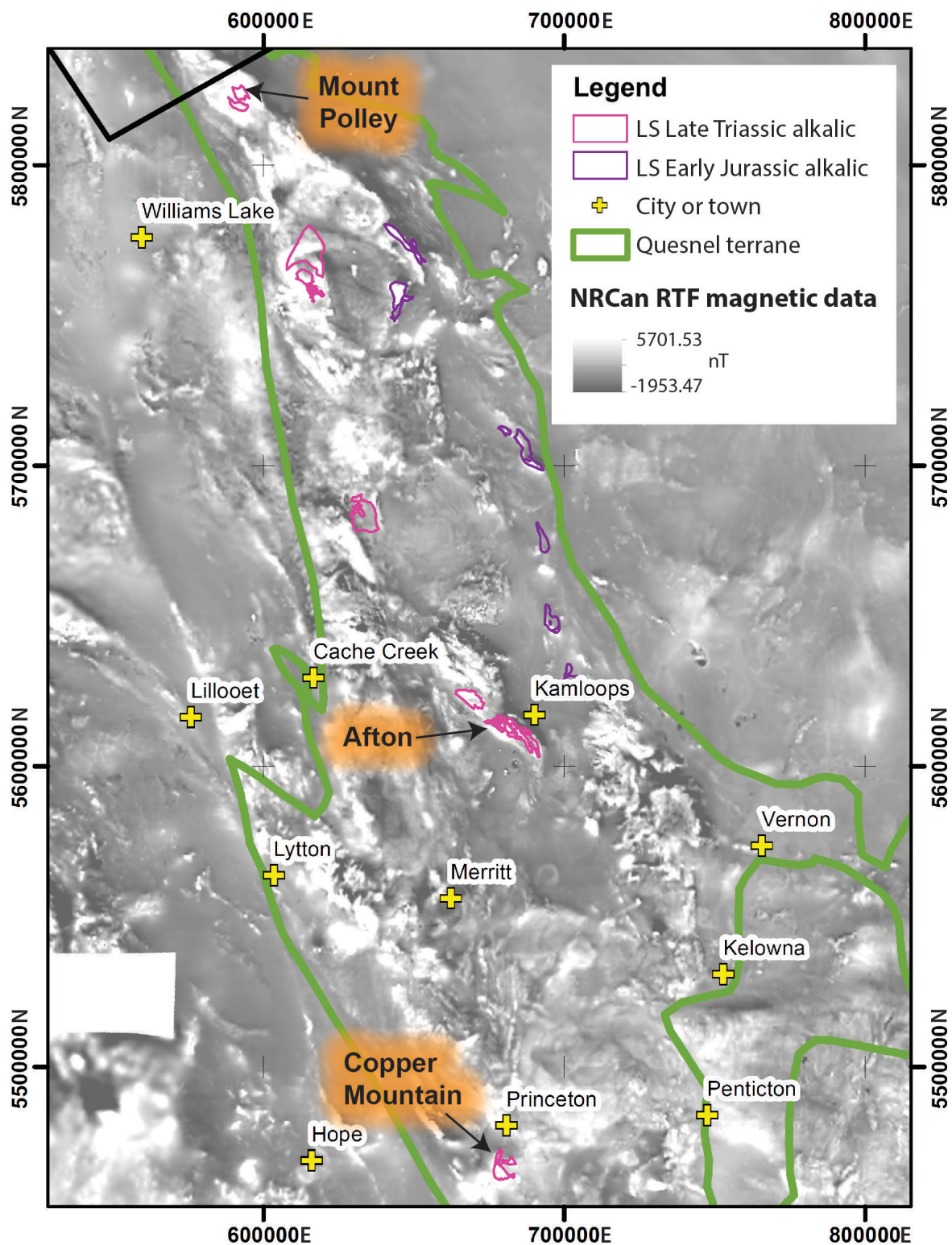


Figure 2. Alkalic-intrusive suites identified within the southern Quesnel terrane by Logan and Schiarizza (2011) are indicated by 'LS' in the legend. The western Late Triassic alkalic belt is shown in pink and the eastern Early Jurassic alkalic belt is shown in red. Several Cu-Au porphyry deposits are indicated, each of which is correlated with magnetic host or source intrusions. Background is NRCan residual-total-field magnetic data (Natural Resources Canada, 2020). The Quesnel terrane is outlined in green. Abbreviation: nT, nanotesla.

Identification of Intrusive Targets

The Natural Resources Canada (NRCan) residual-total-field data (Natural Resources Canada, 2020), as well as several derivatives of the magnetic data, were evaluated to identify magnetic anomalies that appear to be attributed to an intrusive source rock (Figure 3). Fifty-eight anomalies were chosen manually. The selection criteria required that the anomalies be somewhat rounded in shape, that they appear to crosscut stratigraphy or other geological bodies, and that they be of a size similar to intrusive bodies known to be related to the Mount Milligan and Mount Polley porphyry deposits. Comparisons between the magnetic data and bedrock geology maps confirm that some of the volcanic stratigraphy within the Quesnel terrane's Nicola and Takla groups, as well as ultramafic units of various ages, are magnetically anomalous. Positive magnetic anomalies clearly attributed to mapped mafic to ultramafic rock types were avoided.

The magnetic anomalies chosen range in size from approximately 2 km² to 50 km². Some are coincident with intrusive rocks that are mapped at the surface, whereas others do not have an obvious link to mapped or interpreted bedrock geology and may therefore represent a deeper, or undercover, magnetic body. The magnetic targets can be subdivided roughly into four clusters: 1) east and north of Quesnel, where several smaller anomalies are aligned with the regional northwest geological strike; 2) south of Prince George, where 3 to 4 anomalies occur along an east-west trend; 3) north of Prince George, where a north-northeast trend is apparent; and 4) east of Fort St. James, where the cluster of anomalies strikes northwest again.

Overburden-Thickness Modelling

Overburden-thickness modelling was undertaken to improve on current knowledge of the distribution and thickness of surficial geological material across the central Quesnel terrane. Such information is critical to improving target ranking and exploration decision-making. Overburden modelling also provides a constraint for the eventual modelling of selected magnetic anomalies of interest using geophysical inversions. The overburden-thickness model can provide an upper constraint on the location of the tops of magnetic geological bodies in the subsurface.

The VTEM data for the region were collected by Geotech Ltd. in 2008 for Geoscience BC as part of the QUEST program (Geotech Ltd., 2008). This survey collected more than 11 600 line-km of data along east-west lines at a line spacing of 4 km. Following collection, the data were inverted in 1-D and the inversion results concatenated along-line to generate conductivity models along each survey line (Mira Geoscience, 2009). It has been recognized previously that QUEST VTEM conductivity models identify the presence of conductive overburden (Kowalczyk et al.,

2010) and this was, in fact, one of the purposes of running the QUEST VTEM survey. Although the nature of the surficial materials that constitute overburden in this part of BC is highly variable and some are likely more electrically conductive than others, the extent of mapped surficial material correlates well with conductive layers resolved in inversions of the VTEM data.

The VTEM inversion sections and thickness-model data constraints were compiled using the 3-D geological modelling software SKUA-GOCAD (Figure 4). The complete list of data used to constrain the current overburden-thickness model is provided in Table 1.

To confirm independently whether VTEM models could resolve the thickness of the overburden, VTEM line inversions were compared with information from water wells, exploration drillholes and outcrop databases at localities where these data co-occur. The bases of thin near-surface conductors were found to regularly match the bottom of overburden recorded in water-well and exploration drill logs. The thin conductive overburden layer is commonly absent in areas of known outcrop. Figure 5 illustrates examples of correlation between various constraining data and conductivity horizons interpreted to represent overburden.

Two types of overburden-thickness constraints are extracted from VTEM inversions: 1) base of conductive overburden, and 2) locations of no apparent overburden. Interpretations of the apparent base of the overburden were manually digitized line by line. For each line that was interpreted, only those conductors that were most obviously related to overburden were marked. Other conductivity anomalies that had several possible geological, geographic or cultural causes, or were ambiguous, were ignored. Interpretations were consistently checked against groundwater-well and exploration-drillhole data, where available. Once interpretations were complete, all constraints were converted to a 3-D pointset in SKUA-GOCAD.

All constraints were given equal weighting or importance in the model. A 3-D surface was warped to the point constraints to create a new surface that represents the base of overburden. The interpolation was done in SKUA-GOCAD, using discrete smooth interpolation (DSI). On a first attempt in areas of higher or more abrupt relief, the surface was pulled away (down) from the topographic 'peaks' due to smoothing during interpolation. Points were then added manually by digitizing topographic peaks in SKUA-GOCAD, and a second attempt at warping the surface with these additional constraints succeeded in reducing that pull-down effect. In several places, the base of overburden surface was inadvertently smoothed between topographic highs, causing it to sit above the true topographic surface. The base of overburden surface was then simply pushed

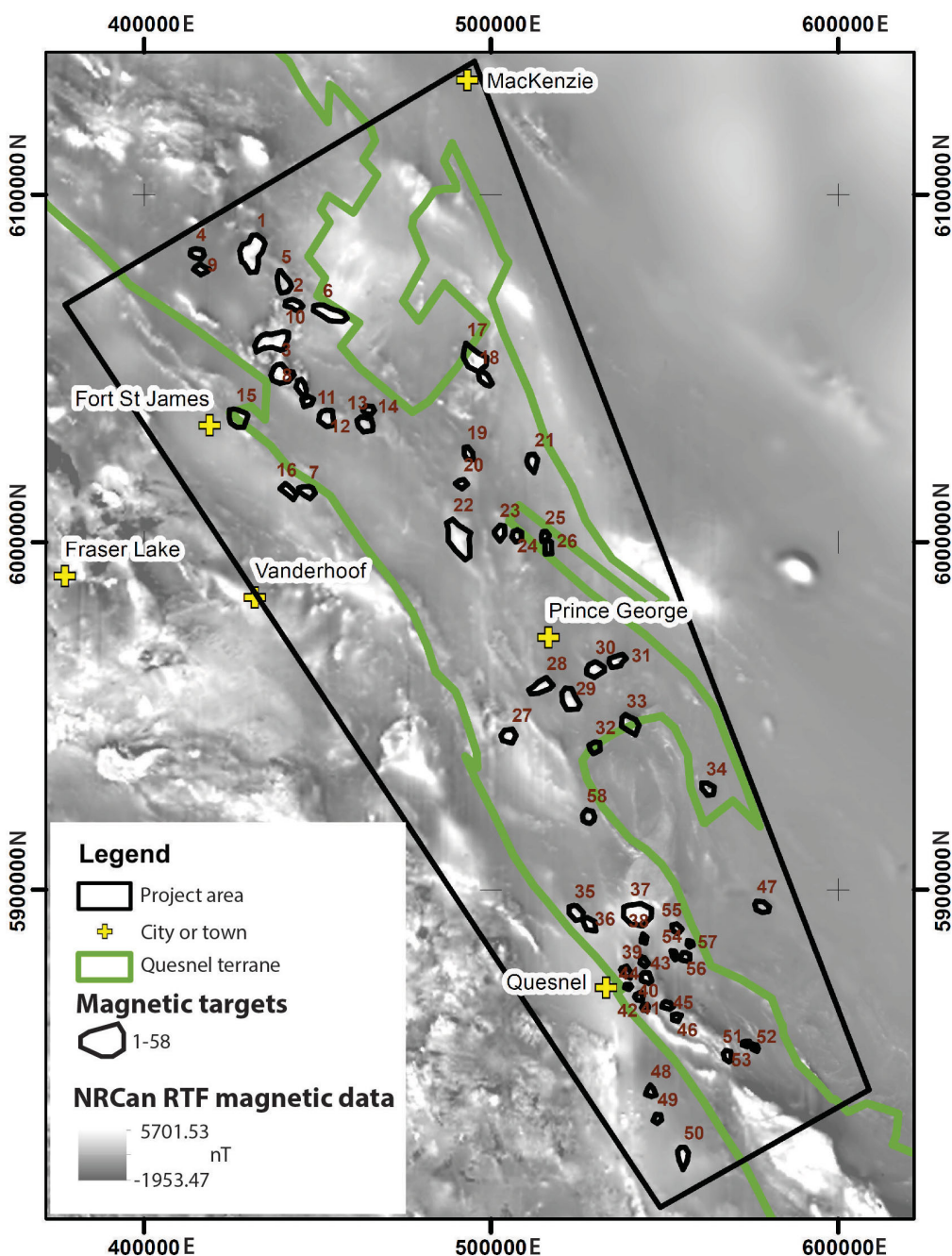


Figure 3. Magnetic targets selected for investigation (outlined in black; $n = 58$) superimposed on the Natural Resources Canada residual-total-field magnetic data grid (Natural Resources Canada, 2020). The Quesnel terrane is outlined in dark green, and the project area lies within the black quadrilateral. Abbreviation: nT, nanotesla.

down everywhere that it occurred above topography using the surface-modelling tools in SKUA-GOCAD.

The results (Figure 6) were reviewed and checked against the constraints to ensure that the constraints continued to honour, within a reasonable margin of error, the surface interpolation.

There is a good spatial correlation between the extents of mapped Quaternary geology and areas of modelled cover

material (Figure 6). The addition of detailed constraints from VTEM interpretations results in more detail about overburden thickness in areas that are difficult to access for mapping, and gives a sense of the significant variability in thickness through the region. The model indicates that there are likely more ‘windows’ of thin to no overburden than indicated on regional Quaternary geology maps. These areas of thinner cover might provide easier access to

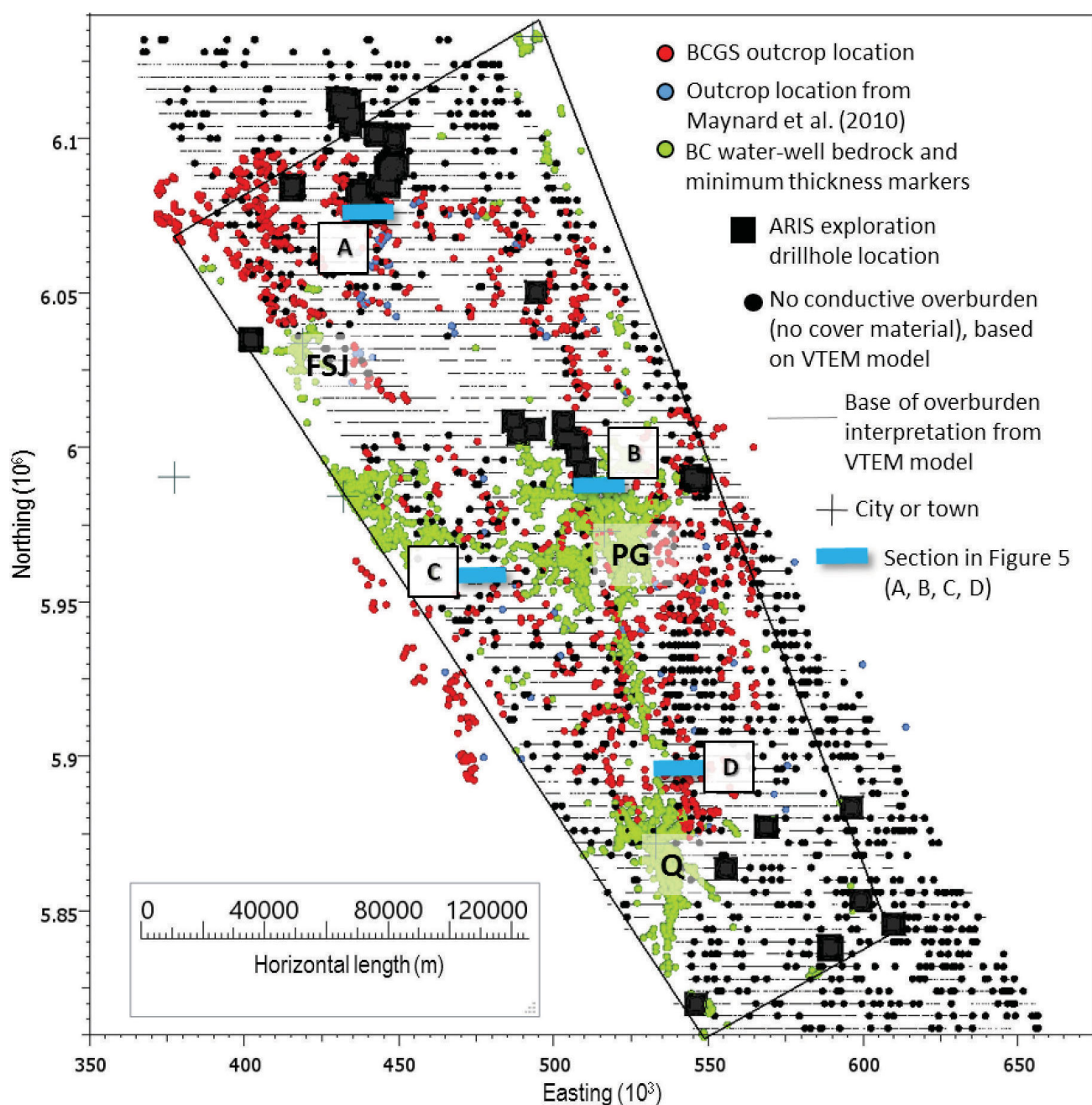


Figure 4. Constraining data used for overburden-thickness modelling. Constraining data from VTEM inversion models are derived from interpretations digitized along line on east-west VTEM lines spaced 4 km apart. Project area lies within the black quadrilateral. Abbreviations: PG, Prince George; FSJ, Fort St. James; Q, Quesnel.

bedrock for mapping and exploration purposes than previously thought.

Based on this model, the overburden thickness ranges from 0 to 297 m and averages 36 m. Most of the magnetic targets identified for this project occur beneath <50 m of overburden according to the model. The thickest overburden areas, with >200 m modelled thickness, occur south of Prince George, about 40 km northwest of Prince George, and in the northernmost part of the project area.

Preliminary Geophysical Characterization of Magnetic Targets

The goals of geophysical characterization of selected targets are to 1) determine if other geophysical data or models in addition to magnetics can help uniquely identify felsic to intermediate intrusive rocks; 2) assess the variability of geophysical signatures of interpreted intrusive rocks; and 3) determine whether differences between the geophysical fingerprints of interpreted intrusive rocks are relevant to

Table 1. Types and numbers of data constraints used for overburden-thickness modelling in this project.

Constraining data	Number of data points	Source
Groundwater wells:		BC Ministry of Environment and Climate Change Strategy (2020)
Bedrock interface	1169	
Minimum thickness where bedrock not recorded	5924	
Exploration drillhole data from BCGS assessment reports:		BC Ministry of Energy, Mines and Low Carbon Innovation (2020)
Bedrock interface	198	
Minimum thickness where bedrock not recorded	30	
Outcrop location:		Logan et al. (2010), Maynard et al. (2010)
BC Geological Survey work by Maynard et al. (2010)	1225 95	
QUEST program VTEM model interpretations:		This study
Points digitized from base of overburden interpretations	25965	
Points digitized from areas of no apparent overburden	1047	

porphyry prospectivity. To gain further insight into the geology of the chosen magnetic targets, a preliminary assessment was made of the regional density and resistivity character of the magnetic targets.

A review of existing rock-property data from the Quesnel terrane (Enkin, 2018) suggests that felsic to intermediate intrusive rocks, like those known to host or otherwise be genetically related to Cu-Au porphyry deposits in BC, should be characterized by high resistivities and low to moderate densities (Figure 7). This makes sense because a massive igneous body like an intrusion should be electrically resistive. Felsic to intermediate rocks will have lower densities than mafic to ultramafic rocks due to their higher proportion of low-density silicate minerals, but should have higher densities than sedimentary rocks, which typically have higher porosity. These characteristics should distinguish them from lower density, higher conductivity sedimentary or volcano-sedimentary rocks, and very high density, massive mafic and ultramafic rocks. Secondary alteration of rocks can lead to changes in rock properties along localized fluid pathways (Mitchinson et al., 2013), but the bulk overall rock response should prevail in the cases of these coarse regional datasets.

The density and resistivity for each chosen magnetic target was sampled from the gravity inversion (Mira Geoscience Ltd., 2009) that modelled QUEST regional airborne-gravity data (Sander Geophysics Ltd., 2008), and from a new 3-D interpolated VTEM conductivity model (this project). The density data were sampled from an inversion depth slice at 125 m and the VTEM conductivity model (converted to resistivity) was sampled from a 160 m inversion depth slice (Figure 8). Sampling the data at depth removes some of the influence of surficial rocks on the model, meaning that the signature should be bedrock driven.

Density and resistivity data were ‘painted’ onto point sets that were created for each magnetic target using SKUA-

GOCAD. In addition, points were extracted that coincide with the British Columbia Geological Survey bedrock geology polygons for intrusions related to the Mount Milligan and Mount Polley deposits, and these were also ‘painted’ with QUEST density and resistivity. Box and whisker plots showing the ranges of inversion-derived density and resistivity for the Mount Milligan and Mount Polley intrusions, and for the 58 magnetic targets, are shown in Figure 9.

Intrusions associated with Mount Milligan and Mount Polley have densities that are moderate compared to the full density dataset that would represent the densities of the varied geology across the QUEST project area. This is consistent with the types of intrusions known to host or be the source of alkalic-porphyry deposits in the Quesnel terrane. Almost all of the selected magnetic targets fall into the same range of moderate densities. Future analysis will attempt to discern the factors that led to the slightly higher densities characteristic of Mount Milligan and the slightly lower densities characteristic of Mount Polley, and whether these factors may influence prospectivity of the source rocks.

The Mount Milligan and Mount Polley intrusions have moderate to high resistivities relative to the full resistivity dataset, as expected from rock properties of felsic to intermediate intrusive rocks. The 58 magnetic targets display a large range of resistivities, with only a subset reaching the higher values seen for Mount Milligan and Mount Polley intrusive rocks. Again, future work will consider additional geological and geophysical data layers, with the goal to expand on what the variability in resistivity between these targets reveals about their geology and prospectivity.

Ongoing Work

The overburden-thickness model will be refined and updated in the final report for this project. Two approaches will be pursued to refine the model. The first addresses the ‘pulling down’ of the base-of-overburden surface during

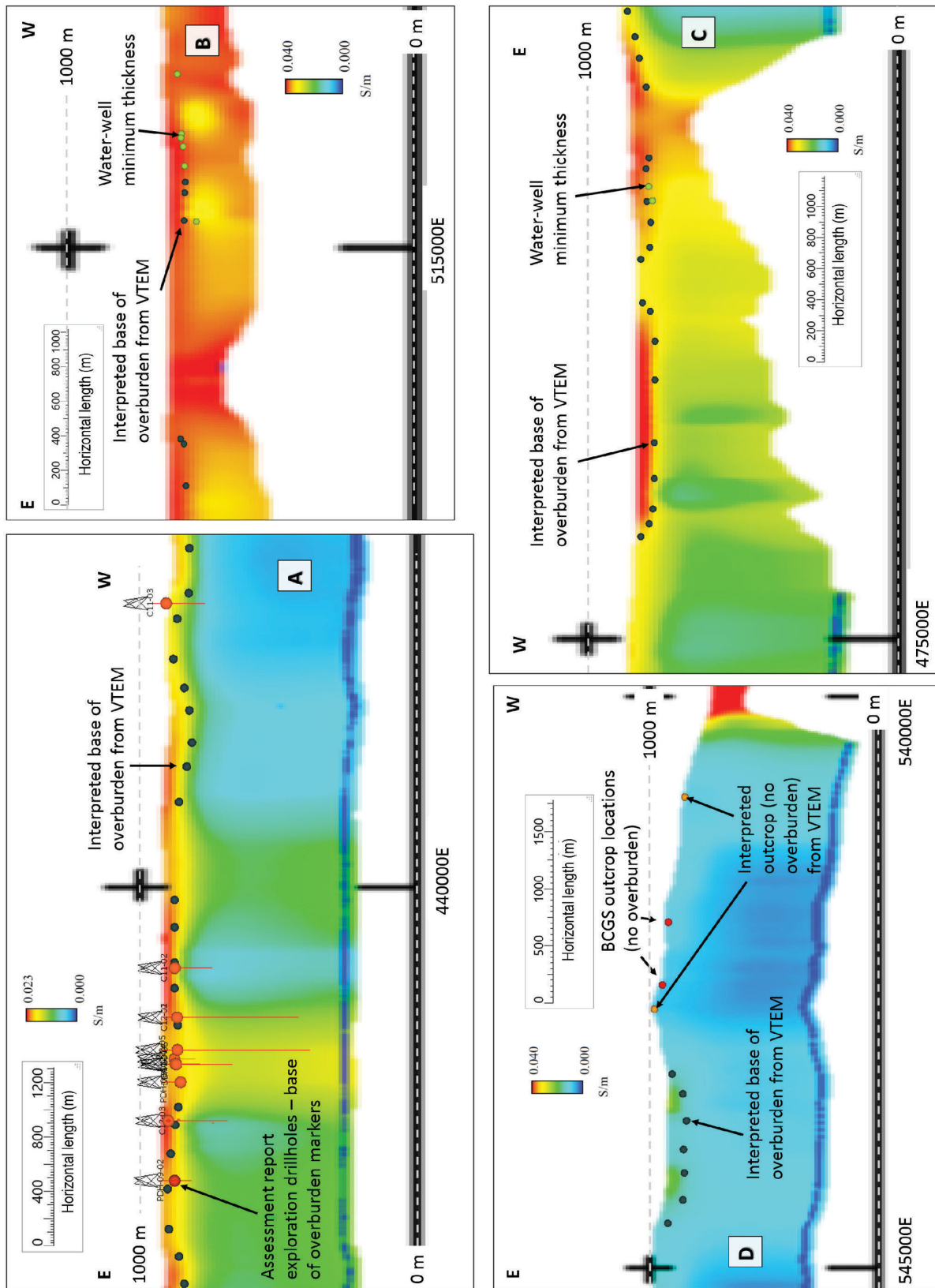


Figure 5. Vertical cross-sections through VTEM conductivity inversions showing correlation between high-conductivity layers resolved near surface and the presence of overburden as indicated in exploration-drilling, water-well and outcrop data. Vertical scale is elevation with 2x exaggeration. Section locations A–D are shown in Figure 4. Abbreviation: S/m, siemens/metre.

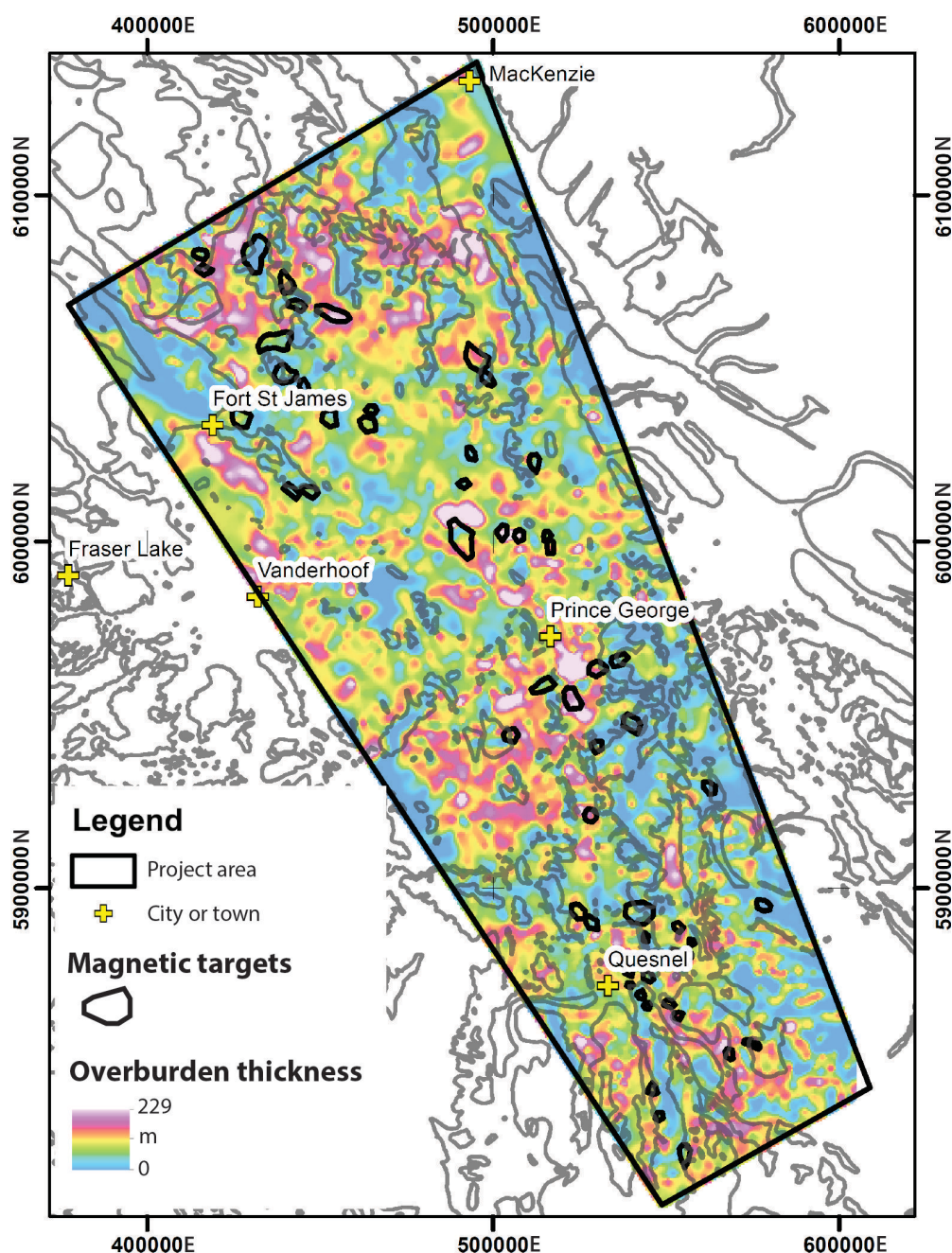


Figure 6. Overburden-thickness model of the project area. Quaternary geology (Cui et al., 2017) shown in dark grey outline.

interpolation. Rather than using manually picked topographic peaks to draw the surface back up to the likely uncovered topographic highs, an attempt will be made to use contours mapping the base of alpine physiography as a hard constraint above which overburden will be removed. The second refinement will focus on an improved interpolation to reduce any ‘line effects’ where VTEM inversion interpolations are exerting a concentrated control on the base of the overburden surface. The final thickness model will be available as both a 3-D surface (DXF and GOCAD surface

objects) and as a 2-D grid (ASCII) recording depth to the base of overburden.

Work on geophysical classification of key magnetic targets will continue and include comparisons to geophysical responses associated with other known porphyry-related intrusions north and south of the project area (north and south Quesnel terrane). An updated gravity inversion will be completed using the overburden-thickness model to refine the bedrock-density estimates. An additional VTEM inver-

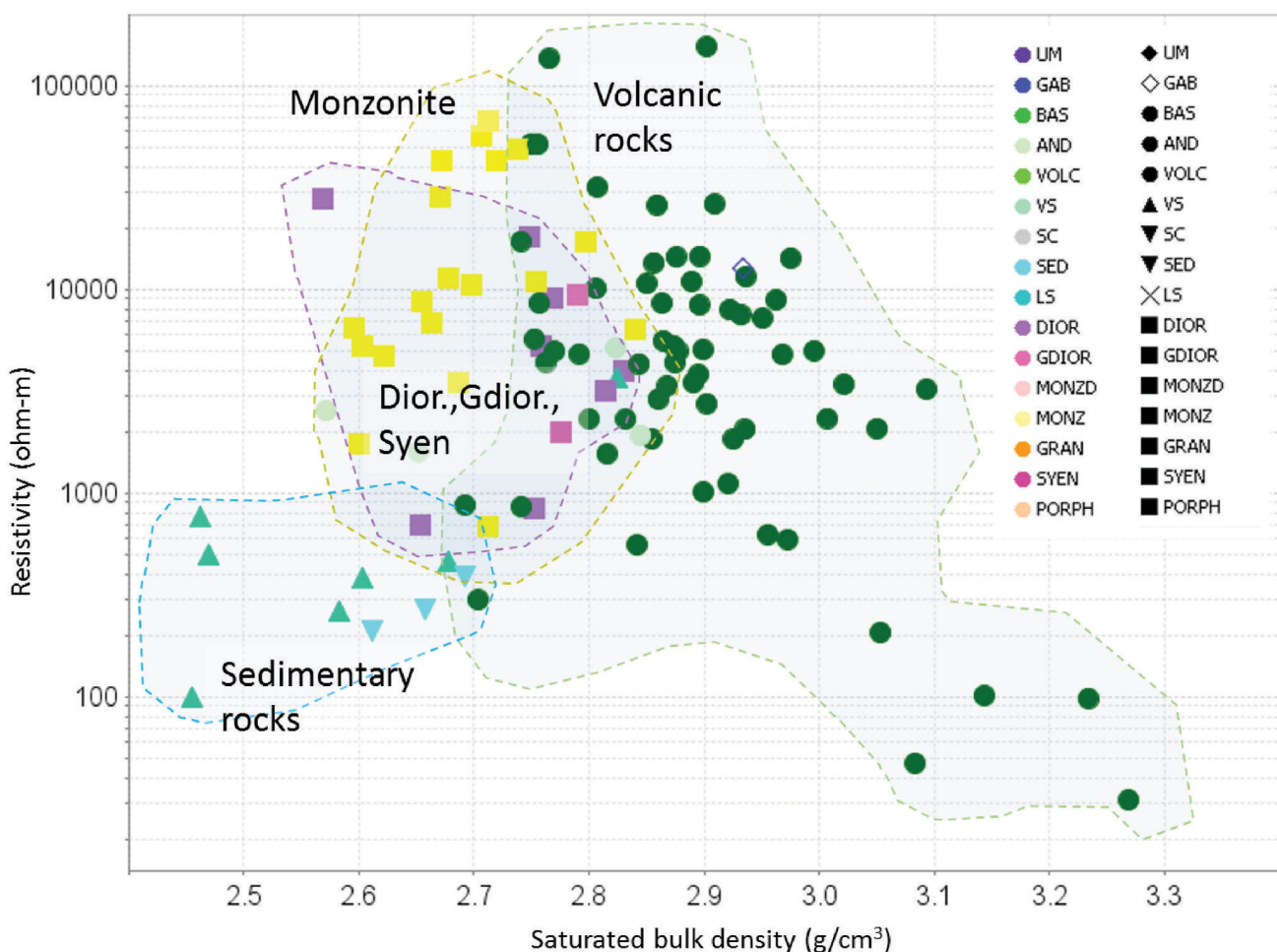


Figure 7. Saturated bulk density versus resistivity of rocks from the Quesnel terrane. Data from the Canadian Rock Property Database (Enkin, 2018). Legend shows colour and shape assigned to each rock type. Abbreviations: $\Omega\text{-m}$, ohm-metres; AND, andesite; BAS, basalt; DIOR, diorite; GAB, gabbro; GDIOR, granodiorite; GRAN, granite; LS, limestone; MONZ, monzonite; MONZD, monzdiorite; PORPH, porphyritic intrusive; SC, schist; SED, sedimentary rock; SYEN, syenite; UM, ultramafic; VOLC, volcanic rock; VS, volcanic sediment.

sion, deriving induced-polarization effect, will be run to generate a model that provides information about the chargeability of rocks across the QUEST project area.

Petrographic, lithogeochemical and petrophysical studies are underway on a set of samples from the project area. The goal of these analyses is to determine whether these properties can be used to further prioritize chosen magnetic targets.

The most prospective interpreted intrusive targets chosen on the basis of geophysical and geochemical characterization will be modelled in 3-D using magnetic inversions to provide details on their shape, size, depth and magnetic properties. This information will further inform mineral explorers on the physical parameters of the target, which will help guide prospecting, planning of local geochemical and geophysical surveys, and drilling.

Acknowledgments

Geoscience BC is thanked for providing the financial support for this project. The authors are grateful for the encouragement, insight and suggestions from peer reviewer P. Kowalczyk. Many people have provided helpful guidance and data during the course of this work thus far, including N. Phillips, P. Schiarizza, Y. Cui, P. Jago, M. Sanchez, D. Sacco and G. Andrews. B. Najafian completed a thorough review of archived exploration drilling for the project area. J. McWhirter is thanked for project management support.

References

- Andrews, G.D.M. and Russell, J.K. (2008): Cover thickness across the southern Interior Plateau, British Columbia (NTS 092O, P; 093A, B, C, F): constraints from water-well records; *in*

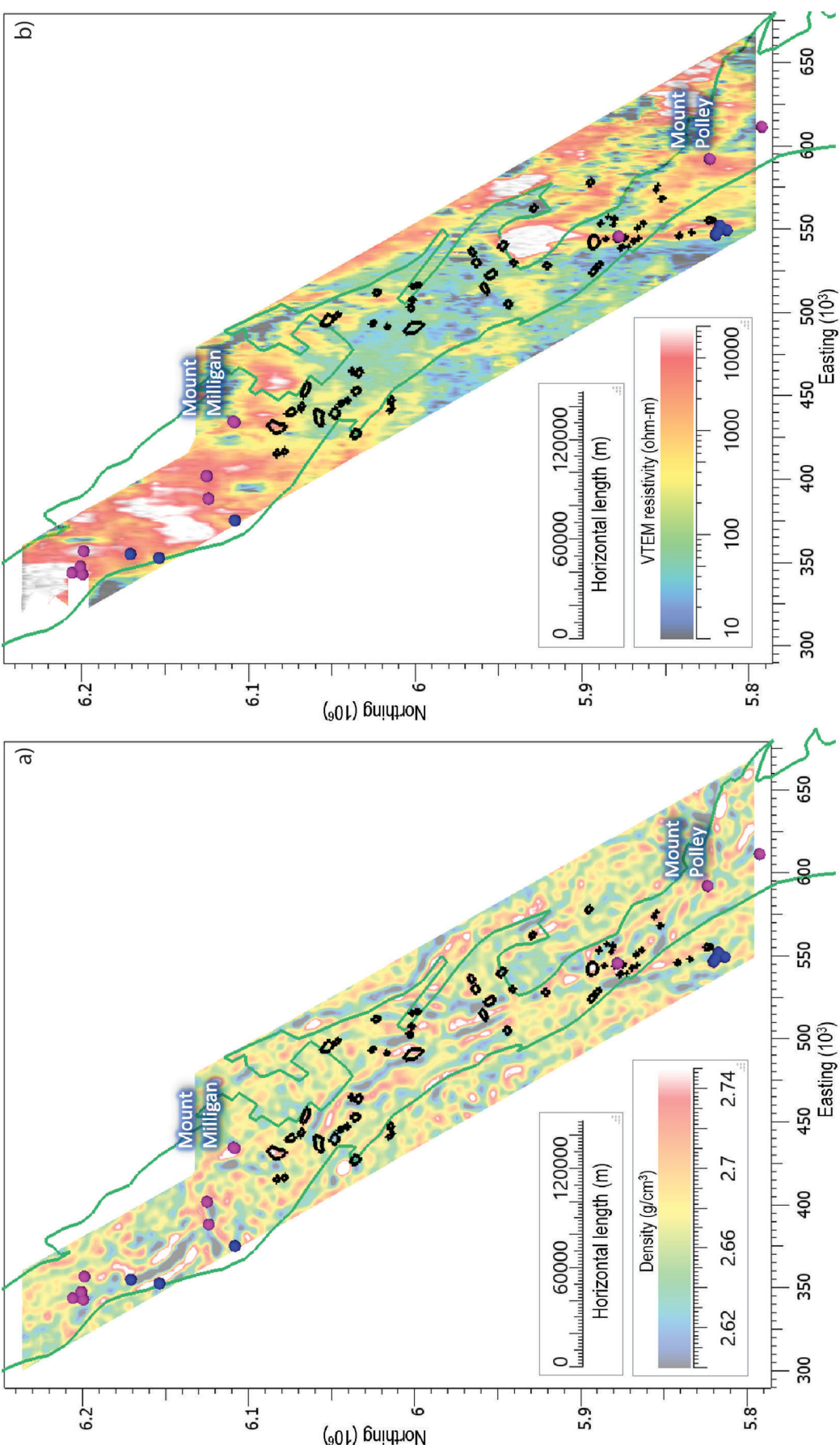


Figure 8. a) QUEST density model at 125 m depth, and b) QUEST VTEM resistivity model at 160 m depth, used to identify density and resistivity character of selected magnetic targets. Quesnel terrane outline in green. Pink dots represent alkalic Cu-Au porphyry deposits and blue dots represent other porphyry-deposit types.

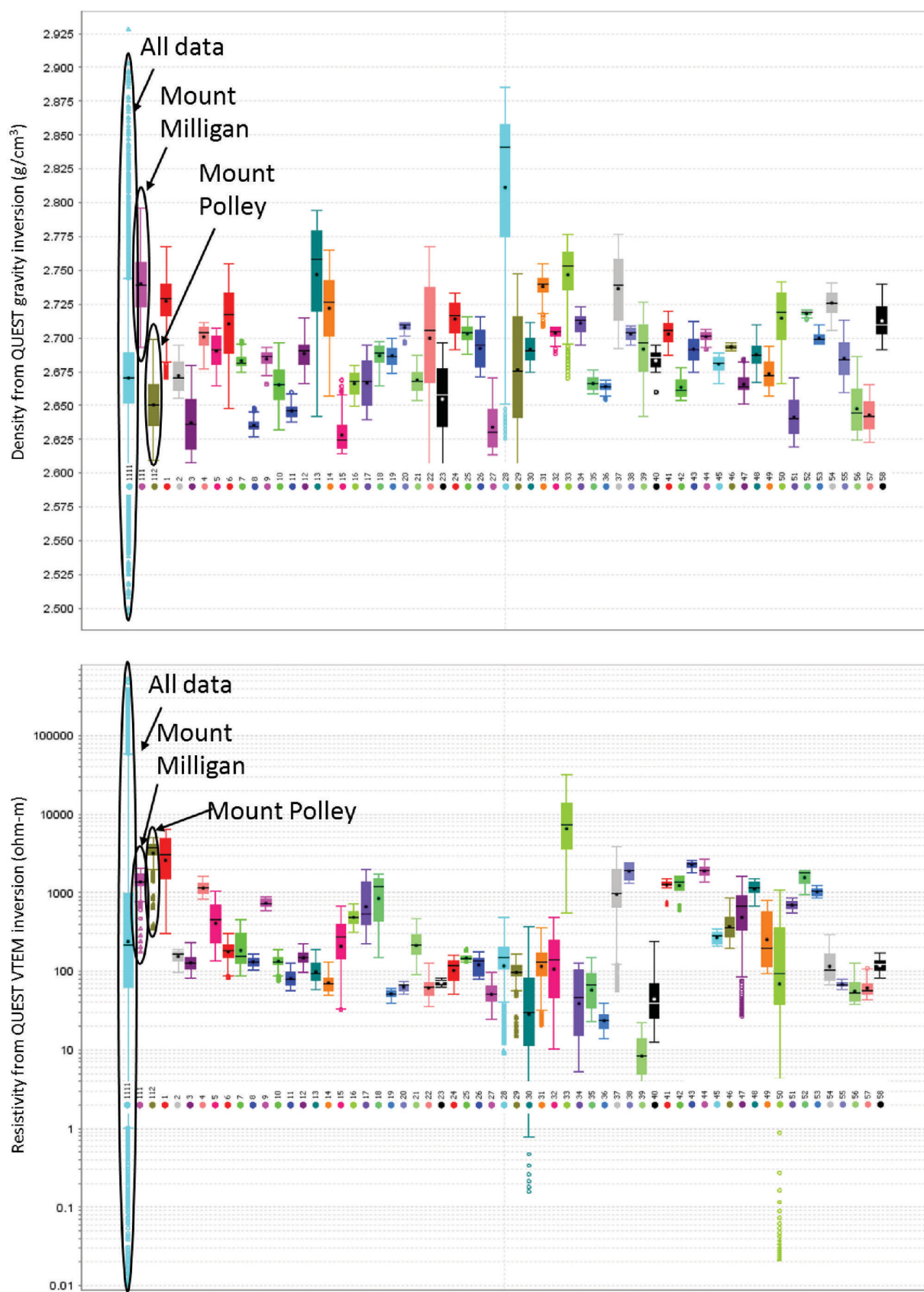


Figure 9. Density (upper plot) and resistivity (lower plot) ranges for each of the 58 magnetic targets (colors assigned randomly) sampled from regional gravity and VTEM inversions, compared to density and resistivity ranges for the entire QUEST project area and those associated with the Mount Milligan and Mount Polley intrusions.

- Geoscience BC Summary of Activities 2007, Geoscience BC, Report 2008-1, p. 11–20, URL <http://www.geosciencebc.com/i/pdf/SummaryofActivities2007/SoA2007-Andrews_original.pdf> [February 2020].
- Barnett, C.T. and Kowalczyk, P.L. (2008): Airborne electromagnetics and airborne gravity in the QUEST Project area, Williams Lake to Mackenzie, British Columbia (parts of NTS 093A, B, G, H, J, K, N, O; 094C, D); *in* Geoscience BC Summary of Activities 2007, Geoscience BC, Report 2008-1, p. 1–6, URL <<http://www.geosciencebc.com/i/pdf/SummaryofActivities2007/SoA2007-Barnett.pdf>> [October 2020].
- BC Geological Survey (2020): MINFILE BC mineral deposits database; BC Ministry of Energy, Mines and Low Carbon Innovation, BC Geological Survey, URL <<http://minfile.ca>> [July 2019].
- BC Ministry of Energy, Mines and Low Carbon Innovation (2020): Assessment Report Indexing System (ARIS); BC Ministry of Energy, Mines and Low Carbon Innovation, BC Geological Survey, URL <<https://www2.gov.bc.ca/gov/content/industry/mineral-exploration-mining/british-columbia-geological-survey/assessmentreports>> [May 2020].
- BC Ministry of Environment and Climate Change Strategy (2020): Groundwater wells database, URL <<https://catalogue.data.gov.bc.ca/dataset/groundwater-wells>> [October 2020].
- Chamberlain, C.M., Jackson, M., Jago, C.P., Pass, H.E., Simpson, K.A., Cooke, D.R. and Tosdal, R.M. (2007): Toward an integrated model for alkaline porphyry copper deposits in British Columbia (NTS 093A, N; 104G); *in* Geological Fieldwork 2006, Geoscience BC Report 2007-1, p. 259–274, URL <http://cmscontent.nrs.gov.bc.ca/geoscience/PublicationCatalogue/GeoscienceBC/GBCR2007-01-26_Chamberlain.pdf> [October 2020].
- Colpron, M. and Nelson, J.L. (2011): Yukon terranes – a digital atlas of terranes for the northern Cordillera; Yukon Geological Survey, URL <<http://data.geology.gov.yk.ca/Compilation/2>> [November 2020].
- Cui, Y., Miller, D., Schiarizza, P. and Diakow, L.J. (2017): British Columbia digital geology; BC Ministry of Energy, Mines and Low Carbon Innovation, BC Geological Survey, Open File 2017-8, 9 p., URL <http://cmscontent.nrs.gov.bc.ca/geoscience/PublicationCatalogue/OpenFile/BCGS_OF-2017-08.pdf> [June 2019].
- Enkin, R.J. (2018): The Canadian Rock Physical Property Database: first public release; Geological Survey of Canada, Open File 8460, 1 zip file, URL <<https://doi.org/10.4095/313389>>.
- Geotech Ltd. (2008): Report on a helicopter-borne versatile time domain electromagnetic (VTEM) geophysical survey: QUEST project, central British Columbia (NTS 93A, B, G, H, J, K, N, O and 94C, D), Geoscience BC, Report 2008-4, 35 p., URL <http://www.geosciencebc.com/i/project_data/QUESTdata/report/7042-GeoscienceBC_final.pdf> [June 2019].
- Kowalczyk, P., Oldenburg, D., Phillips, N., Nguyen, T.N.H. and Thomson, V. (2010): Acquisition and analysis of the 2007–2009 Geoscience BC airborne data; *in* Abstracts from the ASEG-PESA Airborne Gravity 2010 Workshop, Aug. 22–26, Geoscience Australia, Canberra, R.J.L. Lane (ed.), p. 115–124, URL <https://d28rz98at9flks.cloudfront.net/70673/Rec2010_023.pdf> [October 2020].
- Lang, J.R., Lueck, B., Mortensen, J.K., Russell, J.K., Stanley, C.R. and Thompson, J.F.H. (1995): Triassic–Jurassic silica-undersaturated and silica-saturated alkalic intrusions in the Cordillera of British Columbia: implications for arc magmatism; *Geology*, v. 23, p. 451–454.
- Logan, J.M. and Schiarizza, P. (2011): Geology of the Quesnel and Stikine terranes and associated porphyry deposits; Geoscience BC Workshop: Exploration Undercover; a practical example using the QUEST study area, URL <http://www.geosciencebc.com/i/pdf/Presentations/UnderCover-WS2011/Talk_4_Schiarrizza.pdf> [January 2020].
- Logan, J.M., Schiarizza, P., Struik, L.C., Barnett, C., Nelson, J.L., Kowalczyk, P., Ferri, F., Mihalynuk, M.G., Thomas, M.D., Gammon, P., Lett, R., Jackaman, W. and Ferbey, T. (2010): Bedrock geology of the QUEST map area, central British Columbia; Geological Survey of Canada, Open File 6476, 1 sheet, URL <<https://doi.org/10.4095/261517>>.
- Maynard D.E., Ward B.C., Geertsema M., Roberts N., and Sacco D. (2010): Relative drift thickness map, north-central BC, (93G, 93H/w, and 93J/s); Geoscience BC, Map 2010-14-1, scale 1:250 000, URL <http://cdn.geosciencebc.com/project_data/GBC_Report2010-14/GBC_Map_2010-14-1.pdf> [June 2019].
- Mira Geoscience Ltd. (2009): QUEST Project: 3D inversion modeling, integration, and visualization of airborne gravity, magnetic, and electromagnetic data, BC, Canada; Geoscience BC, Report 2009-15, 87 p., URL <http://www.geosciencebc.com/i/project_data/GBC_Report2009-15/Report/MiraAGIC_GeoscienceBC_Quest_Geop_Modelling_Report_2009-15.pdf> [June 2019].
- Mitchinson, D.E., Enkin, R.J. and Hart, C.J.R. (2013): Linking porphyry deposit geology to geophysics via physical properties: adding value to Geoscience BC geophysical data, Geoscience BC, Report 2013-14, 116 p., URL <http://www.geosciencebc.com/i/project_data/GBC_Report2013-14/GBC_Report2013-14.pdf> [November 2019].
- Natural Resources Canada (2020): Canadian Airborne Geophysical Data Base; Airborne Geophysics Section, Geological Survey of Canada, Lands and Minerals Sector, Natural Resources Canada, URL <<http://gdr.agg.nrcan.gc.ca/gdrdap/dap/search-eng.php>> [October 2019].
- Sánchez, M.G., Bissig, T. and Kowalczyk, P. (2015): Toward an improved basis for beneath-cover mineral exploration in the QUEST area, central British Columbia: new structural interpretation of geophysical and geological datasets; Geoscience BC, Report 2015-15, scale 1:500 000, URL <http://cdn.geosciencebc.com/project_data/GBCReport-2015-15/ExecutiveSummary_2015_015.pdf> [May 2020].
- Sander Geophysics Ltd. (2008): Airborne gravity survey, Quesnelia region, British Columbia; Geoscience BC, Report 2008-8, 121 p., URL <http://www.geosciencebc.com/i/project_data/QUESTdata/GBCReport2008-8/Gravity_Technical_Report.pdf> [November 2019].
- Siddorn, J.P. (2011): Interpreting aeromagnetic data for geological and structural mapping in the QUEST area; Geoscience BC Workshop: Exploration Undercover; a practical example using the QUEST study area, URL <http://www.geosciencebc.com/i/pdf/Presentations/UnderCoverWS2011/Talk_11_Siddorn.pdf> [October 2019].

Geophysical Data Compilation Project in British Columbia's Golden Triangle Area (NTS 103O, P, 104A, B, G)

C.L. Pellett, Geoscience BC, Kamloops, British Columbia, pellett@geosciencebc.com

T.A. Ballantyne, in3D Geoscience Inc., Gabriola, British Columbia

B.K. Clift, Geoscience BC, Vancouver, British Columbia

Pellett, C.L., Ballantyne, T.A. and Clift, B.K. (2021): Geophysical data compilation project in British Columbia's Golden Triangle area (NTS 103O, P, 104A, B, G); *in* Geoscience BC Summary of Activities 2020: Minerals, Geoscience BC, Report 2021-01, p. 25–28.

Introduction

Northwestern British Columbia (BC) has a long history of mineral exploration and mining, much of which has been focused in an area known within the exploration industry as the 'Golden Triangle'. The area of the Golden Triangle is only loosely defined, encompassing Stikine terrane from near Dease Lake in the north to south of the District Municipality of Stewart (Figure 1; BC Geological Survey, 2020). The area includes most of the major deposits in the western Stikine terrane, including the operating Red Chris and Brucejack mines, the proposed Galore Creek, KSM, Red Mountain and Kitsault mines, and the past-producing Snip, Eskay Creek, Premier, Dolly Varden, Granduc and Anyox deposits, many of which are experiencing new exploration activity (BC Geological Survey, 2020). Tombe (2020) notes that large porphyry Cu-Au-Mo, high-grade Au-Ag precious metal, Ag-Pb-Zn polymetallic and ultramafic-hosted Ni-Co-Pt-Pd deposits can all be potentially found in the Golden Triangle. In 2019, the Northwest mining region in BC saw over 50% of mineral exploration expenditures in the province, in large part because of industry activity in the Golden Triangle (Clarke et al., 2020).

With high mineral exploration interest in the Golden Triangle, correspondingly there is a huge amount of geoscience knowledge that exists within proprietary industry databases, including high-resolution airborne magnetic data. In contrast, the public airborne magnetic surveys for much of the area are low-resolution, widely spaced surveys that date back to the 1970s, apart from three surveys flown as part of Geoscience BC's QUEST-Northwest project in 2011–2012 (Simpson et al., 2013). Geoscience BC's Golden Triangle Geophysics Data Compilation Project has been designed to update the publicly available airborne magnetic dataset by acquiring privately held airborne magnetic data (and other airborne geophysical datasets if available), and collating them with geophysical data available in assessment reports

to publish a more comprehensive public airborne magnetic dataset for the Golden Triangle.

Updating the publicly available airborne magnetic data will be valuable to the mineral exploration sector, governments, Indigenous groups and academia to guide decisions about mineral exploration. The project can help guide future geoscience research and improve the understanding of the area's major geological features and mineral systems. In a broader sense, compiling quality mineral exploration industry data may help decrease the costs of future airborne surveys by identifying areas that already have excellent coverage.

Public Consultation

During the planning stage, Geoscience BC discussed the project with Indigenous groups in the area (Gitanyow Hereditary Chiefs, Nisga'a Lisims Government, Metlakatla First Nation, Tahltan Central Government). No major concerns were identified, and Indigenous interest in access to public geoscientific data was confirmed. Local economic development professionals (e.g., City of Terrace) have also recognized the importance of the project to attracting mineral exploration investment to the area.

Sources of Airborne Magnetic Data

The Golden Triangle Geophysics Data Compilation Project is focused on updating the publicly available airborne magnetic data in the area highlighted in Figure 2 by combining publicly available regional datasets, proprietary industry-held geophysical data and assessment report data.

Regional Datasets

Public geoscience agencies such as Geoscience BC, the BC Geological Survey and the Geological Survey of Canada collect and host airborne geophysical data and imagery, but these are regional in nature and as such are often flown at wider line spacings and higher elevations than industry-supported surveys. There are also multiple generations of public airborne magnetic data in some areas. Geoscience BC had three 250 m line-spaced airborne magnetic surveys

This publication is also available, free of charge, as colour digital files in Adobe Acrobat® PDF format from the Geoscience BC website: <http://geosciencebc.com/updates/summary-of-activities/>.

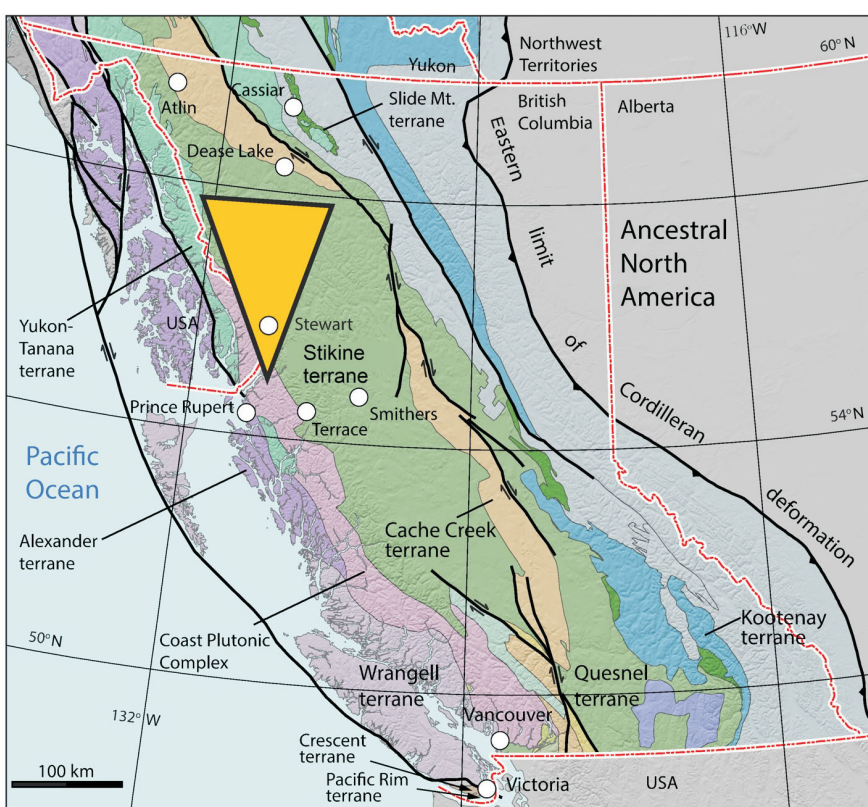


Figure 1. The Golden Triangle (yellow triangle) of northwestern British Columbia. The area of the Golden Triangle is only loosely defined, encompassing western Stikine terrane from south of Dease Lake to south of Stewart. Reproduced from BC Geological Survey Information Circular 2020-06 (modified after BC Geological Survey, 2020) with permission.

flown in the Golden Triangle area in 2011–2012 as part of the QUEST-Northwest project (Simpson et al., 2013; Figure 3a). These surveys are just north of the compilation project area (Figure 2). The rest of the Golden Triangle is covered by 1600 m line-spaced airborne magnetic surveys flown in the mid 1970s for the Geological Survey of Canada (Natural Resources Canada, 2020; Figure 3b).

Purchase of Proprietary Industry Data

Geoscience BC has purchased proprietary airborne geophysical data as part of past initiatives. Data from recent industry surveys were purchased and incorporated into both the QUEST-Northwest and TREK geophysical programs (Simpson et al., 2013; Clifford and Hart, 2014) and industry-held data were contributed as an extension to the Search Project Phase II airborne survey (Sanders Geophysics Ltd., 2017).

In July 2020, Geoscience BC put out a call for industry to sell or donate high-quality privately held geophysical data collected in the compilation project area (Figure 2) with the intention of releasing it to the public. Although Geoscience BC's primary focus for this project is on airborne magnetic data, other airborne geophysical data in the designated area

is being considered. To be considered for purchase, data must be

- well documented and ideally supported by digital copies of a logistics report, flight logs, data archive descriptions and calibration files;
- unavailable to the public, however, maps and images derived from the data may be in the public domain (e.g., news releases, websites, Assessment Report Indexing System [ARIS] reports); and
- collected by a helicopter or fixed-wing aircraft survey.

ARIS Data

The project is benefiting from a collaborative approach to geoscience in the province by Geoscience BC and the BC Geological Survey. As part of a Memorandum of Understanding signed by the two organizations in July 2020, the project has benefited from the compilation of available ARIS geophysical data by BC Geological Survey geoscientists. BC's Mineral Tenure Act Regulation requires that claim holders submit an assessment report, in PDF format, detailing their exploration or development work. The BC Geological Survey now encourages the submission of digital data along with current and previous assessment reports (data are then made available to the public for download after a one-year confidentiality period). For airborne geo-

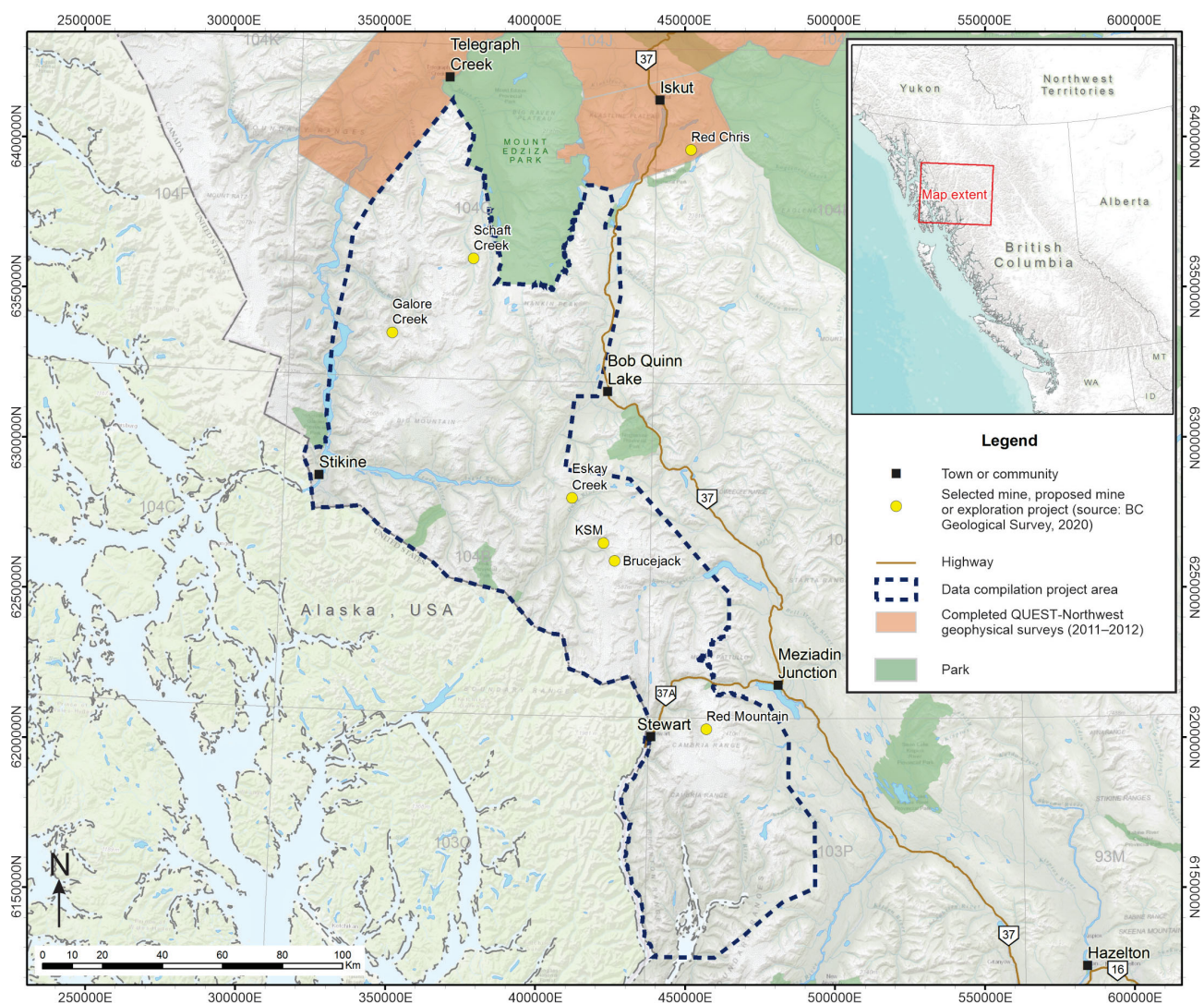


Figure 2. Golden Triangle Geophysics Data Compilation Project area, northwestern British Columbia. Light brown shading north of the project area shows the area of the Geoscience BC QUEST-Northwest project airborne magnetic surveys completed in 2011 and 2012. UTM Zone 09N, NAD 83.

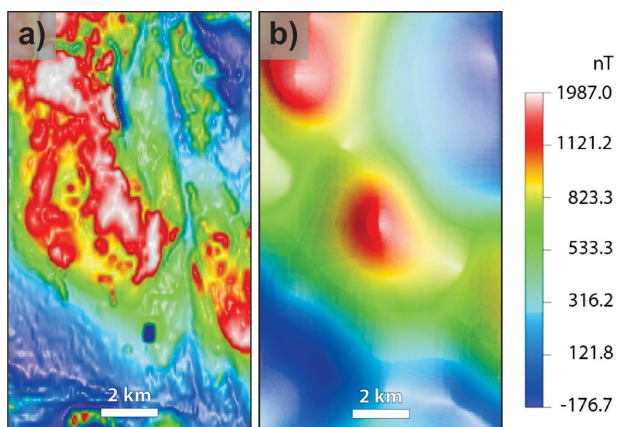


Figure 3. Comparison of regional public aeromagnetic data in the Golden Triangle: **a)** Geoscience BC's QUEST-Northwest project data collected in 2011–2012 at 250 m line spacings, **b)** National Resources Canada data collected in the 1970s at 1600 m line spacings (Natural Resources Canada, 2012). Figure reproduced from Simpson et al. (2013). Abbreviation: nT, nanotesla.

physical data, this includes the raw and processed data files (e.g., .gdb, .xyz, .csv or .grd files; BC Ministry of Energy, Mines and Low Carbon Innovation, 2020).

Project Progress and Future Work

As of mid-November 2020, 11 companies have expressed interest in participating in the program, and data from 17 separate survey blocks are currently being evaluated for purchase based on the age, method of collection and quality/desirability. Data purchases by Geoscience BC are expected to wrap up by the end of 2020. At the same time, BCGS geoscientists have identified nine blocks of ARIS data that are outside of the confidentiality period and contain the raw and processed data files, and therefore can be included as final products for this project. Once the final data are purchased and compiled, Geoscience BC will release the complete compilation of all the data products in early 2021.

Acknowledgments

This paper benefited by reviews from R. Truman, C. Salas and G. Dirom.

References

- BC Geological Survey (2020): The Golden Triangle of northwestern British Columbia; BC Ministry of Energy, Mines and Low Carbon Innovation, BC Geological Survey, Information Circular 2020-06, 8 p., URL <http://cmscontent.nrs.gov.bc.ca/geoscience/PublicationCatalogue/InformationCircular/BCGS_IC2020-06.pdf> [November 2020].
- BC Ministry of Energy, Mines and Low Carbon Innovation (2020): ARIS submission information; BC Ministry of Energy, Mines and Low Carbon Innovation, BC Geological Survey, URL <<https://www2.gov.bc.ca/gov/content/industry/mineral-exploration-mining/british-columbia/geological-survey/assessmentreports/submissionmineral>> [November 2020].
- Clarke, G., Northcote, B., Katay, F. and Tombe, S.P. (2020): Exploration and mining in British Columbia, 2019: a summary; *in* Provincial Overview of Exploration and Mining in British Columbia, 2019, BC Ministry of Energy, Mines and Low Carbon Innovation, BC Geological Survey, Information Circular 2020-01, p. 1-40, URL <http://cmscontent.nrs.gov.bc.ca/geoscience/PublicationCatalogue/InformationCircular/BCGS_IC2020-01-01.pdf> [November 2020].
- Clifford, A. and Hart, C.J.R. (2014): Targeting Resources through Exploration and Knowledge (TREK): Geoscience BC's newest minerals project, Interior Plateau Region, central British Columbia (NTS 093B, C, F, G); *in* Geoscience BC Summary of Activities 2013, Geoscience BC, Report 2014-01, p. 13–18, URL <http://www.geosciencebc.com/i/pdf/SummaryofActivities2013/SoA2013_CliffordHart.pdf> [November 2020].
- Natural Resources Canada (2012): Canadian Aeromagnetic Data Base; Natural Resources Canada, Earth Sciences Sector, URL <http://gdr.nrcan.gc.ca/aeromag/index_e.php> [November 2012; dead link].
- Natural Resources Canada (2020): Geoscience data repository for geophysical data; Natural Resources Canada, URL <<http://gdr.agg.nrcan.gc.ca/gdrdap/dap/search-eng.php>> [July 2020].
- Sander Geophysics Ltd. (2017): Technical report - magnetic gradient & radiometric survey: Search phase II; Geoscience BC, Report 2017-03, 335 p., URL <http://www.geosciencebc.com/i/project_data/GBCReport2017-03/2017-03_FinalTechnicalReport.pdf> [November 2020].
- Simpson, K.A., Kowalczyk, P.L. and Kirkham, G.D. (2013): Update on Geoscience BC's 2012 geophysical programs; *in* Geoscience BC Summary of Activities 2012, Geoscience BC, Report 2013-01, p. 1–4, URL <http://cdn.geosciencebc.com/pdf/SummaryofActivities2012/SoA2012_Simpson.pdf> [November 2020].
- Tombe, S.P. (2020): Exploration and mining in the Northwest Region, British Columbia; *in* Provincial Overview of Exploration and Mining in British Columbia, 2019, BC Ministry of Energy, Mines and Low Carbon Innovation, BC Geological Survey, Information Circular 2020-01, p. 41–58, URL <http://cmscontent.nrs.gov.bc.ca/geoscience/PublicationCatalogue/InformationCircular/BCGS_IC2020-01-02.pdf> [November 2020].

Review of the Structural Geology of the Brucejack Intermediate-Sulphidation Epithermal Deposit, Northwestern British Columbia (NTS 104B)

C. Peddle¹, Department of Earth and Atmospheric Sciences, University of Alberta, Edmonton, Alberta, cpeddle@ualberta.ca

S.T. Johnston, Department of Earth and Atmospheric Sciences, University of Alberta, Edmonton, Alberta

Peddle, C. and Johnston, S.T. (2021): Review of the structural geology of the Brucejack intermediate-sulphidation epithermal deposit, northwestern British Columbia (NTS 104B); *in* Geoscience BC Summary of Activities 2020: Minerals, Geoscience BC, Report 2021-01, p. 29–40.

Introduction

Epithermal Au deposits form at shallow crustal levels (0–2 km) and are associated with hydrothermal-fluid temperatures ranging from <150 to 300°C (White and Hedenquist, 1995). Since these deposits are emplaced at high crustal levels, older epithermal systems are commonly eroded away and there is a bias toward discovery of young (Mesozoic age) deposits (Sillitoe and Hedenquist, 2003). Formation and spatio-temporal relationships of these deposits are linked to key stages in orogenic cycles (Nelson et al., 2013). In general, epithermal deposits form in convergent-margin settings associated with continental and island-arc magmatic systems (Sillitoe and Hedenquist, 2003). Epithermal deposits can form in extensional intra-arc and back-arc environments, as well as in compressive-arc regimes (Sillitoe and Hedenquist, 2003). The state of stress (tensile versus compressive) is determined based on whether an arc is retreating or advancing (Collins, 2002). Retreating arcs undergo extension in response to rollback of the lower plate, promoting the development of back-arc basins (Cawood et al., 2009). In contrast, advancing arcs undergo contraction in response to coupling with, and overriding of, the down-going plate. Flat-slab subduction and high rates of plate convergence are responsible for the development of an advancing arc (Cawood et al., 2009).

In compressive- and extensional-arc settings, there is a variety of controls that influence the formation, distribution and orientation of epithermal systems. Rheological characteristics of rocks, structural processes and stress regime are some of the more important controls on orebodies (Corbett, 2012). Competent hostrocks more readily fracture via brittle failure, opening conduits for migrating fluids (Ramsay and Huber, 1987) and thereby facilitating the passage of metal-rich fluids (Corbett, 2012). Linear ore shoots form where feeder-fault structures intersect permeable or chemi-

cally favourable horizons and other planar features such as dikes and faults (Corbett, 2012). Epithermal deposits can be hosted along extensional structures such as listric- and bookshelf-style normal faults and subsidiary vein systems, but also in compressional structures, including thrusts, shear zones and dilation jogs (i.e., releasing bends) in strike-slip faults (Corbett, 2012).

Brucejack is a high-grade (electrum) intermediate-sulphidation epithermal deposit hosted in early to-mid-Jurassic Hazelton Group volcanic and volcano-sedimentary rocks within the Intermontane Belt (Stikine terrane) of the Canadian Cordilleran Orogen (Tombe et al., 2018; Figure 1). The deposit is located in the Sulphurets mineral district of northwestern British Columbia (BC), a major exploration camp that has been prospected since the 1800s (Kirkham and Margolis, 1995). Electrum is hosted in mildly deformed carbonate and quartz-carbonate stockwork and breccia systems (Tombe et al., 2018).

This paper presents a comprehensive review of the structural relationships that characterize the Sulphurets mineral district, with emphasis placed on the Brucejack deposit. Folds, cleavage, and fault and vein relationships are discussed from tectonic to property scale and then the observations are compared with available interpretations. Published evolutionary models for the Brucejack deposit are discussed and key questions are identified that remain to be resolved regarding the structure of the Brucejack deposit.

Tectonic Setting

The Canadian Cordillera records the complex evolution and interactions of pericratonic and allochthonous island-arc terranes and associated oceanic assemblages that have accreted to the North American continent (Monger et al., 1972). The Brucejack deposit resides in the western domain of the Stikine arc terrane (Stikinia) of the Intermontane Belt (Tombe et al., 2018; Figure 1). The Stikine terrane is flanked to the west by the Coast Plutonic Complex and to the east by Triassic–Jurassic arc-related rocks of the Quesnel terrane (Quesnellia; Nelson and Kyba, 2014). Stikinia formed as an island-arc in the paleo-Pacific Ocean from the

¹The lead author is a 2019 Geoscience BC Scholarship recipient.

This publication is also available, free of charge, as colour digital files in Adobe Acrobat® PDF format from the Geoscience BC website: <http://geosciencebc.com/updates/summary-of-activities/>.

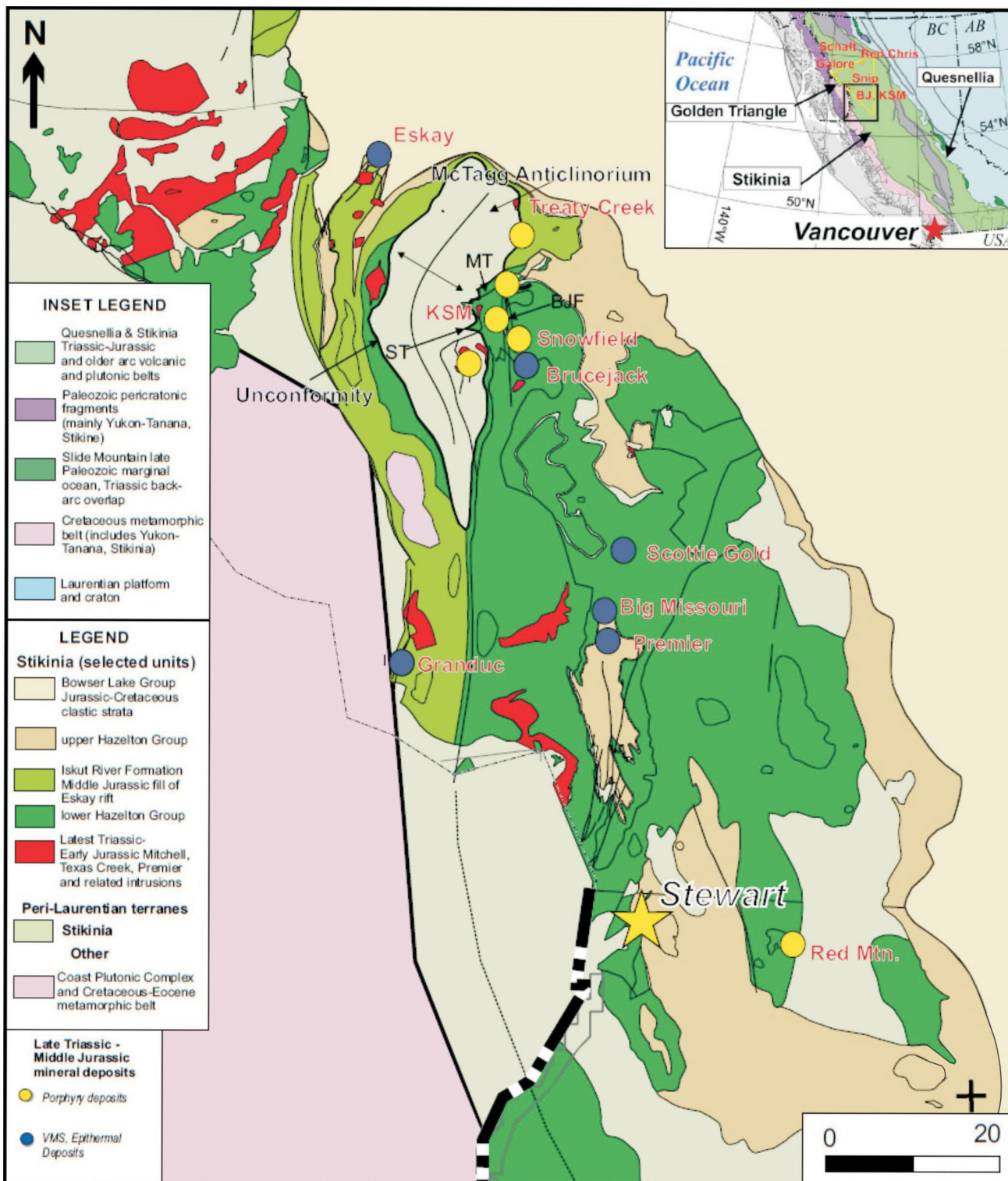


Figure 1. Geology of the McTagg Anticlinorium, showing the Brucejack deposit on the eastern flank of the anticlinorium (labelled) and other well-known prospects in the area. Small inset map in top right corner shows location of the McTagg Anticlinorium in the Canadian Cordillera (modified after Board et al., in press).

mid-Paleozoic to the Mesozoic (Monger et al., 1972). Early to Middle Jurassic subduction beneath Stikinia is indicated by arc magmatism and the development of the Cache Creek accretionary complex (Marsden and Thorkelson, 1992). Early Jurassic subduction caused Stikinia to rift, forming an extensional basin known as the Hazelton Trough, with synchronous volcanism along both of its margins (Marsden and Thorkelson, 1992). The Hazelton Trough is interpreted as an inter-arc basin (Marsden and Thorkelson, 1992). Rocks of Stikinia were deformed by a mid-Jurassic orogenesis (Evenchick, 1991). This is consistent with formation of the Bowser Basin (foreland basin) and the termination of island-arc magmatism within the Hazelton Group (Nelson and Colpron, 2007; Gagnon et al., 2012).

The Skeena fold-and-thrust belt (SFTB) is a 160 km wide fold-and-thrust zone mapped in the Stikine terrane (Evenchick, 1991). It is likely the result of a major mid-Cretaceous collision that variably strained the incompetent sedimentary rocks of this terrane. Rocks of the Bowser Lake Group were shortened by ~44%, whereas the more competent volcanic and volcaniclastic Hazelton Group rocks exhibit much less deformation (Evenchick, 1991). In the Bowser Lake Group, rocks are folded and imbricated along northwest- and southeast-striking faults that likely merge with a sole thrust at a branch point at depth, possibly at the boundary between the Hazelton and Bowser Lake groups (Evenchick, 1991). The one exception is in the northwestern domain of the Bowser Basin, where folds and faults trend and strike northeast (Evenchick, 2001). It is probable that progressive loading during SFTB orogenesis formed the Sustut foreland basin in a newly formed flexure (Evenchick, 1991).

Sulphurets Mineral District

The Sulphurets mineral district occupies the mountainous region of the Canadian Cordillera 70 km north of Stewart, BC (Figure 2; latitude 56°30'N, longitude 130°15'W; Kirkham and Margolis, 1995). This district hosts well-defined, world-class, Cu-Au-porphyry mineralization, including the Kerr-Sulphurets-Mitchell-Iron Capp (Febbo et al., 2019) and Snowfields deposits (Jones, 2013), as well as high-grade Au-Ag epithermal mineralization, including the Brucejack deposit (Tombe et al., 2018). Placer Au prospecting began in the Sulphurets region in the 1880s (Kirkham and Margolis, 1995). More extensive Cu, then Mo and later Au and Ag exploration began in the 1950s (Kirkham and Margolis, 1995). The first Cu-Au-porphyry targets were drilled in the 1960s and, during 2006, Seabridge Gold Inc. drilled the Mitchell porphyry deposit (Febbo et al., 2019). Gold-silver mineralization was first reported near Brucejack in 1959 (Roach and Macdonald, 1992). Subsequent exploration programs by Esso Minerals Canada Ltd. and Granduc Mines Ltd. from 1960 to 1985 identified multiple Au-Ag showings on what is now the

Brucejack property, currently owned by Pretium Resources Inc. (Pretium Resources Inc., 2014).

Lithostratigraphy

The lithostratigraphic relationships of the Stikine assemblage and the Stuhini, Hazelton and Bowser Lake groups are important in understanding the structural geology of the Sulphurets mineral district. The district is underlain by rocks of the Stuhini and Hazelton groups (Kirkham and Margolis, 1995). However, the relationships between the Stikine and Stuhini groups (Brown and Greig, 1990), as well as the Hazelton and Bowser Lake (Evenchick, 1991) groups, are described from observations of the immediate region. Figure 3 illustrates the stratigraphic relationships between the Stikine assemblage and the Stuhini, Hazelton and Bowser Lake groups. The lithostratigraphic development of rocks in the Sulphurets mineral district is described below.

The Stikine assemblage is the basement of the Stikine terrane (Nelson and Kyba, 2014). It consists of mostly Devonian to Mississippian arc-related plutonic and volcanic rocks that are unconformably overlain by arc-related volcanic, pyroclastic and sedimentary rocks of the Stuhini Group (Figures 2, 3; Brown and Greig, 1990). In the Sulphurets mineral district, the Stuhini Group consists of dark grey turbiditic siltstone interbedded with minor limestone, subaqueous pyroclastic rocks and intermediate porphyritic flows (Kirkham and Margolis, 1995).

The latest Triassic to middle Jurassic Hazelton Group unconformably overlies the Stuhini Group (Figures 2, 3; Grieg and Brown, 1990). The Hazelton Group is divided into lower and upper components (Figure 3; Nelson et al., 2018). The lower Hazelton Group includes the Jack and Betty Creek formations (Nelson et al., 2018). The Jack Formation consists of volcaniclastic cobble to boulder conglomerate and arkosic sandstone overlain by thinly bedded siltstone with local interbeds of intermediate pyroclastic rocks (Nelson et al., 2018). The Betty Creek Formation unconformably overlies the Jack Formation (Board et al., in press) and is subdivided into the Unuk River andesite and Brucejack Lake felsic units (Figure 3; Nelson et al., 2018).

The Unuk River andesite unit is characterized by intermediate pyroclastic and epiclastic rocks (Nelson et al., 2018). The epiclastic rocks are typically near the top of the unit, though the transition is only recognized in underground workings at the Brucejack property (Board et al., in press). The overlying Brucejack Lake felsic unit consists of potassium feldspar- and hornblende-phyric flows and welded to nonwelded felsic tuffs (Macdonald, 1993; Nelson et al., 2018). Pyroclastic rocks of the Unuk River andesite unit have detrital zircons that range in age (U-Pb) from 188 to 184 Ma (Tombe et al., 2018). Near the Sulphurets mineral district, the upper Hazelton Group includes the Spatsizi,

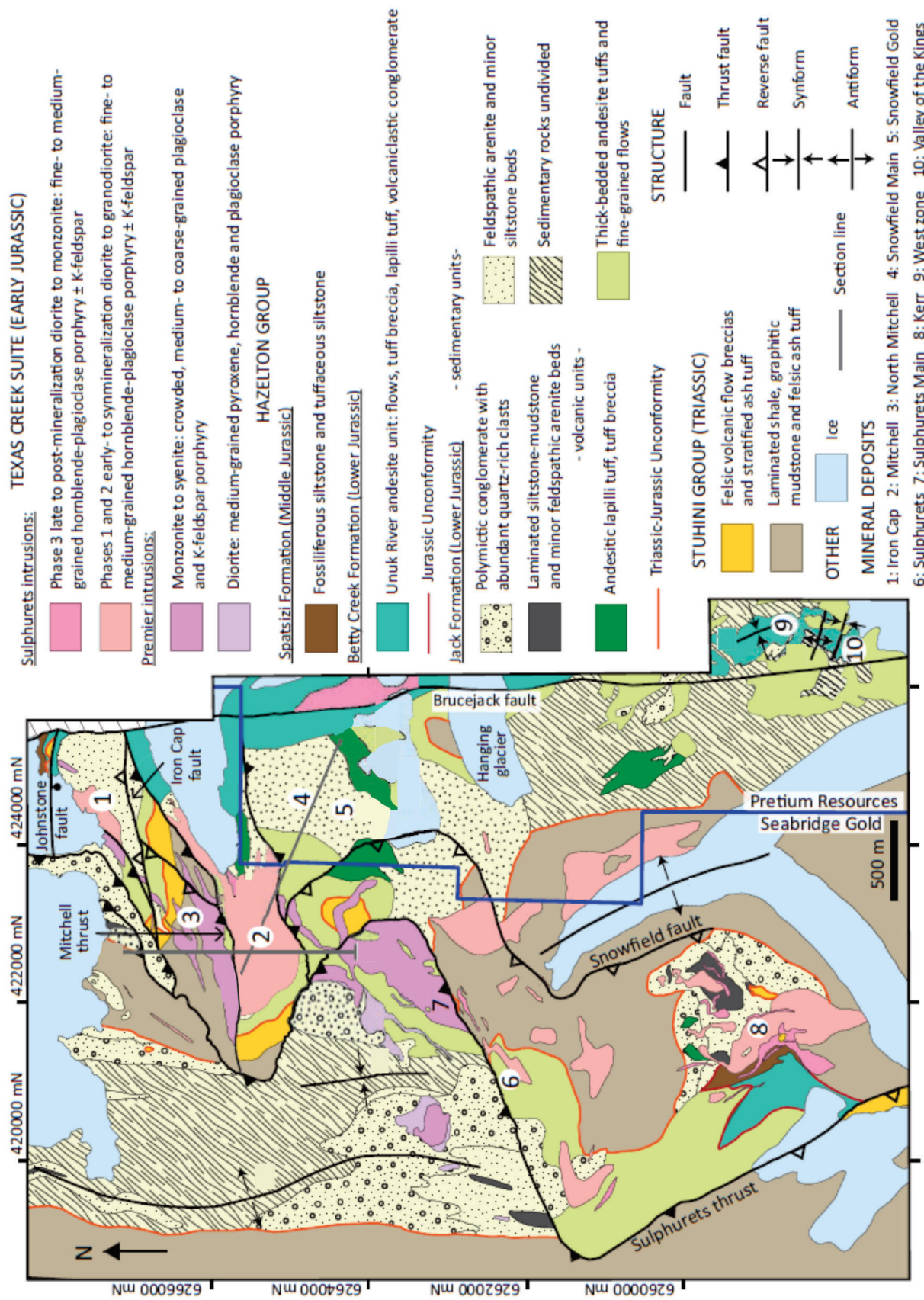


Figure 2. Lithological and structural relationships of the Sulphurets mineral district, with emphasis on known mineral deposits (1–10) and major faults and folds in the area (modified after Febbo et al., 2019).

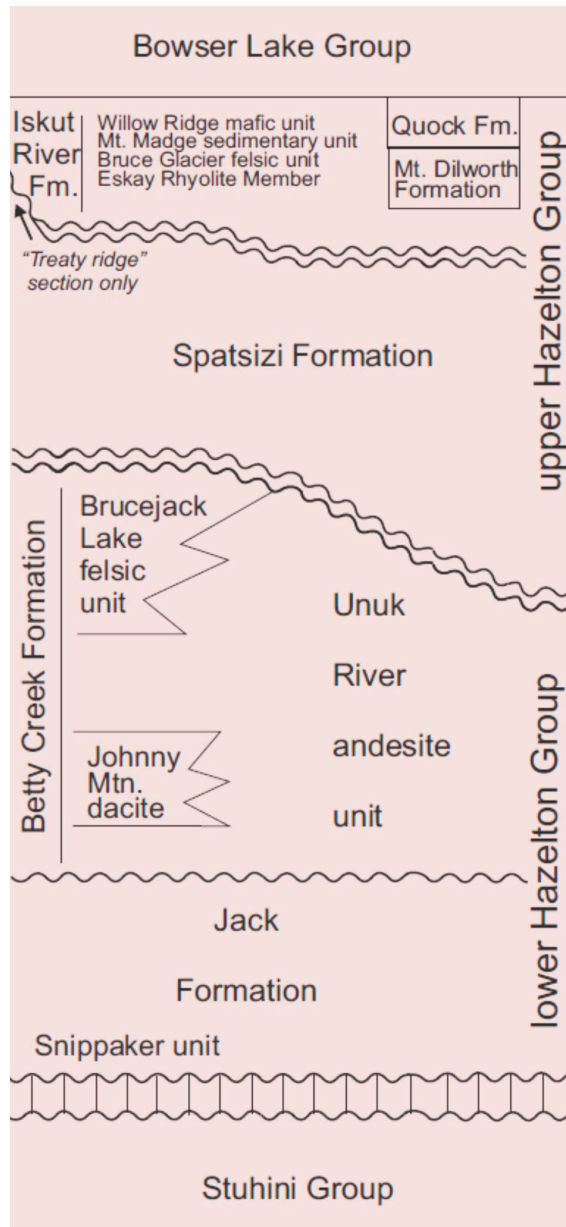


Figure 3. Stratigraphic relationships in the Sulphurets mineral district (modified after Nelson et al., 2018). Abbreviations: Fm., Formation; Mt., Mount; Mtn., Mountain.

Iskut River and Quock formations (Figure 3; Nelson et al., 2018). The Spatsizi Formation unconformably overlies the Betty Creek Formation (Nelson et al., 2018). It consists of volcaniclastic conglomerate, sandstone and siltstone-mudstone rhythmites with local limestone (Nelson et al., 2018). The Spatsizi Formation is overlain by the ca. 179–173 Ma Iskut River Formation (Gagnon et al., 2012). It consists of bimodal volcanic rocks (basalt and rhyolite) and sedimentary rocks, including grey sandstone, siltstone and mudstone (Gagnon et al., 2012). The Quock Formation overlies, and is locally a facies equivalent to, the Iskut River Formation (Gagnon et al., 2012). The Quock Formation includes thin- and medium-bedded mudstone with thin

grey tuffaceous layers (Thomson et al., 1986; Gagnon et al., 2012). The Iskut River and Quock formations are restricted to the Eskay Rift, a mid-Jurassic paleo-back-arc basin (Gagnon et al., 2012).

The Bowser Lake Group both unconformably and conformably overlies Hazelton Group rocks (Figure 3; Evenchick, 1991). It is a package of onlapping successions of fossiliferous conglomerate, sandstone, siltstone and mudstone that were likely deposited in a subsiding foreland basin during the mid-Jurassic (Evenchick, 1991). Fossils constrain deposition of the Bowser Lake Group to the mid-Jurassic to lower Cretaceous (Nelson and Kyba, 2014).

Intrusive Rocks

Arc-related intrusive rocks are documented throughout the Sulphurets mineral district (Figure 2; Davies et al., 1994; Kirkham and Margolis, 1995). Many plutons are of the Texas intrusive suite, which includes the Premier and Sulphurets intrusions (Figure 2; Kirkham and Margolis, 1995; Febbo et al., 2019). The alkaline Premier intrusions include plagioclase- and potassium feldspar-phyric monzogranite to syenite, as well as pyroxene-, hornblende- and plagioclase-phyric diorite (Figure 2; Febbo et al., 2019). Stocks associated with Premier intrusions host the main Sulphurets porphyry mineralization (Febbo et al., 2019). The Sulphurets intrusions comprise three main phases of plutons, diorite to monzodiorite, granodiorite and diorite, which all cut the Premier intrusions (Figure 2; Febbo et al., 2019). These rocks host porphyry-style mineralization of the Mitchell deposit (Febbo et al., 2019).

Three distinct igneous bodies intrude stratified rocks on the Brucejack property (Figure 4; Macdonald, 1993; Davies et al., 1994; Nelson et al., 2018; Board et al., in press). The informally named ‘Office and Bridge zone porphyries (P1)’ are characterized by light green plagioclase- and hornblende-phyric diorite (Figure 4; Davies et al., 1994; Board et al., in press). The informally named ‘P2 porphyry’ comprises potassium feldspar- (locally plagioclase) and hornblende-phyric rocks (Figure 4; Davies et al., 1994; Board et al., in press). The informally named ‘flow dome complex’ is an intrusion mapped north, south and east of Brucejack Lake (Figure 4; Macdonald, 1993). It consists of flow-banded and flow-folded plagioclase- and potassium feldspar-phyric rocks that are likely the subvolcanic equivalent of the Brucejack Lake felsic unit (Macdonald, 1993). The flow-dome complex has a U-Pb age of ca. 183–188 Ma (Lewis, 2013).

Structural Geology

The Sulphurets mineral district resides on the eastern flank of the McTagg Anticlinorium (Figure 1; Nelson and Kyba, 2014). The anticlinorium is an arcuate, fault-bounded, kilometre-scale culmination that likely formed during a mid-

Cretaceous orogenesis (Evenchick, 1991; Febbo et al., 2019). Internal structural relationships within the anticlinorium suggest a long and protracted deformation history that started in the latest Triassic (Brown and Grieg, 1990) and extended into the Cenozoic (Kirkham and Margolis, 1995). This deformation includes multiple con-

fractional events (latest Triassic and mid-Cretaceous) and a major extensional event (latest Triassic to middle Jurassic) that formed many generations of folds, cleavages, faults and veins with varying structural styles and orientations (Davies et al., 1994; Kirkham and Margolis, 1995; Nelson and Kyba, 2014; Febbo et al., 2019). This section is a re-

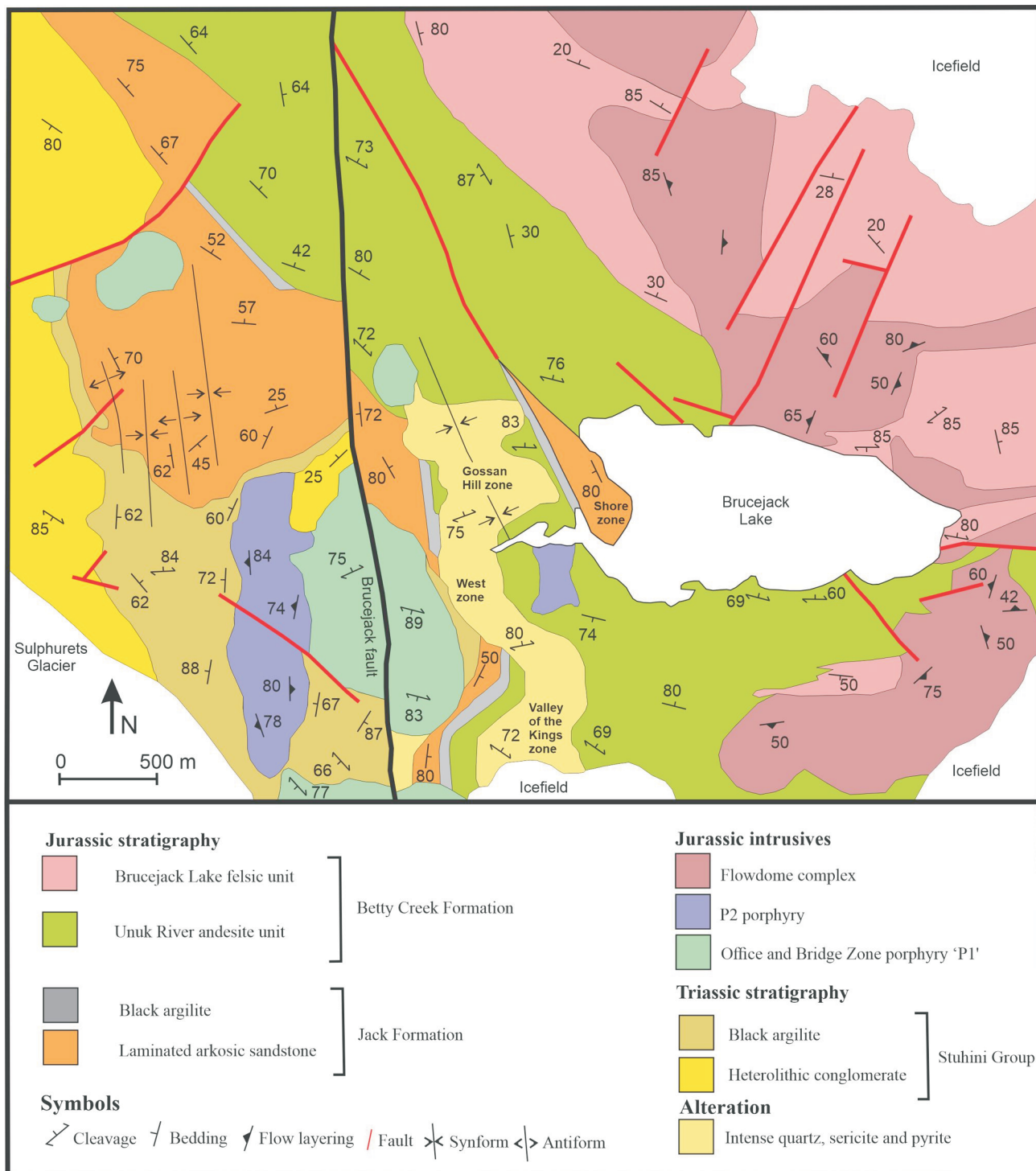


Figure 4. Detailed geology of the Brucejack property, showing lithological and structural relationships (modified after Davies et al., 1994). The Brucejack deposit comprises the Gossan Hill, West, and Valley of the Kings zones, the latter of which is currently being mined.

view of structural observations and interpretations of the Sulphurets mineral district outside the Brucejack deposit.

The oldest documented folds affect the Stuhini Group strata and formed prior to the deposition of Hazelton Group strata (Brown and Greig, 1990; Davies et al., 1994). These north-plunging folds record a major east-west contractional event that occurred during the latest Triassic and earliest Jurassic (Brown and Greig, 1990). Deformation of Jurassic vein systems (Mitchell deposit), plutons (Premier and Sulphurets suites) and Jurassic Hazelton Group strata post-date the basal Hazelton unconformity (Kirkham and Margolis, 1995; Febbo et al., 2019). Workers have attributed these younger structures to progressive mid-Cretaceous SFTB deformation (Kirkham and Margolis, 1995; Febbo et al., 2019). Rocks were folded first about west-plunging axes (north-south shortening) and later about north-plunging axes (east-west shortening; Kirkham and Margolis, 1995; Febbo et al., 2019). This is best documented at the Mitchell deposit, where dome-and-basin fold-interference patterns are observed (Febbo et al., 2019). At this deposit, west-plunging small-scale buckle folds of veins have a weak to strong west-northwest-striking axial-planar flattening cleavage (Kirkham and Margolis, 1995; Febbo et al., 2019). Veins hosted in competent potassically-metasomatized rocks are relatively undeformed, whereas those hosted in quartz-sericite-pyrite-altered rocks are tight to isoclinally folded (Febbo et al., 2019). Likewise, a west-northwest-striking cleavage is absent in potassically altered rocks and well-developed in quartz-sericite-pyrite rocks (Kirkham and Margolis, 1995; Febbo et al., 2019). This cleavage has been documented throughout the entire Sulphurets district, including mid-Jurassic rocks north of the Iron Cap deposit (Kirkham and Margolis, 1995; Lewis, 2013; Febbo et al., 2019). North-plunging folds of the Sulphurets district have been recognized at multiple scales (Davies et al., 1994; Febbo et al., 2019). Regional-scale, open, north-plunging folds define the structural grain of the Sulphurets mineral district, though small-scale folds have been documented in veins at the Mitchell deposit (Figure 2; Davies et al., 1994; Kirkham and Margolis, 1995; Febbo et al., 2019). An approximately north-striking, nonpenetrative, spaced axial-planar fracture cleavage is observed locally (Kirkham and Margolis, 1995; Febbo et al., 2019).

South-verging (north-south compression) and east-verging (east-west compression) thrusts, mapped throughout the Sulphurets mineral district, have been attributed to progressive SFTB deformation (Kirkham and Margolis, 1995; Febbo et al., 2019). South- and east-verging faults are thought to be coeval with west- and north-plunging folds, respectively (Febbo et al., 2019). South-verging thrusts are rare, the largest being the Iron Cap fault near the Mitchell deposit (Figure 2; Febbo et al., 2019). In contrast, east-verging thrusts are common, including the Sulphurets and

Mitchell thrust faults and the Mitchell basal shear zone (Figure 2; Kirkham and Margolis, 1995; Febbo et al., 2019). The Sulphurets thrust lies at the highest structural position and displays 1 km of top-to-the-east displacement (Febbo et al., 2019). The Mitchell thrust (1.6 km displacement) and the Mitchell basal shear zone (1–2 km displacement) are foreland-propagating splays positioned in the footwall of the Sulphurets thrust (Febbo et al., 2019). The Snowfields porphyry deposit is in the hanging wall of the Mitchell thrust and is thought to be the upper, displaced part of the Mitchell porphyry deposit that resides in the fault's footwall (Febbo et al., 2019). The Mitchell porphyry is truncated and displaced by the Mitchell basal shear zone at depth (Febbo et al., 2019).

The east-striking Johnstone fault and the north-striking Brucejack fault are two subvertical orthogonal structures (Figure 2; Kirkham and Margolis., 1995; Febbo et al., 2019). The Johnstone fault is located in the northeasternmost corner of the Sulphurets mineral district on the west side of the Brucejack fault and is suspected to link with the Brucejack fault at a branch point (Figure 2; Febbo et al., 2019). Near the Mitchell Glacier, there is ~500 m of west-side-up reverse displacement on the Brucejack fault, the most recent movements thought to be Eocene (Kirkham and Margolis, 1995). However, the Johnstone and Brucejack faults are interpreted to be long-lived structures that were active during deposition of the Hazelton Group units and were subsequently reactivated during later deformation (Nelson and Kyba, 2014; Tombe et al., 2018; Febbo et al., 2019). Nelson and Kyba (2014) reported that the Sulphurets thrust fault reactivated an early basin-bounding normal fault, the Sulphurets proto-fault. The configuration of early north-striking faults (Brucejack fault and Sulphurets proto-fault) and east-striking subsidiary faults (Johnstone fault) may have been crucial in controlling both the emplacement of porphyry-epithermal systems, including Kerr-Sulphurets-Mitchell-Iron Capp and Snowfields porphyries in the Jurassic, as well as stress distribution during the mid-Cretaceous SFTB (Nelson and Kyba, 2014; Febbo et al., 2019). It is likely that strain first focused on east-west basement faults (early north-south compression) and later focused on north-striking faults (later east-west compression) during progressive SFTB deformation (Febbo et al., 2019).

Brucejack Property Geology and Mineral Zones

The Brucejack property has been subdivided into 10 mineral zones, located in an arcuate north-trending belt of altered Hazelton Group rocks proximal to the Brucejack fault (Figure 4; Jones, 2013). The geology of the property is commonly discussed in relation to these zones, which have distinct geological and structural characteristics. The following discussion of some of the major zones, including

the Valley of the Kings, West, Gossan Hill and Shore zones, focuses on vein paragenesis, composition and mineralogy, as well as lithology and alteration.

Valley of the Kings Zone

The Valley of the Kings stockwork systems are hosted in the siliciclastic rocks of the Jack Formation and intermediate pyroclastic and epiclastic rocks of the Unuk River andesite unit (Figure 4; Board et al., *in press*). Veins are also hosted in hornblende- and plagioclase-phyric intrusive or hypabyssal volcanic flows along the northern (Office porphyry) and southern (Bridge Zone porphyry) boundaries of the Valley of the Kings (Board et al., *in press*). Tombe et al. (2018) classified and described the veins of this zone in six main stages: 1) barren quartz–carbonate–pyrite stringers; 2) barren translucent microcrystalline veinlets; 3) quartz–carbonate–dolomite electrum-rich veins, stockworks and breccias; 4) quartz–calcite–base metal–Ag sulphosalt–electrum veins; 5) calcite (local Mn-rich calcite)–electrum veins; and 6) barren quartz–carbonate–chlorite ‘orogenic style’ shear and extensional veins. The youngest unit that hosts veins of all six stages is the 188–184 Ma Unuk River andesite unit (Tombe et al., 2018). Stages 1–5 are cut by mafic to intermediate dikes with a U–Pb age of 183 Ma (Board et al., *in press*). This constrains the main electrum vein stages (stages 3–5) to the Jurassic (Board et al., *in press*). Because stage 3, 4 and 5 veins and the dikes are all similarly oriented and have mutual crosscutting relationships, they are interpreted to be broadly coeval (Tombe et al., 2018). The hostrocks are affected by pervasive phyllitic alteration, including white mica, pyrite, quartz and calcite, that locally destroyed primary rock textures (Board et al., *in press*). Pods of intense silicification are particularly prevalent in the Conglomerate unit and locally in the underlying Volcaniclastic unit, usually near the boundary between the two (Board et al., *in press*).

West Zone

West zone mineralization is hosted in the volcaniclastic sandstone and argillite of the Jack Formation, intermediate volcanic and pyroclastic rocks of the Unuk River andesite unit, and the P2 porphyry (Figure 4; Jones, 2013; Nelson et al., 2018). The West zone comprises 10 major quartz–carbonate veins and associated stockworks, the largest of which has a strike length of 250 m and can reach 6 m in thickness (Jones, 2013). Mineralized veins of the West zone have 650 m of known vertical continuity (Roach and Macdonald, 1992). The alteration system is ~100–150 m wide and has a silica core that transitions to sericite (\pm quartz and carbonate), then to chlorite (\pm sericite and carbonate; Jones, 2013). Quartz–carbonate veins host electrum, pyrite, sphalerite, chalcopyrite and galena, as well as Ag-bearing tetrahedrite, pyrargyrite, polybasite and sparse stephanite and acanthite (Jones, 2013).

Gossan Hill Zone

The Gossan Hill zone is a circular zone (400 m in diameter) of mineralization, hosted in the Unuk River andesite unit, that is overprinted by intense quartz–sericite–pyrite alteration (Figure 4; Jones, 2003; Nelson et al., 2018). There are 11 deformed quartz veins that strike west, dip steeply north and can have strike lengths of 250 m and thicknesses of 20 m (Jones, 2013). The veins contain electrum, pyrite, sphalerite and galena, as well as Ag-rich tetrahedrite, pyrargyrite and polybasite (Jones, 2013).

Shore Zone

Shore zone mineralization is hosted mainly in intensely quartz–sericite–pyrite–altered Jack Formation and, to a lesser extent, the Unuk River andesitic unit (Figure 4; Nelson et al., 2018). Here, a relatively small quartz–stockwork zone is coincident with a major northwest-trending lineament near the western shore of Brucejack Lake (Jones, 2013). The vein and alteration system together have a 530 m strike length and can be 5 m thick (Jones, 2013).

Structural Geology of the Brucejack Property

Folds and Cleavage

Rocks underlying the Brucejack property record multiple phases of Triassic to Eocene deformation (Figure 4; Brown and Greig, 1990; Kirkham and Margolis, 1995). The earliest deformation is documented in the Stuhini Group to the west of the Brucejack deposit (Davies et al., 1994). The Stuhini Group rocks are imbricated and tightly folded about north-northwest-plunging fold axes (Davies et al., 1994). Folds have wavelengths of tens of metres and are truncated against an angular unconformity that separates them from the overlying Hazelton Group (Davies et al., 1994). The Hazelton Group strata of the Brucejack property are also deformed (Britton and Aldrick, 1987; Roach and Macdonald, 1992; Davies et al., 1994; Kirkham and Margolis, 1995; Harrichhausen, 2015; Tombe et al., 2018). They constitute a concave-to-the-west arcuate, northerly trending belt of eastward-younging and openly folded rocks (Figure 4; Davies et al., 1994; Jones, 2013). East of the Brucejack fault and west of Brucejack Lake, the belt is characterized by a regional-scale, north-plunging syncline. The core of the syncline houses the West zone showing (Figure 4; Davies et al., 1994; Jones, 2013). The western limb of the syncline continues south through an alteration zone near the Brucejack deposit, whereas the eastern limb is cut out against a fault along strike to the north and south (Figure 4; Davies et al., 1994). Although Davies et al. (1994) described folds in the northerly belt as open, their bedding-orientation data indicate that tightly folded domains exist along the axial trace of the syncline (Figure 4). Northerly trending folds lack a penetrative axial-planar

fabric. Tombe et al. (2018) interpreted the Brucejack deposit, as well as the West zone showing, to reside within a series of east-southeast-trending synclines that lie along the axial trace of the north-trending syncline mapped by Davies et al. (1994). However, the synclinal features have also been interpreted as a series of east-southeast-striking paleo-half grabens (Board et al., in press).

A weakly to well-developed, ubiquitous, east-southeast-striking planar fabric can be mapped throughout the Brucejack property (Roach and Macdonald, 1992; Davies et al., 1994; Tombe et al., 2018; Board et al., in press). Early vein and foliation studies by Roach and Macdonald (1992) defined a high-strain region in the West zone. In this high-strain zone, there is a strong east-southeast cleavage that parallels mineralized veins and their margins (Roach and Macdonald, 1992). They interpreted that the high-strain zone, including the mineralized veins and cleavage, formed during simple shear (non-coaxial deformation; Roach and Macdonald, 1992). In contrast, Davies et al. (1994) described the east-southeast-striking cleavage as a flattening fabric (coaxial deformation) that is axial planar to buckle folds observed in veins. This is consistent with fold- and fabric-orientation data collected in stockwork zones on the Brucejack property by Harrichhausen (2015). Davies et al. (1994) argued that the east-southeast-striking cleavage is postmineralization and attributed it to the mid-Cretaceous SFTB deformation (Evenchick, 1991). Davis (2017) defined two east-southeast-striking flattening fabrics (S_1 , east-southeast; S_2 , southeast) at the Brucejack deposit. He documented both foliation-parallel and discordant relationships between mineralized veins at the Brucejack deposit and suggested that both fabrics predate mineralization (B. Davis, unpublished report prepared for Pretium Resources Inc., 2017).

Faults

The Brucejack fault is subvertical and passes through the entire property west of Brucejack Lake (Figure 4; Davies et al., 1994; Tombe et al., 2018). The fault cuts all rock types, veins and alteration zones, and the most recent movements are believed to be Eocene (Kirkham and Margolis, 1995). At regional scale, map patterns suggest there is ~200 m of dextral strike separation (with unknown dip separation) along the fault west of Brucejack Lake (Figure 4; Davies et al., 1994). North of the Brucejack property, Davies et al. (1994) mapped steeply plunging elongated clasts, suggesting dominantly dip-slip movement at some time during the fault's history.

Minor east-northeast-striking cross faults with both dextral and sinistral movements also affect rocks of the Brucejack property (Figure 4; Davies et al., 1994; Harrichhausen, 2015). The largest of the east-northeast-striking cross faults, mapped north of Brucejack Lake, has normal-

dextral shear sense and tens of metres of displacement (Davies et al., 1994).

Proposed Structural Models for the Brucejack Deposit

Roach and Macdonald (1992) conducted a vein and foliation study at the West zone showing and interpreted quartz-carbonate veins of the West zone to have formed in a 130 m wide, southeast-striking and steeply dipping, sinistral, brittle-ductile shear zone. This model interpreted the southeast-striking fabric as synveining and a product of ductile simple shear (Roach and Macdonald, 1992). Extensional veins of the West zone are parallel and subparallel to the orientation of the interpreted shear zone. The veins are described as central and oblique, terms adopted from Hodgson (1989), and are inferred to have formed episodically at elevated fluid pressures through brittle failure (Roach and Macdonald, 1992).

Harrichhausen (2015) studied the structural evolution of mineralized veins of the Brucejack property, placing emphasis on a major east-southeast-striking breccia-stockwork system, Domain 20, at the heart of the Valley of the Kings. This system is well exposed underground but has not been observed at the surface. Higher density of veins at the core of Domain 20, and adjacent lower density systems, are consistent with vein patterns observed in faults and neighbouring damage zones (Harrichhausen, 2015). Inferred offset of lithological units in the hangingwall relative to the footwall of Domain 20 suggests it is a south-side-down normal fault (Harrichhausen, 2015). Harrichhausen (2015) interpreted Domain 20 to have formed in an extensional zone along an east-southeast-striking strike-slip fault. Veins associated with Domain 20 have syntectonic growth textures and likely formed postfaulting during a static period with high fluid pressures and fracture displacement through mode-1 extension (Harrichhausen, 2015). In contrast, other quartz-carbonate stockwork zones mapped at the surface in the Valley of the Kings zone have asymmetries and textures, such as stretched quartz fibres, that suggest they formed during shearing (i.e., synfaulting; Harrichhausen, 2015). Therefore, veins of the Brucejack deposit likely formed in an east-southeast-striking strike-slip system along subsidiary extensional fractures both syn- and postdisplacement (Harrichhausen, 2015).

Davis (B. Davis, unpublished report prepared for Pretium Resources Inc., 2017) reported that veins of the Valley of the Kings formed through two progressive stages of roughly north-south compression prior to and during the main stage of mineralization in the Jurassic. Stage one is characterized by the development of two flattening fabrics, oriented east-southeast and southeast, that formed through northeast-southwest compression. Large-scale, north-striking strike-slip faults, including the 'Cleopatra' vein,

formed as transfer structures (i.e., tear faults) bounding distinct structural domains. During stage two, pre-existing north-striking faults were reactivated during sinistral transpression. This implies a switch in kinematics from northeast-southwest to northwest-southeast compression. Here, ore fluids of the Brucejack deposit focused along north-striking faults and southeast-striking extensional veins that formed through episodic brittle failure. Davis (B. Davis, unpublished report prepared for Pretium Resources Inc., 2017) hypothesized that the two fabrics, in part, controlled the orientation of the southeast-striking mineralized extensional veins. Locally, veins are folded and boudinaged parallel to the fabric, suggesting that ongoing progressive deformation was at a high angle to the mineralized veins. Styolitic and asymmetric geometries observed in electrum hosted in extensional veins are interpreted as syndeformational textures. Board et al. (in press) proposed that the approximately north-south compression noted at the Mitchell Au-Cu porphyry by Febbo et al. (2019), who attributed this deformation to the mid-Cretaceous SFTB, is also likely a product of Jurassic deformation (183 Ma) described by Davis (B. Davis, unpublished report prepared for Pretium Resources Inc., 2017).

Febbo et al. (2019) interpreted the west-northwest-striking veins of the Mitchell deposit as having formed during localized north-south extension within a step-over zone between north-striking faults in an overall east-west extensional regime. It is postulated that the east-southeast-striking veins of the Brucejack also formed in a step-over zone similar to the Mitchell deposit (Febbo et al., 2019).

Preliminary Hypothesis Based on Previous Studies

Detailed mapping of the Brucejack property by Davies et al. (1994) indicated that north-northwest-trending folds (arcuate belt) define at property scale the structural grain of the Jurassic stratigraphy that hosts the mineralized zones of the property. These folds are tight, and locally isoclinal, on the map by Davies et al. (1994), suggesting significant east-west shortening. In contrast, the Au-bearing vein networks at Brucejack are relatively undeformed with exceptional continuity (Board et al., in press). Based on these observations, it would not be unreasonable for the significant east-west shortening documented in the hostrocks of the Brucejack deposit to be premineralization or synmineralization. However, folds and faults of the belt are at present considered a product of the SFTB, based on orientation alone (e.g., Davies et al., 1994). Mineralized zones along the belt could have formed as extensional and transtensional vein systems along east-southeast-trending faults, as previously proposed by Harrichhausen (2015), during the waning stages of folding in the north-trending arcuate belt during approximately east-west Jurassic compression.

One of the most difficult things to explain is parallelism of cleavage and veins, since they imply opposite kinematics, a phenomenon observed at the Brucejack property. Roach and Macdonald (1992) proposed that the east-southeast fabric formed during brittle-ductile shearing, although it has since been well documented as a flattening (coaxial deformation) fabric (e.g., Harrichhausen, 2015; Davis, 2017) and therefore unlikely to have formed through simple shear. In order to justify this relationship in the model of Davis (B. Davis, unpublished report prepared for Pretium Resources Inc., 2017) and Board et al. (in press), this would require cyclical changes in kinematics: 1) northeast-southwest compression to form east-southeast cleavages; 2) northwest-southeast compression to reactivate north-south faults as sinistral shear zones and form east-southeast-striking mineralized veins; and 3) northeast-southwest compression to fold and boudinage the veins along an east-southeast-striking cleavage. Because older veins of the Brucejack mineralized system are interpreted to be more deformed than younger ones (Tombe et al., 2018; Board et al., in press), the model would require numerous kinematic changes. It is possible that relatively undeformed and fabric-oblique, as well as deformed, veins are observed along the east-southeast-striking cleavage as a result of strain partitioning during postmineral deformation, consistent with SFTB deformation, as proposed by Febbo et al. (2019). Rather than trying to explain the observations of previous workers (e.g., Board et al., in press) as being the result of synmineralization deformation, it is possible that mineralized veins that are steeply dipping are symmetrically boudinaged, veins that dip at moderate angles are sheared, and subhorizontal veins are buckled during postmineral deformation. The competency contrast between veins and the hostrock, as well as the spacing of veins in a stockwork zone, will affect whether a vein will partition strain or not, which could explain why many veins are relatively undeformed. Although other interpretations are possible, the authors believe strain partitioning could be a more reasonable alternative for the vein-fabric relationships at the Brucejack deposit and intend to further investigate a strain-partitioning model.

Ongoing and Future Work

This paper summarizes the structural geology of the Sulphurets mineral district, with emphasis on the Brucejack property. It serves as a review for the authors' ongoing research project entitled 'Structural analysis of the Brucejack intermediate-sulphidation epithermal deposit, northwestern British Columbia' as well as a summary of hypotheses and queries that have been developed. The main goal of the project is to define and categorize all structural elements, including folds, faults, cleavage, lineations, fractures and veins, at various scales based on process of formation, structural style, orientation and crosscutting relationships. The aim is to create a holistic kinematic

framework that adheres to all structural observations and clearly defines pre-, syn- and postmineral deformation.

To achieve this goal, detailed surface and underground mapping was conducted during the 2018 and 2019 summer field seasons. During the 2018 field season, emphasis was placed on the Valley of the Kings zone. Detailed structural analysis was conducted on cleavage, fold, fault, fracture, vein and dike systems of both surface and underground workings. The 2019 field season focused on detailed lithology and structural mapping at regional scale, covering the area mapped by Davies et al. 1994 (Figure 4). Using these field and underground observations, an evolutionary model (interpretive) will be developed for the mineralization observed at the Brucejack property that follows this structural framework in hopes that it can be used for future exploration of the area.

Acknowledgments

Funding for this project was provided by a Natural Sciences and Engineering Research Council of Canada (NSERC) Discovery Grant awarded to S. Johnston. Pretium Resources Inc. is thanked for providing accommodations and logistical support during the 2018 and 2019 field seasons while field and underground work was being conducted for this study. The authors also thank D. McLeish, M. McManus and J. Ashburner for reviewing and improving the manuscript. The lead author thanks Geoscience BC for providing financial support through a Geoscience BC scholarship.

References

- Board, W.S., McLeish, D.F., Grieg, C.J., Bath, O.E., Ashburner, J.E., Murphy, T. and Friedman, R.M. (in press): The Brucejack Au-Ag deposit, northwest British Columbia, Canada: multistage porphyry to epithermal alteration, mineralization, and deposit formation in an island-arc setting; Society of Economic Geologists, Inc., SEG Special Publications, no. 23, p. 289–311.
- Britton, J.M. and Alldrick, D.J. (1987): Sulphurets map area; *in* Geological Fieldwork 1987, BC Ministry of Energy, Mines and Low Carbon Innovation, BC Geological Survey, Paper 1988-1, p. 199–209, URL <http://cmscontent.nrs.gov.bc.ca/geoscience/PublicationCatalogue/Paper/BCGS_P1988-01-18_Britton.pdf> [November 2020].
- Brown, D.A. and Greig, C.J. (1990): Geology of the Stikine River–Yehiniko Lake area, northwestern British Columbia (104G/11W and 12E); *in* Geological Fieldwork 1989, BC Ministry of Energy, Mines and Low Carbon Innovation, BC Geological Survey, Paper 1990-1, p. 141–151.
- Cawood, P.A., Kröner, A., Collins, W.J., Kusky, T.M., Mooney, W.D. and Windley, B.F. (2009): Accretionary orogens through Earth history; Geological Society of London, Special Publications, v. 318, p. 1–36, URL <<https://doi.org/10.1144/SP318.1>>.
- Collins, W.J. (2002): Hot orogens, tectonic switching, and creation of continental crust; *Geology*, v. 30, no. 6, p. 535–538, URL <<https://doi.org/10.1130/0091-7613-31.1.e9>>.
- Corbett, G.J. (2012): Structural controls to, and exploration for, epithermal Au-Ag deposits; Australian Institute of Geoscientists Bulletin, v. 56, p. 43–47, URL <<https://corbettgeology.com/wp-content/uploads/2016/07/Structure-of-epithermal-Au-2012.pdf>> [November 2020].
- Davies, A.G.S., Lewis, P.D. and Macdonald, A.J. (1994): Stratigraphic and structural setting of the mineral deposits in the Brucejack Lake area, northwestern British Columbia; *in* Current Research 1994-A, Geological Survey of Canada, p. 37–43.
- Evenchick, C.A. (1991): Geometry, evolution, and tectonic framework of the Skeena Fold Belt, north-central British Columbia; *Tectonics*, v. 10, p. 527–546, URL <<https://doi.org/10.1029/90TC02680>>.
- Evenchick, C.A. (2001): Northeast-trending folds in the western Skeena fold belt, northern Canadian Cordillera: a record of Early Cretaceous sinistral plate convergence; *Journal of Structural Geology*, v. 23, no. 6–7, p. 1123–1140, URL <[https://doi.org/10.1016/S0191-8141\(00\)00178-4](https://doi.org/10.1016/S0191-8141(00)00178-4)>.
- Febbo, G.E., Kennedy, L.A., Nelson, J.L., Savell, M.J., Campbell, M.E., Creaser, R.A., Friedman, R.M., van Straaten, B.I. and Stein, H.J. (2019): The evolution and structural modification of the supergiant Mitchell Au-Cu porphyry, northwestern British Columbia; *Economic Geology*, v. 114, no. 2, p. 303–324, URL <<https://doi.org/10.5382/econgeo.2019.4632>>.
- Gagnon, J.-F., Barresi, T., Waldron, J.W., Nelson, J., Poulton, T., Cordey, F. and Colpron, M. (2012): Stratigraphy of the upper Hazelton Group and the Jurassic evolution of the Stikine terrane, British Columbia; *Canadian Journal of Earth Sciences*, v. 49, no. 9, p. 1027–1052, URL <<https://doi.org/10.1139/e2012-042>>.
- Harrichhausen, N.J. (2015): Role of colloidal transport in the formation of high-grade veins at Brucejack, British Columbia; M.Sc. thesis, McGill University, Montreal.
- Hodgson C.J. (1989): The structure of shear-related, vein-type gold deposits: a review; *Ore Geology Reviews*, v. 4, no. 3, p. 231–273, URL <<https://www.sciencedirect.com/science/article/abs/pii/016913688990019X>> [November 2020].
- Jones, I. (2013): Technical report on the geology of, and results from, the Brucejack Property; prepared for Pretium Resources Inc., Report NI 43-101, Snowden Mining Industry Consultants, URL <https://s23.q4cdn.com/277467366/files/doc_downloads/technical_reports/Brucejack-Feasibility-Study-FINAL-June-26-2013.pdf> [November 2020].
- Kirkham, R.V. and Margolis, J. (1995) Overview of the Sulphurets area, northwestern British Columbia; *in* Porphyry Deposits of the Northwestern Cordillera of North America, T.G. Schroeter (ed.), Canadian Institute of Mining and Metallurgy and Petroleum, Special Volume 46, p. 473–483.
- Lewis, P.D. (2013): Iskut River area geology, northwest British Columbia (104B/08, 09, 10 & part of 104B/01, 07, 11); Geoscience BC, Report 2013-05, maps at 1:50 000 scale, URL <<http://www.geosciencebc.com/projects/2009-003/>> [November 2020].
- Macdonald, A.J. (1993): Lithostratigraphy and geochronometry, Brucejack Lake, northwestern British Columbia (104B/8E); *in* Geological Fieldwork 1992, BC Ministry of Energy, Mines and Low Carbon Innovation, BC Geological Survey, Paper 1993-1, p. 315–324, URL <http://cmscontent.nrs.gov.bc.ca/geoscience/PublicationCatalogue/Paper/BCGS_P1993-01.pdf> [November 2020].

- Marsden, H. and Thorkelson, D.J. (1992): Geology of the Hazelton volcanic belt in British Columbia: implications for the Early to the Middle Jurassic evolution of Stikinia; *Tectonics*, v. 11, p. 1266–1287, URL <<https://doi.org/10.1029/92TC00276>>.
- Monger, J.W.H., Souther J.G. and Gabrielse, H. (1972): Evolution of the Canadian Cordillera: a plate-tectonic model; *American Journal of Science*, v. 272, p. 577–602, URL <<https://doi.org/10.2475/ajs.272.7.577>>.
- Nelson, J.L. and Colpron, M. (2007): Tectonics and metallogeny of the British Columbia, Yukon and Alaskan Cordillera, 1.8 Ga to present; in *Mineral Deposits of Canada: A Synthesis of Major Deposit Types, District Metallogeny, the Evolution of Geological Provinces and Exploration Methods*, W.D. Goodfellow (ed.), Geological Association of Canada, Mineral Deposits Division, Special Publication 5, p. 755–792, URL <<http://cmscontent.nrs.gov.bc.ca/geoscience/PublicationCatalogue/External/EXT060.pdf>> [November 2020].
- Nelson, J.L. and Kyba, J. (2014) Structural and stratigraphic control of porphyry and related mineralization in the Treaty Glacier–KSM–Brucejack–Stewart trend of western Stikinia; in *Geological Fieldwork 2013*, BC Ministry of Energy, Mines and Low Carbon Innovation, BC Geological Survey, Paper 2014-1, p. 111–140, URL <http://cmscontent.nrs.gov.bc.ca/geoscience/PublicationCatalogue/Paper/BCGS_P2014-01-07_Nelson.pdf> [November 2020].
- Nelson, J.L., Colpron, M. and Israel, S. (2013): The Cordillera of British Columbia, Yukon, and Alaska: tectonics and metallogeny; Society of Economic Geologists, Special Publication 17, p. 53–110, URL <<https://doi.org/10.5382/SP.17.03>>.
- Nelson, J.L., Waldron, J., van Straaten, B., Zagorevski, A. and Rees, C. (2018): Revised stratigraphy of the Hazelton Group in the Iskut River region, northwestern British Columbia; in *Geological Fieldwork 2017*, BC Ministry of Energy, Mines and Low Carbon Innovation, BC Geological Survey, Paper 2018-1, p. 15–38.
- Premium Resources Inc. (2014): Feasibility study and technical report update on the Brucejack project, Stewart, BC; Premium Resources Inc., URL <https://s23.q4cdn.com/277467366/files/doc_downloads/technical_reports/FeasibilityStudy-TechReportJune19-2014.pdf> [November 2020].
- Ramsay, J.G. and Huber, M. (1987): *The Techniques of Modern Structural Geology, Volume 2: Folds and Fractures*; Academic Press, Cambridge, Massachusetts, 391 p.
- Roach, S. and Macdonald, A.J. (1992): Silver-gold vein mineralization, West zone, Brucejack Lake, northwestern British Columbia (104B/8E); in *Geological Fieldwork 1991*, BC Ministry of Energy, Mines and Low Carbon Innovation, BC Geological Survey, Paper 1992-1, p. 503–512, URL <http://cmscontent.nrs.gov.bc.ca/geoscience/PublicationCatalogue/Paper/BCGS_P1992-01.pdf> [November 2020].
- Sillitoe, R.H. and Hedenquist, J.W. (2003): Linkages between volcanotectonic settings, ore-fluid compositions, and epithermal precious metal deposits in volcanic, geothermal, and ore-forming fluids: rulers and witnesses of processes within the Earth; Chapter 18 in *Volcanic, Geothermal, and Ore-Forming Fluids: Rulers and Witnesses of Processes Within the Earth*, Society of Economic Geologists, Special Publication 10, p. 315–345, URL <<https://doi.org/10.5382/SP.10.16>>.
- Thomson, R.C., Smith, P.L. and Tipper, H.W. (1986): Lower to Middle Jurassic (Pliensbachian to Bajocian) stratigraphy of the northern Spatsizi area, north-central British Columbia; *Canadian Journal of Earth Sciences*, v. 23, no. 12, p. 1963–1973.
- Tombe, S.P., Richards, J.P., Greig, C.J., Board, W.S., Creaser, R.A., Muehlenbachs, K.A., Larson, P.B., DuFrane, S.A. and Spell, T. (2018): Origin of the high-grade Early Jurassic Brucejack epithermal Au-Ag deposits, Sulphurets mining camp, northwestern British Columbia; *Ore Geology Reviews*, v. 95, p. 480–517, URL <<https://doi.org/10.1016/j.oregeorev.2018.03.003>>.
- White, N.C. and Hedenquist, J.W. (1995): Epithermal gold deposits: styles, characteristics and exploration; *SEG Newsletter*, no. 23, p. 1, 9–13, URL <https://www.researchgate.net/publication/268274871_Epithermal_gold_deposits_Styles_characteristics_and_exploration> [November 2020].

British Columbia Gold Composition Atlas Update 2020: Developing a New Tool for the Exploration Community

R.J. Chapman, School of Earth and Environment, University of Leeds, Leeds, United Kingdom,
r.j.chapman@leeds.ac.uk

R.J. Murphy, School of Earth and Environment, University of Leeds, Leeds, United Kingdom

J.K. Mortensen, MDN Geosciences Ltd, Salt Spring Island, British Columbia

B. Bluemel, Goldspot Discoveries, Toronto, Ontario

D.A. Banks, School of Earth and Environment, University of Leeds, Leeds, United Kingdom

Chapman, R.J., Murphy, R.J., Mortensen, J.K., Bluemel, B. and Banks, D.A. (2021): British Columbia gold composition atlas update 2020: developing a new tool for the exploration community; *in* Geoscience BC Summary of Activities 2020: Minerals and Mining, Geoscience BC, Report 2021-01, p. 41–46.

Introduction

This ongoing project seeks to develop a new tool for use by exploration companies in projects of all sizes, which focus on either orogenic gold, epithermal gold or Cu-Au porphyry deposits, across British Columbia (BC). The background to the project was provided in full in Murphy et al. (2020) and is summarized below.

The use of indicator minerals as a vector to *in situ* mineralization is well established (McClennaghan and Layton-Matthews, 2017). However, detrital gold particles have not found widespread use in this regard thus far because: 1) they are formed in a variety of ore deposits; and 2) they are chemically indestructible and physically durable, thereby permitting recycling into successive surficial facies. Thus, discovery of particulate gold in heavy concentrates collected during routine stream-sediment sampling is not in itself evidence for a specific source-style of mineralization. However, there is significant alloy and mineralogical variations within gold particles. This project utilizes such variations to identify key markers within gold particles, by which their deposit-specific origins may be deduced. The approach is based both on alloy composition according to Au and Ag+Cu, Hg and Pd (where detectable) by electron probe microanalysis (EPMA), and characterization of the suite of ore and gangue minerals present as inclusions within the gold particles using the energy dispersive spectrometry (EDS) facility of the scanning electron microscope (SEM). In addition, trace-element composition of gold particles may be established using laser-ablation inductively coupled plasma–mass spectrometry (LA-ICP-MS; Banks et al., 2018). Combination of these datasets on a particle-by-

particle basis permits ‘microchemical characterization’ of populations of gold particles from a single locality and reconstruction of the nature of the source mineralization, more specifically, whether the gold originates from an orogenic system (Chapman and Mortensen, 2016) or from a Cu-Au porphyry deposit (Chapman et al., 2017). The first stage of the current project has established a database containing microchemical EPMA/EDS characterization of gold particles, with subsets analyzed by LA-ICP-MS. The second stage of the project will involve identifying gold signatures from specific styles of mineralization using exploratory data analysis. The output will be a publicly available template in the form of a data-driven workflow accessible to other researchers, who may then interpret the results of their own sampling projects.

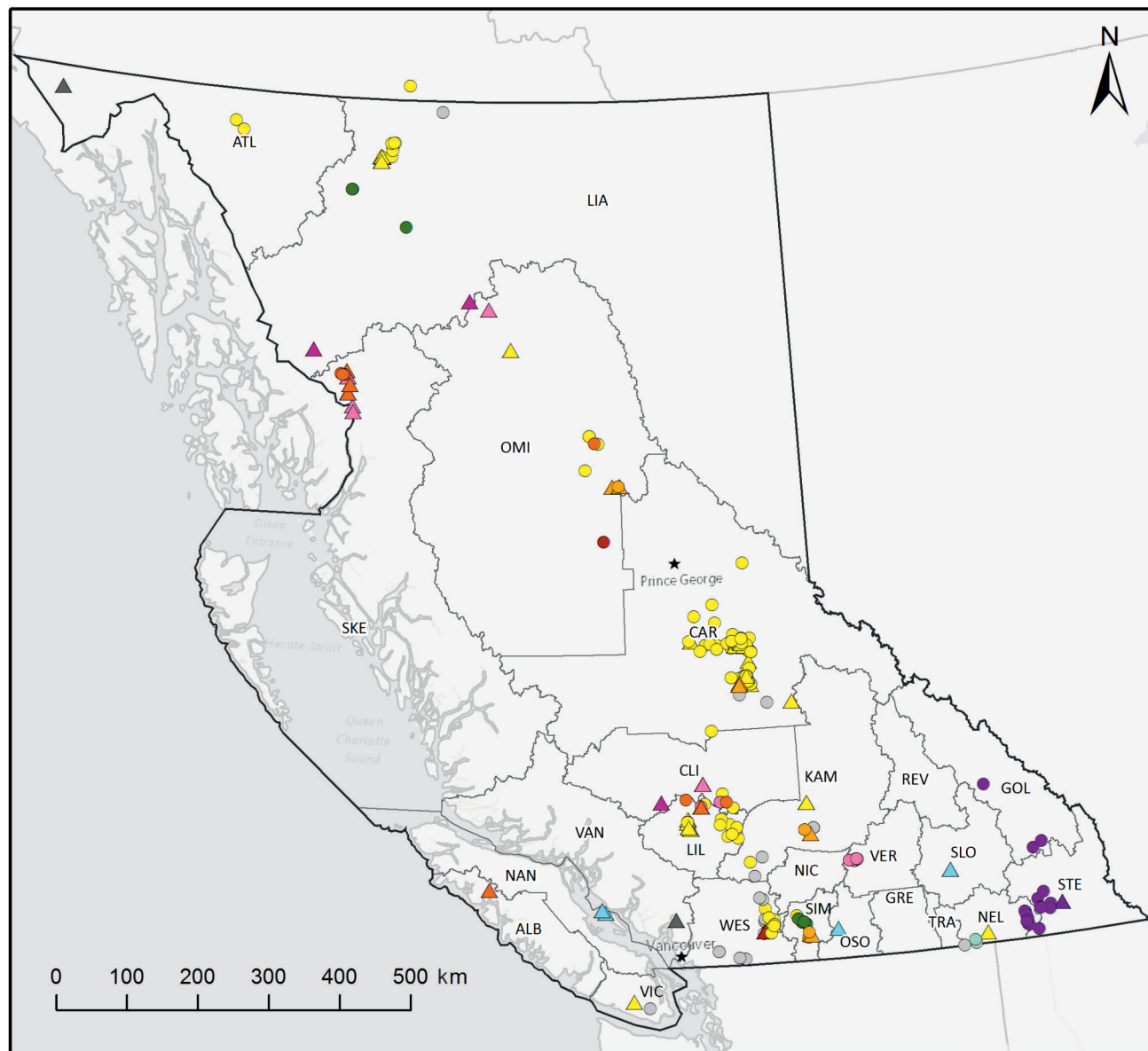
Methodology

Data Acquisition

The geographic distribution of the study samples is presented in Figure 1. Breakdowns of the sample suite according to historical BC mineral districts and deposit type are presented in Figure 2. The microchemical characterizations of 13 999 gold particles from 327 localities populate the database for the project. A description of the sample preparation and microchemical characterization procedures was provided in Murphy et al. (2020).

In addition to the routine gold characterization via EPMA and SEM, 537 gold particles have been analyzed by LA-ICP-MS. The study can draw on some previous data flowing from a Geoscience BC funded project on LA-ICP-MS characterization of gold in BC (Banks et al., 2018) but additional analyses have also been undertaken. These datasets await processing and further interrogation.

This publication is also available, free of charge, as colour digital files in Adobe Acrobat® PDF format from the Geoscience BC website: <http://geosciencebc.com/updates/summary-of-activities/>.



Legend

Sample type		Mineralization style		Mineral districts	
△	Hypogene	Yellow	Orogenic	ALB	Alberni
○	Detrital	Grey	VMS	ATL	Atlin
		Cyan	Skarn	LIA	Liard
		Grey	Unknown	LIL	Lillooet
				NAN	Nanaimo
				NEL	Nelson
				NIC	Nicola
				SIM	Similkameen
				GRE	Greenwood
				OSO	Osoyoos
				WES	New Westminster
				TRA	Trail Creek
				REV	Revelstoke
				SKE	Skookum
				SLO	Slocan
				VER	Vernon
				VAN	Vancouver
				VIC	Victoria

Figure 1. Geographic distribution of study samples according to historical British Columbia mineral districts. Base map created using ArcGIS® software by Esri. ArcGIS® and ArcMap™ are the intellectual property of Esri and are used herein under licence. Copyright© Esri. All rights reserved. Abbreviation: VMS, volcanogenic massive sulphide.

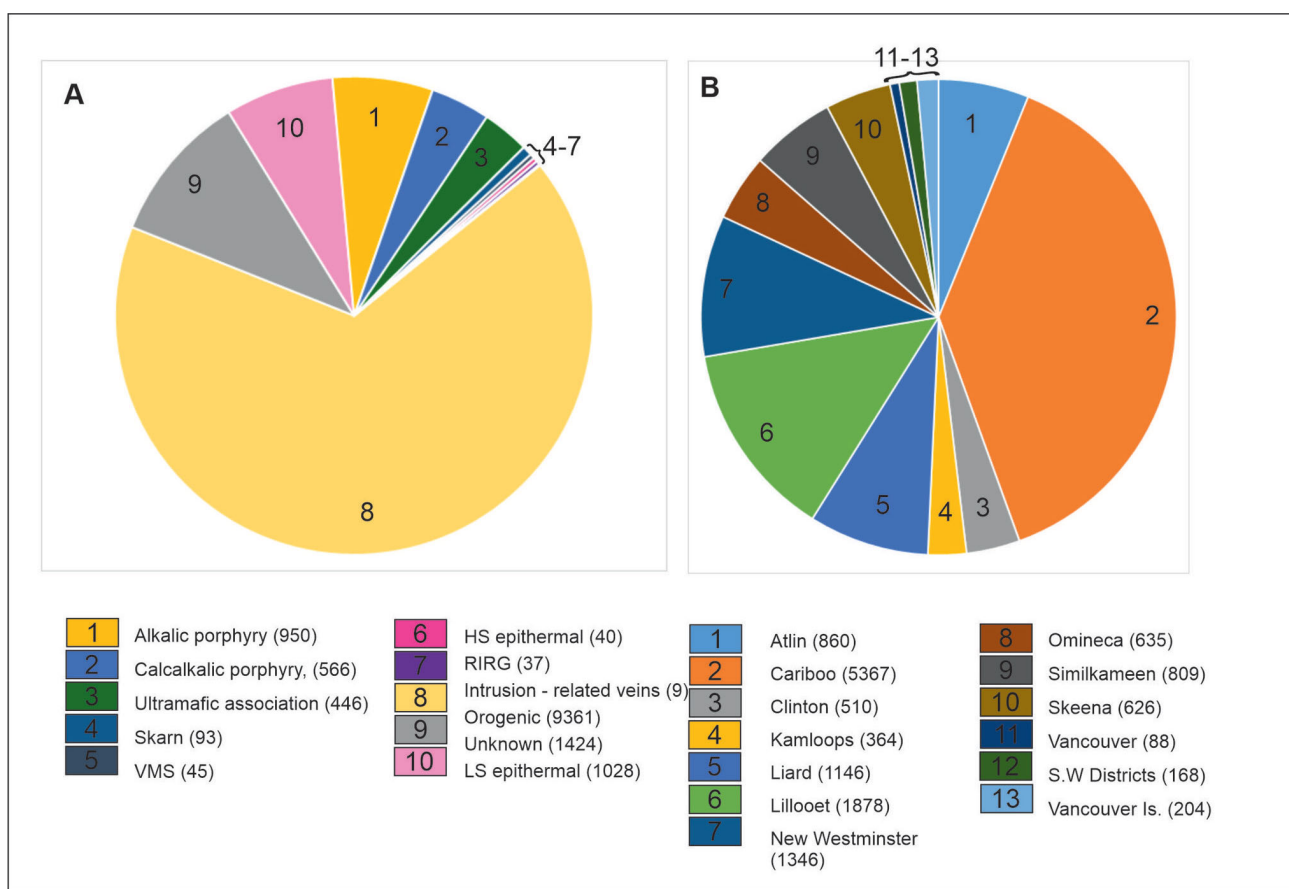


Figure 2. Breakdown of study samples characterized by electron probe microanalysis and scanning electron microscopy, according to **a**) source style and **b**) location in British Columbia mineral districts. Abbreviations: HS, high sulphidation; Is., Island; LS, low sulphidation; RIRG, reduced intrusion-related gold; S.W., southwest; VMS, volcanogenic massive sulphide.

Database Organization

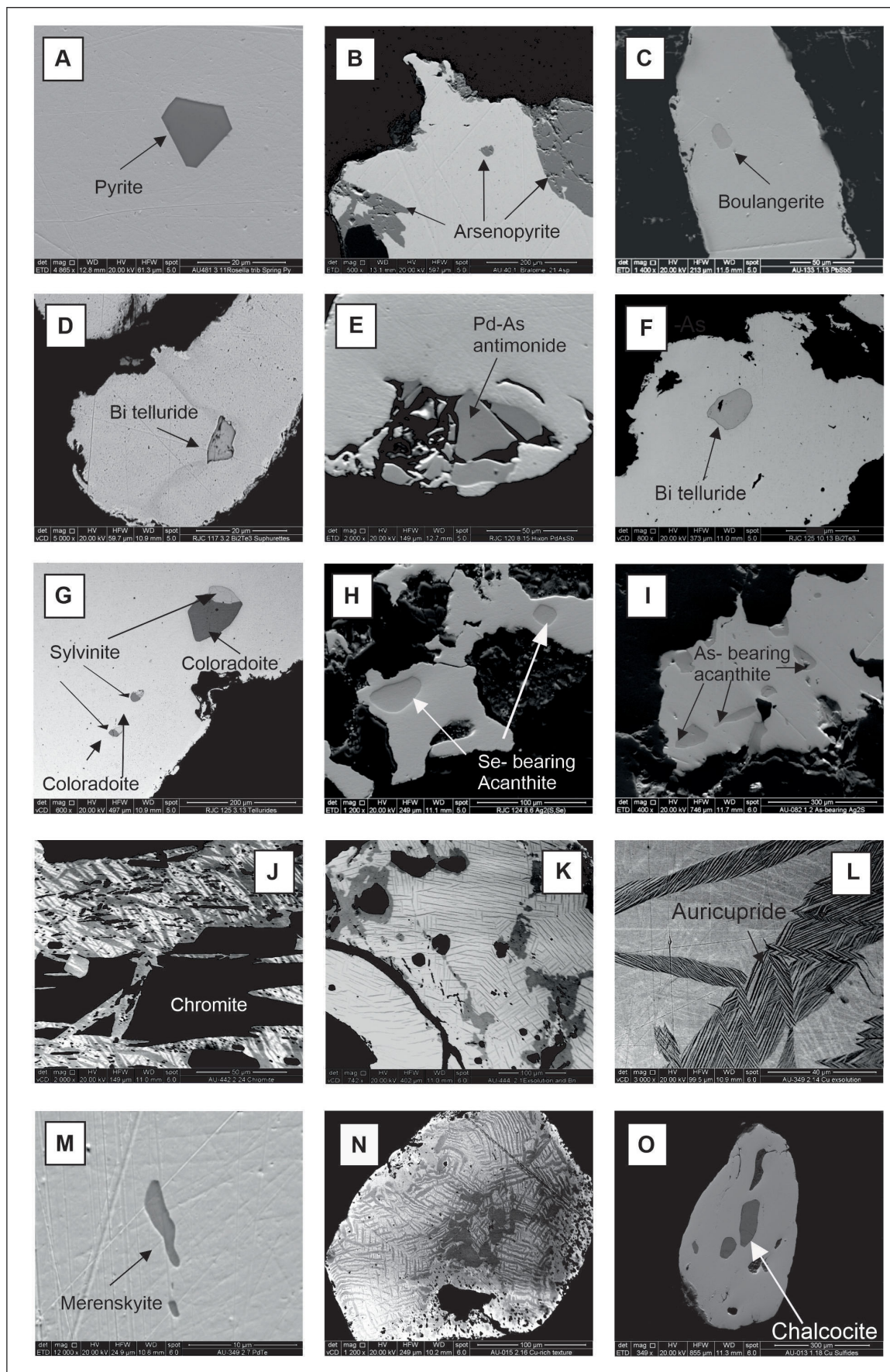
All data have been collated according to a standardized spreadsheet design, which will permit interrogation using various multivariate and geochemical data analysis software packages such as Reflex® ioGASTM, Orange, or the KNIME analytics platform.

Preliminary Results

Previous studies in the Canadian Cordillera have established typical microchemical signatures of gold formed in different styles of mineralization. Gold from orogenic settings is usually a binary Au-Ag alloy, with Cu, Hg and Pd below detection level by EPMA and the inclusion suite is best characterized by the nonmetal components of minerals (i.e., sulphides), including sulphides+sulpharsenides±sulphosalts, sulphides+tellurides or, more rarely, sulphides+sulpharsenides+tellurides (Chapman et al., 2010a, b, 2011; Chapman and Mortensen, 2016). In the Yukon, gold from calcalkalic Cu-Au porphyry deposits has been characterized according to a Pb-Bi-Te-S signature in the inclusion suite (Chapman et al., 2018), whereas alkalic Cu-Au porphyries in BC exhibit an inclusion signature with a small but consistent Pd-Hg component, also evident in alloy

compositions (Chapman et al., 2017). In addition, Knight and Leitch (2001) reported high (>3 wt. %) Cu contents in the gold alloy associated with ultramafic-hosted mineralization in both the Coquihalla River valley and Wheaton Creek (Skeena mineral district).

To date, consideration of new data has focused mainly on inclusion suites, as these can provide the most distinctive signatures, and some noteworthy results have been achieved. Suites of minerals typical for gold from orogenic systems have been identified in areas such as Cassiar and Bralorne, and the Quesnel–Cottonwood area (Figure 3a–c). Similar assemblages have been recorded more widely in the catchment area of the Fraser and Coquihalla rivers. The Bi-Pb-Te-S signature of gold from Yukon calcalkalic porphyry systems reported in Chapman et al. (2018) has also been observed in gold from the environs of the KSM deposit (Figure 3d, e) and the Pd-Hg-bearing inclusion mineralogy associated with alkalic Cu-Au porphyries has been confirmed at Friday Creek, near Copper Mountain (Figure 3f). The Bi-Pb-Hg-Te inclusion signature in gold from Stirrup Creek (Figure 3g, h) has yet to be fully interpreted. Low-sulphidation epithermal gold from Black Dome exhibits a dominant Ag-S-Se inclusion suite, and a Ag-S-As



signature is observed in gold from the Brucejack deposit (Figure 3i). In Omineca, gold from the Germansen Landing area showed a typical orogenic inclusion-signature suite but that from Valleau Creek showed a more complex elemental array, including Bi, Te and minor Mo. Knight and Leitch (2001) observed that gold from some sample sites in the Coquihalla River drainage basin and Wheaton Creek contained >3 wt. % Cu and exhibited strong exsolution of auricupride (Au_3Cu) from a Au-Ag-Cu matrix, which suggests the potential of a generic textural signature for gold with an ultrabasic association (Figure 3j–m). This texture has also been identified from sample populations from the Bridge River area, where a genetic link between placer and source has not yet been established. The distinctive exsolution signature is commonly associated with inclusions of chalcocite (Figure 3n). In addition, the presence of Pd-bearing mineral inclusions (Figure 3o) raises the possibility of a further discriminant.

Outputs to Date

The results of the project were presented at a poster session at the 2020 Mineral Exploration Roundup in Vancouver, BC. Some of the inclusion data have been integrated with previous datasets in a scientific journal contribution (R.J. Chapman, J.K. Mortensen, M.M. Allan, R.D. Walshaw, J. Bond and K. MacWilliam, work in progress), which links inclusion assemblages in gold from throughout the Canadian Cordillera with wider metallogenic interpretations.

Conclusions and Future Work

In the second phase of this project, the implications of the datasets in terms of regional and local metallogenic significance will be evaluated. This will involve depiction of both alloy and inclusion assemblages of EPMA/SEM data, and integration with the datasets generated by LA-ICP-MS. These qualitative characterizations will form the training datasets for use in an exploratory data-analysis approach to compositional definition. The aim of this project element is to remove the future need for an experienced researcher to interpret the significance of gold compositions. Therefore,

 **Figure 3.** Examples of features observed in the gold-particle sample suite (detrital particles observed in backscattered electron scanning electron microscope mode imaging unless otherwise stated), showing inclusion mineralogy typical of orogenic systems (a–c), inclusions in gold from magmatic hydrothermal systems (d–i), exsolution of auricupride (Au_3Cu) from gold alloy matrix in placer particles linked to ultrabasic hosts (j–m) and inclusion species observed in gold from some of the same localities (n, o). Samples were collected at the following locations: **a**) Rosella Creek, Cassiar; **b**) Bralorne (hypogene sample); **c**) Tertiary Creek, near Quesnel; **d, e**) drainage basin in which the KSM property is located; **f**) Friday Creek, near Copper Mountain; **g**) Stirrup Creek, near the Fraser River; **h**) Valleau Creek, Omineca; **i**) the Brucejack property (hypogene sample); **j**) Coquihalla River; **k**) Yalakom River, a tributary of the Bridge River; **l, m**) Wheaton Creek, Stikine; **n**) Bridge River; **o**) Coquihalla River.

use of the classification workflow will replicate dataset interrogation as if performed by such subject-matter experts. A key deliverable of this project will be the detailed description and workflow template, based on expert-derived linear discriminant analysis, to create a classification algorithm (e.g., naïve Bayes, decision trees, or random forest), which can then be used by any nonspecialist to classify new gold particle data. In this way, the project will generate a new tool immediately available to the exploration community in BC, but one with the potential to expand efficiently to encompass both the Canadian and Alaskan cordilleras.

Acknowledgments

The authors are grateful to T. Torvela of the University of Leeds for her review of this manuscript.

References

- Banks, D.A., Chapman, R.J. and Spence-Jones, C. (2018): Detrital gold as a deposit-specific indicator mineral by LA-IPS-MS analysis; Geoscience BC, Report 2018-21, 49 p., URL <http://cdn.geosciencebc.com/project_data/GBCReport-2018-21.pdf> [September 2020].
- Chapman, R.J. and Mortensen, J.K. (2016): Characterization of gold mineralization in the northern Cariboo Gold District, British Columbia, Canada, through integration of compositional studies of lode and detrital gold with historical placer production: a template for evaluation of orogenic gold districts; *Economic Geology*, v. 111, no. 6, p. 1321–1345, URL <<https://pubs.geoscienceworld.org/segweb/economicgeology/article-abstract/111/6/1321/152454>> [September 2020].
- Chapman, R.J., Allan, M.M., Mortensen, J.K., Wrighton, T.M. and Grimshaw, M.R. (2018): A new indicator mineral methodology based on a generic Bi-Pb-Te-S mineral inclusion signature in detrital gold from porphyry and low/intermediate sulfidation epithermal environments in Yukon Territory, Canada; *Mineralium Deposita*, v. 53, no. 6, p. 815–834, URL <<https://link.springer.com/article/10.1007/s00126-017-0782-0>> [September 2020].
- Chapman, R., Mileham, T., Allan, M. and Mortensen, J. (2017): A distinctive Pd-Hg signature in detrital gold derived from alkalic Cu-Au porphyry systems; *Ore Geology Reviews*, v. 83, p. 84–102, URL <<https://www.sciencedirect.com/science/article/pii/S0169136816305005>> [September 2020].
- Chapman, R.J., Mortensen, J.K., Crawford, E. and LeBarge, W. (2010a): Microchemical studies of placer and lode gold in the Klondike District, Yukon, Canada: 1. Evidence for a small, gold-rich, orogenic hydrothermal system in the Bonanza and Eldorado Creek area; *Economic Geology*, v. 105, p. 1369–1392.
- Chapman, R.J., Mortensen, J.K., Crawford, E. and LeBarge, W. (2010b): Microchemical studies of placer and lode gold in the Klondike District, Yukon, Canada: 2. Constraints on the nature and location of regional lode sources; *Economic Geology*, v. 105, p. 1393–1410.
- Chapman, R., Mortensen, J. and LeBarge, W. (2011): Styles of lode gold mineralization contributing to the placers of the Indian River and Black Hills Creek, Yukon Territory, Canada as deduced from microchemical characterization of placer gold grains; *Mineralium Deposita*, v. 46, p. 881–903.

- Knight, J.B. and Leitch, C.H. (2001): Phase relations in the system Au–Cu–Ag at low temperatures, based on natural assemblages; Canadian Mineralogist, v. 39, p. 889–905.
- McClennaghan, M.B. and Layton-Matthews, D. (2017): Application of indicator mineral methods to bedrock and sediments; Geological Survey of Canada, Open File 8345, 86 p., URL <<https://doi.org/10.4095/306305>>.
- Murphy, R.J., Chapman, R.J., Mortensen, J.K., Bluemel, B. and Banks, D.A. (2020): Atlas of gold composition for British Columbia: developing a new tool for the exploration community; in Geoscience BC Summary of Activities 2019: Minerals, Geoscience BC, Report 2020-01, p. 77–82, URL <http://www.geosciencebc.com/i/pdf/SummaryofActivities2019/Minerals/Project%202018-013_Minerals_SOA2019.pdf> [November 2020].

Cryptic Magmatic Skarn of the Merry Widow Deposit, Vancouver Island (NTS 092L)

R. Morris¹, School of Earth and Ocean Sciences, University of Victoria, Victoria, British Columbia,
ramorri@uvic.ca

D. Canil, School of Earth and Ocean Sciences, University of Victoria, Victoria, British Columbia

Morris, R. and Canil, D. (2021): Cryptic magmatic skarn of the Merry Widow deposit, Vancouver Island (NTS 092L); *in* Geoscience BC Summary of Activities 2020: Minerals, Geoscience BC, Report 2021-01, p. 47–54.

Introduction

Skarn deposits are typically defined as calcsilicate assemblages that occur within or adjacent to carbonate-bearing rocks (limestone, dolostone) as a result of metamorphic and metasomatic processes, and are a major source of Fe, Au, Cu, Pb, Zn, W, Mo and Sn (Meinert et al., 2005; Ray, 2013). Skarn is generally associated with intrusions into carbonate wallrock, and the ore deposit forms from a combination of an initial thermal-metamorphic event followed by secondary metasomatic alteration from fluids of magmatic, metamorphic or meteoric origin (Meinert et al., 2005). The resulting skarn is an alteration envelope that can be mapped around the intrusion (Ettlinger and Ray, 1987). Skarn can be further classified as 1) exoskarn, which consists of the decarbonized and silicified carbonate wallrock, or 2) endoskarn, which consists of calcified and desilicified igneous rocks within the intrusion (Sangster, 1964; Meinert et al., 2005).

Less commonly discussed and not evident in outcrop is ‘magmatic skarn’, which occurs as a result of assimilation of Ca-rich wallrock (i.e., carbonate, calcsilicate) within the magma (Barnes et al., 2009). Earlier skarn studies on Vancouver Island, British Columbia (BC) by Sangster (1964) hinted at a potential presence of magmatic skarn, where he noted that contact metamorphism was “most striking” in metasomatized country rocks, but that “endomorphism within the pluton” was less obvious. This endomorphism was noted after observing a common occurrence of mafic margins within skarn-associated intrusions (Sangster, 1964). Such mafic margins may be a result of the initial mafic parental melt cooling along the magma chamber margin, or from fractional crystallization of mafic phases as a result of wallrock assimilation, or from a combination of these processes. If assimilation-driven fractional crystallization occurs, this would be evident by an abundance of mafic cumulates that are proximal to the wallrock contact.

Studies by Barnes et al. (2009) have indicated cumulates of Ca-rich fractionates (clinopyroxene, titanite, plagioclase) within magmatic skarn. These distinct cumulates were termed ‘hortite’ from earlier mapping by Vogt (1916). Calcium-rich cumulates are interpreted to be a result of assimilation, where an increase in Ca within the magma from partially melted carbonate or calcsilicate wallrock induces the fractionation of calcic phases (i.e., clinopyroxene, plagioclase, titanite, apatite). If this process does occur, the latent heat produced by fractional crystallization would enhance wallrock assimilation (Taylor, 1980; De Paolo, 1981; Spera and Bohrson, 2001).

This study quantifies the extent of magmatic skarn within a well-exposed intrusion, the Coast Copper stock, that is associated with the Merry Widow Fe-skarn deposit on Vancouver Island. This paper presents the preliminary field and geochemical work completed on the magmatic skarn thus far.

Merry Widow Deposit

The Merry Widow Fe-skarn deposit occurs at the contact of Jurassic Bonanza arc intrusions with Triassic Quatsino limestone (Figure 1) in Wrangellia on northern Vancouver Island (Sangster, 1964; Lund, 1966; Ray and Webster, 1991; Nixon et al., 2011). The orebody was mined from 1957 to 1967, primarily for magnetite (MINFILE 092L 044, 045 and 046; BC Geological Survey, 2020b). Skarn mineralization at Merry Widow consists of magnetite, pyrrhotite, pyrite, arsenopyrite, cobaltite, erythrite, sphalerite and gold in a gangue of garnet, epidote, actinolite, clinopyroxene, carbonate and quartz (Ray and Webster, 1991). This mineralization is recognizable in outcrop and drillcore. However, determining the precise extent of magmatic skarn within the intrusion requires a fastidious examination of geochemical relationships in order to differentiate contaminated from pristine magmatic rock.

A number of previous studies have been completed on the geology and mineral occurrences at the Merry Widow site (Figure 2; Sangster, 1964; Lund, 1966; Ray and Webster, 1991; Nixon et al., 2011). This study focused on the petrography of dikes, plutonic rocks and carbonate wallrock, and

¹The lead author is a 2020 Geoscience BC Scholarship recipient.

This publication is also available, free of charge, as colour digital files in Adobe Acrobat® PDF format from the Geoscience BC website: <http://geosciencebc.com/updates/summary-of-activities/>.

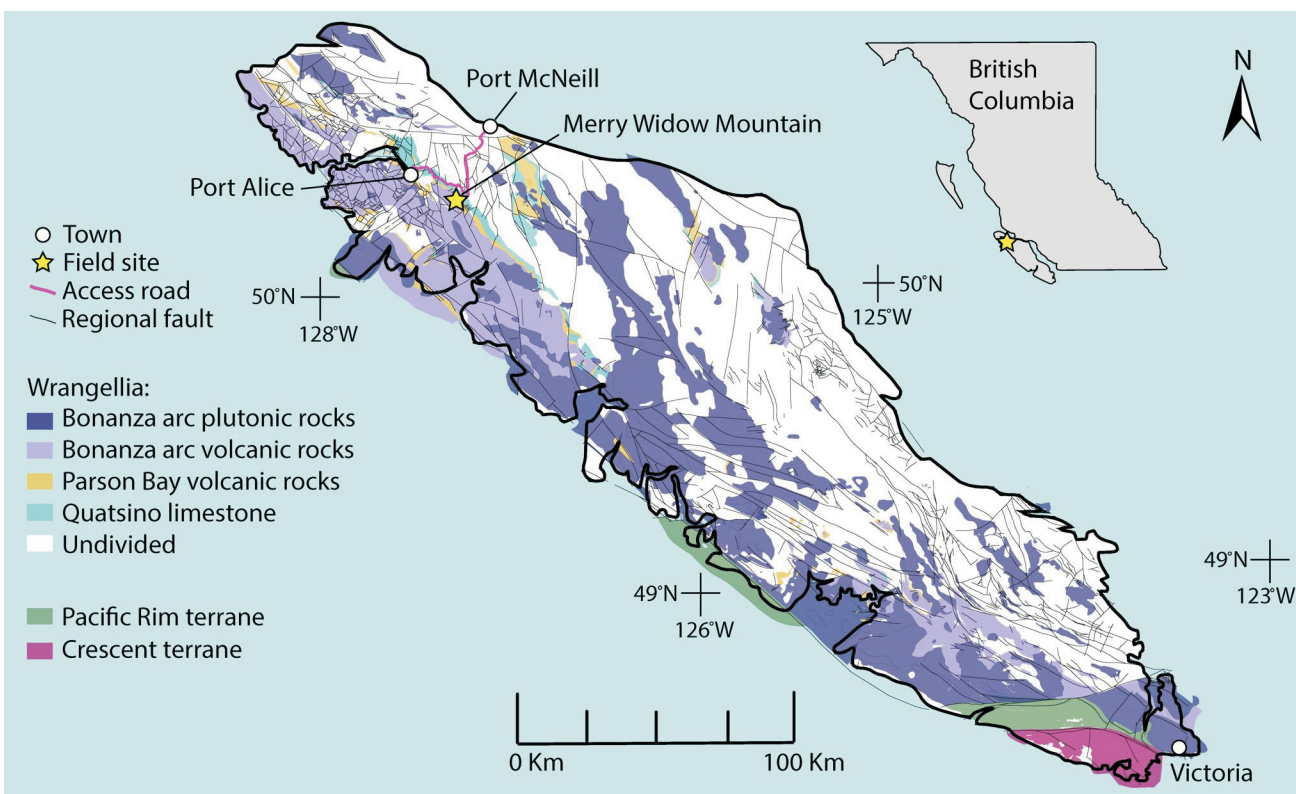


Figure 1. Regional geology of Vancouver Island from Morris and Canil (2020), showing Wrangellia and the Pacific Rim and Crescent terranes. Wrangellia is stripped of its pre- and post-Jurassic rocks, except for the Parson Bay volcanic rocks and Quatsino limestone (both Triassic), which immediately underlie the Jurassic Bonanza arc. Geological unit boundaries and faults are from the BC Geological Survey (BCGS) MapPlace dataset (BC Geological Survey, 2020a). The Merry Widow Mountain area is located within NTS 092L.

the contact relations at the site (Morris and Canil, 2020). Herein, the extent of magmatic skarn within the Coast Copper stock, the main plutonic body at the Merry Widow deposit, is quantified using samples collected during the 2019 field program that were analyzed for whole-rock geochemistry and oxygen isotopes. In addition, publicly available subsurface drillcore logs and whole-rock geochemistry data were compiled and incorporated with mapping from Morris and Canil (2020). The results reveal a far larger volume of magmatic skarn that is not evident in surface field geology.

Fieldwork

During the 2019 fieldwork, the eastern margin of the Coast Copper stock and an ~1 km transect from the pluton-wallrock contact into the interior of the pluton were mapped and sampled in detail (Figure 2; Morris and Canil, 2020). The margin of the Coast Copper stock is gabbro, with lesser amounts of monzonite. The pluton shows heterogeneities that include regions of pegmatite (plagioclase laths up to 5 cm long); spheroidal cumulates (plagioclase + clinopyroxene + magnetite + apatite + titanite) that are proximal (~200 m orthogonal) to the pluton margin; magma-mingling textures between the lesser monzonite and gabbro on a variety of scales; and thin (<0.5 m) monzonite

dikes (Morris and Canil, 2020). Some regions display a greenschist-facies hydrothermal overprint, with occurrences of albitized plagioclase and chlorite.

Historical Core-Log Compilation

Publicly available core logs from 2006 and 2007 drilling programs at Merry Widow were compiled to interpret subsurface relationships between the Coast Copper stock and Quatsino limestone (Nicholson, 2006; Wesley and Nelson, 2008a). Six core logs from these drilling programs show an intersection with the plutonic margin (Figure 2), which includes two core logs from the 2006 program (MW06-08, MW06-15) and four core logs from the 2007 program (MW07-78, MW07-79, MW07-80, MW07-90; Nicholson, 2006; Wesley and Nelson, 2008a). Mapped bedding and contact exposures at the surface (Figure 2), when combined with depths of intersection of the Coast Copper stock based on drillhole trend and plunge, show the pluton margin has an orientation of ~340°/59°NE if generalized to be a planar structure. Contact relationships of the pluton at depth are shown in Figure 3, where the selected cross-section transects a vertical drillhole (MW07-78) south of the main magnetite deposit.

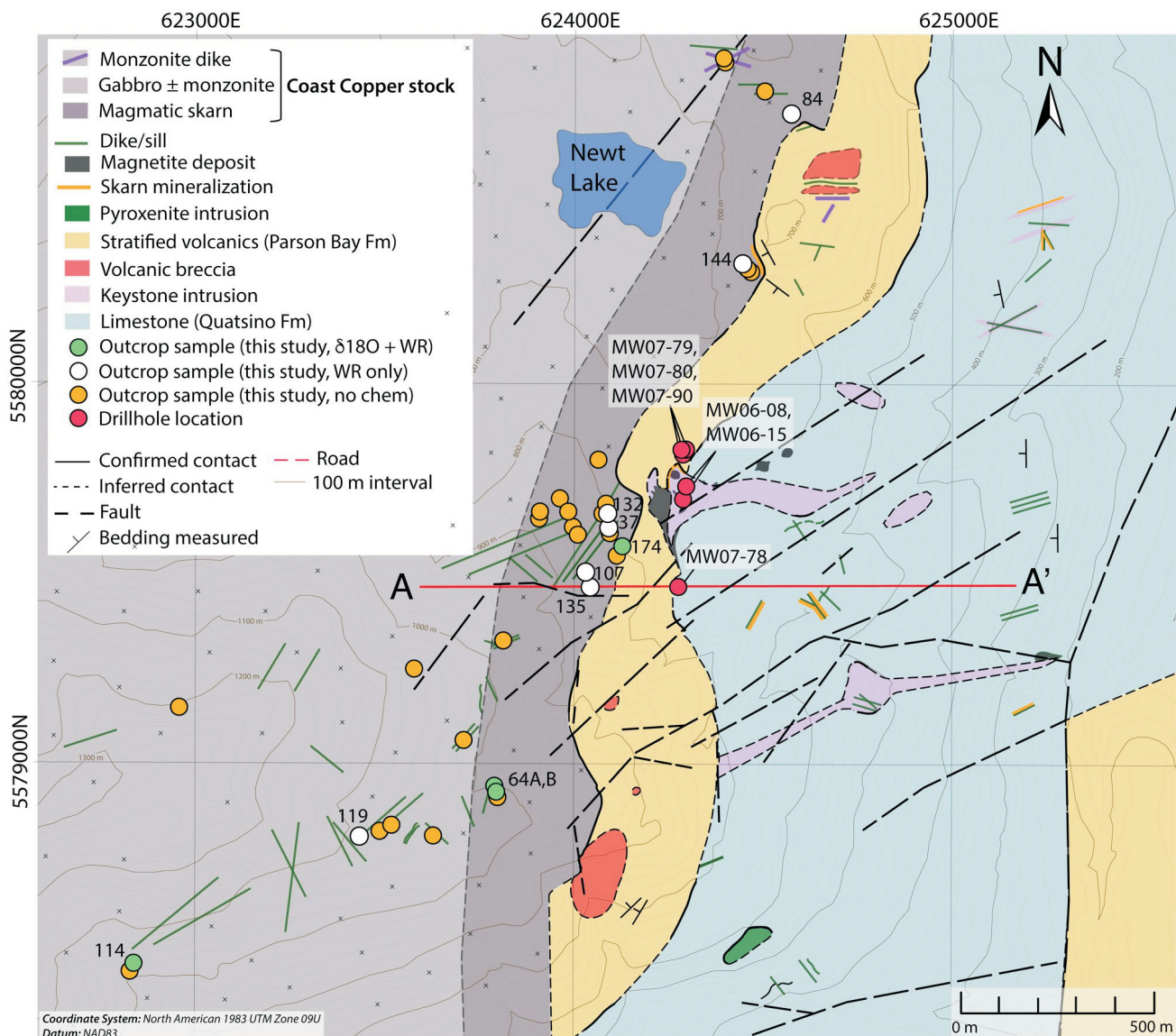


Figure 2. Detailed bedrock geology of the Merry Widow site, modified after Sangster (1964), Lund (1966), Ray and Webster (1991) and Nixon et al. (2011). Drillhole locations from Nicholson (2006) and Wesley and Nelson (2008a) are shown in red. Outcrop samples from this study are shown in white, green and orange. Gabbro collected near dikes was sampled >1 m away from dike margins and appeared fresh in outcrop and hand sample. Samples collected northeast of Newt Lake appear to have been subjected to faulting and hydrothermal alteration, and were not submitted for $\delta^{18}\text{O}$ analyses. Samples from this study were analyzed for whole-rock (WR) geochemistry (white symbol), with some samples also analyzed for $\delta^{18}\text{O}$ (green symbol). The cross-section from the A–A' transect is shown in Figure 3.

At surface, there is no exposure of the Coast Copper stock in direct contact with the Quatsino limestone (Figure 2). Core logs, however, indicate approximate true thicknesses of various units across the transition from wallrock to pluton, which includes: ~100 m of irregular exoskarn, ~10–60 m of volcanic breccia, ±3–10 m of recrystallized limestone, leading into at least ~20 m of magmatic skarn based on the authors' interpretation of core-log descriptions (Nicholson, 2006; Wesley and Nelson, 2008a). The extent of magmatic skarn from core logs is limited by sampled depths (i.e., up to a maximum of 25 m into the pluton was sampled) and is interpreted to extend beyond these sampled limits. Here, the magmatic skarn is defined based on its

abundance of spheroidal mafic cumulates, which occur irregularly along the pluton margin. These cumulates consist of clinopyroxene and plagioclase, are rich in magnetite (>10%), apatite (>3%) and titanite (>1%), and produce unique geochemistry, as described below.

Magmatic Skarn Geochemistry

Whole-Rock Major- and Trace-Element Geochemistry

In this study, whole-rock major- and trace-element geochemistry are used to identify changes in the pluton due to limestone assimilation, such as increased Ca and/or de-

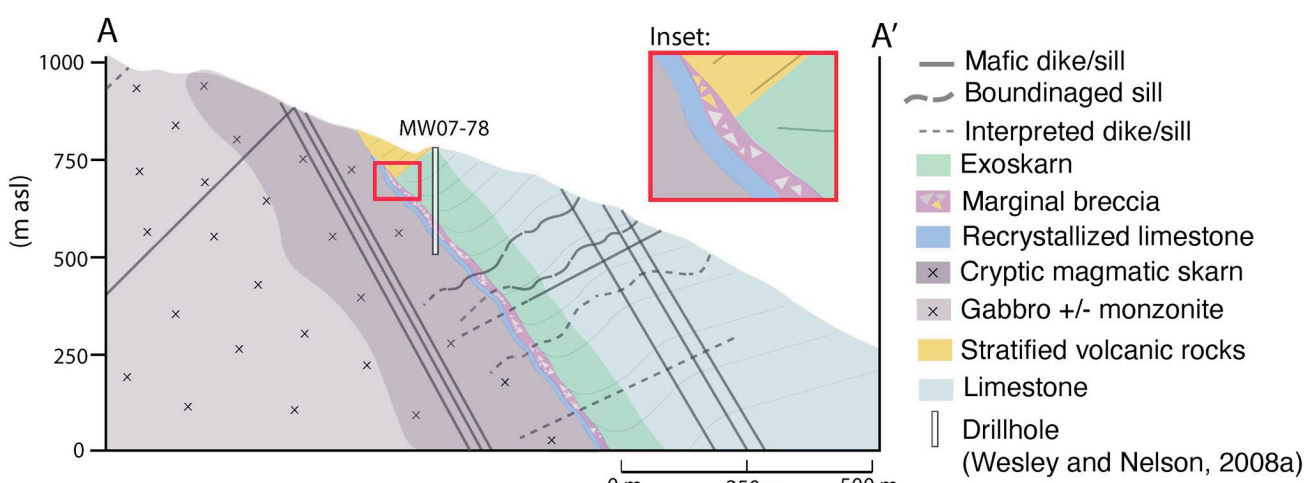


Figure 3. Cross-section A–A' (from Figure 2), representing the authors' interpretation of field relationships at depth, which are established from extrapolation of exposed bedding and contacts and from publicly available core-log data (Nicholson, 2006; Wesley and Nelson, 2008a). The extent of magmatic skarn is based on preliminary field and geochemical results.

creased Si concentrations. Three drillholes that intersected the Coast Copper stock (MW06-08, MW06-15 and MW07-79) have whole-rock major- and trace-element data determined by inductively coupled plasma–emission spectrometry (ICP-ES) that is publicly available (Nicholson, 2006; Wesley and Nelson, 2008b). Based on sample depths and the orientation of drillholes, the Coast Copper stock was intersected from its margin to the approximate orthogonal distances in each of the following drillholes: 1.2–7.5 m for MW06-08 (6 samples), 1.1–16.7 m for MW06-15 (15 samples) and 0.9–25.2 m for MW07-79 (10 samples). Core logs indicate that samples were collected at ~1 m intervals with the exception of drillhole MW07-79, in which three samples were collected <2 m from the margin and the remaining seven collected 19–25 m from the margin.

Whole-rock major-element geochemistry of the Coast Copper stock samples, collected during the 2019 field campaign ($n = 11$), were compiled and compared to drillcore sample results. Samples from the 2019 field campaign included 10 gabbro and 1 cumulate, which were both proximal and distal with respect to the pluton-wallrock margin (Figure 2). The orthogonal distances of outcrop samples collected from the pluton-wallrock margin were calculated for spatial comparison with chemistry of the drillcore samples, using a regionally generalized planar plutonic margin that strikes $\sim 340^\circ/59^\circ\text{NE}$, based on core logs (Nicholson, 2006; Wesley and Nelson, 2008a).

The magmatic skarn intersected in drillcore displays unique chemical trends of increasing P_2O_5 and TiO_2 with increasing distance from the pluton-wallrock contact. Typical mafic igneous values of P_2O_5 (<0.5 wt. %) and TiO_2 (<2 wt. %) are achieved between 200 and 500 m from the pluton-wallrock contact, as indicated in outcrop sample chemistry (Figure 4). Results also show an overall increase in FeO^* , MgO and CaO with increasing distance from the

pluton-wallrock contact. However, the boundary from contaminated (magmatic skarn) to pristine magmatic rock is less obvious with these elements, as high concentrations are sustained in the most distal samples. The chemical compositions observed in distal drillcore samples (~20 m inward from the margin) are either similar to, or trend toward, those of the cumulate sampled in outcrop approximately 200 m orthogonal from the pluton margin (Figure 4). Drillcore analytical reports provided no Si concentrations, so it is assumed that magmatic skarn is low in SiO_2 , similar to the cumulate (<45 wt. % SiO_2).

The irregularity of major-element abundances in drillcore and in sampled outcrops along the pluton margin is interpreted to be a result of simultaneous assimilation and fractional crystallization. This is obvious in drillcore samples from MW06-08 and MW06-15, which display similar trends and were well sampled, with continuous data from 1 to 20 m, as demonstrated by the increasing TiO_2 . However, samples from MW07-79 do not show this trend, likely due to no sample collection between 2 and 19 m from the margin. In addition, MW06-08 and MW06-15 were drilled at similar locations within the main pit, whereas MW07-79 was drilled north of the main pit (Figure 2).

Overall, major- and trace-element chemistry indicates substantial accumulation of magnetite (up to 30%), titanite and apatite within intervals of magmatic skarn at the margin of the Coast Copper stock, some of which are marked by increasing Co concentration (Figure 4), a metal also enriched in exoskarn at the Merry Widow deposit (Ray and Webster, 1991). No surface samples collected during the 2019 field campaign were analyzed for Co, so the extent of Co concentrations is currently limited to the publicly available geochemical data from drillcore samples (Nicholson, 2006; Wesley and Nelson, 2008b).

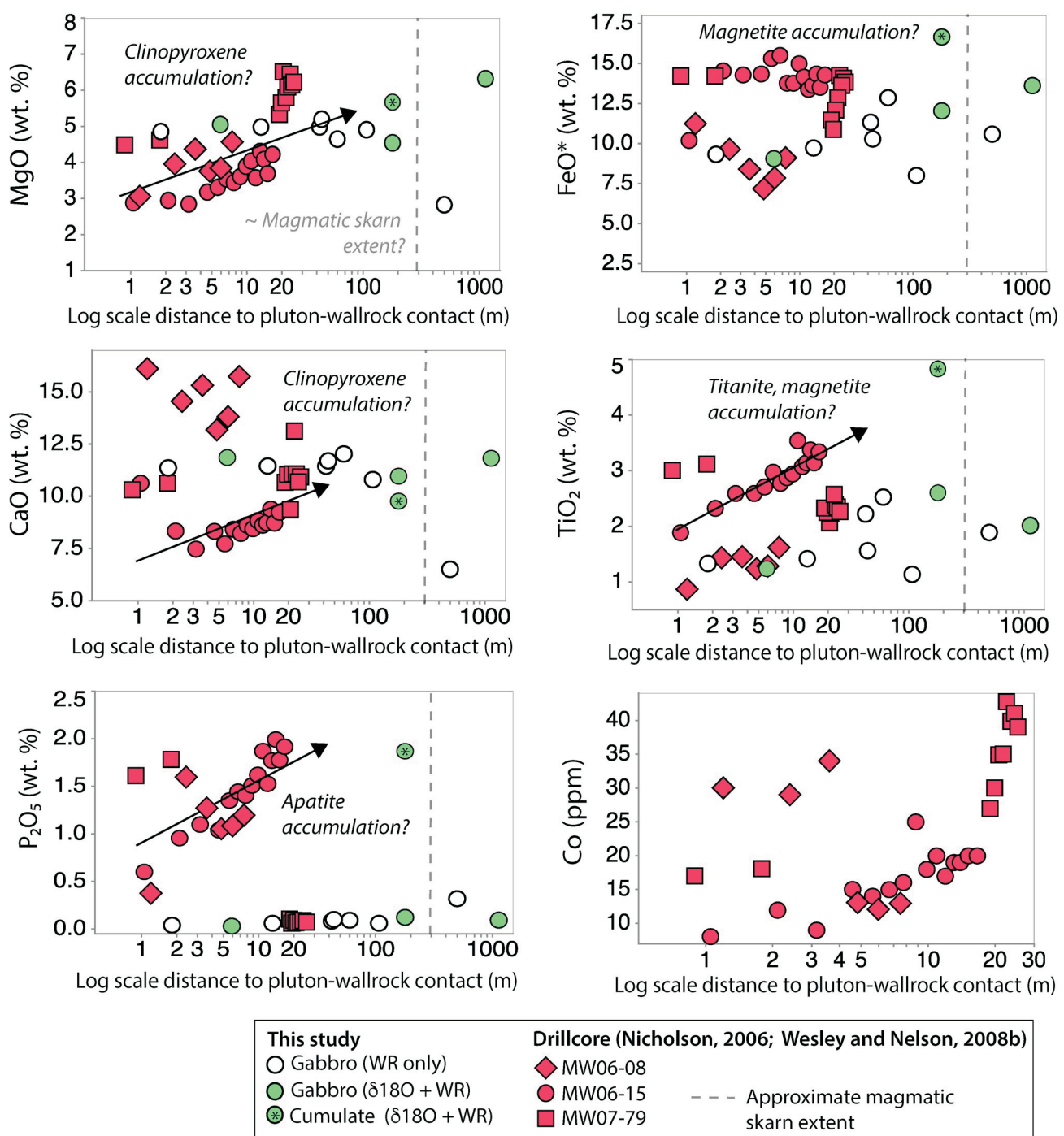


Figure 4. Major- and trace-element concentrations of whole-rock (WR) pluton samples from drillcore (published in Nicholson, 2006; Wesley and Nelson, 2008b) and this study, plotted against the approximate orthogonal distance from the pluton-wallrock margin. Trace-element chemistry is only available from drillcore data. Samples intersected by drilling are shown in red (drillcore symbols).

Due to the nature of skarn deposits, it is likely that the margin of the pluton experienced metasomatism in some regions, a factor that should be considered when evaluating whole-rock chemistry. Nevertheless, the high levels of P_2O_5 in magmatic skarn suggest accumulation of at least 5% apatite, also noted previously in petrographic examination of cumulates in the pluton (Morris and Canil, 2020). Accessory phases such as titanite and apatite are relatively

resistant to metasomatic replacement and, in this instance, can be interpreted as a good indicator of carbonate assimilation.

Oxygen Isotopes

Whole-rock samples collected from the 2019 field campaign were analyzed for $\delta^{18}\text{O}$ to quantitatively measure the

extent of assimilation within the Coast Copper stock, which ultimately affects major-element geochemical trends (Figure 4). Four samples from the Coast Copper stock were analyzed for $\delta^{18}\text{O}$ at the University of Oregon Stable Isotope Laboratory using methods given in Watts et al. (2019). The submitted samples included a proximal gabbro <10 m from the margin (sample 174), a distal gabbro ~1 km from the margin (sample 114), a cumulate (sample 64B) and the cumulate host (sample 64A; Figure 2). In addition, two Quatsino limestone wallrock samples, unaltered and collected off site, were analyzed for $\delta^{18}\text{O}$ at the University of Victoria using isotope-ratio mass spectrometry (IRMS). Methods for limestone $\delta^{18}\text{O}$ analyses involved heating sample powders (<1.0 mg) and standards (IAEA-603, IAEA-CO-8 and one internal standard) at 90°C overnight in borosilicate reaction vials to remove volatiles. Vials were placed in a heated block and samples were dissolved with ~15 drops of 100% H_3PO_4 and allowed to react for a minimum of 1 hour. The resulting CO_2 gas was measured on a Sercon Ltd. 20-22 gas-source mass spectrometer with a Gas Box 2 front end. Results were reported relative to Vienna Standard Mean Ocean Water (VSMOW). Precision, based upon measurement of the internal standard, is 0.2 per mille (‰) for $\delta^{18}\text{O}$ (1σ ; Vanwieren, 2019).

The gabbro $\delta^{18}\text{O}$ values range from 3.8 to 13.3‰ (Figure 5) and are highly variable compared to the narrow range of 5.5–5.9‰ for $\delta^{18}\text{O}$ in mantle-derived basalts (Bindeman, 2008). Values of $\delta^{18}\text{O}$ above 5.9‰ may indicate assimilation of the Quatsino limestone ($\delta^{18}\text{O} \sim 22\text{‰}$; Figure 5) or low-temperature (<100°C) hydrothermal alteration, whereas values below 5.5‰ may indicate assimilation of hydrothermally altered material, high-temperature hydrothermal alteration or a high modal percentage of minerals with low $\delta^{18}\text{O}$, such as magnetite ($\delta^{18}\text{O} \sim 3.5\text{‰}$; Cartwright and Barnicoat, 1999; Bindeman, 2008). Preliminary examination suggests limestone assimilation may be evident in a fresh proximal gabbro with $\delta^{18}\text{O}$ of 8.7‰ reported <10 m from the plutonic margin (sample 174; Figures 2, 5), as well as within the cumulate host gabbro, as indicated by a sample (sample 64A) taken ~200 m from the margin that has a highly enriched $\delta^{18}\text{O}$ value of 13.3‰. Low $\delta^{18}\text{O}$ signatures in both the sampled cumulate (sample 64B) and distal gabbro (sample 114) may be a result of the high abundance of magnetite (~30%) within these samples. Future additional $\delta^{18}\text{O}$ analyses from fresh outcrop will provide a better representation and coverage of gabbro $\delta^{18}\text{O}$ within the Coast Copper stock to help in understanding the extent of magmatic skarn and the process behind its generation.

Conclusions

This paper summarizes preliminary results to quantify the size and extent of magmatic skarn within the Coast Copper stock at the Merry Widow deposit from surface geology

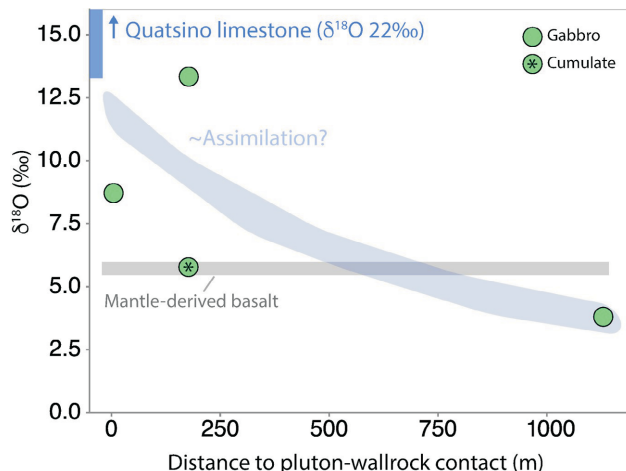


Figure 5. Oxygen-isotope results from Coast Copper stock gabbro plotted against the distance orthogonal to the pluton-wallrock contact with Quatsino limestone. Results show a variable range in comparison to typical mantle-derived basalts (Bindeman, 2008). Results suggest possible assimilation with $\delta^{18}\text{O}$ -enriched wallrock, such as the Quatsino limestone. Enriched $\delta^{18}\text{O}$ can also occur from low-temperature hydrothermal alteration. Depleted $\delta^{18}\text{O}$ may indicate high modal percentages of minerals with low $\delta^{18}\text{O}$ (i.e., ~3.5‰ in magnetite) or high-temperature hydrothermal alteration. Oxygen isotope values are standardized to Vienna Standard Mean Ocean Water (VSMOW).

(Morris and Canil, 2020) and core logs, and to examine its formation using $\delta^{18}\text{O}$ and whole-rock geochemistry. The transition from wallrock to pluton at Merry Widow is characterized by ~100 m of irregular exoskarn, ~10–60 m of volcanic breccia, ±3–10 m of recrystallized limestone and potentially >200 m of magmatic skarn. Assimilation of Triassic Quatsino limestone by the ~197 Ma Coast Copper stock enriches the gabbro $\delta^{18}\text{O}$ and results in a pluton margin characterized by an accumulation of magnetite, apatite and titanite. More $\delta^{18}\text{O}$ analyses will be completed for a better representation and coverage of the magmatic skarn within the Coast Copper stock. Results from this research can be used to estimate the extent of magmatic skarn and possible mineralization within other Fe-skarn deposits located throughout Wrangellia.

Acknowledgments

This project was supported by Geoscience BC scholarships (RM) and a Natural Sciences and Engineering Research Council of Canada (NSERC) Discovery Grant (DC). The authors thank G. Simandl for his comments and suggestions. They also thank J. Husson for access to his IRMS facility and J. Lei for analytical assistance.

References

- Barnes, C.G., Prestvik, T., Yujia, L., McCulloch, L., Yoshinobu, A.S. and Frost, C.D. (2009): Growth and zoning of the Hortavær intrusive complex, a layered alkaline pluton in the Norwegian Caledonides; *Geosphere*, v. 5, p. 286–301, URL <<http://doi.org/10.1130/GES00210.1>>.

- BC Geological Survey (2020a): MapPlace GIS internet mapping system; BC Ministry of Energy, Mines and Low Carbon Innovation, BC Geological Survey, MapPlace website, URL <<http://www.MapPlace.ca>> [October 2020].
- BC Geological Survey (2020b): MINFILE BC mineral deposits database; BC Ministry of Energy, Mines and Low Carbon Innovation, BC Geological Survey, URL <<http://minfile.ca/>> [October 2020].
- Bindeman, I. (2008): Oxygen isotopes in mantle and crustal magmas as revealed by single crystal analysis; Mineralogical Society of America Reviews in Mineralogy, v. 30, p. 157–186, URL <<http://doi.org/10.2138/rmg.2008.69.12>>.
- Cartwright, I. and Barnicoat, A.C. (1999): Stable isotope geochemistry of alpine ophiolites: a window to ocean-floor hydrothermal alteration and constraints on fluid-rock interaction during high-pressure metamorphism; International Journal of Earth Sciences, v. 88, p. 219–235, URL <<https://doi.org/10.1007/s005310050261>>.
- De Paolo, D.J. (1981): Trace element and isotopic effects of combined wallrock assimilation and fractional crystallization; Earth and Planetary Science Letters, v. 53, p. 189–202, URL <[https://doi.org/10.1016/0012-821X\(81\)90153-9](https://doi.org/10.1016/0012-821X(81)90153-9)>.
- Ettlinger, A.D., and Ray, G.E. (1987): Gold-enriched skarn deposits of British Columbia; in Geological Fieldwork 1987, BC Ministry of Energy, Mines, and Petroleum Resources, Paper 1988-1, p. 263–279, URL <http://cmscontent.nrs.gov.bc.ca/geoscience/PublicationCatalogue/Paper/BCGS_P1988-01.pdf> [October 2020].
- Lund, J.C. (1966): Structural geology of Empire mine, Empire Development Limited, Port McNeil, British Columbia; M.Sc. thesis, The University of British Columbia, URL <<http://hdl.handle.net/2429/37080>> [October 2020].
- Meinert, L.D., Dipple, G.M., and Nicolescu, S. (2005): World skarn deposits; Society of Economic Geologists, Economic Geology 100th Anniversary Volume, p. 299–336, URL <<https://doi.org/10.5382/AV100.11>>.
- Morris, R. and Canil, D. (2020): Skarn mineralization along magma-carbonate contacts in the Merry Widow Mountain area, Vancouver Island, British Columbia (NTS 092L); in Geoscience BC Summary of Activities 2019: Minerals, Geoscience BC, Report 2020-01, p. 5–12, URL <http://www.geosciencebc.com/i/pdf/SummaryofActivities2019/Minerals/Sch_Morris_Minerals_SOA2019.pdf> [October 2020].
- Nicholson, G. (2006): Assessment report on the diamond drilling on the Merry Widow property, Nanaimo Mining Division, Vancouver Island; BC Ministry of Energy, Mines and Low Carbon Innovation, Assessment Report 28863, 423 p., URL <<https://aris.empr.gov.bc.ca/ArisReports/28863.PDF>> [October 2020].
- Nixon, G.T., Snyder, L.D., Payie, G.J., Long, S., Finnie, A., Orr, A.J., Friedman, R.M., Archibald, D.A., Orchard, M.J., Tozer, E.T., Poulton, T.P. and Haggart, J.W. (2011): Geology, geochronology, lithogeochemistry and metamorphism of the Alice Lake area, northern Vancouver Island, NTS 092L/06 and part of 092L/03; BC Ministry of Energy, Mines and Low Carbon Innovation, BC Geological Survey, Geoscience Map 2011-4, scale 1:50 000, URL <<http://>
- cmscontent.nrs.gov.bc.ca/geoscience/PublicationCatalogue/GeoscienceMap/BCGS_GM2011-04.pdf> [October 2020].
- Ray, G.R. (2013): A review of skarns in the Canadian Cordilleran; BC Ministry of Energy, Mines and Low Carbon Innovation, BC Geological Survey, Paper 2013-08, 52 p., URL <http://cmscontent.nrs.gov.bc.ca/geoscience/PublicationCatalogue/OpenFile/BCGS_OF2013-08.pdf> [October 2020].
- Ray, G.E. and Webster, I.C.L. (1991): Geology and mineral occurrences of the Merry Widow skarn camp, northern Vancouver Island; BC Ministry of Energy, Mines and Low Carbon Innovation, BC Geological Survey, Open File 1991-08, 1 map at 1:5000 scale, URL <http://cmscontent.nrs.gov.bc.ca/geoscience/PublicationCatalogue/OpenFile/BCGS_OF1991-08.pdf> [October 2020].
- Sangster, D.F. (1964): The contact metasomatic magnetite deposits of southwestern British Columbia, Ph.D. thesis, The University of British Columbia, URL <<https://open.library.ubc.ca/circus/collections/ubctheses/831/items/1.0053070>> [October 2020].
- Spera, F.J., and Bohrson, W.A. (2001): Energy-constrained open-system magmatic processes I: general model and energy-constrained assimilation and fractional crystallization (EC-AFC) formulation; Journal of Petrology, v. 42, p. 999–1018, URL <<https://doi.org/10.1093/petrology/42.5.999>>.
- Taylor, H.P. (1980): The effects of assimilation of country rocks by magmas on $^{18}\text{O}/^{16}\text{O}$ and $^{87}\text{Sr}/^{86}\text{Sr}$ in igneous rocks; Earth and Planetary Science Letters, v. 47, p. 243–254, URL <[https://doi.org/10.1016/0012-821X\(80\)90040-0](https://doi.org/10.1016/0012-821X(80)90040-0)>.
- Vanwieren, C.S. (2019): Characterizing the Triassic/Jurassic boundary through stratigraphy of northern Vancouver Island carbonates; B.Sc. thesis, University of Victoria.
- Vogt, T. (1916): Petrographisch-chemische studien an einigen assimilations-gesteinen der Nordnorwegischen gebirgskette; Videnskapsselskapets Skrifter, v. 1, p. 1–33.
- Watts K.E., John, D.A., Colgan, J.P., Henry, C.D., Bindeman, I.N. and Valley, J.W. (2019): Oxygen investigation of silicic magmatism in the Stillwater caldera complex, Nevada: generation of large-volume, low $\delta^{18}\text{O}$ rhyolite tuffs and assessment of their regional context in the Great Basin of the western United States; GSA Bulletin, v. 131, p. 1133–1156, URL <<https://doi.org/10.1130/B35021.1>>.
- Wesley, R. and Nelson, M. (2008a): Diamond drilling, geochemical and geophysical assessment report for the 2007 program at the Merry Widow project, Nanaimo Mining Division, Vancouver Island; BC Ministry of Energy, Mines and Low Carbon Innovation, Assessment Report 30002a, 242 p., URL <<https://aris.empr.gov.bc.ca/ArisReports/3000-2A.PDF>> [October 2020].
- Wesley, R. and Nelson, M. (2008b): Diamond drilling, geochemical and geophysical assessment report for the 2007 program at the Merry Widow project, Appendix 3 – Analytical certificates, Nanaimo Mining Division, Vancouver Island; BC Ministry of Energy, Mines and Low Carbon Innovation, Assessment Report 30002b, 589 p., URL <<https://aris.empr.gov.bc.ca/ArisReports/30002B.PDF>> [October 2020].

Paleogene Penticton Group, Boundary area, Southern British Columbia (Parts of NTS 082E): Geochronology and Implications for Precious Metal Mineralization

T. Höy, Geological consultant, Sooke, British Columbia, thoy@shaw.ca

R. Friedman, Pacific Centre for Isotopic and Geochemical Research, The University of British Columbia, Vancouver, British Columbia

J. Gabites, Pacific Centre for Isotopic and Geochemical Research, The University of British Columbia, Vancouver, British Columbia

Höy, T., Friedman, R. and Gabites, J. (2021): Paleogene Penticton Group, Boundary area, southern British Columbia (parts of NTS 082E): geochronology and implications for precious metal mineralization; *in* Geoscience BC Summary of Activities 2020: Minerals, Geoscience BC, Report 2021-01, p. 55–66.

Introduction

Paleogene volcanic and sedimentary rocks of the Penticton Group are exposed in numerous localities throughout southern British Columbia (BC), commonly preserved in north-trending structural basins. Regional mapping in the Boundary area in the eastern half of the Penticton map area (NTS 082E), in conjunction with Ar/Ar and U-Pb zircon dating, has helped to constrain the age of the Penticton Group, its relation to extensional tectonics and its control of precious-metal mineralization. This project is a continuation and enhancement of systematic 1:50 000 geological mapping that has resulted in the publication of six maps (Figure 1): Grand Forks (NTS 082E/01), Greenwood (NTS 082E/02), Almond Mountain (NTS 082E/07), Deer Park (NTS 082E/08), Burrell Creek (NTS 082E/09) and Christian Valley (NTS 082E/10). The Boundary area has had an extensive history of exploration and mining, particularly in the Greenwood, Franklin and Beaverdell mining camps, where intermittent production of base and precious metals continued from the late 1880s to the early 1990s. Exploration continues to be active throughout the area, still largely focused on precious-metal targets.

Geology

The Penticton Group in the Boundary area of the Penticton map area (NTS 082E) includes a basal succession of dominantly conglomerate, sandstone, reworked tuff and minor volcanic flows of the Kettle River Formation that unconformably overlies Paleozoic and Triassic metavolcanic rocks and large suites of intrusive rocks of varying ages (Figure 2). The Kettle River Formation is conformably overlain by a thick sequence of dominantly alkalic volcanic

rocks and minor sedimentary units of the Marron Formation. Farther west in the White Lake basin area, the Marron Formation is unconformably overlain by basal conglomerate, felsic lava and tuff of the Marama Formation, and interlayered sedimentary and volcanic rocks of the White Lake and Skaha formations (Church, 1973).

Paleozoic basement rocks in the Boundary area have been studied extensively by Massey (2006). In the Greenwood map area (NTS 082E/02; Figure 1), they include poorly dated metavolcanic and metasedimentary rocks, minor gabbro, serpentinite and locally paragneiss of the Carboniferous to Permian Knob Hill complex (Little, 1983; Church, 1986; Fyles, 1990; Massey, 2007). The Attwood Formation comprises mainly Mississippian to Permian metasedimentary rocks; their relationship to the Knob Hill complex is not known as there are no recognized stratigraphic contacts between the units. Farther north and to the east in the Grand Forks map area (NTS 082E/01; Figure 1), Attwood Formation rocks are correlated with the lithologically similar Wallace group or Mount Roberts Formation.

Middle to late Triassic chert breccia, limestone and volcanic ‘greenstone’ of the Brooklyn Formation unconformably overlie the Attwood Formation or Knob Hill Group in the Greenwood area (Little, 1983; Fyles, 1990). Volcanic rocks correlated with the Jurassic Rossland Group are in thrust contact with serpentinites and gabbro, assumed to be part of the Knob Hill complex, in the southern part of the Grand Forks map area (Höy and Jackaman, 2005).

A large part of the Penticton map area is underlain by granitic and alkalic intrusive rocks that have variously been assigned to granodiorite of the ‘Nelson’ plutonic complex, granite of the Okanagan batholith or Coryell syenite (Tempelman-Kluit, 1989; Höy and Jackaman, 2019; Höy et al., 2020). Locally, the Penticton Group unconformably overlies Triassic to Jurassic Nelson intrusions and in the Almond Mountain map area (NTS 082E/07; Figure 1), a

This publication is also available, free of charge, as colour digital files in Adobe Acrobat® PDF format from the Geoscience BC website: <http://geosciencebc.com/updates/summary-of-activities/>.

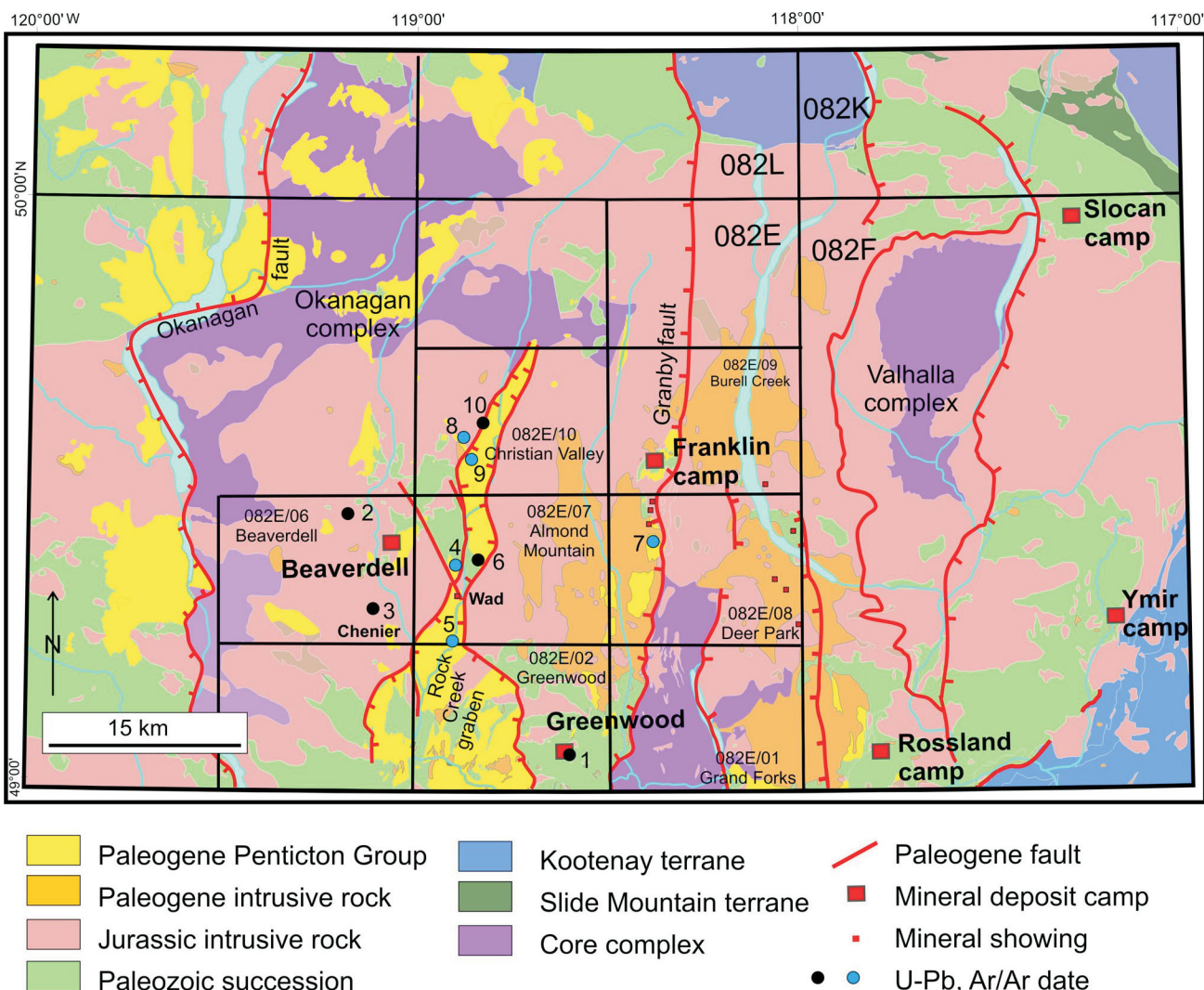


Figure 1. Regional terrane map of the Boundary area of southern British Columbia, showing location of major deposit camps, mineral occurrences discussed in this paper, and samples (numbered 1–10) collected for Ar/Ar and U-Pb dating.

Paleocene granite that has been informally named the ‘Taurus Creek stock’ (Höy and Jackaman, 2016). Dikes and small stocks of the Paleocene to Eocene Okanagan batholith and Eocene Coryell syenite locally intrude the Penticton Group, which helps constrain the age of these rocks.

The Kallis Formation (Figure 2) is preserved in isolated topographic highs throughout the area, unconformably overlying either the Penticton Group or intrusive rocks. It represents the remains of widespread Miocene–Pliocene plateau basalts.

Penticton Group

The Penticton Group is exposed mainly within the north-trending Rock Creek graben, shown on the western part of the Penticton east-half map area, in the northern extension of the Republic graben in the Greenwood area and farther north in the western part of the Deer Park map area

(NTS 082E/08; Figure 1; Tempelman-Kluit, 1989; Höy and Jackaman, 2019). The widespread distribution of the Penticton Group rocks and correlations are described by Church (1973), who inferred that they represented the erosional remnants of a continuous belt of dominantly volcanic rocks that extended across southern BC and the northern State of Washington. Alternatively, the distribution of basal Penticton Group rocks, particularly the Marron Formation, may be considerably more limited, largely restricted to the fault-bounded, north-trending grabens.

Kettle River Formation

The Kettle River Formation is the dominantly sedimentary succession that overlies basement rocks, extending upward into a generally conformable contact with alkalic volcanic rocks of the Marron Formation. It has been described in considerable detail by Monger (1968), Little (1983) and

Fyles (1990), and the following description is based largely on these works.

The formation includes pale grey to buff feldspathic sandstone, grey to green-tinged volcanic sandstone and conglomerate, and locally felsic crystal-lithic tuff. The conglomerates occur at several stratigraphic levels but the thickest and coarsest are generally at the base of the formation. Clasts, locally to several tens of centimetres in diameter, are generally composed of local volcanic and chert fragments of the Paleozoic basement, granite and granodiorite of the Nelson plutonic complex and, in the Rock Creek graben, clasts and broken crystals of the immediately underlying Paleocene Taurus Lake granite.

Volcanic rocks are a minor component of the Kettle River formation but include dacitic crystal-lithic tuffs comprising lithic fragments, euhedral feldspar crystals, pyroxene and quartz. Locally, white to pink porphyritic dacite with phenocrysts of plagioclase, orthoclase and rounded quartz in a light green aphanitic matrix also occur, generally near the upper contact with the Marron Formation.

Correlation

The Kettle River Formation correlates with the contiguous O'Brien Formation in the Republic District, Washington (Pearson and Obradovich, 1977), and with the Springbrook Formation in the White Lake basin, 90 km northwest of Greenwood (Church, 1973, 1986).

Age

Numerous plant fossils and spores from the Kettle River Formation have been identified as ranging in age from Paleocene to Eocene (e.g., Rouse and Mathews, 1961). Potassium-argon dating of dacite has returned a range of ages, from 53.1 ± 1.5 Ma (Pearson and Obradovich, 1977) to 46.2 ± 2 Ma (Mathews, 1963).

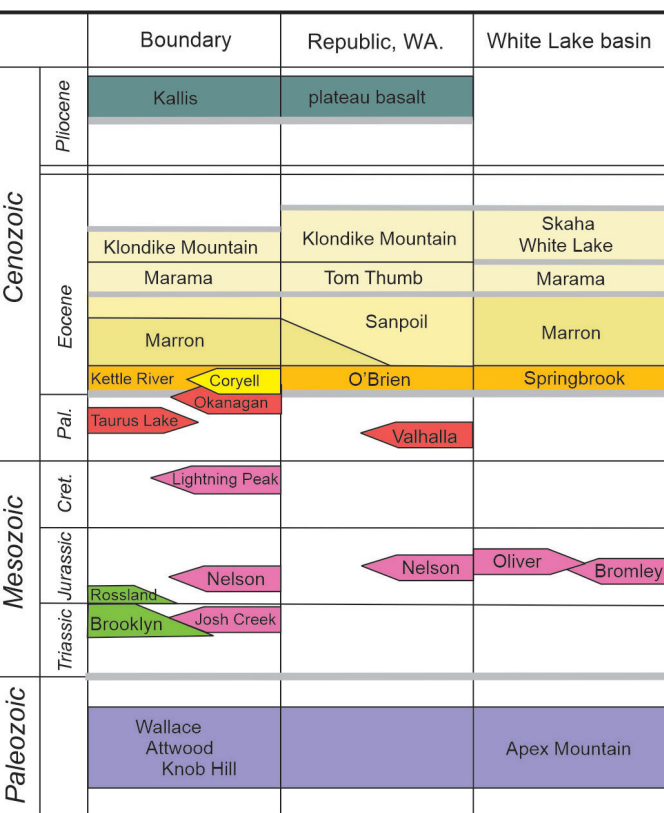


Figure 2. Schematic stratigraphy of the Boundary area, and correlations with the Republic District in the State of Washington (Cheney, 1994, 1998) and the White Lake basin (Church, 1973) area. Abbreviations: Cret., Cretaceous; Pal., Paleocene.

Three samples of the Kettle River Formation were submitted to the Pacific Centre for Isotopic and Geochemical Research (PCIGR) for U-Pb zircon dating (Figure 1, Table 1). Petrographic descriptions of these samples are not yet completed and, hence, the following descriptions are based on field observations.

Table 1. Summary of U-Pb zircon and Ar⁴⁰/Ar³⁹ mineral ages obtained for selected samples of intrusive and Penticton Group rocks collected during mapping in the Boundary area; more complete sets of the data have also been studied (Höy et al., 2019; T. Höy, J. Gabites and R. Friedman, work in progress). Abbreviations: Bi, biotite; Ksp, K-feldspar; WR, whole rock; Zr, zircon.

No.	Sample	Easting	Northing	NTS map area	Unit	Rock type	Method	Age	Error	
1	H20-60	383577	5438992	082E/02	Greenwood	Kettle River	crystal-lithic tuff	U-Pb Zr	50.80	0.49
2	H19-149	344974	5482539	082E/06	Beaverdell	Marama	trachyte	U-Pb Zr	48.88	0.44
3	H20-09	344093	5464081	082E/06	Beaverdell	Kettle River	crystal-lithic tuff	U-Pb Zr	51.45	0.47
4	AM-470	361491	5471677	082E/07	Almond Mountain	Marron	basalt	Ar/Ar Ksp	57.80	2.10
5	AM-557	361478	5457103	082E/07	Almond Mountain	Marron	andesite	Ar/Ar Ksp	59.22	0.83
6	H20-59	366290	5471486	082E/07	Almond Mountain	Kettle River	tuffaceous sandstone	U-Pb Zr	51.50	0.44
7	H19-26	399631	5475801	082E/08	Deer Park	Marron	alkali basalt	Ar/Ar Ksp	53.22	0.79
8	CV-41	364772	5497380	082E/10	Christian Valley	Marron	lava or possible dike	Ar/Ar WR	50.60	0.90
9	CV-159	365992	5491657	082E/10	Christian Valley	Marron	mafic lava	Ar/Ar Bi	52.77	0.38
10	CV-294	368478	5498093	082E/10	Christian Valley	dike(?)	andesite dike	U-Pb Zr	49.40	0.77

Sample H20-60: Greenwood

Sample H20-60 (no. 1 on Figure 1) is a vaguely layered, medium to fine-grained, light grey volcanic sandstone or reworked tuff from the Phoenix deposit pit near Greenwood (Figures 3, 4). It contains dominantly feldspar and quartz crystals and small, generally dark, lithic fragments. It is within a succession of massive to layered siltstone, sandstone, grit, conglomerate and dacitic tuff, approximately 80 m in thickness, that is bracketed by unconformably underlying Paleozoic basement and overlying Marron Formation volcanic rocks. Plant fossils are common in the succession. The sample was collected from a pit wall, several tens of metres above the base of the formation.

The weighted $^{207}\text{Pb}/^{206}\text{Pb}$ average of 12 zircon grains yielded a date of 50.80 ± 0.49 Ma (Table 1) and is assumed to record the age of extrusion of the dacitic tuff. Other dates obtained from individual zircons range from ca. 87 to 65 Ma and may record inclusion of detrital grains from underlying granitic rocks.

Sample H20-59: Lost Horse Creek

Sample H20-59 (no. 6 on Figure 1) is from a thick succession of bedded to massive conglomerate, quartzite, siltstone, minor shale and minor tuff that unconformably overlies late Paleozoic Wallace group volcanics and is overlain by Marron Formation. The sample is a massive to vaguely bedded light grey, green-tinged crystal-lithic tuff or tuffaceous sandstone, comprising mainly light grey and pink-tinged feldspar, quartz and dark (volcanic) lithic fragments.

The weighted $^{206}\text{Pb}/^{238}\text{U}$ average of 15 zircons gave a date of 51.50 ± 0.44 Ma (Table 1) and is assumed to record the depositional age of dacitic tuff within the Kettle River Formation. Other probable detrital zircon dates may reflect the ages of underlying lower Jurassic, Cretaceous and Paleogene granitic rocks.

Sample H20-09: Chenier Creek

Sample H20-09 (no. 3 on Figure 1) is from a succession of conglomerate, breccia, volcanic flows and tuff that unconformably overlies Middle Jurassic granite, probable Paleocene granite and minor Paleozoic metasedimentary rocks in the Kelly River area, approximately 30 km north of Rock Creek. Mineral exploration in the immediate vicinity has been directed toward a porphyry copper-gold prospect, the Chenier or CuAu property (Höy, 2007; Thompson et al., 2018), and the following description of the Kettle River Formation is largely taken from the cited reports. Crystal-lithic tuff, in part interlayered with polymictic breccia and conglomerate, occurs at the base of the succession immediately overlying Jurassic granodiorite. The conglomerate comprises numerous angular to rounded fragments of dominantly granite or granodiorite and dark fragments of either mafic volcanic rocks or dikes. The crystal-lithic units com-



Figure 3. Phoenix deposit pit near Greenwood, British Columbia; sample H20-60 was taken from the pit wall at the far end of the lower bench.



Figure 4. Well-bedded, reworked Kettle River Formation felsic tuff and tuffaceous sandstone from the Phoenix deposit pit near Greenwood, British Columbia.

prise mainly broken feldspar crystals, quartz and lithic granite fragments. Feldspar (\pm pyroxene) flows, interlayered with tuff and breccia, locally overlie the basal succession. Massive conglomerate, consisting mainly of granitic clasts and occasional dark fragments, interlayered with volcanic sandstone, may represent a lateral facies change of

the crystal-lithic tuffs and breccia units (Thompson et al., 2018, p 56). The dated sample (H20-09) is from a poorly bedded, medium-grained crystal-lithic tuff that contains mainly white feldspar, quartz and minor biotite (Figure 5). It is lithologically similar to the other dated samples of the Kettle River Formation.

The weighted $^{206}\text{Pb}/^{238}\text{U}$ average of 18 zircons returned a date of 51.45 ± 0.47 Ma (Table 1) and is assumed to record the depositional age of dacitic tuff on the Chenier property. Numerous other zircon grains range in age up to ca. 70 Ma and reflect the age of underlying Paleogene granitic rocks. However, the only dated intrusion in the immediate vicinity, 1.2 km east of the Kettle River contact, is Middle Jurassic in age.

Marron Formation

The Marron Formation was first defined by Bostock (1941) as an early Tertiary¹ volcanic succession in the Okanagan area, southwest of the town of Penticton. Church (1973) defined a type section in that area, and Monger (1968) and Little (1983) subsequently applied the terminology to correlative rocks in the southern part of the Penticton map area (NTS 082E), a succession previously referred to as the ‘Midway Volcanic Group’ (Daly, 1912) or the ‘Phoenix Volcanic Group’ (Little, 1957). The Marron Formation in the Greenwood map area (NTS 082E/02) has been mapped and subdivided by Monger (1968) and Little (1983) but little work other than regional (1:50 000 scale) mapping has been done farther north in the Penticton map area.

The Marron Formation unconformably overlies the Kettle River Formation and is locally overlain by Miocene plateau basalts of the Kallis Formation. In the Greenwood area, it has been subdivided into three informal divisions: a lower division comprising dominantly rhomb-porphyry soda trachyte and phonolite; a middle division comprising pyroxene andesite and trachyandesite; and an upper division comprising mainly andesite (Monger, 1968; Little, 1983). These subdivisions are not readily apparent farther north, perhaps due to lack of detailed mapping. The thickness of the exposed Marron Formation varies considerably, from locally less than 100 m in the Greenwood area in the south to 900–1800 m farther west in the Rock Creek graben. The original thicknesses of the formation are not known, as the upper limit is often either an erosional surface or, as in the Greenwood area, a faulted contact.



a)



b)

Figure 5. Kettle River Formation lapilli tuff (a) and sampled quartz-crystal lapilli tuff (b) from the Chenier property, south of Beaverdell.

Correlation

Based on gross lithological similarities, Church (1973, 1986) correlated the Marron Formation in the White Lake basin area with the exposed sections of Marron Formation in the Greenwood map area. Although it is difficult to correlate individual members of the type White Lake basin section with those in the Penticton area, both Church (1973) and Little (1983) suggested that the basal Yellow Lake member correlated with the lower division in the

¹‘Tertiary’ is a historical term. The International Commission on Stratigraphy recommends using ‘Paleogene’ (comprising the Paleocene to Oligocene epochs) and ‘Neogene’ (comprising the Miocene and Pliocene epochs). The author used the term ‘Tertiary’ because it was used in the source material for this paper.

Greenwood area; the Kitley Lake, Kearns Creek and Nimpit Lake members correlated with the middle division; and the Park Rill member, with the upper division in the Greenwood area. Direct correlations with sections immediately south in the Republic District, Washington, are also difficult. Pearson and Obradovich (1977) and Cheney (1994, 1998) suggested that the Sanpoil volcanics correlated with the lithologically similar Park Rill member in the White Lake basin and the upper division of the Marron Formation in the Penticton map area (Figure 2).

Age

The Marron Formation, and correlative rocks, are generally poorly dated. In the Penticton map area, the formation is underlain by the middle Eocene (ca. 52–51 Ma) Kettle River Formation and locally overlain by the Miocene–Pliocene (ca. 6–4 Ma) Kallis Formation. Several K-Ar mineral dates of volcanic rocks in the Marron Formation range from ca. 49–48 Ma in the Greenwood area (Mathews, 1964) to 51.6 ±1.8 Ma in the White Lake basin (Church, 1973). Pearson and Obradovich (1977) obtained 13 K-Ar mineral dates from samples of Sanpoil volcanics that range from 53.4 ±2.0 Ma to 48.4 ±3.0.

Four samples of the Marron Formation have been analyzed at the PCIGR:

- Sample AM-470 (no. 4 on Figure 1), a medium grey, amygdaloidal alkali andesite with minor disseminated biotite and hornblende and small euhedral plagioclase grains, was collected near the base of the formation, on a paleotectonic high within the north-trending Rock Creek graben (Höy and Jackaman, 2016); an Ar/Ar plateau age of 57.8 ±2.1 Ma was determined on K-feldspar (Table 1).
- Sample AM-557 (no. 5 on Figure 1), a sample of light grey plagioclase-phyric porphyritic andesite with minor disseminated biotite in a fine-grained matrix, was collected from a roadcut near the base of the Marron Formation in the Rock Creek graben along the Christian Valley road, 10 km north of Westbridge; an Ar/Ar plateau age of 59.22 ±0.83 Ma was determined on K-feldspar (Table 1).
- Sample CV-41 (no. 8 on Figure 1) was sampled from a small exposure of altered, pale grey crowded feldspar porphyry located 1 km northwest of Little Sandrift Lake (Höy and Jackaman, 2017) and is associated with either a Marron dike or an outcrop of Marron Formation that overlies Paleocene granite; an Ar/Ar plateau age of 53.8 ±1.8 Ma was determined on feldspar and the whole rock produced a plateau age of 50.6 ±0.9 Ma (Table 1).
- Sample CV-159 (no. 9 on Figure 1), a black, fine-grained amygdaloidal basalt flow unit located in the upper member of the Marron Formation near the centre of the Rock Creek graben, was petrographically analyzed and the results indicate it is a biotite-clinopyroxene

trachyte lava, with approximately 5% disseminated biotite and 3–5% plagioclase phenocrysts (Höy et al., 2019); an Ar/Ar plateau age of 52.77 ±0.38 Ma was determined on biotite (Table 1).

Discussion on the Radiometric Dating

The plateau Ar/Ar dates determined for three of the known Marron Formation flows cannot be reconciled with the younger U-Pb zircon ages of the underlying Kettle River Formation. There is no petrographic evidence to suggest that the biotites or feldspars used for the radiometric dating are xenocrystic or detrital grains. However, analyses of the oldest feldspars revealed they contained extremely low volumes of ^{39}Ar (K) which could lead to spurious older ages. The age of the Marron is therefore assumed to be bracketed by the ca. 51.5 Ma age of the underlying Kettle River formation and the age of overlying Marama Formation, ca. 48.9 Ma (see below).

Marama Formation

The Marama Formation is defined as a succession of dominantly rhyolitic and rhyodacitic rocks that unconformably overlie the Marron Formation in the White Lake basin (Church, 1973). The formation comprises basal “conglomerate, minor sandstone and shale with seams of pyroclastic rocks throughout” (Church, 1973, p. 40). These are overlain by rhyolite breccia and pyroclastic deposits, and capped by thick rhyodacite lavas. The Marama Formation is unconformably overlain by stream and lake deposits interlayered with trachyte and trachyandesites of the White Lake Formation, and dominantly slide breccias, conglomerate and lava flows of the Skaha formation, which are the youngest Paleogene deposits in the White Lake basin (Church, 1973).

The Marama Formation has been correlated with the upper part of the Sanpoil Formation in the Toroda Creek graben in Washington, south of Greenwood (Church, 1973; Pearson and Obradovich, 1977). However, it is lithologically similar to rhyolitic and rhyodacitic rocks of the Tom Thumb member, which forms the basal part of the Klondike Mountain Formation that overlies the Sanpoil in northern Washington. Both units unconformably overlie correlative Marron and Sanpoil formations, contain distinctive interbedded rhyolitic and dacitic tuffs and shales, and locally contain abundant plant fossil remains. Hence, a correlation of the Marama Formation with the Tom Thumb member is preferred (Figure 2), with the overlying White Lake and Skaha formations correlating with middle and upper divisions of the Klondike Mountain Formation (Cheney, 1994, 1998).

The Marama Formation has not been recognized previously in the Boundary area. However, Little (1983) described an epiclastic breccia-tuff succession south of Greenwood that he correlated with the Klondike Mountain

Formation; subsequently, Fyles (1990) included this unit in the Marron Formation. Reconnaissance geological mapping west of Beaverdell has recognized a distinctive tuff succession that unconformably overlies Paleocene granite and Paleozoic metavolcanics; based in part on similar rock types and a U-Pb zircon date, this unit has been tentatively correlated with the Marama Formation, or possibly the overlying White Lake Formation.

Age

The Marama Formation is clearly younger than the underlying Kettle River (ca. 51.5 Ma) and Marron formations. Klondike Mountain Formation rock samples have yielded several K-Ar mineral dates that range from 49.1 to 41.3 Ma, with a mean age of ca. 46 Ma, which is assumed to be the age of the middle member of the formation (Pearson and Obradovich, 1977). However, due to possible inherent Ar loss, older K-Ar dates are considered more reliable and hence the ca. 49.1 Ma date may more closely reflect the age of the Klondike Mountain Formation.

Sample H19-149: Beaverdell

A poorly exposed succession of dacitic to trachytic tuff, unconformably overlying Paleocene granite and Paleozoic metavolcanics was recognized west of Beaverdell during reconnaissance mapping in 2019 (no. 2 on Figure 1). It is lithologically similar to some phases of the Klondike Mountain Formation and to the Marama Formation, although the latter is typically more felsic.

A sample of the bedded trachytic tuff (Figure 6), taken from a large angular block directly downslope from surface exposures, was dated at The University of British Columbia. The weighted $^{206}\text{Pb}/^{238}\text{U}$ average of 19 zircons gave a date of 48.8 ± 0.44 Ma (Table 1), with a fairly wide scatter of older dates to ca. 53 Ma. The date is close to the average K-Ar mineral date of the Klondike Mountain Formation, in contrast to the older dates of the basal Kettle River Forma-



Figure 6. Sample of poorly bedded to massive trachytic tuff (no. 2 on Figure 1, Table 1), taken immediately downslope from similar tuff of the Marama(?) Formation northeast of Beaverdell.

tion. Hence, this exposure is considered the first evidence of post-Marron volcanism in the Boundary area.

Eocene Dike

Regional mapping throughout the Boundary area has recognized numerous suites of dominantly alkalic dikes. Many of these are assumed to be comagmatic with, and similar to, the Marron Formation, and commonly intrude lower stratigraphic levels of the formation.

In the eastern part of the Christian Valley map area (NTS 082E/10; Höy and DeFields, 2017) the western margin of the Rock Creek graben is characterized locally by several fault splays marked by shearing, brecciation and alteration (Figure 7). In one of these exposures (Figure 8), highly broken and sheared Eocene(?) granite containing

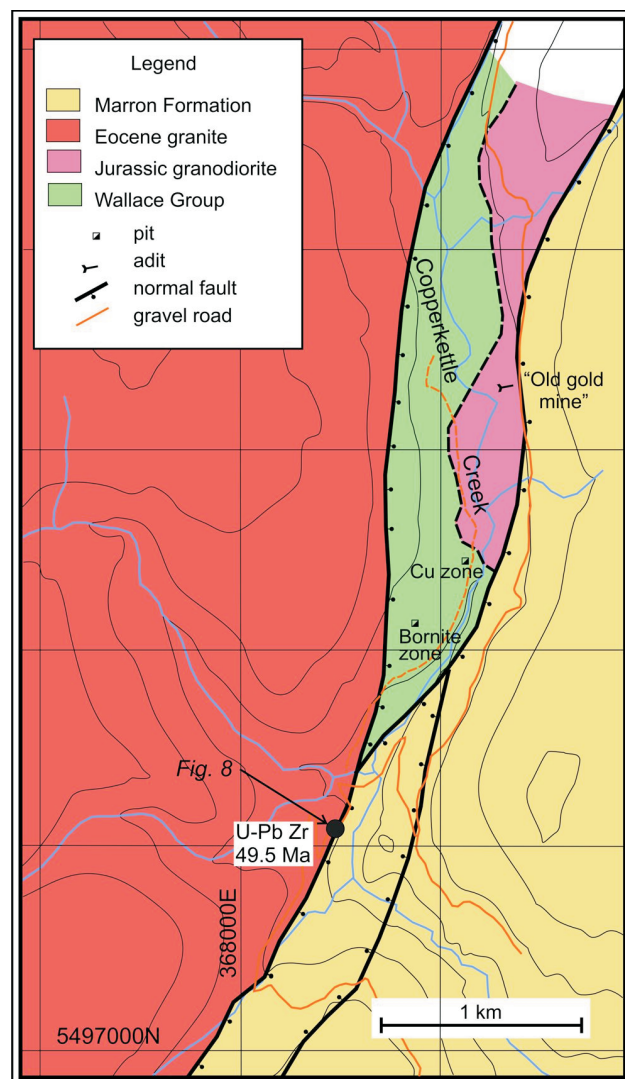


Figure 7. Geology of the western margin of the Rock Creek graben in the Boundary area, showing fault splays and location of chalcopyrite-galena-gold vein and skarn mineralization of the Copket property (location of the Eocene(?) dike, sample CV-294 and Figure 8 are also shown). Map modified from Whiting (1991) and Höy and DeFields (2017).

blocks of crushed Wallace group, is cut by a fresh, unaltered north-trending hornblende-porphyry dike. A U-Pb zircon date on the dike constrains the timing of movement along this fault splay to predate 49.4 ± 0.77 Ma (sample CV-294; no. 10 on Table 1).

Penticton Group: Depositional Controls

The Penticton Group in the Boundary area is mainly exposed in the northern extension of the Republic graben north of Greenwood and in the Rock Creek graben, which is the northern extension of the Toroda Creek graben. Several studies have either stated or implied that the Penticton Group extended over a large part of southern BC and northern Washington, and its present distribution is due largely to its preservation in postdepositional downdropped fault blocks.

However, considerable evidence exists for syndeposition of the Kettle River and Marron formations during extension, and within, the grabens. The basal Kettle River Formation is considerably coarser and thicker in exposures within the graben than it is in the few exposures both to the west, at the Chenier deposit area (Figure 1), and in a cross-cutting northwest-trending paleotectonic high, in the Rock Creek graben. Furthermore, the total thickness of the Marron Formation exceeds 1800 m in the Rock Creek graben (Little, 1983) in contrast to a few tens of metres at the Chenier and Wad deposit areas (see below). Northwest of Beaverdell, the Kettle River and Marron formations are missing, and ‘basement’ granite is unconformably overlain by tuff and tuffaceous sands of the Marama or Klondike Mountain formations. It is possible, but unlikely, that these older formations were eroded away prior to deposition of the Marama Formation, though this in itself would be evidence of considerable vertical movements during Penticton Group deposition.

The Marron Formation is geochemically similar in all downdropped blocks throughout the Okanagan and Boundary areas and northern Washington. This evidence further supports a model according to which “these deposits occur as scattered erosional remnants of what was probably a once continuous belt composed mainly of volcanic rocks extending from at least central Washington through the Interior to central British Columbia” (Church, 1973, p. 17). However, individual members within the well-recognized succession in the White Lake basin (Church, 1973) do not match those in the Marron Formation in the Rock Creek graben, nor those in the Sanpoil Formation of Washington.

Growth faulting along the western margin of the Rock Creek graben is constrained by the age of the basal Kettle River Formation at ca. 51.5 Ma. As the graben faults cut both the Marron and Kettle River formations, movement must also clearly postdate deposition of these rocks. The

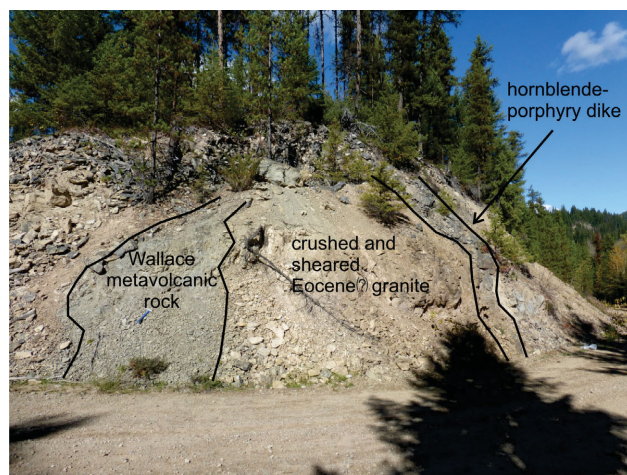


Figure 8. Crushed and altered Eocene(?) granite in the fault along the western margin of the Rock Creek graben in the Boundary area, containing blocks of altered and sheared Paleozoic Wallace group and cut by a fresh, unaltered hornblende dike. The age of the dike (ca. 49.4 Ma) constrains the timing of the latest movement along this splay of the fault (location shown on Figures 1 and 7).

age of the post-fault, crosscutting dike at ca. 49.4 Ma constrains the timing of fault movement along the western margin of the graben, thereby limiting deposition of the Kettle River and Marron formations to a few million years (Figure 9). This supports the contention of Bardoux and Irving (1989) that all but the lower beds of the Marron Formation were deposited in a limited period of normal geomagnetic polarity between 51.5 and 50.5 Ma. There is little record of Penticton Group rocks on the upthrown blocks, though thinned successions may have been largely eroded during continued movement along these extensional faults. Therefore, the Marama Formation or younger Penticton Group rocks may have formed a more extensive, regional cover over both the graben fill and the marginal highlands.

In the northern extension of the Republic graben, the basal Kettle River Formation in the Phoenix deposit pit near Greenwood may be slightly younger at 50.8 ± 0.49 Ma. Farther north, within the projected northern extension of the graben, large exposures of undifferentiated Penticton Group appear to unconformably overlie Coryell syenite (Tempelman-Kluit, 1989), dated at 51.1 Ma (Carr and Parkinson, 1989). This contrasts with small, higher level Coryell dikes in the Rock Creek graben that intrude Marron Formation rocks (Höy and Jackaman, 2016) and support a model of essentially contemporaneous intrusion of Coryell syenite with extrusion of Marron Formation volcanic rocks and graben development (Figure 9).

Grabens formed in a zone of regional extension in the hangingwall of the Granby fault, a relatively low-angle crustal structure that separates high-grade Proterozoic metamorphic rocks of the Grand Forks complex in the east (Preto, 1970) from lower grade Paleozoic to Eocene rocks in its hangingwall to the west (Tempelman-Kluit and Par-

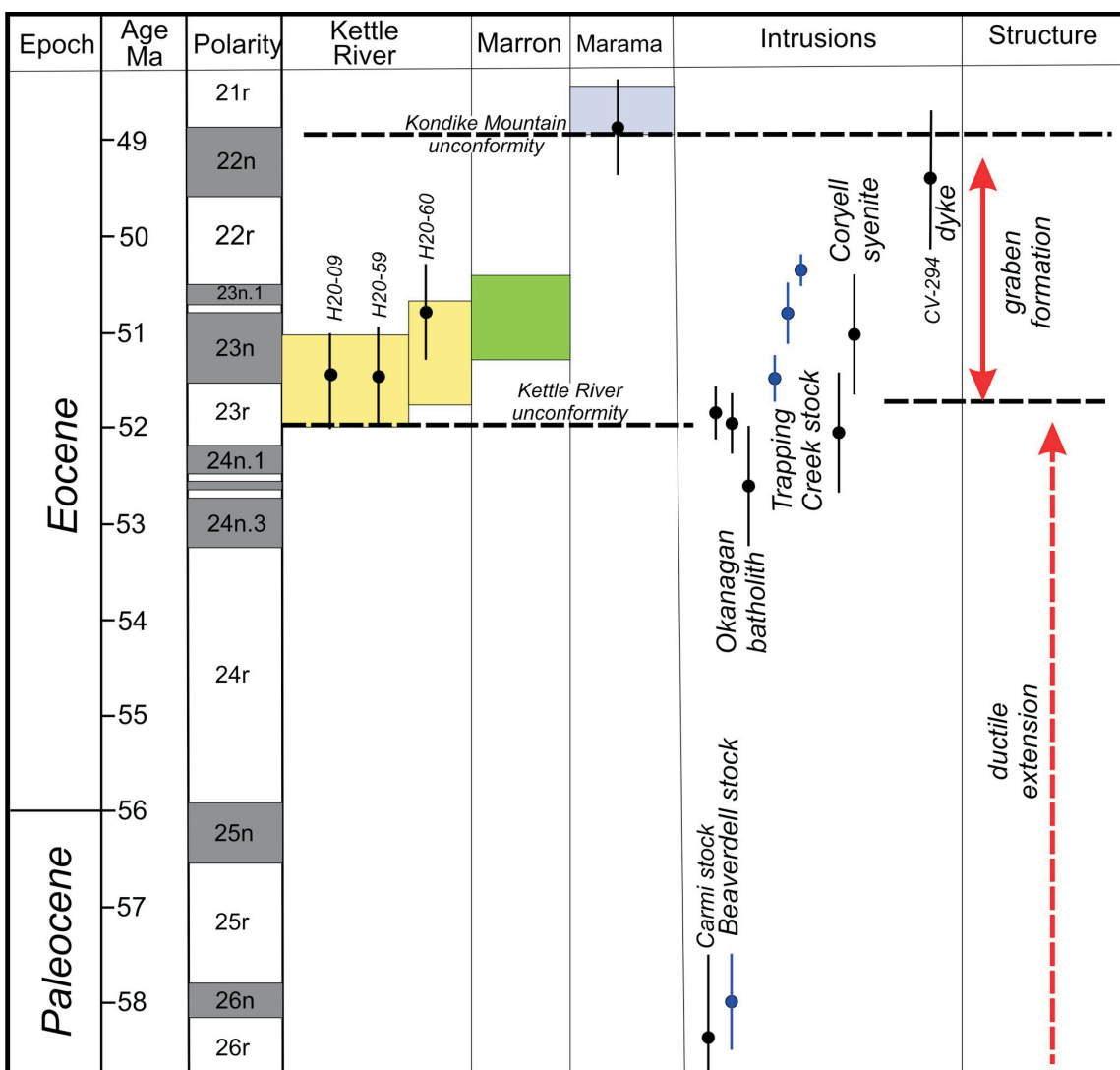


Figure 9. Geochronological chart of the Paleocene and Eocene Penticton Group and intrusions in the Boundary area, showing geochronology discussed in the text and geomagnetic polarities (after Wingate and Irvine, 1994). Note that the entire Kettle River and Marron formations were deposited in the developing grabens between ca. 51.5 and 49.5 Ma (intrusion ages from Höy et al., 2019).

kinson, 1986; Tempelman-Kluit, 1989). The Granby fault cuts Coryell syenite, dated at ca. 51.1 Ma (Carr and Parkinson, 1989), but is locally cut by Coryell dikes (Laberge and Pattison, 2007), which lends support to movement in the area continuing up to ca. 50 Ma (Parrish et al., 1988). Based on evidence from paleomagnetic data, Wingate and Irving (1994) argued that motion along the Granby fault began at or after 50.6 Ma and that motion along this and other extensional faults was limited to ‘short intervals’ of 1 to 2 million years. However, a number of regional studies indicate that extension and exhumation occurred over approximately 12 million years, from ca. 61 to 49 Ma (Kruckenberg et al., 2008) with early ductile movements and associated formation of migmatite and granite melts, followed by late, more brittle extensional faulting at higher structural levels. Based on $\text{Ar}^{40}/\text{Ar}^{39}$ analyses of biotite and

titanite in the Okanagan dome, Washington, Kruckenberg et al. (2008) determined that rapid cooling of leucosome pegmatites from ca. 51 to 47 Ma was related to rapid exhumation during graben formation.

Eocene Epithermal Mineralization

More than 2.5 million ounces of gold have been produced from Eocene low-sulphidation epithermal veins in the Republic and Curlew areas of Washington, less than 20 km south of Greenwood (Lasmanis, 1966; Muessig, 1967). The Greenwood area has seen an extended period of exploration and mining dating back to the 1880s, and much of this work is described by Peatfield (1978), Church (1986) and Fyles (1990). Recent exploration in the camp is described in numerous industry assessment reports, including summaries by Dufresne (2015) and Caron (2016). This pa-

per is intended to highlight the potential for discovery of epithermal deposits in Eocene volcanic rocks in the Boundary area north of Greenwood.

Most of the production from epithermal deposits in the Republic and Curlew areas are from a paleohorizon in the basal part of the Klondike Mountain Formation. However, as noted by Caron (2016), this paleosurface can cut down into and bevel any underlying stratigraphic horizon and, hence, epithermal mineralization can form in any host, including the Sanpoil, Marron or Kettle River formations, or in the underlying granitic rocks. Furthermore, examples of epithermal mineralization in Kettle River rocks that are overlain by Marron Formation imply mineralization is also related to the Kettle River paleosurface (L. Caron, pers. comm., 2020).

Two factors enhance the potential for discovery of epithermal mineralization in the Boundary area north of the Greenwood mining camp:

- recognition that the Marama or Klondike Mountain stratigraphy is locally present
- recognition that the basal Kettle River formation may also control epithermal mineralization

Klondike Mountain Formation Target Areas

There is little evidence of Klondike Mountain stratigraphy in the Boundary area north of the United States border. Little (1983) mapped some heterogeneous nonvolcanic epiclastic breccia south of Greenwood as Klondike Mountain but, subsequently, Fyles (1990) included these in the Marron Formation. Caron (2016) also suggested that some exposures with epithermal-style mineralization in the Marsh Creek area west of Midway, may be Klondike Mountain Formation. Farther north, northwest of Beaverdell, a succession of dacitic to trachytic tuff, similar to some exposures of either Marama, Klondike Mountain or Kettle River formations, unconformably overlies Eocene granite and Paleozoic metavolcanic rocks. There is no immediately underlying or overlying volcanic stratigraphy to constrain the age of the horizon. However, the U-Pb zircon age of 48.9 Ma (sample H19-149; no. 2 on Figure 1) defines this succession as part of the Marama Formation (or Klondike Mountain Formation), and possibly correlative with the Tom Thumb tuff member.

The age, or correlation, of other similar horizons throughout the Boundary area, characterized by basal conglomerate and felsic tuff or rhyolite, is generally not known. At the recently discovered Wad epithermal gold showing (Murton, 2020), tuffaceous sandstone and felsic tuff that unconformably overlie Eocene megacrystic granite may be equivalent in age to either the Kettle River or Marama formations (see below). Farther north, several other Eocene basins contain felsic tuff and rhyolite, and generally their

age or stratigraphic position is not well established (e.g., Tempelman-Kluit, 1983; Okulitch, 2013). These and other horizons have been variously and successfully explored for epithermal mineralization (e.g., Lenard, 1996; Caron, 2015).

Kettle River Host

Several occurrences of epithermal precious-metal deposits are documented in the Greenwood camp (e.g., Dufresne, 2015; Caron, 2016) and farther north in the Franklin camp (Caron, 2005). Recently, a low-sulphidation epithermal-gold occurrence, the Wad property, was discovered in rocks correlated with the Kettle River Formation in the central part of the Rock Creek graben, approximately 30 km north of Rock Creek (Murton, 2020).

Hostrocks on the Wad property are mainly highly altered tuffaceous sandstone, felsic tuff, trachyte and trachyte breccia that have been mapped as Kettle River Formation (Höy and Jackaman, 2016) but which could possibly be correlated with the younger Tom Thumb member of the Klondike Mountain Formation, as suggested by Murton (2020). These rocks unconformably overlie Taurus Lake megacrystic granite dated at ca. 67–63 Ma (Höy et al., 2019) and are unconformably overlain by basalt of the Miocene Kallis Formation. The deposit is within a northwest-trending, fault-bounded paleohigh that crosses the western margin of the Rock Creek graben (Höy and Jackaman, 2016).

At the Wad property, a zone of intense alteration, with carbonate (calcite), drusy quartz and chalcedony, adularia and possibly alunite, occurs within breccias over a strike length of approximately 1 km, with anomalous values of gold ranging up to 2.4 g/t (Murton, 2020).

Summary

The basal part of the Eocene Penticton Group, the Kettle River and Marron formations, was deposited mainly in the north-trending Rock Creek graben and along the northern inferred extension of the Republic graben over a relatively short time period, from ca. 51.5 to 49.5 Ma. Graben development initiated in the hangingwall of the Granby fault, along with deposition of basal Kettle River conglomerate, sandstone and locally felsic tuff, after an extended period of regional ductile extension and magma generation lasting 10 to 12 million years.

Marama Formation conglomerate, sandstone and felsic to alkalic tuff unconformably overlie Marron formation rocks in several locations north and west of the Boundary area. Exposures of Marama trachytic tuff northwest of Beaverdell and west of the Rock Creek graben are similar in age (48.9 Ma) and are correlated with the basal part of the Klondike Mountain Formation in Washington. Northwest

of Beaverdell, the Marron and Kettle River formations are missing, and the Marama unconformably overlies Eocene granite and Paleozoic ‘basement’ on a tectonic high along the margins of the graben. It is probable that other similar exposures record Marama or basal Klondike Mountain stratigraphy rather than the lithologically similar basal Kettle River Formation.

Most epithermal mineralization in the highly productive Republic and Curlew camps in northern Washington is related to the basal Klondike Mountain Formation unconformity, within or directly overlying Sanpoil volcanic rocks. The recognition of correlative Marama Formation rocks in the Boundary area enhances the potential for discovery of epithermal mineralization here as well.

A recently discovered, low-sulphidation epithermal-gold prospect, the Wad occurrence, in a structural paleohigh in the Rock Creek graben may be evidence of mineralization in the basal Kettle River horizon, which is similarly host to some epithermal deposits in the Greenwood camp to the south.

In summary, geological mapping and geochronological dating in the Boundary area have more clearly defined the relationship between the deposition of the early Penticton Group volcanic rocks, brittle extensional faulting and intrusion of high-level Eocene plutonic rocks (Höy et al., 2020). The early Eocene, specifically ca. 51.5 to 49.5 Ma, was a period of extensive volcanism, graben formation, rapid uplift and intrusive activity, conditions that were conducive to the formation of mineral deposits, including epithermal precious-metal mineralization.

Acknowledgments

Field assistance by I. Hutcheon in 2020, and G. DeFields and Chilco in 2019 is gratefully acknowledged. Discussions with industry personnel L. Carron, M. Dufresne and W. Murton were much appreciated. The manuscript benefited from the editorial comments of G. Ray, G. DeFields, F. Katay and staff members of Geoscience BC.

References

- Bardoux, M. and Irving, E. (1989): Paleomagnetism of Eocene rocks of the Kelowna and Castlegar areas, British Columbia: studies in determining paleohorizontal; Canadian Journal of Earth Sciences, v. 26, p. 829–844.
- Bostock, H.S. (1941): Okanagan Falls, Similkameen and Osoyoos districts, British Columbia; Geological Survey of Canada, Map 627A, scale 1:63 360, URL <<https://doi.org/10.4095/106956>>.
- Caron, L. (2005): Assessment report on the 2004 exploration program: rock sampling, trenching, diamond drilling, Union property, Franklin camp, Greenwood Mining Division, British Columbia; BC Ministry of Energy, Mines and Low Carbon Innovation, Assessment Report 27 604, 37 p., URL <http://aris.empr.gov.bc.ca/search.asp?mode=repsum&rep_no=27604> [November 2012].
- Caron, L. (2015): Assessment report, soil and rock geochemistry, IP, biogeochemistry and diamond drilling on the Brett property, Whiteman Creek area; BC Ministry of Energy, Mines and Low Carbon Innovation, Assessment Report 35447, URL <http://aris.empr.gov.bc.ca/search.asp?mode=repsum&rep_no=35447> [November 2020].
- Caron, L. (2016): 2016 Assessment report: geology, rock, soil and silt geochemistry, trenching on the Grizzly Greenwood property, Greenwood Mining Division, British Columbia; BC Ministry of Energy, Mines and Low Carbon Innovation, Assessment Report 36633, 45 p., URL <http://aris.empr.gov.bc.ca/search.asp?mode=repsum&rep_no=36633> [November 2020].
- Carr, S.D. and Parkinson, D.L. (1989): Eocene stratigraphy, age of the Coryell batholith, and extensional faults in the Granby valley, southern British Columbia; in Current Research Part A, Geological Survey of Canada, Paper 89-1E, p. 79–87.
- Cheney, E.S. (1994): Cenozoic unconformity-bounded sequences of central and eastern Washington; Washington Division of Geology and Earth Resources, Bulletin 80, p. 115–139.
- Cheney, E.S. (1998): Guide to the geology of north-central Washington; Northwest Geological Society, Guidebook 17, 97 p.
- Church, B.N. (1973): Geology of the White Lake basin; BC Ministry of Energy, Mines and Low Carbon Innovation, BC Geological Survey, Bulletin 61, 120 p., URL <<http://www2.gov.bc.ca/gov/content/industry/mineral-exploration-mining/british-columbia-geological-survey/publications/bulletins>> [November 2020].
- Church, B.N. (1986): Geological setting and mineralization in the Mount Attwood-Phoenix area of the Greenwood camp; BC Ministry of Energy, Mines and Low Carbon Innovation, BC Geological Survey, Paper 1986-2, 70 p., URL <<http://www2.gov.bc.ca/gov/content/industry/mineral-exploration-mining/british-columbia-geological-survey/publications/papers-1999-1980>> [November 2020].
- Daly, R.A. (1912): Geology of the North American Cordillera at the forty-ninth parallel; Geological Survey of Canada, Memoir 249, 857 p.
- Dufresne, M. (2015): Assessment report for 2012 exploration, Greenwood property, southern British Columbia; BC Ministry of Energy, Mines and Low Carbon Innovation, Assessment Report 34747, 66 p.
- Fyles, J.T. (1990): Geology of the Greenwood–Grand Forks area, British Columbia; BC Ministry of Energy, Mines and Low Carbon Innovation, Open File 1990-25, 19 p.
- Höy, T. (2007): Geology and rock geochemistry, Chenier property, Kelly Creek area, southern British Columbia; BC Ministry of Energy, Mines and Low Carbon Innovation, Assessment Report 28 960, 32 p., URL <http://aris.empr.gov.bc.ca/search.asp?mode=repsum&rep_no=28960> [September 2019].
- Höy, T. and DeFields, G.M. (2017): Geology of the northern extension of the Rock Creek graben, Christian Valley map area, south-central British Columbia (NTS 082E/10); in Geoscience BC Summary of Activities 2016, Geoscience BC, Report 2017-1, p. 245–256, URL <http://www.geosciencebc.com/i/pdf/SummaryofActivities2016/SoA2016_Hoy.pdf> [December 2020].
- Höy, T. and Jackaman, W. (2005): Geology of the Grand Forks map sheet, British Columbia (NTS 082E/01); BC Ministry

- of Energy, Mines and Low Carbon Innovation, Geoscience Map 2005-2, scale 1:50 000.
- Höy, T. and Jackaman, W. (2016): Geology of the Almond Mountain map sheet (NTS 82E/07); Geoscience BC, Map 2016-08, scale 1:50 000, URL <http://cdn.geosciencebc.com/project_data/GBCReport2016-08/GBC_Map2016-08_Almond.pdf> [November 2020].
- Höy, T. and Jackaman, W. (2017): Geology of the Christian Valley map sheet (NTS082E/10); Geoscience BC, Map 2017-10, scale 1:50 000, URL <http://www.geosciencebc.com/i/project_data/GBCReport2017-10/GBC_Map2017-10_CV.pdf> [December 2020].
- Höy, T. and Jackaman, W. (2019): Geology of the Penticton map sheet (east-half); Geoscience BC, Map 2019-04, scale 1:150 000, URL <http://cdn.geosciencebc.com/project_data/GBCR2019-04/GBCMap2019-04.pdf> [November 2020].
- Höy, T., Friedman, R. and Gabites, J. (2020): Porphyry, base-metal and gold potential in the Boundary area, southern British Columbia (NTS 082E); *in* Geoscience BC Summary of Activities 2019: Minerals, Geoscience BC, Report 2020-01, p. 23–33, URL <http://www.geosciencebc.com/summary-of-activities-2019/Minerals/Project%2018-011_Minerals_SOA2019.pdf> [November 2020].
- Höy, T., Gabites, J., Friedman, R. and Dunne, K. (2019): Summary report, U-Pb and Ar/Ar dating, Penticton east-half (082E½); Geoscience BC, supplementary report to Geoscience BC Map 2019-04, 122 p., URL <http://www.geosciencebc.com/i/project_data/GBCR2019-04/GBCMap2019-04-Supp_Geochronology_PetrographyRpt.pdf> [November 2020].
- Kruckenberg, S.C., Whitney, L., Teyssier, C., Fanning, C.M. and Dunlap, W.J. (2008): Paleocene–Eocene migmatite crystallization, extension, and exhumation in the hinterland of the northern Cordillera: Okanogan dome, Washington, USA; Geological Society of America, Bulletin, v. 120, p. 912–929.
- Laberge, J.R. and Pattison, D.R.M. (2007): Geology of the western margin of the Grand Forks complex: high grade Cretaceous metamorphism followed by early Tertiary extension on the Granby fault; Canadian Journal of Earth Sciences, v. 44, p. 199–208.
- Lasmanis, R. (1966): A historical perspective on ore formation, concepts, Republic Mining Districts, Ferry County, Washington; Washington State Department of Natural Resources, Washington Geology, v. 24, no. 2, p. 8–14.
- Lenard, N.C. (1996): Host claim, Mount Swite: 15 km NW of the city of Kelowna, Vernon Mining Division, British Columbia; BC Ministry of Energy, Mines and Low Carbon Innovation, Assessment Report 24 594, 15 p.
- Little, H.W. (1957): Kettle River, east half, Similkameen, Kootenay and Osoyoos districts, British Columbia; Geological Survey of Canada, Map 6-1957, scale 1:253 440, URL <<https://doi.org/10.4095/108451>>.
- Little, H.W. (1983): Geology of the Greenwood map-area, British Columbia; Geological Survey of Canada, Paper 79-22, 37 p.
- Massey, N. (2006): Boundary project: reassessment of Paleozoic rock units of the Greenwood area (NTS 082E/02), southern BC; *in* Geological Fieldwork 2005, BC Ministry of Energy, Mines and Low Carbon Innovation, BC Geological Survey, Paper 2006-01, p. 99–108, URL <<http://www2.gov.bc.ca/gov/content/industry/mineral-exploration-mining/british-columbia-geological-survey/publications/papers#2006>> [November 2020].
- Massey, N. (2007): Geology and mineral deposits of the Rock Creek area, British Columbia; BC Ministry of Energy, Mines and Low Carbon Innovation, BC Geological Survey, Open File 2007-7, 1 map, scale 1:25 000, URL <<http://www2.gov.bc.ca/gov/content/industry/mineral-exploration-mining/british-columbia-geological-survey/publications/openfiles-2009-2000>> [November 2020].
- Mathews, W.H. (1963): Thirteen potassium-argon dates of Cenozoic volcanic rocks from British Columbia; University of British Columbia, Department Geological Report 2.
- Mathews, W.H. (1964): Potassium-argon age determinations of Cenozoic volcanic rocks from British Columbia; Geological Society of America, Bulletin, v. 47, p. 465–468.
- Monger, J.W.H. (1968): Early Tertiary stratified rocks, Greenwood map area (82E/02), British Columbia; Geological Survey of Canada, Paper 67-42, 39 p.
- Muessig, S. (1967): Geology of the Republic Quadrangle and a part of the Aeneas Quadrangle, Ferry County, Washington; U.S. Geological Survey, Bulletin 1216, 141 p.
- Murton, J.W. (2020): 2020 Assessment report, rock sampling and geological mapping program on the Wad claims, Greenwood Mining Division; BC Ministry of Energy, Mines and Low Carbon Innovation, Assessment Report 39 060, 18 p.
- Okulitch, A.V. (2013): Geology, Okanagan watershed, British Columbia; Geological Survey of Canada, Open File 6839, 1 map, scale 1:100 000.
- Parrish, R.R., Carr, S.D. and Parkinson, D.L. (1988): Eocene extensional tectonics and geochronology of the southern Omineca belt, British Columbia and Washington; Tectonics, v. 72, p. 181–212.
- Pearson, R.C. and Obradovich, J.D. (1977): Eocene rocks in northeast Washington – radiometric ages and correlations; United States Geological Survey, Bulletin 1433, 41 p.
- Peatfield, G.R. (1978): Geologic history and metallogeny of the “Boundary District”, southern British Columbia and northern Washington; Ph.D. thesis, Queens University, Kingston, Ontario.
- Preto, V.A. (1970): Structure and petrology of the Grand Forks Group; Geological Survey of Canada, Paper 69-2, 80 p.
- Rouse, G.E. and Mathews, W.H. (1961): Radioactive dating of Tertiary plant-bearing deposits: Science, v. 133, p. 1079–1080.
- Tempelman-Kluit, D.J. (1989): Geology, Penticton, west of the sixth meridian, British Columbia; Geological Survey of Canada, Map 1736A, scale 1:250 000, URL <<https://doi.org/10.4095/127379>>.
- Tempelman-Kluit, D.J. and Parkinson, D. (1986): Extension across the Eocene Okanagan crustal shear in southern British Columbia; Geology, v. 14, p. 318–321.
- Thompson, R.I., Cook, F. and Hetherington, R. (2018): Cu-Au property, Kelly River area, southcentral British Columbia: the case for a Paleogene porphyry Cu system; BC Ministry of Energy, Mines and Low Carbon Innovation, Assessment Report 37 196, 132 p.
- Whiting, F.B. (1991): Geological sampling report, Copket Group, Copperkettle Creek; BC Ministry of Energy, Mines and Low Carbon Innovation, Assessment Report 21 534, 22 p.
- Wingate, M.T.D. and Irvine, E. (1994): Extension in high-grade terranes of the southern Omineca Belt, British Columbia: evidence from paleomagnetism; Tectonics, v. 13, p. 686–711.

Development of Rare-Earth Elements Database for the East Kootenay Coalfield of Southeastern British Columbia (NTS 082G/10, 15) Using Field Collected Samples: Preliminary Results

V.K. Kuppusamy, NBK Institute of Mining Engineering, The University of British Columbia, Vancouver, British Columbia, vinothkumar@alumni.ubc.ca

M.E. Holuszko, NBK Institute of Mining Engineering, The University of British Columbia, Vancouver, British Columbia

Kuppusamy, V.K. and Holuszko, M.E. (2021): Development of rare-earth elements database for the East Kootenay coalfield of southeastern British Columbia (NTS 082G/10, 15) using field collected samples: preliminary results; *in* Geoscience BC Summary of Activities 2020: Minerals, Geoscience BC, Report 2021-01, p. 67–74.

Introduction

Rare-earth elements (REEs) are the group of 17 elements in the periodic table that include 15 lanthanides and two chemically similar transition metals—scandium and yttrium. Using their atomic number, REEs are classified as heavy REEs (HREEs) or light REEs (LREEs), with elements from Tb to Lu and Y belonging to the former group and La to Gd and Sc belonging to the latter group (Moldoveanu and Papangelakis, 2013; Zhang et al., 2015). With the emergence of new clean energy and defence-related technologies, consumption of REEs has increased rapidly (Tse, 2011). For example, it is projected that the demand for dysprosium, one of the REEs, is expected to increase by as much as 2600% by 2025 (Standing Committee on Natural Resources, 2014). In addition, traditional rare-earth ore deposits are fast depleting and supply is only expected to meet demand for next 15–20 years (Seredin and Dai, 2012). Based on the projected dwindling supply and increasing demand, REEs are classified as critical elements by the United States and the European Union due to their importance in clean energy and defence applications (U.S. Department of Energy, 2010; Deloitte Sustainability et al., 2017). The National Energy Technology Laboratory (NETL) in the United States has conducted a prospective analysis of coal deposits as a source of REEs using the U.S. Geological Survey's (USGS) coal database, which contains the concentrations of REEs in coalfields across the United States (Bryan et al., 2015). The NETL has launched a research and development program to demonstrate the techno-economic feasibility of developing domestic technologies to separate REEs from coal and/or its byproducts. The study uses samples that contain a minimum of 300 ppm total REEs and concentrating the REEs to a level greater than or equal to 2% (by weight) in processed streams (U.S.

Department of Energy, 2016). The program will focus on areas of research such as resource sampling and characterization, separation technology development, REE sensor development, process and systems modelling, and techno-economic analyses (U.S. Department of Energy, 2016).

There is indication of the presence of REEs in some Canadian coal deposits, especially in British Columbia (BC) coalfields (Goodarzi, 1988; Birk and White, 1991; Goodarzi et al., 2009), however, there is no proper quantification, characterization and extraction analysis currently available for coal deposits in BC or for other coal deposits across Canada. The first objective of this study is to develop a database of REE occurrences in the East Kootenay coalfield (Figure 1), from samples collected in the field, and to identify the best potential coal sources of REEs in the study area. Using the collected data, phase two of the study will explore the possibility of extracting these critical elements from these sources. Some of the initial results of this study were reported previously (Kumar et al., 2018; Kuppusamy and Holuszko, 2019).

Background

Abundance of REEs in Coal

Table 1 shows the average concentration of REEs in coal from different countries, such as the United States, China, the Democratic People's Republic of Korea and Turkey, in comparison to average values for the upper continental crust, black shale and world coal on a whole coal basis. The average REE concentration in world coal on a whole coal basis is 72 ppm (Seredin and Finkelman, 2008; Ketris and Yudovich, 2009), which is 2.5 times lower than the upper continental crust (179 ppm; Taylor and McLennan, 1985) and the average black shale value (182 ppm; Ketris and Yudovich, 2009). The average concentration of REEs in Chinese coal is 101–138 ppm (Dai et al., 2008; Zhang et al., 2015) and is 1.5–2 times the world's average. Similar results were observed for Turkish coal (Karayigit et al., 2000;

This publication is also available, free of charge, as colour digital files in Adobe Acrobat® PDF format from the Geoscience BC website: <http://geosciencebc.com/updates/summary-of-activities/>.

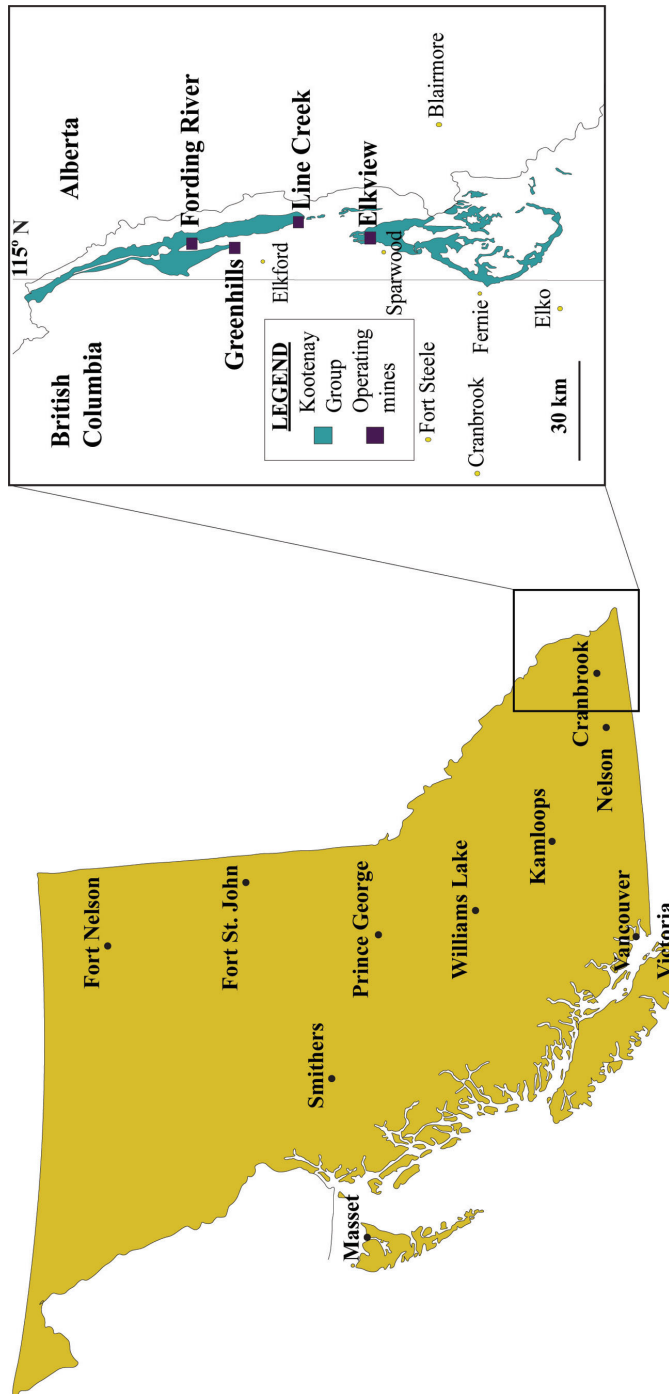


Figure 1. Location of East Kootenay coalfield and operating coal mines in southeastern British Columbia (adapted from BC Geological Survey, 2019).

Table 1. Concentration of rare-earth elements (on a whole coal basis; ppm) in coal from different countries in comparison to concentrations in the upper continental crust and black shale. Abbreviations: HREE, heavy rare-earth elements; LREE, light rare-earth elements; ND, no data; REE, rare-earth elements.

Coal	La	Ce	Pr	Nd	Sm	Eu	Gd	Tb	Dy	Y	Ho	Er	Tm	Yb	Lu	Sc	Total REEs	LREEs	HREEs
Upper continental crust ¹	30	64	7.1	26	4.5	0.88	3.8	0.64	3.5	22	0.8	2.3	0.33	2.2	0.32	11	179	147	32
Black shale ²	28	58	4.2	33	5.4	1.2	4.7	0.75	3	26	0.52	1.9	0.4	2.8	0.4	12	182	147	36
World coal ^{2,8}	11	23	3.5	12	2	0.47	2.7	0.32	2.1	8.4	0.54	0.93	0.31	1	0.2	3.9	72	59	14
American coal ³	12	21	2.4	9.5	1.7	0.4	1.8	0.3	1.9	8.5	0.35	1	0.15	0.95	0.14	ND	62	49	13
Chinese coal ⁴	26	49	5.5	22	4.3	0.9	3.7	0.7	3.1	18	0.7	1.9	0.27	2.1	0.3	ND	138	111	27
Chinese coal ⁵	18	35	3.8	15	3	0.5	3.4	0.52	3.1	9	0.73	2.1	0.34	2	0.32	4	101	83	18
Turkish coal ^{6,8}	21.12	39.24	4.71	16.85	3.18	0.76	3	0.45	2.42	12.76	0.47	1.37	0.21	1.35	0.21	7.92	116	97	19
North Korean coal ⁷	14.5	27.2	2.9	11.1	2.3	0.5	1.4	0.3	2	7.2	0.4	1.1	0.3	1	ND	4.9	77	65	12

¹Taylor and McLennan, 1985; ²Ketris and Yudovich, 2009; ³Finkelman, 1993; ⁴Dai et al., 2008; ⁵Zhang et al., 2000; ⁶Karayigit et al., 2015; ⁷Hu et al., 2006; ⁸Seredin and Finkelman, 2008

Zhang et al., 2015). But the average concentration in coals from the United States and Democratic People's Republic of Korea is close to the world's average (Finkelman, 1993; Hu et al., 2006). The average REEs concentration in world coal on an ash basis is 404 ppm (Seredin and Dai, 2012). However, coal with enriched concentrations of REEs on an ash basis have been found in different coalfields such as in the Sydney Coal Basin, Nova Scotia, Canada (72–483 ppm; Birk and White, 1991), the Far East, Russia (300–1000 ppm; Seredin, 1996) and the Fire Clay coal bed, central Appalachian basin, United States (500–4000 ppm; Hower et al., 1999). Approximately 80% of the total concentration of REEs in coal is LREEs (Zhang et al., 2015). The anomalies of REE enrichment in coal and REE distribution patterns are discussed in detail elsewhere (Dai et al., 2016).

Some of the enriched coal (0.68 to 2.03% of rare earth oxide) has REE concentrations comparable to traditional commercial rare-earth deposits and coal ashes from coal mining operations can be viewed as a potential source for these elements (Seredin and Dai, 2012).

U.S. Geological Survey's COALQUAL Database

During the 1970s energy crisis, the USGS developed the National Coal Resources Data System (NCRDS), which is a comprehensive database on coal resources in the United States (Finkelman et al., 1994). The USCHEM, a coal quality geochemical database for the United States, is an interactive digital version of the NCRDS, which contains information on more than 13 000 samples from major coal basins in the United States (Palmer et al., 2015). The COALQUAL database, which contains a subset of 7430 samples from USCHEM database, was published in 1994 (Bragg et al., 1994). For each sample, 136 parameters were collected including coal type, proximate analysis data, ultimate analysis data, and major-, minor- and trace-elements analysis data (Finkelman et al., 1994). Figure 2 shows an example of a COALQUAL sample detail page. In 2015, the updated version (3.0) of the COALQUAL database was published with 7657 samples (Palmer et al., 2015). Using the original database as a guideline, further investigations were carried out to characterize and physically enrich the REE from coal-related feedstocks (e.g., produced coals, coal waste, coal ash from power plants) in the United States (Akdogan and Ghosh, 2014; Honaker et al., 2015; Miskovic, 2015; Soundarajan et al., 2015).

Objectives

The purpose of this investigation is to assess BC coal deposits as possible sources for extraction of REEs. The assessment will be performed by creating a database of REE distribution in the East Kootenay coalfield; it will be a simplified version of the USGS COALQUAL database. The

first phase of the project will be the development of a database, which starts with the collection of roof, floor, partings and coal samples in the study area. These samples will be characterized and analyzed by inductively coupled plasma–mass spectrometry (ICP-MS), sequential extraction, X-ray diffraction (XRD) and scanning electron microscope (SEM). Phase two of the project will focus on the advanced characterization of the REEs and development of the physical methods used to enrich the REE from the coal-related feedstocks.

Materials and Methods

Sampling

For the purpose of developing the REE database, coal seam (referred to as coal) samples along with their corresponding roof, floor and partings samples were collected from the East Kootenay coalfield and shipped in barrels to the Coal and Mineral Processing Laboratory at The University of British Columbia (Vancouver, BC). All the samples used in this study were collected by geologists from their respective mines to enhance the quality of the collected samples. Representative samples were obtained for further testing using the standard procedure for coal sample preparation—ASTM D2013/D2013M-12 (2012). Proximate analysis was conducted in duplicate on the representative samples using the standard methods—ASTM D3172-13 (2013), D3173/D3173M-17a (2017), D3174-12 (2012) and D3175-17 (2017).

Chemical Analysis of REEs and Other Minor Elements

For total REE quantification, feed and test product samples (0.2 g) were added to lithium metaborate and lithium tetraborate flux and mixed thoroughly. The samples were then fused in a furnace at 1025°C. Finally, resulting melts were cooled and digested in an acid mixture containing nitric, hydrochloric and hydrofluoric acids. The digested solutions were then analyzed by ICP-MS. The analytical results were corrected for interelemental spectral interference. In this study, REEs in coal are expressed as follows: on a whole coal basis (REE concentration in the coal sample) and on an ash basis (REE concentration in the ash of the coal sample).

Base metal and other minor elements were analyzed by four-acid digestion followed by inductively coupled plasma–emission spectroscopy (ICP-ES). For a few highly reactive samples, aqua-regia digestion was used for the analysis. All the chemical analysis was conducted by ALS-Geochemistry (North Vancouver, BC).

Results and Discussions

Since more samples are currently being collected for the study, this paper only contains preliminary results based on

Sample Detail for W218790

Sample Description		Proximate & Ultimate		Oxide	Trace Element
Sample ID	W218790	Sample ID	W218790	Sample ID	W218790
State	Kentucky	Moisture	3.53	Remnant Moisture	1.23
County	CLAY	Moisture Q		Remnant Moisture Q	<u>g</u>
Latitude	37.2203	Volatile Matter	39.99	GSAsh	4.1
Longitude	-83.8561	Volatile Matter Q		GSAsh Q	
Province	EASTERN	Fixed Carbon	52.34	SiO ₂	49.2
Region	CENTRAL APPALACHIAN	Fixed Carbon Q		SiO ₂ Q	<u>g</u>
Field		Standard Ash	4.14	Al ₂ O ₃	32.7
District	SOUTHWESTERN	Standard Ash Q		Al ₂ O ₃ Q	<u>g</u>
Formation	BREATHITT	Proximate Validation	Acceptable	CaO	1.65
Group		Hydrogen	5.38	CaO Q	<u>g</u>
Bed	MANCHESTER	Hydrogen Q		MgO	0.764
Member		Carbon	77.2	MgO Q	<u>g</u>
Coal Zone		Carbon Q		MnO	0.0057
Depth (in)	0	Nitrogen	1.8	MnO Q	
Thickness (in)	9.4	Nitrogen Q		Na ₂ O	0.932
System	Pennsylvanian	Oxygen	7.39	Na ₂ O Q	<u>g</u>
Series/Epoch		Oxygen Q		K ₂ O	1.26
Literature		Sulfur	0.56	K ₂ O Q	<u>g</u>
Comments		Sulfur Q		Fe ₂ O ₃	3.27
Map	MANCHESTER (7.5')	Ultimate Validation	Excellent	Fe ₂ O ₃ Q	<u>g</u>
Collector	KYGS-CURRENS J C	Btu	13915	TiO ₂	1.49
Mine/Power Plant	SURFACE MINE	Btu Q		TiO ₂ Q	<u>g</u>
Drill Core No		Sulfate Sulfur	0.01	P ₂ O ₅	
Point Id	KGS 698	Sulfate Sulfur Q		P ₂ O ₅ Q	<u>g</u>
Submit Date	12/16/1982	Pyritic Sulfur	0.03	SO ₃	
Sample Description	BITUMINOUS COAL	Pyritic Sulfur Q		SO ₃ Q	<u>g</u>
Estimated Rank	BITUMINOUS	Organic Sulfur	0.52	LOI	
Apparent Rank	High volatile A bituminous	Organic Sulfur Q			
Analytical Labs	GT and USGS	Ash Deformation	2800		
Sample Type	Channel	Ash Deformation Q	<u>G</u>		
Analysis Type	As Received	Ash Softening	2800		
Values Represent	Single sample	Ash Softening Q	<u>G</u>		
Township		Ash Fluid	2800		
Range		Ash Fluid Q	<u>G</u>		

Figure 2. Example of a 'Sample Detail' page from the U.S. Geological Survey's (USGS) COALQUAL database (Palmer et al., 2015).

the early sample data from 49 samples. Results of the proximate analysis of the coal samples are shown in Table 2. According to ASTM D388-17 (2017), all the coal samples are classified as medium volatile bituminous coal, which is largely a metallurgical quality grade. For the database, more than 60 parameters were collected for each sample including type, proximate analysis results and major-, minor- and trace-elements data. The complete dataset will be released in the future. Seam ID and the specific locations of the individual samples are not supplied to maintain a confidentiality agreement.

Among the samples analyzed, the REE concentration on ash basis varies from 137 to 686 ppm. Table 3 shows that REE concentrations on ash basis are similar for roof, floor and partings material, whereas coal showed enhanced concentrations of REEs. Among the 17 REEs, the five elements of Ce, La, Nd, Y and Sc accounted for more than 80% of the total REE present in these samples. Figure 3 shows that on a whole coal basis, however, the concentration of REE increases with the ash content of the material. This

indicates the association of REE with mineral matter, which is comparable with previously published results (Kuppusamy and Holuszko, 2019). During the coal beneficiation process, the REEs associated with mineral matter are generally concentrated into waste tailings streams.

Preliminary Economic Evaluation for BC Coal Samples

Seredin and Dai (2012) estimated that a coal seam with a thickness greater than 5 m may be considered as a potential source of REEs if its rare-earth oxide content is above 800–900 ppm on an ash basis. Zhang et al. (2015) estimated the minimum average REE content to be 720 ppm on an ash basis, assuming a valence state of +3 for all of the REEs and a relative atomic mass of 132.5. In the United States, coal seams with an REE content of more than 300 ppm on ash basis are considered a potential source of REEs (U.S. Department of Energy, 2016).

It can be inferred that the REE concentration in the feed samples (see Figure 4) did not meet the cutoff grade as pro-

Table 2. Proximate analysis results for coal samples (as-determined basis) from the East Kootenay coalfield, southeastern British Columbia.

Sample ID	Type	Moisture content (%)	Ash content (%)	Volatile matter (%)	Fixed carbon (%)
10	Coal	2.41	7.24	22.85	67.5
11	Coal	2.81	10.12	21.92	65.14
12	Coal	2.39	7.66	23	66.95
13	Coal	2.41	7.52	22.92	67.14
14	Coal	2.43	7.93	23.02	66.62
15	Coal	2.5	10.46	22.3	64.74
16	Coal	2.62	5.1	24.08	68.2
17	Coal	2.1	5.29	23.69	68.93
18	Coal	2.09	20.24	27.29	50.38
19	Coal	2.75	7.37	25.68	64.2
20	Coal	1.36	12.39	24.67	61.59
22	Coal	0.85	19.05	19.39	60.71
26	Coal	1.25	7.84	22.73	68.19
27	Coal	1.24	13.19	19.32	66.26
41	Coal	1.31	20.74	23.11	54.84
48	Coal	0.66	20.34	20.15	58.85
49	Coal	0.87	15.06	22.16	61.91

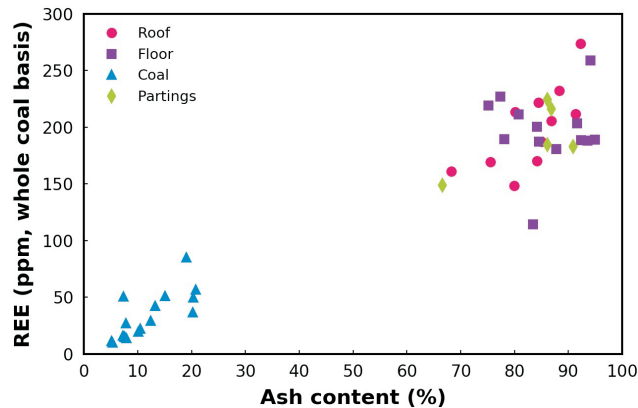


Figure 3. Rare-earth element (REE) concentration (on whole coal basis; ppm) versus ash content (%) for the roof, floor, coal and partings samples from the East Kootenay coalfield, southeastern British Columbia.

posed by Seredin and Dai (2012), but some of the coal showed significant potential. Using the U.S. Department of Energy's (2016) resource cutoff of 300 ppm of REE on an ash basis, it can be concluded that some of the samples met the cutoff grade requirements.

Outlook coefficient (C_{outl}) is another factor that can be used to assess the quality of the REEs present in the coal seam. It is defined as the ratio between the relative amounts of critical REEs in the sample to the relative amounts of excessive REEs in the sample (Seredin and Dai, 2012). It can be calculated as

$$C_{outl} = \frac{\text{sum concentrations of Nd, Eu, Tb, Dy, Er, Y}}{\text{total REE concentration}} / \frac{\text{sum concentrations of Ce, Ho, Tm, Yb, Lu}}{\text{total REE concentration}}$$

A higher value for this index represents a higher market value for the REEs in the coal seam since the concentration of critical REEs increases with the index. Dai et al. (2017) proposed an evaluation plot using REE concentration and C_{outl} . In this study, a similar plot was used (Figure 4) but modified to accommodate the resource cutoff suggested by the U.S. Department of Energy (2016). Accordingly, all of the samples were divided into five categories: unpromising

source ($\text{REE} < 300 \text{ ppm}$ on ash basis or $C_{outl} < 0.7$); promising resource ($300 < \text{REE} < 720 \text{ ppm}$ on ash basis and $0.7 < C_{outl} < 2.4$); highly promising resource ($300 < \text{REE} < 720 \text{ ppm}$ on ash basis and $C_{outl} > 2.4$); promising source ($\text{REE} > 720 \text{ ppm}$ on ash basis and $0.7 < C_{outl} < 2.4$); and highly promising source ($\text{REE} > 720 \text{ ppm}$ on ash basis and $C_{outl} > 2.4$).

The C_{outl} values for most of the samples are greater than 1, implying that the critical REE concentration is significant and accounts for,

Table 3. Maximum, minimum and average rare-earth element (REE) concentrations (on ash basis; ppm) in the roof, floor, coal and partings samples from the East Kootenay coalfield, southeastern British Columbia.

Type	Maximum	Minimum	Average
Roof	296.8	185.7	238.8
Floor	293.3	136.9	230.2
Coal	685.9	172.8	273.5
Partings	260.4	201.2	229.6

Table 4. Maximum, minimum and average heavy rare-earth elements (HREEs) to light rare-earth elements (LREEs) ratio and outlook coefficient in the different coal sample types from East Kootenay coalfield, southeastern British Columbia.

Type	HREEs/LREEs			Outlook coefficient		
	Maximum	Minimum	Average	Maximum	Minimum	Average
Roof	0.36	0.20	0.27	1.28	0.83	1.03
Floor	0.33	0.18	0.26	1.22	0.85	1.02
Coal	0.54	0.27	0.36	1.54	0.92	1.21
Partings	0.34	0.21	0.28	1.27	0.82	1.10

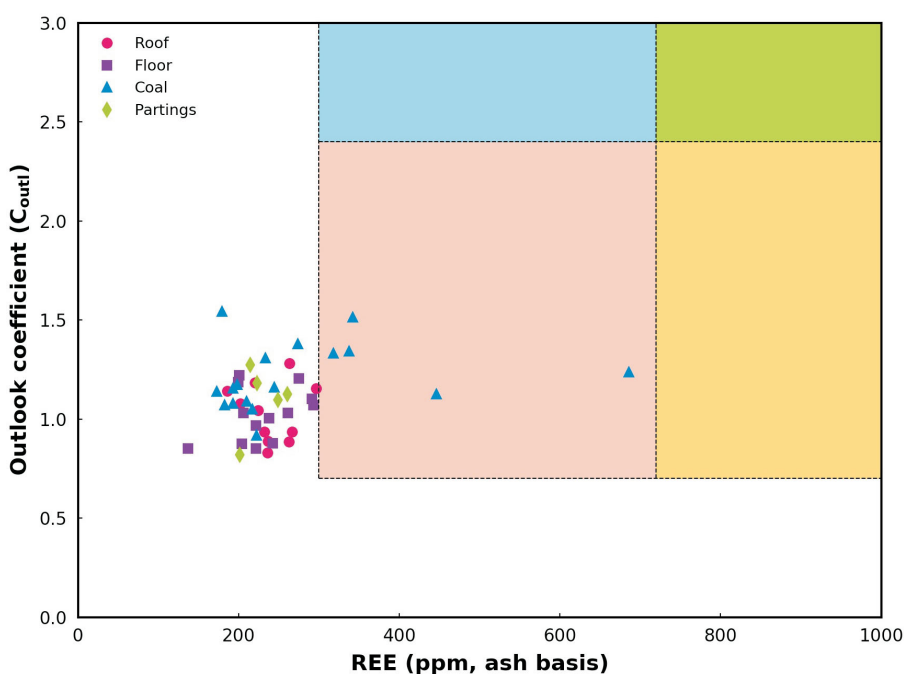


Figure 4. Outlook coefficient (C_{outl}) versus rare-earth element (REE) concentration for various types of coal samples from the East Kootenay coalfield, southeastern British Columbia. The REE resource categories for coal sources: green, highly promising source; yellow, promising source; blue, highly promising resource; light salmon: promising resource.

on average, 35% of the total REEs. Further, it can be noticed from Table 4 that HREE concentrations are more significantly concentrated in coal, in some cases they total more than 50% of total LREEs, than in roof, partings and floor materials, which contributes to the better C_{outl} values. The average C_{outl} for the coal samples is found to be 1.2. Since the reported C_{outl} for world coal is 0.64 (Zhang et al., 2015, Dai et al., 2017), these results show that BC coals may be a viable source of REEs if extraction practices are refined.

Correlation analysis also shows a strong correlation between coal ash and REE content (except Sc) when calculated on a whole coal basis ($r = +0.88$ to $+0.96$). This indicates the presence of mineral phases containing REEs in the coal samples. One of the rare-earth carriers in these types of metalliferous coal is zircon, which can originate from volcanic ash or authigenic minerals and it can be identified by enrichment of Hf, Th, U and HREEs (Finkelman, 1981; Seredin, 2004). A compelling correlation between Hf, Th, U, Y and other REEs implies that zircon is one of the source minerals of REEs and indicates an input of volcanic ash containing REEs into the coal. Elemental analysis results using ICP-MS proved the presence of zirconium in the samples. Also, volcanic ash is believed to be the source of tonsteins associated with the coal beds in the Mist Mountain Formation in the East Kootenay coalfield (Grieve, 1993), which further validates the inference made in this study.

No correlation was observed between ash and REEs content when calculated on an ash basis ($r = -0.03$ to 0.18). This points toward an insignificant association of REEs with organic matter in the studied samples. To confirm this, the next step was to look for a strong correlation between REEs and W, which is believed to be organically fixed in coal. However, a very weak correlation was shown between REE and W in the studied samples ($r = +0.21$ to 0.34) indicating inorganically associated REEs.

In the samples, on the whole coal basis, REEs strongly correlated with uranium ($r > +0.84$) and thorium ($r > +0.85$). This suggests that one of the REE mineral phases could be monazite, but a more detailed mineralogical study is required to confirm this.

Most of these preliminary results are similar to those previously reported for this study (Kumar et al., 2018).

Conclusions

One of the main objectives of the study is the development of a rare-earth element (REE) database for the East Kootenay coalfield. In this regard, coal samples from the East Kootenay coal deposits were tested for the presence of REEs and it was found that total REE concentrations on ash basis varied from 137 to 686 ppm. It was inferred from the data that REEs in the coal samples are associated with both organic and inorganic portions of the coal constituents, but inorganic association seems to be dominant. The information presented in this paper represents only the preliminary

data and the final database will be reported on in future reports. As part of phase two of the study, a few select samples will be identified and detailed characterization of the REEs will be undertaken. In addition, REE enrichment of the coal using physical separation will be tested.

With the development of extraction techniques, REEs could be extracted from coal as byproducts of coal mining, which can strengthen brownfield operations by increasing profitability and possibly generating green credits, as these REEs are used in clean energy technologies. In the case of greenfield operations, REE extraction will increase the economic viability of the deposit and the potential for its future development. Overall, it will enhance British Columbia's coal resources.

Acknowledgments

Financial support for the project from Geoscience BC is greatly appreciated. The authors gratefully acknowledge the scholarship received from Geoscience BC in 2017–2018. Sincere gratitude is extended to industrial partner Teck Coal Limited. The authors would also like to thank M. Mastalerz, Indiana University, for her valuable comments and suggestions to improve this manuscript.

References

- Akdogan, G. and Ghosh, T. (2014): Identification of REE in some Alaskan coal and ash samples; U.S. Department of Energy, National Energy Technology Laboratory, final report, 27 p., URL <<https://edx.netl.doe.gov/dataset/netl-ree-technical-reports/resource/cd514839-bb19-44ef-bd9a-137054619127>> [November 2020].
- ASTM D2013/D2013M-12 (2012): Standard practice for preparing coal samples for analysis; ASTM International, West Conshohocken, Pennsylvania, 2012, URL <https://doi.org/10.1520/D2013_D2013M-12>.
- ASTM D3172-13 (2013): Standard practice for proximate analysis of coal and coke; ASTM International, West Conshohocken, Pennsylvania, 2013, URL <<https://doi.org/10.1520/D3172>>.
- ASTM D3173/D3173M-17a (2017): Standard test method for moisture in the analysis sample of coal and coke; ASTM International, West Conshohocken, Pennsylvania, 2017, URL <https://doi.org/10.1520/D3173_D3173M-17A>.
- ASTM D3174-12 (2012): Standard test method for ash in the analysis sample of coal and coke from coal; ASTM International, West Conshohocken, Pennsylvania, 2012, URL <<https://doi.org/10.1520/D3174-12>>.
- ASTM D3175-17 (2017): Standard test method for volatile matter in the analysis sample of coal and coke; ASTM International, West Conshohocken, Pennsylvania, 2017, URL <<https://doi.org/10.1520/D3175-17>>.
- ASTM D388-17 (2017): Standard classification of coals by rank; ASTM International, West Conshohocken, Pennsylvania, 2017, URL <<https://doi.org/10.1520/D0388-17>>.
- BC Geological Survey (2019): British Columbia coal industry overview 2018; BC Ministry of Energy, Mines and Low Carbon Innovation, Information Circular 2019-2, 13 p., URL <http://cmscontent.nrs.gov.bc.ca/geoscience/PublicationCatalogue/InformationCircular/BCGS_IC2019-02.pdf> [September 2019].
- Birk, D. and White, J.C. (1991): Rare earth elements in bituminous coals and underclays of the Sydney Basin, Nova Scotia: element sites, distribution, mineralogy; International Journal of Coal Geology, v. 19, p. 219–251.
- Bragg, L.J., Oman, J.K., Tewalt, S.J., Oman, C.L., Rega, N.H., Washington, P.M. and Finkelman, R.B. (1994): U.S. Geological Survey coal quality (COALQUAL) database version 1.3; U.S. Geological Survey, Open-File Report 94-205, URL <<https://pubs.er.usgs.gov/publication/ofr94205>> [October 2019].
- Bryan, R.C., Richers, D., Andersen, H.T. and Gray, T. (2015): Assessment of rare earth elemental contents in select United States coal basins; U.S. Department of Energy, National Energy Technology Laboratory, 47 p., URL <<https://edx.netl.doe.gov/dataset/ae5aa8e1-77f9-45fb-a2bc-aa361505706c/resource/137a0880-7c47-40d1-bc23-80b07264ab13>> [November 2020].
- Dai, S., Graham, I.T. and Ward, C.R. (2016): A review of anomalous rare earth elements and yttrium in coal; International Journal of Coal Geology, v. 159, p. 82–95.
- Dai, S., Li, D., Chou, C., Zhao, L., Zhang, Y., Ren, D., Ma, Y. and Sun, Y. (2008): Mineralogy and geochemistry of boehmite-rich coals: new insights from the Haerwusu surface mine, Jungar coalfield, Inner Mongolia, China; International Journal of Coal Geology, v. 74, p. 185–202.
- Dai, S., Xie, P., Jia, S., Ward, C.R., Hower, J.C., Xiaoyun, Y. and French, D. (2017): Enrichment of U-Re-V-Cr-Se and rare earth elements in the Late Permian coals of the Moxinpo coalfield, Chongqing, China: genetic implications from geochemical and mineralogical data; Ore Geology Reviews, v. 80, p. 1–17.
- Deloitte Sustainability, British Geological Survey, Bureau de Recherches Géologiques et Minières and Netherlands Organisation for Applied Scientific Research (2017): Study on review of the list of critical raw materials; European Commission, 92 p., URL <<https://publications.europa.eu/en/publication-detail/-/publication/08fdab5f-9766-11e7-b92d-01aa75ed71a1/language-en>> [September 2017].
- Finkelman, R.B. (1981): Modes of occurrence of trace elements in coal; U.S. Geological Survey, Open File Report 81-99, 301 p., URL <<https://pubs.usgs.gov/of/1981/0099/report.pdf>> [September 2017].
- Finkelman, R.B. (1993): Trace and minor elements in coal; in Organic geochemistry principles and applications, M.H. Engel and S.A. Macko (ed.), Springer Science+Business Media, New York, New York, p. 593–604.
- Finkelman, R.B., Oman, C.L., Bragg, L.J. and Tewalt, S.J. (1994): The U.S. Geological Survey coal quality data base (COALQUAL); U.S. Geological Survey, Open-File Report 94-177, 46 p., URL <<https://pubs.er.usgs.gov/publication/ofr94177>> [October 2019].
- Goodarzi, F. (1988): Elemental distribution in coal seams at the Fording coal mine, British Columbia, Canada; Chemical Geology, v. 68, issue 1–2, p. 129–154, URL <[https://doi.org/10.1016/0009-2541\(88\)90092-7](https://doi.org/10.1016/0009-2541(88)90092-7)>.
- Goodarzi, N.N., Goodarzi, F., Grieve, D.A., Sanei, H. and Gentzis, T. (2009): Geochemistry of coals from the Elk Valley coalfield, British Columbia, Canada; International Journal of Coal Geology, v. 77, p. 246–259.

- Grieve, D.A. (1993): Geology and rank distribution of the Elk Valley coalfield, southeastern BC (82G/15, 82J/2, 6, 7, 10, 11); BC Ministry of Energy, Mines and Low Carbon Innovation, Bulletin 82, 188 p., URL <http://cmscontent.nrs.gov.bc.ca/geoscience/PublicationCatalogue/Bulletin/BCGS_B0-82.pdf> [September 2017].
- Honaker, R., Hower, J.C., Eble, C.F., Weisenfluh, J., Groppo, J., Rezaee, M., Bhagavatula, A., Luttrell, G.H., Bratton, R.C., Kiser, M. and Yoon, R.H. (2015): Laboratory and bench scale testing for rare earth elements; U.S. Department of Energy, National Energy Technology Laboratory, final report, 537 p., URL <<https://edx.netl.doe.gov/dataset/ae5aa8e1-77f9-45fb-a2bc-aa361505706c/resource/bac07c25-ed3c-434e-8972-6be1fa22b2c6>> [November 2020].
- Hower, J.C., Ruppert, L.F. and Eble, C.F. (1999): Lanthanide, yttrium, and zirconium anomalies in the Fire Clay coal bed, eastern Kentucky; International Journal of Coal Geology, v. 39, p. 141–153.
- Hu, J., Zheng, B., Finkelman, R.B., Wang, B., Wang, M., Li, S. and Wu, D. (2006): Concentration and distribution of sixty-one elements in coals from DPR Korea; Fuel, v. 85, p. 679–688.
- Karayigit, A.I., Gayer, R.A., Querol, X. and Onacak, T. (2000): Contents of major and trace elements in feed coals from Turkish coal-fired power plants; International Journal of Coal Geology, v. 44, p. 169–184.
- Ketris, M.P. and Yudovich, Y.E. (2009): Estimations of Clarkes for carbonaceous biolithes: world averages for trace element contents in black shales and coals; International Journal of Coal Geology, v. 78, p. 135–148.
- Kumar, V., Kumar, A. and Holuszko, M.E. (2018): Occurrence of rare-earth elements in selected British Columbian coal deposits and their derivative products; in Geoscience BC Summary of Activities 2017: Minerals and Mining, Geoscience BC, Report 2018-01, p. 87–100, URL <http://cdn.geosciencebc.com/pdf/SummaryofActivities2017/MM/SoA2017_MM_Kumar.pdf> [February 2018].
- Kuppusamy, V.K. and Holuszko, M.E. (2019): Characterization and extraction of rare-earth elements from East Kootenay coalfield samples, southeastern British Columbia; in Geoscience BC Summary of Activities 2018: Minerals and Mining, Geoscience BC, Report 2019-01, p. 33–44, URL <http://cdn.geosciencebc.com/pdf/SummaryofActivities2018/MM/Schol_SoA2018_MM_Kuppusamy.pdf> [October 2019].
- Miskovic, S. (2015): Extraction of REE from Western coal; U.S. Department of Energy, National Energy Technology Laboratory, project report, 85 p., URL <<https://edx.netl.doe.gov/dataset/ae5aa8e1-77f9-45fb-a2bc-aa361505706c/resource/9eb06c86-b085-49f2-abc9-1bb3b87db97b>> [November 2020].
- Moldoveanu, G. and Papangelakis, V. (2013): Recovery of rare earth elements adsorbed on clay minerals: II. leaching with ammonium sulfate; Hydrometallurgy, v. 131, p. 158–166.
- Palmer, C.A., Oman, C.L., Park, A.J. and Luppens, J.A. (2015): The U.S. Geological Survey coal quality (COALQUAL) database version 3.0; U.S. Geological Survey, Data Series 975, 50 p., URL <<https://pubs.er.usgs.gov/publication/ds975>> [June 2019].
- Seredin, V.V. (1996): Rare earth element-bearing coals from the Russian Far East deposit; International Journal of Coal Geology, v. 30, p. 101–129.
- Seredin, V.V. (2004): Metalliferous coals: formation conditions and outlooks for development; Coal Resources of Russia, v. 6, p. 452–519.
- Seredin, V.V. and Dai, S. (2012): Coal deposits as potential alternative sources for lanthanides and yttrium; International Journal of Coal Geology, v. 94, p. 67–93.
- Seredin, V.V. and Finkelman, R.B. (2008): Metalliferous coals: a review of the main genetic and geochemical types; International Journal of Coal Geology, v. 76, p. 253–289.
- Soundarajan, N., Pulati, N., Klima, M.S., Ityokumbul, M. and Pisupati, S.V. (2015): Separation of rare earth elements from coal and coal products; U.S. Department of Energy, National Energy Technology Laboratory, final report, 70 p., URL <<https://edx.netl.doe.gov/dataset/ae5aa8e1-77f9-45fb-a2bc-aa361505706c/resource/2421dac9-b310-4d30-a5f4-87ebd33c0a01>> [November 2020].
- Standing Committee on Natural Resources (2014): The rare earth elements industry in Canada - summary of evidence; House of Commons Canada, 26 p., URL <https://www.ourcommons.ca/Content/Committee/412/RNNR/WebDoc/WD6669744/412_RNNR_reldoc_PDF/RareEarth-Elements-Summary-e.pdf> [November 2020].
- Taylor, S.R. and McLennan, S.M. (1985): The continental crust: its composition and evolution: an examination of the geochemical record preserved in sedimentary rocks; Blackwell Scientific Publications, Oxford, United Kingdom, 312 p.
- Tse, P.K. (2011): China's rare-earth industry; U.S. Geological Survey, Open-File Report 2011-1042, 11 p., URL <<https://pubs.usgs.gov/of/2011/1042/of2011-1042.pdf>> [September 2017].
- U.S. Department of Energy (2010): Critical materials strategy; U.S. Department of Energy, 190 p., URL <https://energy.gov/sites/prod/files/DOE_CMS2011_FINAL_Full.pdf> [September 2017].
- U.S. Department of Energy (2016): Rare earth elements program; U.S. Department of Energy, National Energy Technology Laboratory, 19 p., URL <<https://www.netl.doe.gov/FileLibrary/Research/Coal/RareEarthElements/REE-Project-Portfolio-2016.pdf>> [September 2017].
- Zhang, W., Rezaee, M., Bhagavatula, A., Li, Y., Groppo, J. and Honaker, R. (2015): A review of the occurrence and promising recovery methods of rare earth elements from coal and coal by-products; International Journal of Coal Preparation and Utilization, v. 35, p. 295–330.

Evolution of the Southern Quesnel Arc: Potential to Distinguish Variability in Magmatic Porphyry Fertility, South-Central British Columbia (NTS 082E, L, 092H, I, P, 093A, B)

T.J. Ledoux¹, MDRU – Mineral Deposit Research Unit, The University of British Columbia, Vancouver, British Columbia, tledoux@eoas.ubc.ca

C.J.R. Hart, MDRU – Mineral Deposit Research Unit, The University of British Columbia, Vancouver, British Columbia

Ledoux, T.J. and Hart, C.J.R. (2021): Evolution of the southern Quesnel arc: potential to distinguish variability in magmatic porphyry fertility, south-central British Columbia (NTS 082E, L, 092H, I, P, 093A, B); *in* Geoscience BC Summary of Activities 2020: Minerals, Geoscience BC, Report 2021-01, p. 75–90.

Introduction

Porphyry Cu deposits are the world's largest repositories of Cu and Mo, and are major sources of Au and Ag (International Copper Study Group, 2019). Most porphyry Cu deposits have a spatial and temporal association with active plate margins, such as the continental-margin arc along western North and South America. Porphyry Cu deposits are critical contributors to the British Columbia (BC) economy. In 2018, 293.5 kt of Cu concentrate was extracted from BC porphyry deposits, equating to over \$2 billion in annual revenues and contributing more than half of Canada's Cu production (Natural Resources Canada, 2018; PricewaterhouseCoopers Inc., 2019).

The most fundamental process in forming large porphyry Cu deposits is the exsolution of hydrothermal fluids from magma in large, crystallizing, midcrustal batholiths below the site of porphyry Cu deposit formation (Dilles and Einaudi, 1992). These fluids accumulate Cl, S and metals that preferentially partition from the magma to the fluid, and together they buoyantly stream through the upper crust to where gases exsolve and break the rock. With decreasing temperature, fluids condense and precipitate silicate and sulphide minerals to form porphyry Cu deposits.

Formation of an economic porphyry Cu deposit is dependent on six key magmatic parameters: 1) oxidation state, 2) temperature, 3) water content, 4) metal content, 5) chlorine content, and 6) sulphur content (Burnham and Ohmoto, 1980). A magma may be considered fertile and therefore capable of generating an economic deposit if it 1) is oxidized, 2) cooled quickly, 3) has a high water content, 4) contains enough Cu±Au±Mo, 5) has enough Cl to transport Cu in solution, and 6) has enough S (and Fe) to

precipitate Cu-sulphide minerals. Research in mineral chemistry by Ballard et al. (2002), Lee (2008), Celis (2015), Dilles et al. (2015), Bouzari et al. (2016), Williamson et al. (2016) and Lee et al. (2020) has identified trace-element signatures and grain morphology of zircon, apatite, titanite and plagioclase that correlate with many attributes of magma fertility. For example, indicators of a magma's oxidation state and water content are recorded in and reflected by the characteristics and compositions of magmatic zircon grains. As a result, zircon grains, in addition to being robust U-Pb geochronometers, can also provide insights that contribute to evaluating the fertility of its host magmas and ultimately to exploration decision-making.

Previous research in magmatic porphyry fertility focused primarily on zircon composition and variability within a single deposit, pluton or mineral district (e.g., Wainright et al., 2011; Lee et al., 2017; Kobylinski et al., 2020; Lee et al., 2020), or more generally compared the signatures of fertile and barren plutonic rocks from different and tectonically unrelated locations (Belousova et al., 2006; Dilles et al., 2015; Lu et al., 2016). Some recent research (e.g., Shen, 2015; Rezeau et al., 2019; Bouzari et al., 2020; Pizzaro et al., 2020) has examined magmatic porphyry fertility of numerous bodies within a belt or arc. These studies demonstrate the variability of zircon as a porphyry-fertility indicator within an arc, although further research is needed to establish the scale of variability within an evolving arc, along an arc segment or across a migrating arc. How do zircon magmatic-fertility indicators vary between arcs or arc segments with different basements, or with different crustal thicknesses, or within an arc in time and space?

The authors anticipate that there would be links between the fertility characteristics and the petrogenetic, magmatic and tectonic processes that control the magma formation. Porphyry deposits can be formed from calc-alkaline, high-K, silica-saturated alkaline, silica-undersaturated alkaline and even tholeiitic diorites, and high-silica granites (Mo

¹The lead author is a 2020 Geoscience BC Scholarship recipient.

This publication is also available, free of charge, as colour digital files in Adobe Acrobat® PDF format from the Geoscience BC website: <http://geosciencebc.com/updates/summary-of-activities/>.

deposits), so their associated mineral chemistry signatures are expected to vary. The ability to identify fertile-arc magmas and understand variability within and between different arc settings will enable explorers to better recognize those magmas that have the potential to form an economic porphyry Cu deposit, and to differentiate them from barren magmas.

Since the BC phase of the project just started with field sampling, this paper provides appropriate background geological information and context for the samples, as well as sample descriptions, as a foundation for subsequent analytical results.

Geological Setting

Much of British Columbia is underlain by a series of Mesozoic island-arc and associated accretionary-margin assemblages that were accreted onto the ancestral North American margin. Porphyry Cu deposits in the Canadian Cordillera formed mainly during two separate time periods in response to different tectonic settings: Early Mesozoic (Late Triassic to Middle Jurassic) deposits are associated with calcalkaline to alkaline intrusive suites that formed in the Stikinia and Quesnellia island-arc settings prior to their accretion onto continental North America; and younger Mesozoic–Cenozoic (Late Cretaceous to Eocene) calc-alkaline deposits were emplaced into previously accreted terranes that formed the western North American continental margin (McMillan et al., 1996).

Quesnellia comprises Middle Triassic to Early Jurassic island-arc assemblages and related intrusions that, in part, unconformably overlie late Paleozoic island-arc and oceanic subterranea (Figure 1; Read and Okulitch, 1977; Smith, 1979). Quesnellia was accreted onto ancestral North America in the Early Jurassic (~186 Ma; Nixon et al., 1993). The late Paleozoic through mid-Mesozoic oceanic Cache Creek terrane is faulted against the western margin of Quesnellia as an accretionary mélange above an east-dipping subduction zone (Travers, 1978). Eastern Quesnellia is marked by unconformable contacts on the Slide Mountain terrane oceanic sedimentary rocks and the adjacent pericratonic Harper Ranch subterrane and Kootenay terrane (Colpron and Price, 1995).

Southern Quesnellia Arc

The lower parts of Mesozoic Quesnellia are composed primarily of the Middle to Late Triassic Nicola Group volcanic arc in the west and the coeval Slocan Group siliciclastic basin to the east (Little, 1960; Preto, 1979). Preto (1979) recognized that the Nicola Group formed parallel, linear, fault-bounded magmatic belts between Merritt and Princeton. McMillan (1981) and Monger (1985) expanded this classification farther north to Kamloops and recognized a new eastern sedimentary belt and a few good stratigraphic

contacts. Mortimer (1987) determined that the older volcanic rocks in the western belt of the southern Nicola Group are type-2, low- to medium-K, calcalkaline to tholeiitic rocks; and younger volcanic rocks in the central and eastern belts of the Nicola Group are type-1, high-K, shoshonitic, calcalkaline to alkaline rocks. Schiarizza (2016) established a stratigraphic framework of the Nicola Group in the Bridge Lake–Quesnel River area, breaking it into four assemblages that define a regional syncline and roughly correlate with the belts first described by Preto (1979) farther to the south.

Assemblage 1 of Schiarizza (2016) correlates with the eastern sedimentary belt, is Middle to Late Triassic based on conodonts (Struik, 1988; Schiarizza et al., 2013), and is exposed along the eastern margin of the Nicola belt. This assemblage consists of basinal sedimentary rocks with lesser volcaniclastic and basaltic rocks. Assemblage 2 correlates with the western volcanic belt, is Late Triassic based on conodonts and macrofossils (Schiarizza, 2016), and defines the west and east limbs of a regional syncline in the north and spans the west limb of the Nicola Group in the south. This assemblage is composed of volcaniclastic rocks, locally intercalated with subaerial pyroxene-phyric basalt, epiclastic sedimentary rocks and limestone. Assemblage 3 correlates with the central volcanic belt, is inferred to be Norian based on the stratigraphic position between Assemblages 2 and 3, and crops out as two belts in the north and spans the centre of the Nicola Group in the south. This assemblage consists primarily of pyroxene-phyric basalt and andesite, with lesser interbedded sedimentary rocks in the southern portion of the Nicola Group. Assemblage 4 correlates with the eastern volcanic belt, is Late Triassic based on a U-Pb zircon date of 203.9 ± 0.4 Ma from a plagioclase-phyric andesite (Schiarizza et al., 2013), unconformably overlies the rest of the Nicola Group as the central belt in the north, and is fault bounded between the central volcanic belt and eastern sedimentary belt in the south. This assemblage consists of polymictic conglomerate with abundant plutonic rocks, sandstone, basalt and andesite (Preto, 1979; Schiarizza, 2019).

Southern Quesnellia Plutonism

The magmatic axis of Late Triassic to Early Jurassic Quesnellia plutonism migrated episodically eastward, constructing three subparallel linear plutonic axes (Table 1; Schiarizza, 2014). The plutonic episodes occurred over an ~36 m.y. period (229–193 Ma; Parrish and Monger, 1992; Kobylinski et al., 2020) as part of the longer, ~54 m.y. period (247–193 Ma; Schiarizza, 2019) of arc evolution above an east-dipping subduction zone. As the magmatic axis moved toward the back arc in the east, plutonic episodes evolved from a calcalkaline affinity to an alkaline affinity, and back to calcalkaline; and porphyry-deposit metal assemblages transitioned from Cu-Mo to Cu-Au and back

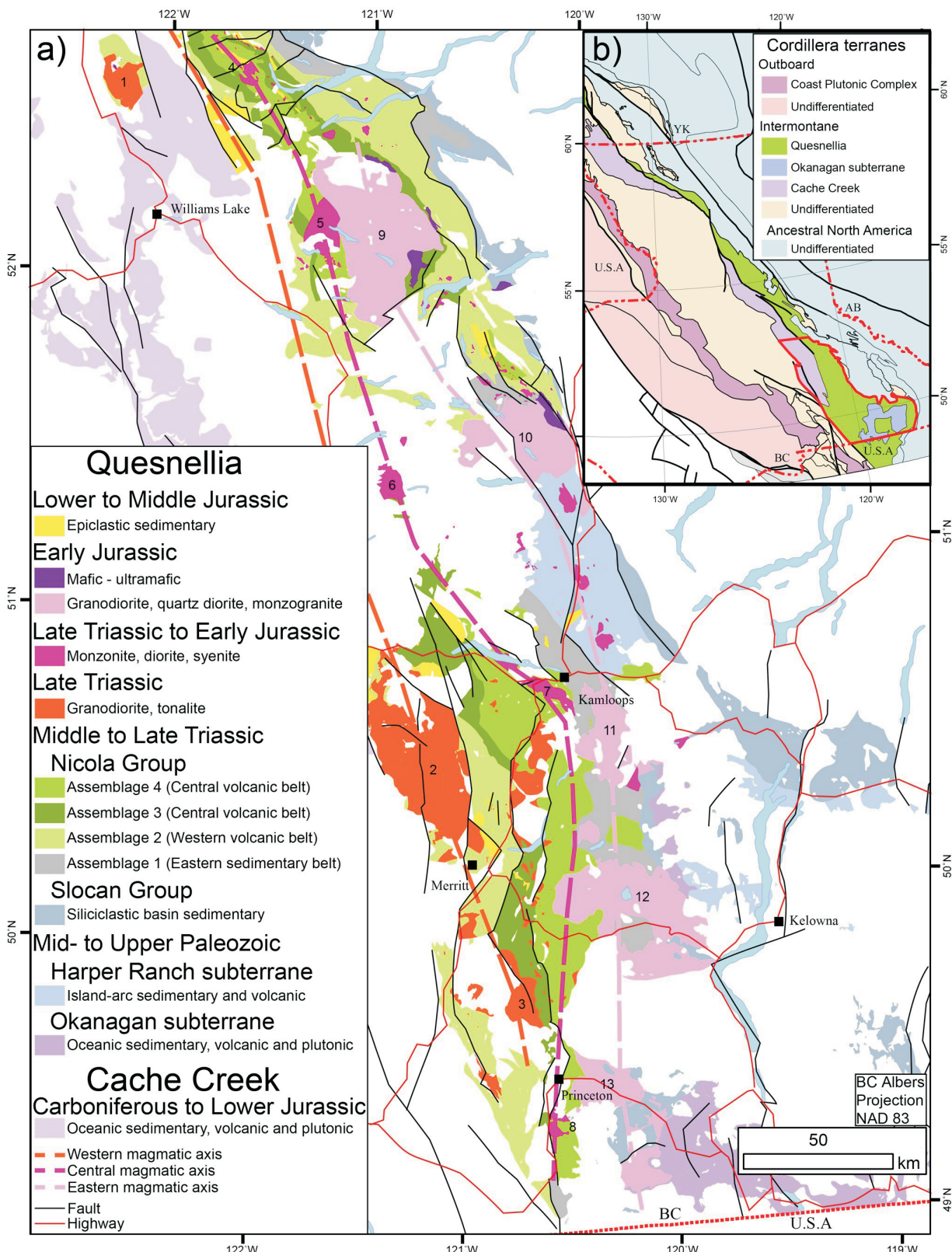


Figure 1. a) Geology of southern Quesnellia and the Cache Creek terrane, south-central British Columbia (modified after Cui et al., 2017). Nicola Group assemblages after Preto (1979), McMillan (1981), Monger (1985) and Schiarizza (2019). Symbols: red dashed line, Western magmatic axis; fuchsia dashed line, Central magmatic axis; pink dashed line, Eastern magmatic axis (modified after Schiarizza (2014)). Numbers: 1, Granite Mountain batholith; 2, Guichon Creek batholith; 3, Alice Lake pluton; 4, Mount Polley; 5, Spout Lake pluton; 6, Rayfield River; 7, Iron Mask batholith; 8, Copper Mountain; 9, Takomkane batholith; 10, Thuya batholith; 11, Wild Horse batholith; 12, Pennask batholith; 13, Bromley batholith. **b)** Terranes of British Columbia (modified after Colpron and Nelson, 2020).

to Cu-Mo (Logan and Mihalynuk, 2014; Schiarizza, 2014). Most Quesnellia porphyry deposits formed between 210 and 195 Ma, with an especially prolific 6 m.y. long mineralizing event centred at 205 Ma (Mortensen et al., 1995).

Western Magmatic Axis (Late Triassic Calcalkaline Plutonism)

The Western magmatic axis is characterized by plutonism of Late Triassic age (229–206 Ma; D’Angelo et al., 2017; Kobylinski et al., 2020; Lee et al. 2020), specifically calcalkaline granodiorite-tonalite suite intrusive rocks and associated Cu-Mo porphyry deposits. Intrusions here are large (up to 2000 km²), thick (>6 km), consist of multiple concentrically zoned phases and were typically emplaced at depths of ~5 km (Sutherland Brown, 1976). The Guichon Creek and Granite Mountain batholiths are the main intrusions that define this magmatic axis; they were emplaced into Assemblage 2 of the Nicola group. These bodies also host the giant Highland Valley Copper and Gibraltar porphyry Cu districts, respectively. Several other intrusive bodies, such as the Nicola batholith, Alice Lake pluton and other smaller intrusions southeast of the Guichon Creek batholith, make up a contemporaneous but smaller volume subset within the rest of the Western magmatic axis. Much of the Western magmatic axis between the Guichon Creek batholith and the Granite Mountain batholith is covered in Cenozoic volcanic and sedimentary units that could overlie potentially prolific porphyry Cu-hosting intrusions.

Guichon Creek Batholith

The Late Triassic Guichon Creek batholith, 65 km southwest of Kamloops, trends north, measures 65 by 30 km and was emplaced at depths between 2.6 and 7.4 km in Assemblage 2 of the Nicola group (Northcote, 1969; McMillan, 1976, 1985; Byrne et al., 2013; D’Angelo, 2016) as a flattened funnel shape with an average thickness of 6 km on the

edges and a maximum thickness of >12 km at the centre (Ager, 1974). The batholith is calcalkaline, composite and concentrically zoned (McMillan, 1976), comprising an earlier granodioritic to quartz monzonitic stock on the edge (218 ± 0.18 Ma; Lee et al., 2020) and a larger zoned batholith in the centre that youngs from a quartz diorite phase at the margin (211.2 ± 0.17 Ma) to a predominantly granodiorite core (206.95 ± 0.22 Ma; D’Angelo et al., 2017). The margin of the batholith is composed of heterogeneous, equigranular gabbroic to monzodioritic rocks that include minor olivine, orthopyroxene and clinopyroxene in the gabbroic phases and abundant hornblende and minor quartz in the dioritic phases. Toward the core of the batholith, the rocks transition from equigranular granodiorite through porphyritic granodiorite to monzogranite with a few percent of mafic minerals. Mafic minerals in the units at the margin of the batholith are pyroxenes with hornblende rims and hornblende with relict cores of pyroxene. Mafic minerals in the units near the core of the batholith comprise hornblende and biotite, and, at the core of the batholith, only biotite phenocrysts (Byrne et al., 2013; D’Angelo et al., 2017).

The Guichon Creek batholith hosts five deposits related to two mineralization events: an ~210 Ma event that formed the deposits in the Bethlehem area (Ash et al., 2007; Byrne et al., 2013) and a 208.4 ± 0.9 Ma event that formed the Valley, Lornex, Highmont and J.A. deposits (D’Angelo et al., 2017). The Highland Valley deposits contained 6.2 Mt Cu, between the 4.89 Mt of Cu production over the last 35 years (BC Geological Survey, 2020) and a current resource of 484 Mt at 0.28% Cu and 0.009% Mo (Teck Resources Limited, 2019).

Table 1. Characteristics of the Western, Central, and Eastern magmatic axes of the Quesnellia arc. * indicates inferred resources. All other resources are measured and indicated.

	Western magmatic axis	Central magmatic axis	Eastern magmatic axis
Age (Ma)	229–206	204–200	202–193
Magmatic affinity	Calcalkaline	Alkaline	Calcalkaline, high-K calcalkaline
Predominant rock type	Granodiorite and tonalite	Diorite and monzonite	Granodiorite and quartz diorite
Average batholith dimensions: length x width x thickness (km)	42 x 23 x 8	16 x 7 x 4	32 x 33
Average emplacement depth (km)	5	1	4
Major porphyry districts	Highland Valley and Gibraltar	Copper Mountain, Afton-Ajax, and Mount Polley	Brenda and Woodjam
Metal assemblages	Cu-Au-Mo	Cu-Au	Cu-Mo ± Au
Historical copper production (Mt)	6.39	1.83	0.28
Current copper resource (Mt)	2.81	4.1	0.79*
Total contained copper (Mt)	9.2	5.93	1.07

* inferred resource

Granite Mountain Batholith

The Late Triassic Granite Mountain batholith, 60 km north of Williams Lake, measures 18 by 10 km and was emplaced at a depth of ~5 km (Sutherland Brown, 1976). The batholith was originally considered to intrude the Cache Creek terrane (Bysouth et al., 1995), but mapping by Schiarizza (2014) identified Assemblage 2 Nicola Group rocks on the margins of the batholith, indicating that it is part of Quesnellia. The batholith is calcalkaline and composite (Panteleyev, 1978), and comprises multiple tonalitic to dioritic intrusions that have gradational contacts. In the north, it is composed of tonalite with quartz > plagioclase and 5–10% mafic minerals (biotite > hornblende) that grades to a more mafic tonalite near the centre and to a border phase at the southern margin that is composed of equigranular quartz diorite grading locally into tonalite or diorite with >25% hornblende. The northeastern margin consists of an older composite stock of equigranular tonalite and variably equigranular to porphyritic tonalite and diorite (Schiarizza, 2015). The batholith was constructed over an ~25 m.y. period beginning at 229.2 ± 4.4 Ma with crystallization of barren tonalite and followed by emplacement of multiple mineralizing tonalitic intrusions from 218.9 ± 3.1 to 205.8 ± 2.1 Ma (Kobylinski et al., 2020).

The Granite Mountain batholith hosts the Gibraltar Cu-Mo porphyry deposit that consists of a cluster of three chimney-like orebodies (Ash and Riveros, 2001), formed during multiple, distinct, magmatic-hydrothermal events that have Re-Os ages on molybdenite ranging from 215.0 ± 1.0 to 210.1 ± 0.9 Ma (Harding, 2012). The Gibraltar deposit contained 3.0 Mt of Cu, between the 1.5 Mt of Cu extracted from the Gibraltar mine (BC Geological Survey, 2020) and the current resource of 594 Mt at 0.25% Cu and 0.008% Mo (Weymark, 2019).

Central Magmatic Axis (Late Triassic to Early Jurassic Alkaline Plutonism)

The Central magmatic axis is characterized by plutonism of latest Triassic to Early Jurassic (204–200 Ma; Mortensen et al., 1995), alkaline, silica-saturated to -undersaturated intrusive rocks of the syenite-diorite suite containing Au-rich Cu-Au deposits. The Mount Polley, Spout Lake and Rayfield River intrusive complexes, Iron Mask batholith and Copper Mountain intrusive complex are the main intrusions that define the Central magmatic axis. The Copper Mountain intrusion and the Iron Mask batholith are silica saturated and locally silica undersaturated, whereas the Mount Polley and Rayfield River intrusions are silica undersaturated (Lang et al., 1995). The Iron Mask batholith hosts a number of Cu-Au occurrences, most notably the Afton and Ajax deposits; and the Copper Mountain and Mount Polley intrusive complexes each host a porphyry Cu-Au district of the same name.

Copper Mountain Intrusive Complex

The Early Jurassic Copper Mountain intrusive complex is located 15 km south of Princeton, measures 8 by 6 km and was emplaced in a subvolcanic environment in Assemblage 4 of the Nicola Group (Preto, 1972; Schiarizza, 2019) at a depth of ~1.1 km (Sutherland Brown, 1976). This intrusive complex is composed of multiple alkalic stocks and dike swarms. The Copper Mountain stock, in the southern part of the intrusive complex, is concentrically differentiated and grades from equigranular clinopyroxene diorite with local gabbro at the margins through clinopyroxene-biotite monzonite to inequigranular syenite at the core (Holbek and Joyes, 2013). Zircons from the monzodiorite in the Copper Mountain stock have a U-Pb age of 202.7 ± 4.4 Ma (Mortensen et al., 1995). The Smelter Lake and Voight stocks are in the northeastern and northwestern parts of the intrusive complex, respectively, and are composed of nearly identical equigranular biotite-clinopyroxene diorite. The Lost Horse intrusive complex, situated between these stocks, is a nearly continuous mass of dikes composed of 1) porphyritic syenite to diorite that consist of euhedral plagioclase, subhedral to anhedral clinopyroxene and varying amounts of interstitial alkali feldspar and biotite; and 2) trachytic latite and trachyte to porphyritic micromonzonite and microsyenite that consist of euhedral plagioclase and clinopyroxene, well-formed biotite and interstitial alkali feldspar (Preto, 1972).

Since production at the Copper Mountain mine began in 1917, 1.05 Mt of Cu and 28.5 t of Au have been mined from the Copper Mountain and Ingerbelle deposits (BC Geological Survey, 2020). These deposits have a combined remaining resource of 584 Mt of 0.23% Cu and 0.1 g/t Au (Copper Mountain Mining Corp., 2020), making for a total of 2.34 Mt Cu and 82.9 t Au in past production and current resources.

Iron Mask Batholith

The Late Triassic to Early Jurassic Iron Mask batholith southwest of Kamloops is a 35 by 5 km, northwest-trending intrusion (Logan and Mihalynuk, 2005) that was emplaced at a depth of ~0.9 km (Sutherland Brown, 1976) as a 2–6 km thick, elongate, funnel-shaped body (Ager, 1974; Thomas, 2019). The batholith was apparently emplaced in a comagmatic environment of alkaline volcanic rocks of Nicola Group Assemblage 4 (Northcote, 1978; Schiarizza, 2019). The Iron Mask batholith is a polyphase alkalic intrusive complex composed of the Pothook, Cherry Creek, Sugarloaf and Hybrid phases. The Pothook phase is an equigranular biotite-pyroxene diorite with 25% clinopyroxene, 22% biotite and magnetite; the Cherry Creek phase is an equigranular biotite monzonite; the Sugarloaf phase is a porphyritic plagioclase- and hornblende-phyric diorite; and the Hybrid phase is a xenolith-rich phase that marks the contacts between the three intrusions and the sur-

rounding Nicola Group country rock, and is composed primarily of Nicola Group xenoliths in a matrix of the Pothook phase and locally the Cherry Creek and Sugarloaf phases (Snyder and Russell, 1995; Logan and Mihalynuk, 2005). The Pothook and Cherry Creek phases are Late Triassic with zircon U-Pb ages of 204.7 ± 3 and 204.5 ± 0.6 Ma, respectively, and the Sugarloaf diorite has a slightly younger Ar/Ar cooling date of 200.1 ± 2.5 Ma (Logan et al., 2007).

The Iron Mask batholith hosts the currently producing New Afton Cu-Au-Ag mine, which is directly beneath the historical Afton open pit (New Gold Inc., 2019), and multiple past-producing Cu-Au deposits that include the Ajax West, Ajax East, Crescent, Pothook and Python-Makao deposits (Lang and Stanley, 1995). Porphyry Cu-Au deposits are associated with all three phases of the Iron Mask batholith. A total of 0.51 Mt Cu and 38.9 t Au have come from historical production from the Afton, Ajax, Crescent and Pothook deposits, with a majority coming from Afton (Logan and Mihalynuk, 2005; BC Geological Survey, 2020). Ajax has a remaining resource of 442.3 Mt of 0.29% Cu and 0.19 g/t Au (Ghaffari et al., 2009) and Afton has a remaining reserve of 47.3 Mt of 0.77% Cu and 0.66 g/t Au, and a resource of 57 Mt of 0.74% Cu and 0.61 g/t Au (New Gold Inc., 2019), making for a combined remaining resource of 2.06 Mt Cu and 113.3 t Au. All of the deposits in the Iron Mask batholith contained a total of 2.57 Mt Cu and 152.2 t Au in past production and current resources.

Eastern Magmatic Axis (Early Jurassic Calcalkaline Plutonism)

The Eastern magmatic axis is characterized by Early Jurassic (202–193 Ma; Parrish and Monger, 1992; Schiarizza et al., 2009), calcalkaline to high-K calcalkaline intrusive rocks of the granodiorite–quartz diorite suite, containing Cu-Mo deposits. The eastern axis is defined by the large, composite and zoned Bromley, Pennask, Wild Horse, Thuya and Takomkane batholiths. The Pennask and Takomkane batholiths host the past-producing Brenda Cu-Mo mine and Woodjam district, respectfully. This axis also includes several smaller granite to diorite plutons farther east, such as the Cahill Creek pluton and Hedley intrusion, in addition to several smaller, concentrically zoned, Alaskan-type ultramafic bodies that intrude the Nicola Group along the easternmost margins of the axis.

Pennask Batholith

The Early Jurassic Pennask batholith, 35 km west of Kelowna, measures 38 by 50 km and was emplaced into Nicola Group Assemblages 1 and 4 (Soregaroli and Whitford, 1976; Schiarizza, 2019) at a depth of ~4.6 km (Sutherland Brown, 1976). The batholith is composed of polyphase granodiorite and quartz diorite with a U-Pb zircon date of 194 ± 1 Ma (Parrish and Monger, 1992). Within the ‘Brenda stock’, an informal subdivision within the much larger batholith, quartz diorite is equigranular with

euhedral acicular hornblende > anhedral biotite; and granodiorite is equigranular to inequigranular with anhedral biotite = euhedral acicular hornblende. The contact between the two units is typically diffuse, but, where sharp, the granodiorite is chilled against the quartz diorite (Soregaroli and Whitford, 1976; this study).

The Brenda Cu-Mo deposit is located near the margin of the batholith and is hosted within the Brenda stock. The deposit formed over a period of less than 1 m.y., based on a 193.9 ± 0.9 Ma Re-Os model age of molybdenite taken from one of the younger vein sets (Logan et al., 2011). The Brenda mine produced 0.28 Mt of Cu and 0.07 Mt of Mo from 177 Mt of ore grading 0.17% Cu and 0.043% Mo throughout the 20-year mine life (Weeks et al., 1995; BC Geological Survey, 2020).

Takomkane Batholith

The latest Triassic to Early Jurassic Takomkane batholith, located 50 km east of Williams Lake, measures 50 by 40 km and was emplaced in Assemblages 2, 3 and 4 of the Nicola Group and the Spout Lake pluton (Schiarizza, 2019) at a depth of ~3 km (del Real et al., 2017). The batholith is a calcalkaline composite intrusion, consisting of the Boss Creek, Schoolhouse Lake and Woodjam Creek units (Schiarizza et al., 2009). The Boss Creek unit, dated at 202.5 ± 0.5 and 199.6 ± 0.3 Ma (Schiarizza et al., 2009), is an equigranular quartz monzodiorite to granodiorite that locally grades into quartz diorite and diorite. The unit is typically composed of 15–25% mafic minerals, typically consisting of hornblende > biotite, and local clinopyroxene. The Schoolhouse Lake unit, dated at 193.5 ± 0.6 Ma (Whiteaker et al., 1998) and 195.0 ± 0.4 Ma (Schiarizza et al., 2009), is an inequigranular granodiorite to monzogranite that is characterized by alkali-feldspar megacrysts with 10–20% mafic minerals, consisting of hornblende > biotite. The Woodjam Creek unit (197.48 ± 0.44 to 194.99 ± 0.16 Ma; del Real et al., 2017) is equigranular to locally inequigranular granodiorite, monzogranite, quartz monzonite and quartz monzodiorite with 10–15% mafic minerals, consisting of hornblende > biotite (Schiarizza et al., 2009).

The Woodjam Creek unit hosts the Woodjam district, which is a cluster of Early Jurassic Cu-Au±Mo porphyry deposits, including the Southeast Zone Cu-Mo porphyry, the Deerhorn and Megabuck Au-Cu porphyries, and the Takom and Three Firs Cu-Au porphyries. The Deerhorn and Megabuck porphyries are related to 196.48 ± 0.21 Ma, high-K calcalkaline monzonite pencil stocks that intruded the upper strata of the Nicola Group at an emplacement depth of ~1.5–2 km (del Real et al., 2017). The Southeast Zone deposit is hosted within the Woodjam Creek phase and likely formed at a depth of ~3 km (del Real et al., 2017) at 196.9 ± 0.9 Ma, based on a Re-Os model age of molybdenite by Logan et al. (2011). The Southeast Zone, Deerhorn

and Takom deposits currently have an inferred resource of 227.5 Mt of 0.31% Cu, 32.8 Mt of 0.22% Cu and 0.49 g/t Au, and 8.3 Mt of 0.22% Cu and 0.26 g/t Au, respectively (Consolidated Woodjam Copper Corp., 2013), making for a total current resource of 0.79 Mt of contained Cu.

Samples and Methods

Roadside sampling was conducted in 2018, 2019 and 2020 to collect samples that reflect the regional plutonic variability within and between the three magmatic axes of the Late Triassic to Early Jurassic southern Quesnellia arc. These samples will be supplemented with the existing zircon trace-element data on the Guichon Creek, Granite Mountain, and Takomkane batholiths completed by Bouzari et al. (2020), Lee et al. (2020) and Lee et al. (in press). Nine rock samples have been collected: one from the Alison Lake pluton in the Western magmatic axis; four from the Iron Mask batholith in the Central magmatic axis; and one from each of the Brenda stock (Pennask batholith), Bromley batholith, Cahill Creek pluton and Hedley intrusion in the Eastern magmatic axis (Table 2). The Copper Mountain intrusive complex will be sampled at a future date to better characterize the Central magmatic axis. Magnetic susceptibility of the rocks was measured using a recently calibrated, handheld KT-9 magnetic susceptibility meter. Two to four readings were taken of the exterior of each rock sample in pin mode and two readings were taken from the cut rock slabs in no-pin mode, and the averages from both sets of readings were combined.

Glacial-till and stream-sediment samples were collected to test the effectiveness of using detrital zircons as an exploration tool; to get broader representation of the Quesnellia arc and its intrusive bodies; and to increase the potential of obtaining zircons from silica-undersaturated to weakly silica-saturated intrusions, such as the Iron Mask batholith and Copper Mountain intrusive complex, that typically have low zircon yields. Till samples were taken in arid areas with low topographic relief because the streams lack sufficient energy to move clasts and are choked with organic material. Stream-sediment samples were taken from areas with sufficient topographic relief and rainfall for running water to erode and transport rock clasts and presumably mineral grains.

Four till samples were taken from the banks of small streams or roadcuts using a trowel and dry sieved to <1 mm in the field (Table 2). At the Iron Mask batholith, three till samples were taken progressively farther down ice from each other to sample an increased proportion of the Iron Mask intrusive rocks in the till relative to the Nicola Group volcanic rocks that are up ice of the batholith. One glaciofluvial-till sample was collected from down ice of the Pennask batholith.

One stream-sediment sample was collected from a major drainage that is a catchment point downstream of the Pennask batholith and was wet sieved to <1 mm in the stream (Table 2). Additional stream-sediment samples will

Table 2. Southern Quesnellia rock, glacial-till and stream-sediment samples.

Sample ID	Latitude	Longitude	Magmatic Axis	Batholith	Unit	Magnetic Susceptibility	Sample Description
18CH-ALP	49.71231	-120.61026	Western	Alice Lake Pluton		21.15	Porphyritic diorite
20TL-BC-IMR1	50.660178	-120.467954	Central	Iron Mask Batholith	Pothook Phase	116.25	Equigranular biotite-pyroxene diorite
20TL-BC-IMR3	50.550568	-120.473389	Central	Iron Mask Batholith	Cherry Creek Phase	4.86	Equigranular biotite monzonite
20TL-BC-IMR4	50.6048	-120.3779	Central	Iron Mask Batholith	Sugarloaf Phase	39.81	Porphyritic hornblende diorite
20TL-BC-IMR5	50.563915	-120.419418	Central	Iron Mask Batholith	Hybrid Phase	1.19	Xenolith-rich diorite
20TL-BC-PR1	49.89825	-119.92915	Eastern	Pennask Batholith	Brenda Stock	18.03	Equigranular hornblende-biotite granodiorite
18CH-Toronto	49.37	-120.04	Eastern		Hedley Intrusion	0.84	Equigranular pyroxene-hornblende quartz diorite
18CH-CGP	49.33771	-120.04016	Eastern	Cahill Creek Pluton		14.63	Inequigranular hornblende-biotite granite
19CH-Bromley	49.43459	-120.29439	Eastern	Bromley Batholith		21.00	Inequigranular hornblende granodiorite
20LT-BC-IMT1	50.660178	-120.467954	Central	Iron Mask Batholith			Glacial till
20LT-BC-IMT2	50.563915	-120.419418	Central	Iron Mask Batholith			Glacial till
20LT-BC-IMT3	50.606215	-120.373081	Central	Iron Mask Batholith			Glacial till
20TL-BC-PT1	49.864029	-120.929117	Eastern	Pennask Batholith			Glaciofluvial till
20TL-BC-PF1	49.89970	-119.92893	Eastern	Pennask Batholith			Stream sediment

be collected from creeks draining the Copper Mountain intrusive complex.

Sample Descriptions

Western Magmatic Axis (Calcalkaline Granodiorite-Tonalite Suite)

Alice Lake Pluton

The fresh rock is a dark green-grey, porphyritic, crowded, plagioclase-phyric diorite (Figure 2). It is composed of creamy white tabular euhedral plagioclase (60%), translucent anhedral quartz eyes (1%), small shiny black euhedral magnetite (1%), and a fine-grained matrix of dark grey-green mafic minerals (38%). Most of the outcrops of this pluton were altered, with chlorite and epidote on fracture surfaces and locally with quartz veins displaying 2–10 mm saussurite alteration selvages along the vein margins. The rock has a magnetic susceptibility of 21.15×10^{-3} SI.

Central Magmatic Axis (Alkaline, Monzodiorite Suite)

Iron Mask Batholith

Pothook Diorite

Pothook diorite forms the northwestern core of the Iron Mask batholith and is in gradational contact with the hybrid unit to the southeast and intrusive contact with the younger Cherry Creek monzonite to the north and east and the Sugarloaf diorite to the southwest (Logan and Mihalynuk, 2005). The Pothook phase hosts the past-producing Magnet mine and the Python prospect. Sample 20TL-BC-IMR1 was collected from a fractured subcrop exposed along a small creek that cuts through the 2 m of glacial-till overburden.

The fresh rock is a pale green, equigranular, medium- to coarse-grained, biotite-pyroxene diorite (Figure 3a). It is composed of subhedral white plagioclase (45%), euhedral green clinopyroxene (25%), poikilitic biotite (22%), anhedral translucent quartz (2%) and small, shiny, black euhedral grains of magnetite (2%). Plagioclase is locally sericitized and biotite grains are weakly chloritized. The rock is locally fractured, with chlorite-magnetite veinlets in the fractures. It has a magnetic susceptibility of 116.25×10^{-3} SI.

Cherry Creek Monzonite

Cherry Creek monzonite accounts for the largest proportion of the Iron Mask batholith and forms the northernmost margin, central core and southeastern edge. The Cherry Creek phase hosts the Afton mine, which is the largest porphyry deposit in the batholith, and the past-producing Crescent mine. Sample 20TL-BC-IMR3 was collected from an outcrop that was exposed along a roadcut east of Iron Mask hill (unofficial place name; UTM Zone 10U, 680616E,

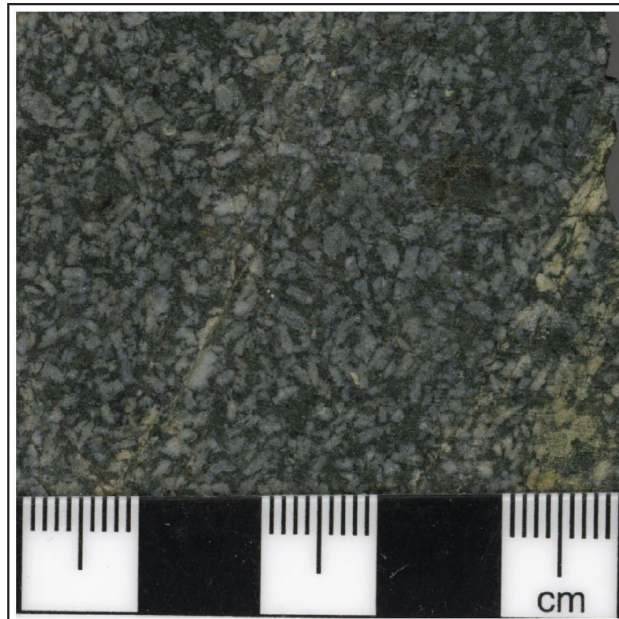


Figure 2. Porphyritic diorite of the Alice Lake pluton in the calcalkaline Western magmatic axis.

5613488N, NAD 83). The outcrop is brownish orange where not freshly exposed by the roadcut covered in black lichen.

The fresh rock is a creamy orange, equigranular, medium-grained, biotite monzonite (Figure 3b). It is composed of creamy orange subhedral alkali feldspar (56%), white subhedral plagioclase (18%), greenish black subhedral biotite (22%), translucent anhedral quartz (2%), small, shiny, black, euhedral grains of magnetite (1%), and partially to completely oxidized anhedral pyrite (1%). The rock locally contains clots (up to 1 cm) of fine-grained mafic minerals. Biotite is moderately chloritized, and the rock is weakly oxidized and has sheeted calcite veinlets. It has an average magnetic susceptibility of 4.86×10^{-3} SI that increases to 8.3×10^{-3} SI if results from oxidized rocks are excluded.

Sugarloaf Diorite

Sugarloaf diorite has the least surface exposure of the Iron Mask batholith phases and forms the western margin of the batholith. The Sugarloaf phase hosts the past-producing Pothook and Ajax deposits. Sample 20TL-BC-IMR4 was collected from a roadcut on the southeastern margin of the batholith, east of the Ajax open pits. The outcrop is dark grey and mostly fresh.

The fresh rock is a dark greenish grey, porphyritic, plagioclase- and hornblende-phyric diorite (Figure 3c). It is composed of creamy white, 1–2 mm, round anhedral and tabular euhedral plagioclase phenocrysts (25%); 1–3 mm, dark green, anhedral hornblende phenocrysts (10%); translucent anhedral quartz eyes (1%); small, shiny, black euhedral magnetite (1%); and a groundmass of dark grey-

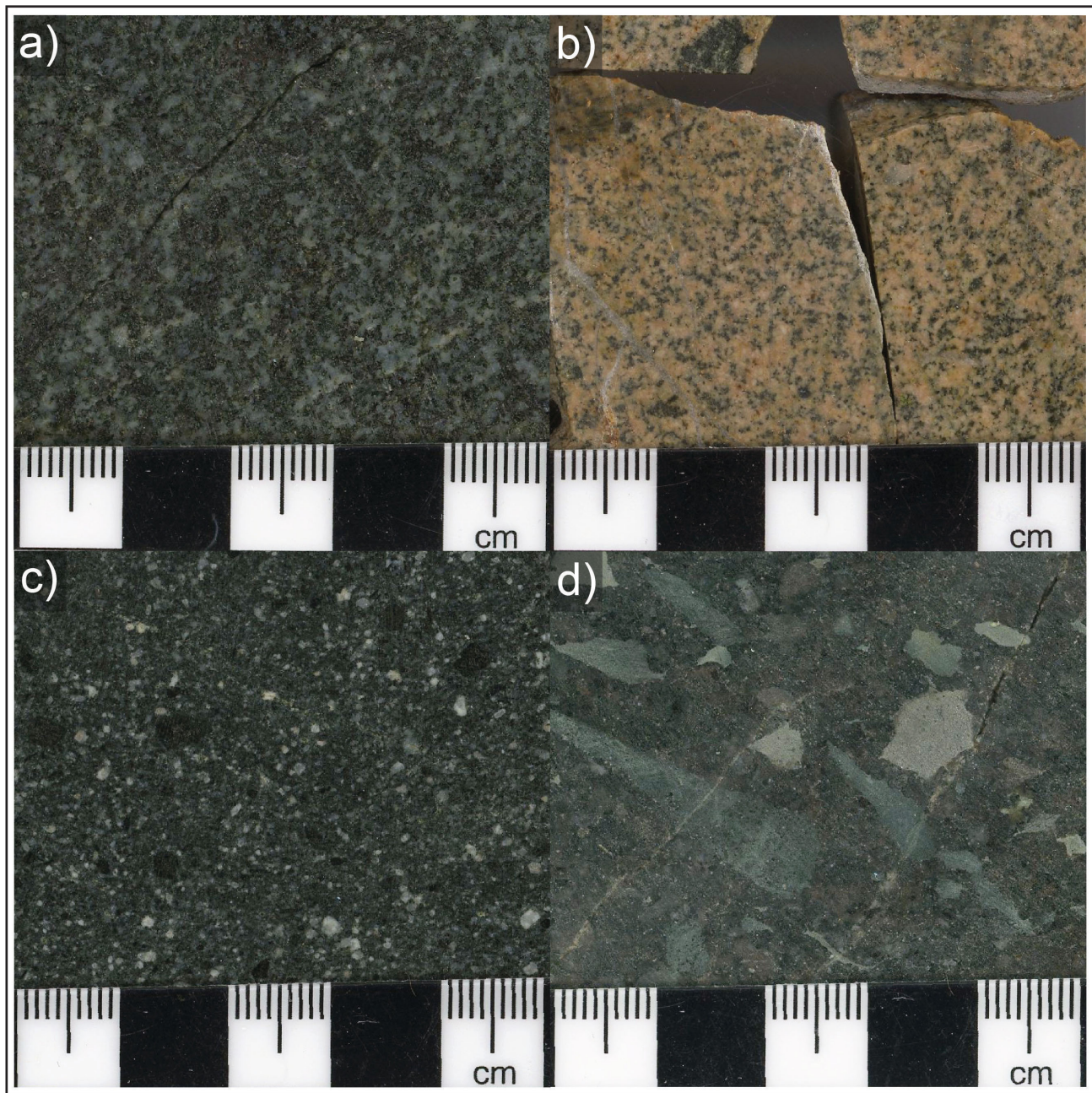


Figure 3. Rocks of the Iron Mask batholith in the alkaline Central magmatic axis: **a)** diorite of the Pothook phase, **b)** equigranular monzonite of the Cherry Creek phase, **c)** porphyritic diorite of the Sugarloaf phase, and **d)** xenolith-rich diorite of the Hybrid phase.

green, fine-grained mafic minerals (42%). It locally contains 1–2 cm xenoliths of fine-grained, strongly chloritized, Nicola group volcanic rocks (5%). Mafic minerals are strongly chloritized and there are multiple clusters of the mafic groundmass that are almost completely replaced by epidote. The rock has a magnetic susceptibility of 39.81×10^{-3} SI.

Hybrid Phase

The hybrid phase is a xenolith-rich, heterogenous unit that forms about half of the surface exposure of the Iron Mask

batholith. Hybrid rocks mark the contacts between the individual phases of the batholith and can locally have a matrix consisting of all the phases in the batholith (Logan and Mihalynuk, 2005). Sample 20TL-BC-IMR5 was collected as a rounded clast in glacial till near the centre of the batholith.

The fresh rock is a pinkish green, xenolith-rich, fine-grained, equigranular diorite (Figure 3d). It is composed of 2–10 mm angular clasts of volcanic and sedimentary Nicola Group xenoliths (37%), dark green poikilitic biotite

(30%), creamy white subhedral plagioclase (22%), creamy orange anhedral alkali feldspar (4%), translucent anhedral quartz (2%) and trace magnetite. The rock is strongly altered to albite. It has a magnetic susceptibility of 1.19×10^{-3} SI.

Till Samples

Most of the Iron Mask Batholith is covered by a glacial-till veneer that was transported to the southeast (Fulton, 1963). Three till samples were taken progressively farther south and down ice from each other.

Sample 20TL-BC-IMT1 was collected at the northeast edge of the batholith, 3 km east of the Afton mine. It is composed of clay (47%), silt (30%) sand (10%), subrounded, pebble-size (2–40 mm) clasts of Nicola Group volcanic rocks (10%) and subrounded to angular, pebble- to cobble-size (20–80 mm) clasts of monzonite and lesser diorite (3%).

Sample 20TL-BC-IMT2 was collected near the centre of the batholith, southeast of Sugarloaf hill (unofficial place name; UTM Zone 10U, 678753E, 5612737N, NAD 83). The sample is composed of clay (45%), silt (33%), sand (10%) and subrounded to angular, pebble- to cobble-size (10–80 mm) clasts of mostly diorite with lesser amounts of xenolith-rich hybrid phase and monzonite (8%), and subrounded, pebble-size (2–30 mm) clasts of Nicola Group volcanic rocks (4%).

Sample 20TL-BC-IMT3 was collected near the south-central portion of the batholith, 1 km southeast of the Ajax deposits. It is composed of clay (42%), silt (35%), sand (10%) and subrounded to angular, pebble- to cobble-size (10–50 mm) clasts of mostly diorite with lesser amounts of monzonite and xenolith-rich hybrid phase (10%), and subrounded, pebble-size (2–20 mm) clasts of Nicola Group volcanic rocks (3%).

Eastern Magmatic Axis (Calcalkaline, Granodiorite Suite)

Pennask Batholith

Brenda Stock

Sample 20TL-BC-PR1 was collected from the southwest side of the Trepanier Creek ravine 6 km east of the past-producing Brenda Cu-Mo mine. The outcrop was weathered a brownish grey colour and strongly fractured.

The fresh rock is light brownish grey, hypidiomorphic, equigranular, coarse-grained, hornblende-biotite granodiorite (Figure 4a). It is composed of creamy white subhedral plagioclase (40%), translucent subhedral quartz (28%), creamy orange subhedral alkali feldspar (18%), greenish black subhedral biotite (8%), black euhedral acicular needles of hornblende (6%) and trace magnetite. Plagioclase is weakly sericitized, biotite is weakly

chloritized and there are several quartz veinlets with sericite alteration selvages. The rock has a magnetic susceptibility of 18.03×10^{-3} SI.

Till Sample

Sample 20TL-BC-PT1 was collected from a bank along a roadcut 4 km southeast of the Brenda mine and downslope of the Brenda tailings dam. This till is likely sourced from the Pennask batholith, located up ice to the north. The sample is graded and composed of sand (50%), pebbles (20%), silt (15%) and clay (15%).

Stream-Sediment Sample

Sample 20TL-BC-PF1 was collected from Trepanier Creek, which drains the northern half of the Pennask batholith, 8 km east of the Brenda mine. The sample is composed of fine-grained sand (60%), silt (30%) and small pebbles (10%).

Bromley Batholith

The fresh rock is a light creamy pink, coarse-grained, hypidiomorphic, inequigranular hornblende granodiorite (Figure 4b). It is composed of creamy white subhedral plagioclase (44%), translucent subhedral quartz (30%), creamy orange subhedral alkali feldspar (10%), greenish black, euhedral, acicular needles of hornblende (15%) and small, shiny, black euhedral grains of magnetite (1%). Feldspars are weakly sericitized, hornblende is weakly chloritized and locally altered to epidote. There are several quartz veinlets with sericite alteration selvages bordering the vein margins. The rock has a magnetic susceptibility of 21.0×10^{-3} SI.

Cahill Creek Pluton

The fresh rock is a light creamy pink, coarse-grained, inequigranular, xenolith-bearing, hornblende-biotite granite (Figure 4c). It is composed of creamy white subhedral plagioclase (25%), pinkish orange subhedral alkali feldspar (19%), translucent subhedral quartz (20%), black subhedral biotite (3%), black acicular hornblende (2%) and irregular 1–40 mm xenoliths of a fine- to medium-grained clinopyroxene-hornblende quartz diorite (30%), possibly from the Hedley intrusion. Feldspars are moderately sericitized and there are several chlorite veinlets with sericite alteration selvages bordering the vein margins. The rock has a magnetic susceptibility of 14.36×10^{-3} SI.

Hedley Intrusion

The fresh rock is a dark green, medium-grained, equigranular, pyroxene-hornblende quartz diorite (Figure 4d). It is composed of creamy white subhedral plagioclase (25%), black subhedral hornblende (30%), green euhedral clinopyroxene (25%), translucent subhedral quartz eyes (8%), creamy orange subhedral alkali feldspar (2%) and trace magnetite. Plagioclase is moderately sericitized and hornblende is weakly chloritized,

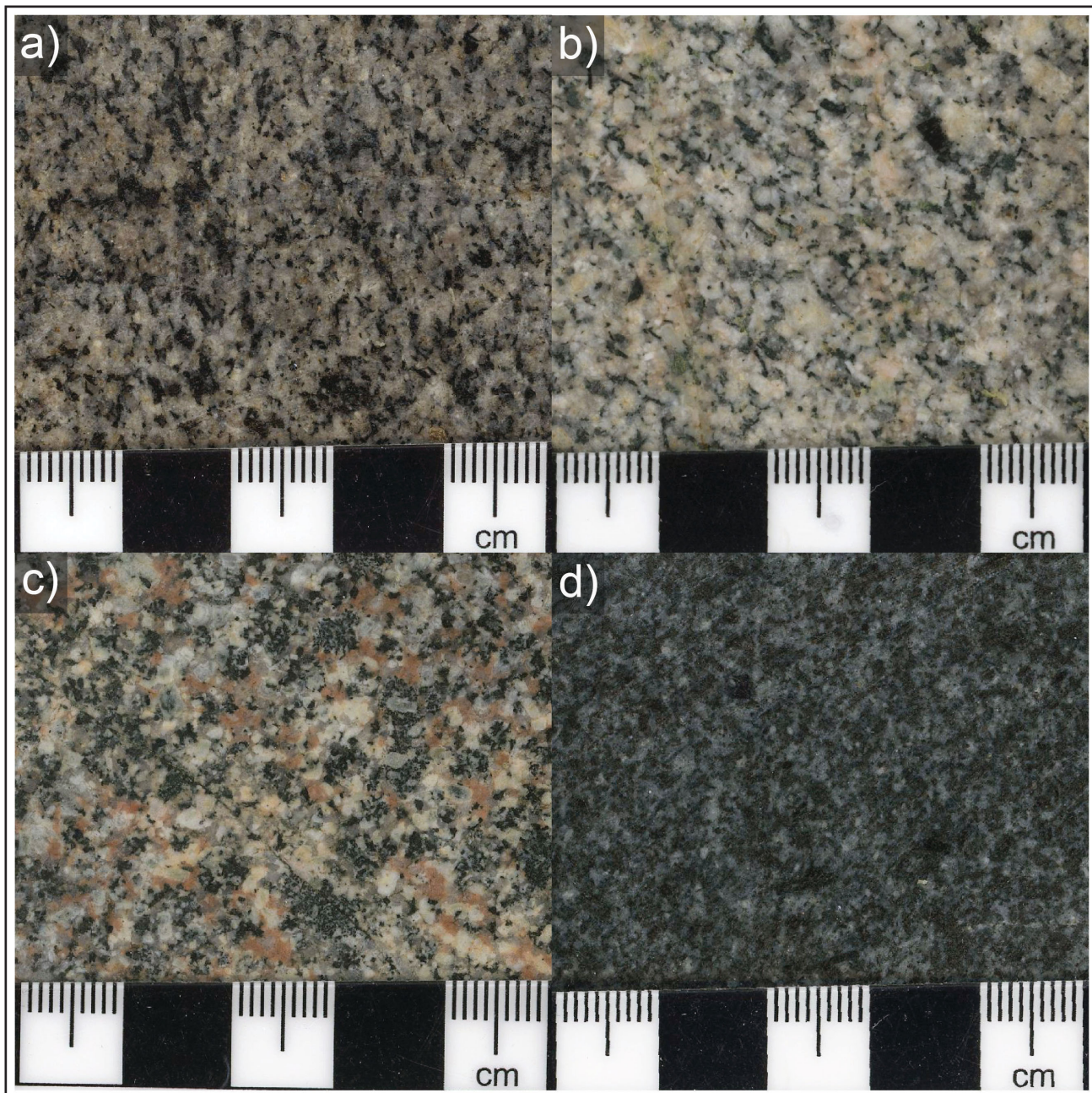


Figure 4. Rocks of the calc-alkaline Eastern magmatic axis: **a)** equigranular granodiorite of the Brenda stock, Pennask batholith; **b)** inequigranular granodiorite of the Bromley pluton, **c)** inequigranular granite of the Cahill Creek pluton, and **d)** equigranular diorite of the Hedley intrusion.

and there are a few calcite-chlorite veinlets. The rock has a magnetic susceptibility of 0.84×10^{-3} SI.

Future Sample Processing and Analysis

Samples will be crushed, sieved, washed and hand-panned prior to heavy-liquid separation using methylene iodide solution to separate them into heavy and light fractions. Approximately 30–50 zircons will be picked from each rock sample and 100–200 zircons from each stream-sediment and till sample, and mounted in an epoxy puck. Zircons will

be imaged in reflected light and cathodoluminescence, and the morphology of the crystals will be classified to identify zircon populations with characteristic habit and growth bands. Appropriate inclusion-free spots will be chosen and analyzed at The University of British Columbia Pacific Centre for Isotopic and Geochemical Research using laser-ablation inductively coupled plasma–mass spectrometry (LA-ICP-MS) to determine the trace-element composition as well as the U-Pb dates. Zircon cores and rims will both be analyzed in each sample when possible. Alkali feldspars will be picked from the light fraction and mounted on a

puck to be analyzed for composition and Pb isotopes via LA-ICP-MS. A fresh portion of the rock samples will be analyzed for major oxides, trace elements and iron speciation.

Summary

There is a very strong geological and geochronological framework that documents the changes in the Quesnellia arc throughout time, resulting in varying magma chemistries, emplacement depths, and styles of plutons and associated porphyry mineralization (Mortensen et al., 1995; McMillan et al., 1996; Logan et al., 2011; Logan and Mihalynuk, 2014; Schiarizza, 2014). This provides a foundation upon which investigations of variability in magmatic porphyry fertility throughout arc evolution can be undertaken, in this case by evaluating the chemistry of zircons.

Glacial-till and stream-sediment samples have been taken to test the effectiveness of using detrital zircons as an exploration tool, and as a means to increase the zircon representation of the arc and to increase the potential for obtaining zircons from silica-undersaturated to weakly silica-saturated intrusions that typically have low zircon yields.

The ability to identify fertile arc magmas and understand variability within and between different arc settings will enable explorers to better recognize magmas with the potential to form an economic porphyry Cu deposit and differentiate them from barren intrusions. This research will be applied to develop an exploration toolkit for porphyry Cu deposits that uses detrital and primary zircons to characterize the magmatic fertility of a district or belt to improve explorers' ability to discover economic porphyry mineralization beneath cover.

Acknowledgments

This project is part of the Mineral Deposit Research Unit's Porphyry Indicator Minerals (PIMS) project. Geoscience BC is thanked for its financial contribution in support of this project in the form of a 2020 Geoscience BC Scholarship. Additional funding was provided by the Society of Economic Geologists Canada. The authors thank R.G. Lee for his comments, insights, and suggestions for improvement.

References

- Ager, C.A. (1974): The three-dimensional structure of batholiths as deduced from gravity data; Ph.D. thesis, The University of British Columbia, 143 p., URL <<https://doi.org/10.14288/1.0052998>>.
- Ash, C.H. and Riveros, C.P. (2001): Geology of the Gibraltar copper-molybdenite deposit, east-central British Columbia (93B/9); in Geological Fieldwork 2000, BC Ministry of Energy, Mines and Low Carbon Innovation, BC Geological Survey, Paper 2001-1, p. 119–133, URL <http://cmscontent.nrs.gov.bc.ca/geoscience/PublicationCatalogue/Paper/BCGS_P2001-01-09_Ash.pdf> [October 2020].
- Ash, C.H., Reynolds, P.H., Creaser, R.A. and Mihalynuk, M.G. (2007): $^{40}\text{Ar}/^{39}\text{Ar}$ and Re-Os isotopic ages for hydrothermal alteration and related mineralization at the Highland Valley Cu-Mo deposit (NTS 092I), southwestern British Columbia; in Geological Fieldwork 2006, BC Ministry of Energy, Mines and Low Carbon Innovation, BC Geological Survey, Paper 2007-1, p. 19–24, URL <http://cmscontent.nrs.gov.bc.ca/geoscience/PublicationCatalogue/Paper/BCGS_P2007-01-02_Ash.pdf> [October 2020].
- Ballard, J.R., Palin, M.J. and Campbell, I.H. (2002): Relative oxidation states of magmas inferred from Ce(IV)/Ce(III) in zircon: application to porphyry copper deposits of northern Chile; Contributions to Mineralogy and Petrology, v. 144, p. 347–364, URL <<https://doi.org/10.1007/s00410-002-0402-5>>.
- BC Geological Survey (2020): MINFILE BC mineral deposits database; BC Ministry of Energy, Mines and Low Carbon Innovation, BC Geological Survey, URL <<http://minfile.ca>> [October 2020].
- Belousova, E.A., Griffin, W.L. and O'Reilly, S.Y. 2006. Zircon crystal morphology, trace element signatures and Hf isotope composition as a tool for petrogenetic modelling: examples from eastern Australian granitoids; Journal of Petrology, v. 47, p. 329–353, URL <<https://doi.org/10.1093/petrology/egi077>>.
- Bouzari, F., Hart, C.J.R. and Bissig, T. (2020): Assessing British Columbia porphyry fertility in British Columbia batholiths using zircons; Geoscience BC Report 2020-07, MDRU Publication 450, 24 p.
- Bouzari, F., Hart, C.J.R., Bissig, T. and Barker, S. (2016): Hydrothermal alteration revealed by apatite luminescence and chemistry: a potential indicator mineral for exploring covered porphyry copper deposits; Economic Geology, v. 111, p. 1397–1410, URL <<https://doi.org/10.2113/econgeo.111.6.1397>>.
- Burnham, C.W. and Ohmoto, H. (1980): Late stage processes of felsic magmatism; in Granitic Magmatism and Related Mineralization, S. Ishihara and S. Takenouchi (ed.), Society of Mining Geologists of Japan, Special Issue 8, p. 1–11.
- Byrne, K., Stock, E., Ryan, J., Johnson, C., Nisenson, J., Alva Jimenez, T., Lapointe, M., Stewart, H., Grubisa, G. and Sykora, S. (2013): Porphyry Cu-(Mo) deposits in the Highland Valley district, south-central British Columbia; Society of Economic Geologists, Field Trip Guidebook Series, v. 43, p. 99–116.
- Bysouth, G.D., Campbell, K.V., Barker, G.E. and Gagnier, G.K. (1995): Tonalite trondhjemite fractionation of peraluminous magma and the formation of syntectonic porphyry copper mineralization, Gibraltar mine, central British Columbia; in Porphyry Deposits of the Northwestern Cordillera of North America, T.G. Schroeter (ed.), Canadian Institute of Mining, Metallurgy and Petroleum, Special Volume 46, p. 201–213.
- Celis, A. (2015): Titanite as an indicator mineral for alkalic porphyry Cu-Au deposits in south-central British Columbia; M.Sc. thesis, The University of British Columbia, 247 p., URL <<https://doi.org/10.14288/1.0166663>>.
- Colpron, M. and Nelson, J.L. (2020): A digital atlas of terranes for the northern Cordillera; Yukon Geological Survey, URL <<http://data.geology.gov.yk.ca/Compilation/2>> [October 2020].

- Colpron, M. and Price, R.A. (1995): Tectonic significance of the Kootenay terrane, southeastern Canadian Cordillera: an alternative model; *Geology*, v. 23, p. 25–28, URL <[https://doi.org/10.1130/0091-7613\(1995\)023<0025:TSOT-KT>2.3.CO;2](https://doi.org/10.1130/0091-7613(1995)023<0025:TSOT-KT>2.3.CO;2)>.
- Consolidated Woodjam Copper Corp. (2013): Woodjam projects; Consolidated Woodjam Copper Corp., URL <[https://www.woodjamcopper.com/projects/](http://www.woodjamcopper.com/projects/)> [October 2020].
- Copper Mountain Mining Corp. (2020): Mineral reserve and mineral resource for the Copper Mountain operation; Copper Mountain Mining Corp., URL <<https://www.cumtn.com/operations/copper-mountain-mine/overview/>> [October 2020].
- Cui, Y., Miller, D., Schiarizza, P. and Diakow, L.J. (2017): British Columbia digital geology; BC Ministry of Energy, Mines and Low Carbon Innovation, BC Geological Survey, Open File 2017-8, 9 p., URL <http://cmscontent.nrs.gov.bc.ca/geoscience/PublicationCatalogue/OpenFile/BCGS_OF-2017-08.pdf> [October 2020].
- D'Angelo, M. (2016): Geochemistry, petrography and mineral chemistry of the Guichon Creek and Nicola batholiths, south-central British Columbia; M.Sc. thesis, Lakehead University, 435 p.
- D'Angelo, M., Miguel, A., Hollings, P., Byrne, K., Piercy, S. and Creaser, R. (2017): Petrogenesis and magmatic evolution of the Guichon Creek batholith: Highland Valley porphyry Cu±(Mo) district, south-central British Columbia; *Economic Geology*, v. 112, p. 1857–1888, URL <<https://doi.org/10.5382/econgeo.2017.4532>>.
- del Real, I., Bouzari, F., Rainbow, A., Bissig, T., Blackwell, J., Sherlock, R., Thompson, J.F.H. and Hart, C.J.R. (2017): Spatially and temporally associated porphyry deposits with distinct Cu/Au/Mo ratios, Woodjam district, central British Columbia; *Economic Geology*, v. 112, p. 1673–1717, URL <<https://doi.org/10.5382/econgeo.2017.4526>>.
- Dilles, J.H. and Einaudi, M.T. (1992): Wall-rock alteration and hydrothermal flow paths about the Ann-Mason porphyry copper deposit, Nevada – a 6-km vertical reconstruction; *Economic Geology*, v. 87, p. 1963–2001, URL <<https://doi.org/10.2113/gsecongeo.87.8.1963>>.
- Dilles, J.H., Kent, A.J.R., Wooden, J.L., Tosdal, R.M., Koleszar, A., Lee, R.G. and Farmer, L.P. (2015): Zircon compositional evidence for sulfur-degassing from ore-forming arc magmas; *Economic Geology*, v. 110, p. 241–251, URL <<https://doi.org/10.2113/econgeo.110.1.241>>.
- Fulton, R.J. (1963): Surficial geology, Kamloops Lake, British Columbia; Geological Survey of Canada, Map 9-1963, 1 sheet, 1:126 720 scale., URL <<https://doi.org/10.4095/108672>>.
- Ghaffari, H., Stubens, T.C., de Ruijter, A., Ulansky, R., Borntraeger, B. and Newcomen, H.W. (2009): Ajax copper/gold project, Kamloops, British Columbia – preliminary assessment technical report, July 31, 2009; Abacus Mining and Exploration Corp., 172 p., URL <https://www.amemining.com/site/assets/files/5750/2009-08-05_ajaxpatechnicalreport.pdf> [November 2020].
- Harding, B. (2012): The characterization of molybdenum mineralization at the Gibraltar mines Cu-Mo porphyry, central British Columbia; B.Sc. thesis, Queen's University, 52 p.
- Holbek, P. and Joyes, R. (2013). Copper Mountain: an alkalic porphyry copper-gold-silver deposit in the southern Quesnel terrane, British Columbia; *in Porphyry Systems of Central and Southern BC: Tour of Central BC Porphyry Deposits* from Prince George to Princeton, J.M. Logan and T.G. Schroeter (ed.), Society of Economic Geologists, Field Trip Guidebook Series, v. 44, p. 129–143.
- International Copper Study Group (2019): The World Copper Factbook 2019; International Copper Study Group, URL <<https://www.icsg.org/index.php/component/jdownloads/finish/170/3046>> [October 2020].
- Kobylinski, C., Hattori, K., Smith, S. and Plouffe, A. (2020): Protracted magmatism and mineralized hydrothermal activity at the Gibraltar porphyry copper-molybdenum deposit, British Columbia; *Economic Geology*, v. 115, no. 5, p. 1119–1136, URL <<https://doi.org/doi:10.5382/econgeo.4724>>.
- Lang, J.R., and Stanley, C.R. (1995): Contrasting styles of alkalic porphyry copper-gold deposits in the northern Iron Mask batholith, Kamloops, British Columbia; Canadian Institute of Mining, Metallurgy and Petroleum, Special Volume 46, p. 581–592.
- Lang, J.R., Lueck, B., Mortensen, J.K., Russell, J.K., Stanley, C.R. and Thompson, J.F.H. (1995): Triassic–Jurassic silica-undersaturated and silica-saturated alkalic intrusions in the Cordillera of British Columbia: implications for arc magmatism; *Geology*, v. 23, p. 451–454, URL <[https://doi.org/10.1130/0091-7613\(1995\)023<0451:TJS-UAS>2.3.CO;2](https://doi.org/10.1130/0091-7613(1995)023<0451:TJS-UAS>2.3.CO;2)>.
- Lee, R.G. (2008): Genesis of the El Salvador porphyry copper deposit, Chile and distribution of epithermal alteration at Lassen Peak, California; Ph.D. thesis, Oregon State University, 344 p.
- Lee, R.G., Bryne, K., D'Angelo, M.D., Hart, C.J.R., Hollings, P., Gleeson, S.A. and Alfaro, M. (2020): Using zircon trace element composition to assess porphyry copper potential of the Guichon Creek batholith and Highland Valley Copper deposit, south-central British Columbia; *Mineralium Deposita*, URL <<https://doi.org/10.1007/s00126-020-00961-1>>.
- Lee, R.G., Dilles, J.H., Tosdal, R.M., Wooden, J.L. and Mazdab, F.K. (2017): Magmatic evolution of granodiorite intrusions at the El Salvador porphyry copper deposit, Chile, based on trace element composition and U/Pb age of zircons; *Economic Geology*, v. 112, p. 245–273, URL <<https://doi.org/10.2113/econgeo.112.2.245>>.
- Lee, R.G., Plouffe, A., Ferbey, T., Hart, C.J.R., Hollings, P. and Gleeson, S.A. (in press): Recognizing porphyry copper potential from till zircon composition: a case study from the Highland Valley porphyry district, south-central British Columbia; *Economic Geology Scientific Communications*, accepted for publication.
- Little, H.W. (1960): Nelson map-area, west half, British Columbia (82F W1/2); Geological Survey of Canada, Memoir 308, 205 p., URL <<https://doi.org/10.4095/100535>>.
- Logan, J.M. and Mihalynuk, M.G. (2005): Porphyry Cu-Au deposits of the Iron Mask batholith, southeastern British Columbia; *in Geological Fieldwork 2004*, BC Ministry of Energy, Mines and Low Carbon Innovation, BC Geological Survey, Paper 2005-1, p. 249–270, URL <http://cmscontent.nrs.gov.bc.ca/geoscience/PublicationCatalogue/Paper/BCGS_P2005-RR07_Logan.pdf> [October 2020].
- Logan, J.M. and Mihalynuk, M.G. (2014): Tectonic controls on Early Mesozoic paired alkaline porphyry deposit belts (Cu-Au ± Ag-Pt-Pd-Mo) within the Canadian Cordillera; *Economic Geology*, v. 109, p. 827–858, URL <<https://doi.org/10.2113/econgeo.109.4.827>>.

- Logan, J.M., Mihalynuk, M.G., Friedman, R.M. and Creaser, R.A. (2011): Age constraints of mineralization at the Brenda and Woodjam Cu-Mo+/-Au porphyry deposits – an Early Jurassic calc-alkaline event, south-central British Columbia; in Geological Fieldwork 2010, BC Ministry of Energy, Mines and Low Carbon Innovation, BC Geological Survey, Paper 2011-01, p. 129–144, URL <http://cmscontent.nrs.gov.bc.ca/geoscience/PublicationCatalogue/Paper/BCGS_P2011-01-09_Logan.pdf> [October 2020].
- Logan, J.M., Mihalynuk, M.G., Ullrich, T. and Friedman, R.M. (2007): U-Pb ages of intrusive rocks and $^{40}\text{Ar}/^{39}\text{Ar}$ plateau ages of copper-gold-silver mineralization associated with alkaline intrusive centres at Mount Polley and the Iron Mask batholith, southern and central British Columbia; in Geological Fieldwork 2006, BC Ministry of Energy, Mines and Low Carbon Innovation, BC Geological Survey, Paper 2007-1, p. 93–116, URL <http://cmscontent.nrs.gov.bc.ca/geoscience/PublicationCatalogue/Paper/BCGS_P2007-01-10_Logan.pdf> [October 2020].
- Lu, Y., Loucks, R.R., Fiorentini, M., McCuaig, T.C., Evans, N.J., Yang, Z., Hou, Z., Kirkland, C.L., Parra-avila, L.A. and Kobussen, A. (2016): Zircon compositions as a pathfinder for porphyry Cu ± Mo ± Au deposits; Economic Geology Special Publications, v. 19, p. 329–347.
- McMillan, W.J. (1976): Geology and genesis of the Highland Valley ore deposits and the Guichon Creek batholith; in Porphyry Deposits of the Canadian Cordillera, A. Sutherland Brown (ed.), Canadian Institute of Mining and Metallurgy, Special Volume 15, p. 85–104.
- McMillan, W.J. (1981): Nicola project – Merritt area; BC Ministry of Energy, Mines and Low Carbon Innovation, BC Geological Survey, Preliminary Map 47 (2 sheets), scale 1:25 000, URL <http://cmscontent.nrs.gov.bc.ca/geoscience/PublicationCatalogue/PreliminaryMap/BCGS_PM47.pdf> [October 2020].
- McMillan, W.J. (1985): Geology and ore deposits of the Highland Valley camp; Field Guide and Reference Manual Series, A.J. Sinclair (ser. ed.), Geological Association of Canada, Mineral Deposits Division, no. 1, 121 p.
- McMillan, W.J., Thompson, J.F.H., Hart, C.J.R. and Johnston, S.T. (1996): Porphyry deposits of the Canadian Cordilleran; Geoscience Canada, v. 23, p. 125–134.
- Monger, J.W.H. (1985): Structural evolution of the southwestern Intermontane belt, Ashcroft and Hope map areas, British Columbia; in Current Research, Part A, Geological Survey of Canada, Paper 85-1A, p. 349–3523.
- Mortensen, J.K., Ghosh, D.K. and Ferri, F. (1995): U-Pb geochronology of intrusive rocks associated with copper-gold porphyry deposits in the Canadian Cordillera; in Porphyry Deposits of the Northwestern Cordillera of North America, T.G. Schroeter (ed.), Canadian Institute of Mining, Metallurgy and Petroleum, Special Volume 46, p. 142–158.
- Mortimer, N. (1987): The Nicola Group: Late Triassic and Early Jurassic subduction-related volcanism in British Columbia; Canadian Journal of Earth Sciences, v. 24, p. 2521–2536, URL <<https://doi.org/10.1139/e87-236>>.
- New Gold Inc. (2019): New Gold mineral reserves and resources summary on December 31, 2019; New Gold Inc., URL <<https://www.newgold.com/investors/financial-information/reserves-and-resources/default.aspx>> [October 2020].
- Nixon, G.T., Archibald, D.A. and Heaman, L.M. (1993): $^{40}\text{Ar}/^{39}\text{Ar}$ and U-Pb geochronometry of the Polaris Alaskan type complex, British Columbia: precise timing of Quesnellia–North America interaction, Geological Association of Canada–Mineralogical Association of Canada, Joint Annual Meeting, Waterloo, Ontario, Program with Abstracts, p. 76.
- Northcote, K.E. (1969): Geology and geochronology of the Guichon Creek Batholith; BC Ministry of Energy, Mines and Low Carbon Innovation, BC Geological Survey, Bulletin 56, 77 p., URL <http://cmscontent.nrs.gov.bc.ca/geoscience/PublicationCatalogue/Bulletin/BCGS_B-056.pdf> [October 2020].
- Northcote, K.E. (1978): Iron Mask batholith (92 119, 10); in Geological Fieldwork 1977, BC Ministry of Energy, Mines and Low Carbon Innovation, BC Geological Survey, Paper 1978-01, p. 37–38.
- Natural Resources Canada. (2018): Canadian mine production of copper, by province and territory, 2018, URL <<https://www.nrcan.gc.ca/our-natural-resources/minerals-mining/copper-facts/20506#L2>> [October 2020].
- Panteleyev, A. (1978): Granite Mountain project (93B/8); in Geological Fieldwork 1977, BC Ministry of Energy, Mines and Low Carbon Innovation, BC Geological Survey, Paper 1977-1, p. 39–42.
- Parrish, R.R. and Monger, J.W.H. (1992): New U-Pb dates from southwestern British Columbia; in Radiogenic Age and Isotopic Studies, Report 5, Geological Survey of Canada, p. 87–108.
- Pizarro, H., Campos, E., Bouzari, F., Rousse, S., Bissig, T., Gregoire, M. and Riquelme, R. (2020): Porphyry indicator zircons (PIZs): application to exploration of porphyry copper deposits; Ore Geology Reviews, v. 126, URL <<https://doi.org/10.1016/j.oregeorev.2020.103771>>.
- Preto, V.A. (1972): Geology of Copper Mountain, British Columbia; BC Ministry of Energy, Mines and Low Carbon Innovation, BC Geological Survey, Bulletin 59, 87 p., URL <http://cmscontent.nrs.gov.bc.ca/geoscience/PublicationCatalogue/Bulletin/BCGS_B059.pdf> [October 2020].
- Preto, V.A. (1979): Geology of the Nicola Group between Merritt and Princeton; BC Ministry of Energy, Mines and Low Carbon Innovation, BC Geological Survey, Bulletin 69, 90 p., URL <http://cmscontent.nrs.gov.bc.ca/geoscience/PublicationCatalogue/Bulletin/BCGS_B069.pdf> [October 2020].
- PricewaterhouseCoopers Inc. (2019): ESG: Resilience and opportunity in uncertain times—the mining industry in British Columbia 2019; PricewaterhouseCoopers Canada, URL <<https://www.pwc.com/ca/en/mining/publications/p688279-bc-mines-report-2019-report-en.pdf#page=8>> [November 2020].
- Read, P.B. and Okulitch, A.V. (1977): The Triassic unconformity of south-central British Columbia; Canadian Journal of Earth Sciences, v. 14, p. 606–638, URL <<https://doi.org/10.1139/e77-063>>.
- Rezeau, H., Moritz, R., Wotzlaw, J.-F., Hovakimyan, S. and Tayan, R. (2019): Zircon petrochronology in the ore-bearing Meghri-Ordubad pluton, Lesser Caucasus: fingerprinting igneous processes with implications for the exploration of porphyry Cu-Mo deposits; Economic Geology, v. 114, p. 1365–1388, URL <<https://doi.org/10.5382/econ-geo.4671>>.
- Schiarizza, P. (2014): Geological setting of the Granite Mountain batholith, host to the Gibraltar porphyry Cu-Mo deposit, south-central British Columbia; in Geological Fieldwork 2013, BC Ministry of Energy, Mines and Low Carbon Innovation, BC Geological Survey, Paper 2014-1, p. 95–110,

- URL <http://cmscontent.nrs.gov.bc.ca/geoscience/PublicationCatalogue/Paper/BCGS_P2014-01-06_Schiarizza.pdf> [October 2020].
- Schiarizza, P. (2015): Geological setting of the Granite Mountain batholith, south-central British Columbia; *in* Geological Fieldwork 2014, BC Ministry of Energy, Mines and Low Carbon Innovation, BC Geological Survey, Paper 2015-1, p. 19-39, URL <http://cmscontent.nrs.gov.bc.ca/geoscience/PublicationCatalogue/Paper/BCGS_P2015-01-02_Schiarizza.pdf> [October 2020].
- Schiarizza, P. (2016): Toward a regional stratigraphic framework for the Nicola Group: preliminary results from the Bridge Lake–Quesnel River area; *in* Geological Fieldwork 2015, BC Ministry of Energy, Mines and Low Carbon Innovation, BC Geological Survey, Paper 2016-1, p. 13–30, URL <http://cmscontent.nrs.gov.bc.ca/geoscience/PublicationCatalogue/Paper/BCGS_P2016-01-02_Schiarizza.pdf> [October 2020].
- Schiarizza, P. (2019): Geology of the Nicola Group in the Bridge Lake–Quesnel River area, south-central British Columbia; *in* Geological Fieldwork 2018, BC Ministry of Energy, Mines and Low Carbon Innovation, BC Geological Survey, Paper 2019-01, p. 15–30, URL <http://cmscontent.nrs.gov.bc.ca/geoscience/PublicationCatalogue/Paper/BCGS_P2019-01-02_Schiarizza.pdf> [October 2020].
- Schiarizza, P., Bell, K. and Bayliss, S. (2009): Geology and mineral occurrences of the Murphy Lake area, south-central British Columbia (NTS 93A/03); *in* Geological Fieldwork 2013, BC Ministry of Energy, Mines and Low Carbon Innovation, BC Geological Survey, Paper 2014-1, p. 95–110, URL <http://cmscontent.nrs.gov.bc.ca/geoscience/PublicationCatalogue/Paper/BCGS_P2009-01-15_Schiarizza.pdf> [October 2020].
- Schiarizza, P., Israel, S., Heffernan, S., Boulton, A., Bligh, J., Bell, K., Bayliss, S., Macauley, J., Bluemel, B., Zuber, J., Friedman, R.M., Orchard, M.J. and Poulton, T.P. (2013): Bedrock geology between Thuya and Woodjam creeks, south-central British Columbia, NTS 92P/7, 8, 9, 10, 14, 15, 16; 93A/2, 3, 6; BC Ministry of Energy, Mines and Low Carbon Innovation, BC Geological Survey, Open File 2013-05; 4 sheets, scale 1:100 000, URL <http://cmscontent.nrs.gov.bc.ca/geoscience/PublicationCatalogue/OpenFile/BCGS_OF2013-05.pdf> [October 2020].
- Shen, P., Hattori, K., Pan, H., Jackson, S. and Seitmuratova, E. (2015): Oxidation condition and metal fertility of granitic magmas: zircon trace-element data from porphyry Cu deposits in the central Asian orogenic belt; *Economic Geology*, v. 110, p. 1861–1878, URL <<https://doi.org/10.2113/econgeo.110.7.1861>>.
- Smith, R.B. (1979): Geology of the Harper Ranch Group (Carboniferous–Permian) and Nicola Group (Upper Triassic) northeast of Kamloops, British Columbia; M.Sc. thesis, The University of British Columbia, 211 p., URL <<https://doi.org/10.14288/1.0052516>>.
- Snyder, L.D. and Russell, J.K. (1995): Petrogenetic relationships and assimilation processes in the alkalic Iron Mask Batholith, south-central British Columbia; *in* Porphyry Deposits of the Northwestern Cordillera of North America, Schroeter, T.G. (ed.), Canadian Institute of Mining, Metallurgy and Petroleum, Special Volume 46, p. 593–608.
- Soregaroli, A.E. and Whitford, D.F. (1976): Brenda; *in* Porphyry Deposits of the Canadian Cordillera, A. Sutherland Brown (ed.), Canadian Institute of Mining and Metallurgy, Special Volume 15, p. 186–194.
- Struik, L.C. (1988): Regional imbrication within Quesnel Terrane, central British Columbia, as suggested by conodont ages; *Canadian Journal of Earth Sciences*, v. 25, p. 1608–1617, URL <<https://doi.org/10.1139/e88-153>>.
- Sutherland Brown, A., editor (1976): Porphyry deposits of the Canadian Cordillera; Canadian Institute of Mining, Metallurgy and Petroleum, Special Volume 15, 510 p.
- Teck Resources Limited (2019): Annual information form; Teck Resources Limited, public filing, URL <<https://www.teck.com/investors/reserves-&-resources/reserves-and-resources>> [October 2020].
- Thomas, M.D. (2019): Gravity and magnetic models of the Iron Mask Batholith, south-central Canadian Cordillera, British Columbia; *Geological Survey of Canada, Current Research* 2019-1, 24 p., URL <<https://doi.org/10.4095/314517>>.
- Travers, W.B. (1978): Overturned Nicola and Ashcroft strata and their relations to the Cache Creek Group, southwestern Intermontane belt, British Columbia; *Canadian Journal of Earth Sciences*, v. 15, p. 99–116, URL <<https://doi.org/10.1139/e78-009>>.
- Wainwright, A.J., Tosdal, R.M., Wooden, J.L., Mazdab, F.K. and Friedman, R.M. (2011): U-Pb (zircon) and geochemical constraints on the age, origin, and evolution of Paleozoic arc magmas in the Oyu Tolgoi porphyry Cu-Au district, southern Mongolia; *Gondwana Research*, v. 19, p. 764–787, URL <<https://doi.org/10.1016/j.gr.2010.11.012>>.
- Weymark, R. (2019): Technical report on the mineral reserve update at the Gibraltar mine, British Columbia, Canada, 228 p., URL <http://www.sedar.com/issuers/issuers_en.htm> [October 2020].
- Weeks, R.M., Bradburn, R.G., Flintoff, B.C., Harris, G.R. and Malcolm, G. (1995): The Brenda mine: the life of a low-cost porphyry copper-molybdenum producer (1970–1990), southern British Columbia, *in* Porphyry Deposits of the Northwestern Cordillera of North America, T.G. Schroeter (ed.), Canadian Institute of Mining and Metallurgy, Special Volume 46, p. 192–200.
- Williamson, B.J., Herrington, R.J. and Morris, A. (2016): Porphyry copper enrichment linked to excess aluminium in plagioclase; *Nature Geosciences*, v. 9, p. 237–242, URL <<https://doi.org/10.1038/ngeo2651>>.
- Whiteaker, R.J., Mortensen, J.K. and Friedman, R.M. (1998): U-Pb geochronology, Pb isotopic signatures and geochemistry of an Early Jurassic alkalic porphyry system near Lac La Hache; *in* Geological Fieldwork 1997, BC Ministry of Energy, Mines and Low Carbon Innovation, BC Geological Survey, Paper 1998-01, p. 33-1–33-14.

Mineralogical and Geochemical Vectors within Advanced Argillic-Altered Rocks of North-Central British Columbia (NTS 094E/02, 15, 104I/05)

F. Bouzari, MDRU - Mineral Deposit Research Unit, The University of British Columbia, Vancouver, British Columbia, fbouzari@eoas.ubc.ca

R.G. Lee, MDRU - Mineral Deposit Research Unit, The University of British Columbia, Vancouver, British Columbia

C.J.R. Hart, MDRU - Mineral Deposit Research Unit, The University of British Columbia, Vancouver, British Columbia

B.I. van Straaten, British Columbia Geological Survey, British Columbia Ministry of Energy, Mines and Low Carbon Innovation, Victoria, British Columbia

Bouzari, F., Lee, R.G., Hart, C.J.R. and van Straaten, B.I. (2021): Mineralogical and geochemical vectors within advanced argillic-altered rocks of north-central British Columbia (NTS 094E/02, 15, 104I/05); *in* Geoscience BC Summary of Activities 2020: Minerals, Geoscience BC, Report 2021-01, p. 91–104.

Introduction

Advanced argillic-alteration zones in the upper parts of porphyry copper systems, also known as ‘lithocaps’, have a blanket-like geometry with areal extents of $>10 \text{ km}^2$, reach up to 1 km in thickness and form the largest near-surface footprints of porphyry copper systems. Indeed, two or more porphyry copper deposits may underlie some large, coalesced advanced argillic zones (Sillitoe, 2010), which may themselves host high-sulphidation epithermal-type gold deposits where they are preserved from erosion.

Zones of advanced argillic alteration are formed by an early stage of intense acid leaching of the wallrocks and a subsequent stage of weakly acidic fluid flow, which deposits sulphides and quartz (Simmons et al. 2005; Heinrich, 2007; Hedenquist and Taran, 2013). Advanced argillic-altered rocks contain various proportions of minerals such as sericite, andalusite, pyrophyllite, topaz, diaspore, corundum, zunyite, dickite, alunite, kaolinite, dumortierite and quartz (Meyer and Hemley, 1967). Similar to the deeper alteration in porphyry deposits, the advanced argillic-alteration zones are typically zoned. Minerals such as diaspore and andalusite with pyrophyllite occur at the roots of advanced argillic alteration above the porphyry system, whereas zones of residual quartz, quartz-alunite and quartz-kaolinite occur laterally in more permeable hostrocks at higher levels (Sillitoe, 1993, 2010; Hedenquist et al., 1998; Watanabe and Hedenquist, 2001).

The recognition of mineralogical and geochemical patterns within areas of advanced argillic alteration provides a fun-

damental opportunity to identify the presence of high-sulphidation epithermal gold and potential underlying porphyry mineralization. Advanced argillic-alteration zones in some porphyry deposits overprint earlier and deeper porphyry alteration, a phenomenon called ‘telescoping’ (Sillitoe, 2010) that results from the rapid collapse of the isotherms (Heinrich et al., 2004) or rapid uplift and erosion of the volcanic edifice (Sillitoe, 2010). Therefore, identification and characterization of advanced argillic alteration from pre-existing higher temperature alteration is important in establishing the vertical profile of the deposit and its potential hypogene enrichment at depth.

Advanced Argillic Alteration in BC

Advanced argillic alteration is not a common feature in many porphyry deposits in British Columbia (BC); this is attributed to the erosion that has destroyed and removed the shallow parts of porphyry systems in many districts. However, advanced argillic-alteration zones are preserved in some locations in BC, typically within districts that are also highly prospective to host porphyry-type copper mineralization. More particularly, zones of advanced argillic alteration cover large areas in northern BC and Vancouver Island. Studies in the Toodoggone district (Bouzari et al., 2019), the Bonanza volcanic field in northern Vancouver Island (Panteleyev and Koyanagi, 1994), Limonite Creek in central BC (Deyell et al., 2000) and several other locations in BC have recognized linkages of these altered zones to porphyry-type mineralization at depth.

Mineral exploration within advanced argillic zones is traditionally difficult because of the large size of the altered areas, the intense nature of the alteration and the subtle mineralogical changes that can be difficult to identify in the field or with tools such as a hand lens. Identification of the tex-

This publication is also available, free of charge, as colour digital files in Adobe Acrobat® PDF format from the Geoscience BC website: <http://geosciencebc.com/updates/summary-of-activities/>.

tural, mineralogical and geochemical trends within these advanced argillic-alteration zones will guide BC explorers to better identify porphyry copper potential and to provide tools that point toward associated mineralization.

In this study, alteration-mineral assemblages and compositions across advanced argillic-alteration zones in three BC mineral properties are characterized: the Tanzilla mineral property, near Dease Lake, and the Alunite Ridge and Kemess North mineral properties, both in the Toodoggone district (Figure 1). The mineralogical and geochemical data from these locations are used to establish tools and protocols that can be used to explore for porphyry deposits in areas with advanced argillic alteration anywhere in BC. This paper provides an update to the Geoscience BC-sponsored research project on advanced argillic alteration (Bouzari et al., 2020) and will be superseded by a final report to be published later in 2021.

Geological Setting

Advanced argillic-alteration zones occur in several locations in BC, particularly in porphyry-prospective areas of northern BC and Vancouver Island (Panteleyev and Koyanagi, 1994; Bouzari et al., 2020). Tanzilla, Alunite Ridge and Kemess North are located in the Stikine terrane of northern BC. The geological setting and mineral occurrences of these mineral properties have been described in several previous studies (e.g., Diakow, et al., 1993, 2006; van Straaten and Gibson 2017). The geological setting of these research sites has also been reviewed previously (Bouzari et al., 2020) and only brief summaries are provided here.

Tanzilla

The Tanzilla property is underlain by a volcanic succession assigned to the Horn Mountain Formation (late Early to

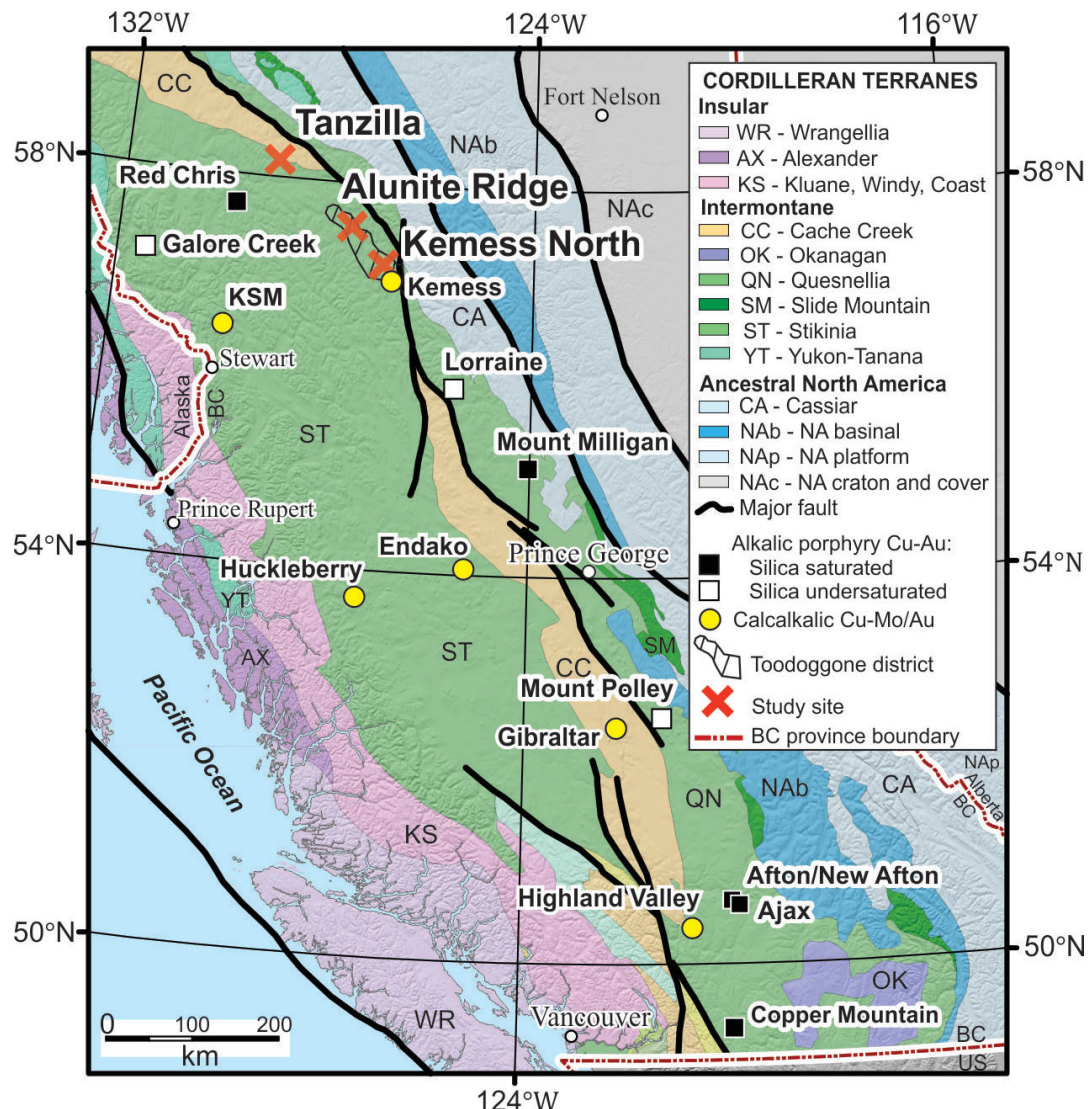


Figure 1. Cordilleran terranes of British Columbia showing the location of the study areas (after Bissig and Cooke, 2014).

Middle Jurassic; van Straaten and Nelson, 2016) in the upper part of the Hazelton Group (Figure 2). The lower part of the Horn Mountain Formation includes massive green augite-plagioclase–phyric volcanic breccia (not exposed in the study area), whereas the middle part is mainly maroon volcanic breccias, autobreccias and flows, and includes minor laminated felsic tuffs to bedded lapillistone. The upper parts of the Horn Mountain Formation consist of a felsic volcanic unit of mainly aphanitic and plagioclase-phyric clasts capped by a mafic volcanic unit of augite-plagioclase–phyric volcanic breccia and flows (van Straaten and Gibson, 2017). These units are unconformably overlain by sedimentary rocks of the Bowser Lake Group. The Late Jurassic Snowdrift Creek pluton cuts the Horn Mountain strata and the Kehlechoa thrust fault. The Horn Mountain Formation hosts areally extensive advanced argillic alteration at the Tanzilla-McBride property for at least 17 km along strike (van Straaten and Gibson, 2017; van Straaten and Bouzari, 2018). At Tanzilla, the advanced argillic-alteration zone is at least 5 by 2 km and overlies porphyry-style alteration at depth, which is characterized by quartz-sericite-pyrite to potassic alteration with anomalous copper and molybdenum hosted in a 173 Ma plagioclase porphyry intrusion (van Straaten and Nelson, 2016; van Straaten and Gibson, 2017).

Alunite Ridge

Alunite Ridge is located within the Toodoggone district of northeastern BC. The district hosts several preserved Early Jurassic high- and low-sulphidation epithermal-type deposits with advanced argillic-alteration zones (Diakow et

al., 1993; Bouzari et al., 2019). The Alunite Ridge area near Quartz Lake hosts several mineral occurrences, including Quartz Lake, Alunite Ridge, North Ridge and Sickle Creek (Figure 3). The underlying geology consists of the Lower Toodoggone Formation, which is equivalent to the Telkwa Formation of the Hazelton Group (Diakow et al., 1991), and consists of andesitic lava flows, tuff, breccia and epiclastic rocks that are intruded by small dikes and stocks of monzonite (Figure 3). The Jock Creek monzonitic pluton forms a large body to the south and east. Zones of intense alteration are northwest-trending and about 200 m wide. Gold mineralization occurs in a 10–15 m wide zone of silicified rock with quartz-alunite alteration, locally with vuggy textures and zones of buff-grey intense diaspore alteration (Bouzari et al., 2019). Banded quartz veins with calcite and K-feldspar host low-sulphidation–type chalcopyrite-sphalerite-galena-pyrite mineralization and occur 200–300 m south of the advanced argillic-altered zone at Alunite Ridge and at the base of the valley near Quartz Lake.

Kemess North

The Kemess North porphyry is located about 6.5 km north of the main Kemess deposit (Kemess South) in the southern part of the Toodoggone district. Hostrocks at Kemess North include Upper Triassic Takla Group andesite/basaltic volcanic rocks locally overlain by Lower Jurassic Toodoggone Formation dacitic fragmental volcanic rocks (Figure 4). Several Early Jurassic stocks or dikes of quartz monzonite to quartz rhyolite composition of the Black Lake intrusive suite have intruded the volcanic succession (McKinley,

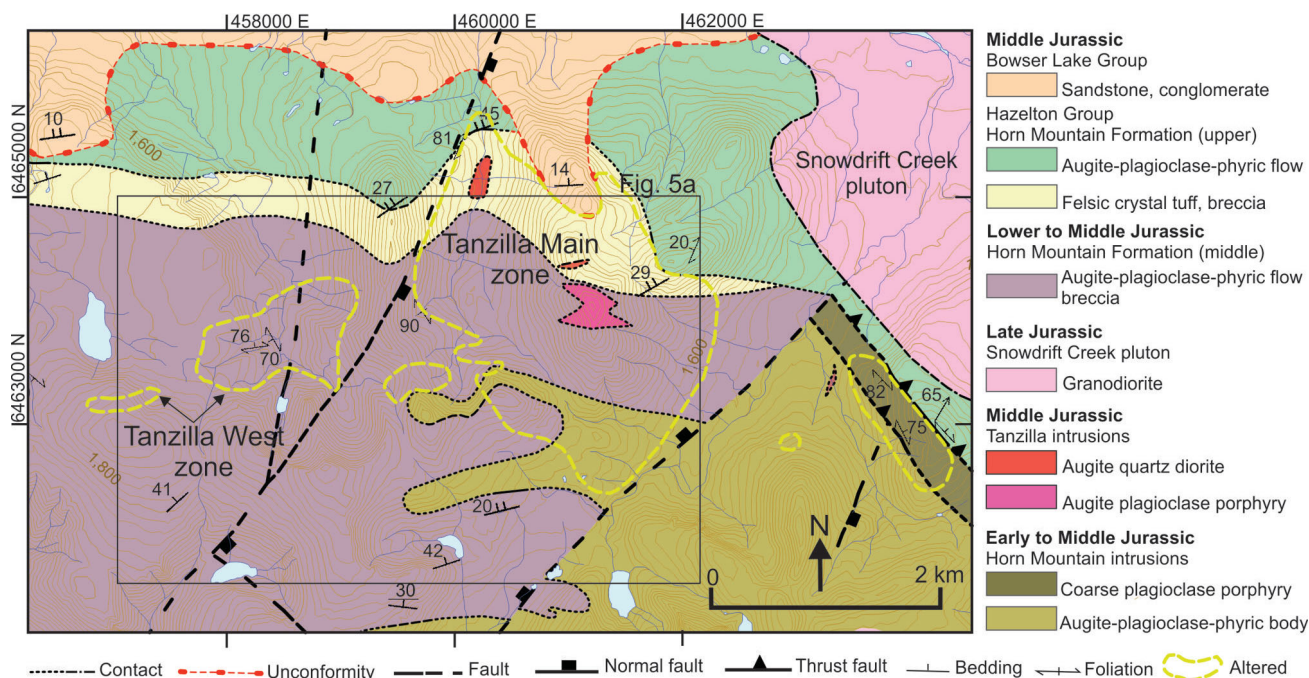


Figure 2. Geology of the Tanzilla study area (after van Straaten et al., 2017).

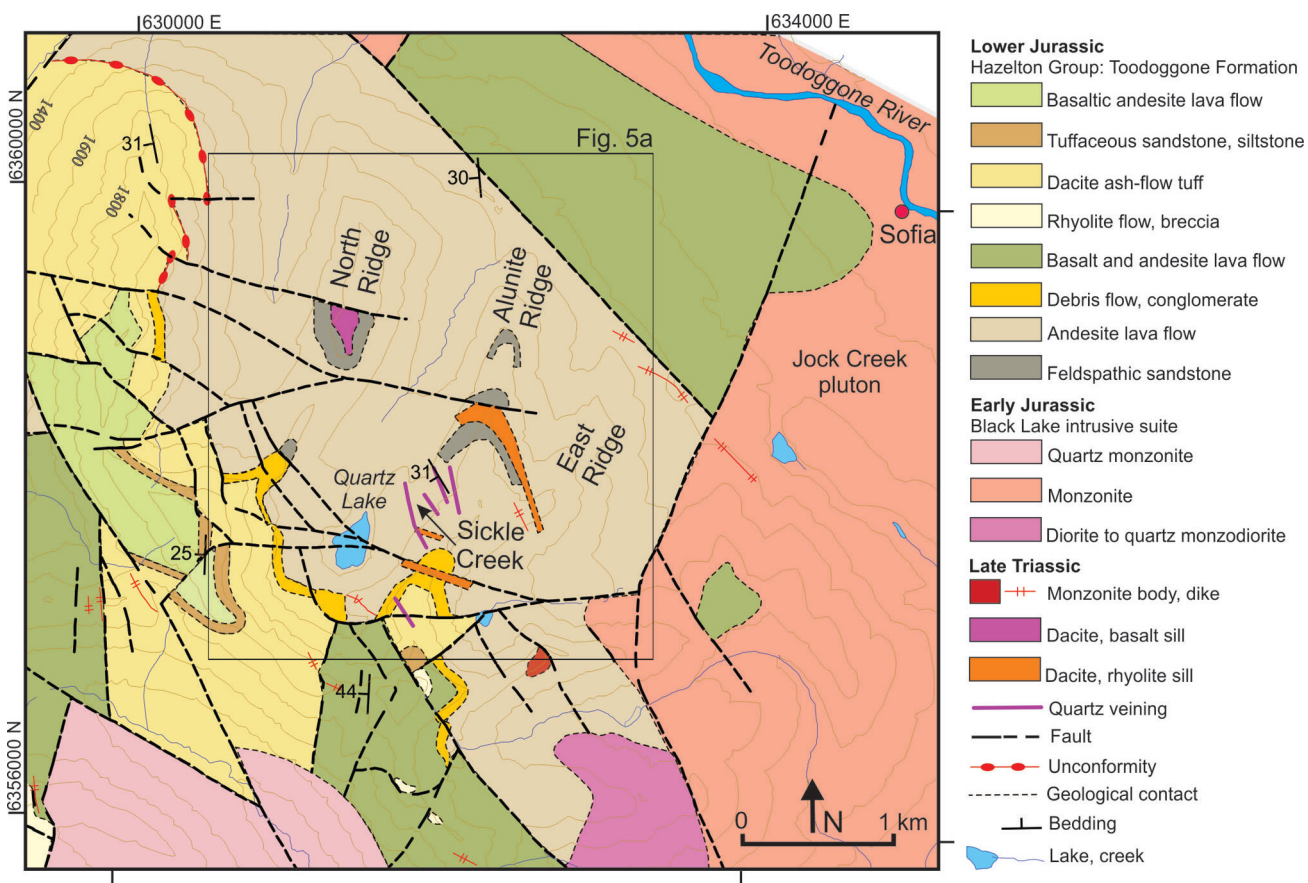


Figure 3. Geology of the Alunite Ridge study area (after Diakow et al., 2006).

2006). The east-trending, south-dipping mineralization at Kemess North seems to have formed along faults with distinct sericite-clay alteration near the surface, which transitions to typical K-silicate alteration at depth.

Sampling and Analytical Work

At Tanzilla, advanced argillic alteration was mapped and sampled across a 3.5 km north-south profile and a 4 km east-west profile. A total of 54 samples were collected from surface outcrops. Drillhole TZ15-01 (Barresi and Luckman, 2016), which tested mineralization below the Main zone hill to the depth of 840 m (-60°) was examined, and 20 core samples were collected to characterize alteration and mineralization at depth. At Alunite Ridge, the footprint of alteration was mapped and sampled along three northeast-trending profiles with a total length of approximately 5 km in an area of 2 by 2 km. In total, 63 samples from surface outcrops ranging in elevation from 1908 to 1560 m asl and 10 samples from drillhole SG-04-18 (Kuran and Barrios, 2005) to a depth of 227 m below surface (1642 m asl) were collected. At Kemess North, advanced argillic alteration was mapped and sampled along a north-south profile of approximately 0.5 km. In total, 18 samples were collected from surface outcrops. Drillholes KN-01-12 and KN-02-09 (SRK Consulting Inc., 2016), which tested

mineralization below the advanced argillic alteration to a depth of ~500 m below surface, were examined and 44 core samples were collected to characterize alteration and mineralization at depth. Surface sample locations are shown on Figure 5a and results for drillhole samples will be provided in a subsequent publication.

All rock samples were characterized in the field, and again after being cut into slabs. To further characterize alteration assemblages, all samples were analyzed at The University of British Columbia's Mineral Deposit Research Unit (MDRU) using the tabletop version of the Terraspec® by Analytical Spectral Devices (ASD) Inc., with full range visible and near-infrared (VNIR) and shortwave infrared (SWIR) wavelengths for the range of 350–2500 nm. Petrographic thin-section studies were completed for 56 selected rock samples. A total of 223 whole-rock samples were analyzed for major- and trace-elements at Bureau Veritas Minerals (Vancouver, BC). Samples were analyzed by X-ray fluorescence (XF700 method) for SiO₂, Al₂O₃, Fe₂O₃, CaO, MgO, Na₂O, K₂O, MnO, TiO₂, P₂O₅, Cr₂O₃, SO₃ and Sr; inductively coupled plasma (ICP)-mass spectrometry using lithium borate fusion (LF100) for Ba, Be, Co, Cs, Ga, Hf, Nb, Rb, Sn, Sr, Ta, Th, U, V, W, Zr, Y, La, Ce, Pr, Nd, Sm, Eu, Gd, Tb, Dy, Ho, Er, Tm, Yb and Lu; multi-acid digestion followed by ICP-emission spectrome-

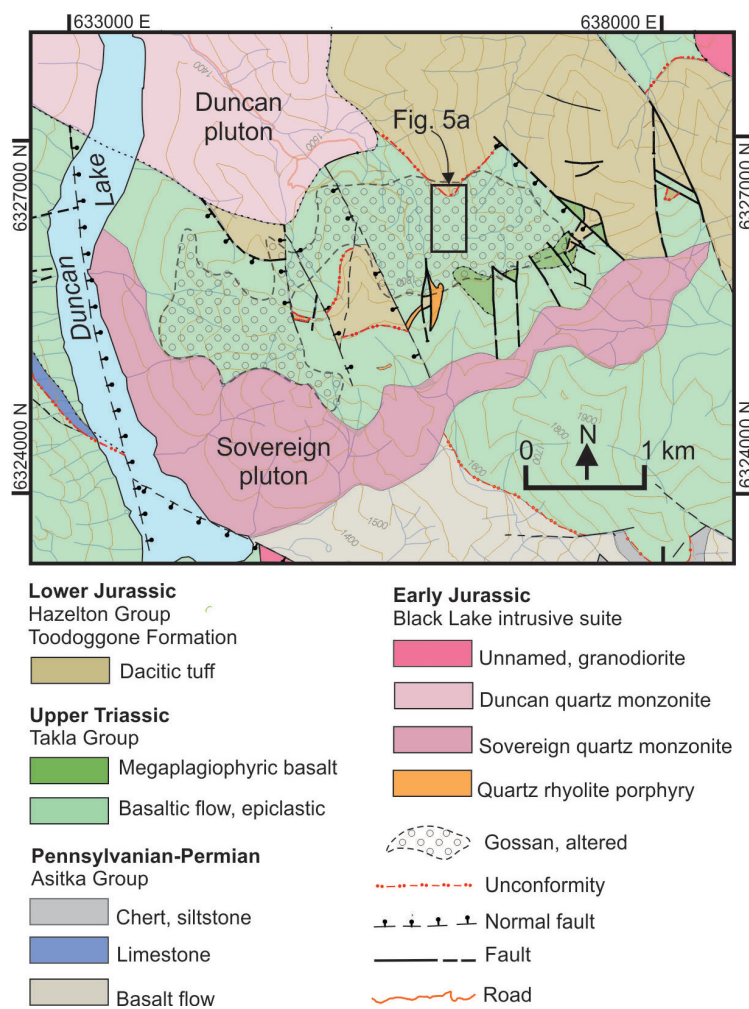


Figure 4. Geology of the Kemess North study area (after Diakow, 2001), showing location of area sampled (Figure 5a).

try and ICP–mass spectrometry (MA200) for Mo, Cu, Pb, Zn, Ag, Ni, As, Cd, Sb, Bi, Sc, Se and Tl; and Au by fire assay/atomic absorption spectroscopy. In addition, magnetic susceptibility of all collected rocks was measured with a KT-10 magnetic susceptibility meter manufactured by Terraplus Inc. Rock density and porosity of all collected rocks were measured using saturation and buoyancy techniques at MDRU (Ulusay and Hudson, 2007). Results of the physical properties of the rock samples will be provided in the final report.

Alteration Mineralogy

Tanzilla

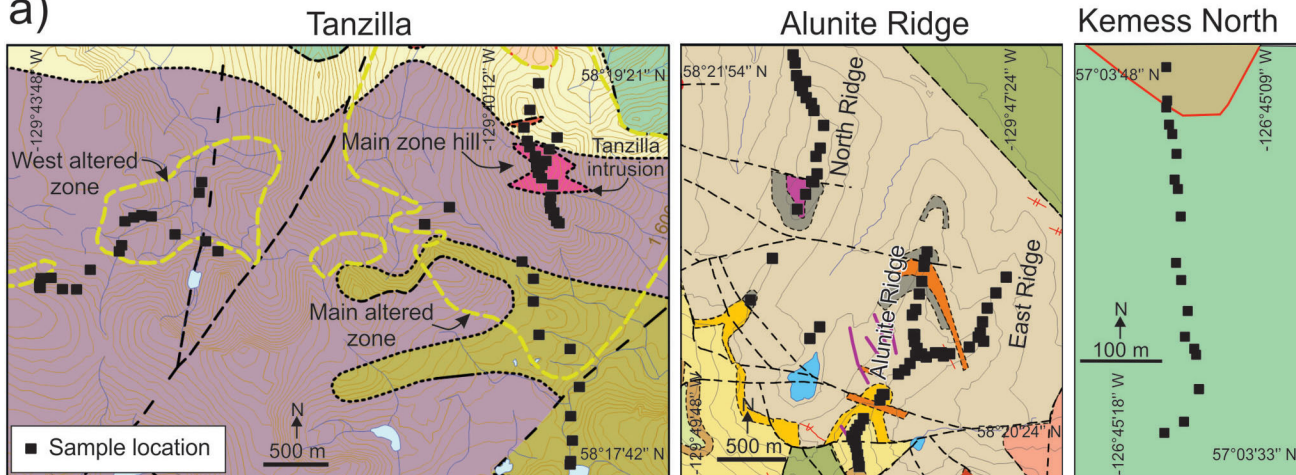
Tanzilla includes two alteration zones: the Main zone ($>4 \text{ km}^2$) and the West zone (Figure 2). Field and SWIR data (Bouzari et al., 2020) show that alteration at Tanzilla is characterized by a green sericite-chlorite-assemblage (Figures 6e, 7a) zone that grades, toward the zones of advanced argillic alteration at the hill in the Tanzilla Main zone, to a pale green sericite and then to a white sericite assemblage

(Figures 6c, 7c) with pyrophyllite and topaz (Figure 5b). In more central locations and commonly at higher elevations, the alteration is characterized by highly silicified rock with remnant sericite, pyrite, and locally abundant pyrophyllite and topaz (Figures 6a, 7d). The sericite at the Main zone is typically muscovite and strongly crystalline (Bouzari et al., 2020). Alteration outside of the green sericite-chlorite assemblage zone is dominantly darker green chlorite-sericite (Figure 6f) and more distal patchy chlorite-epidote alteration occurs within the volcanic rocks (Figure 5b). The chlorite alteration is pervasive and locally alters an earlier biotite alteration.

Alunite Ridge

Advanced argillic alteration in the Alunite Ridge area occurs for over 2 km along a north-northeast-trending ridge (Alunite Ridge) and extends further to the north along North Ridge and to the east along East Ridge (Figures 3, 5b). Field observations backed by SWIR data indicate that the central part of the Alunite Ridge property is characterized by an alteration zone of strong silicification

a)



b)

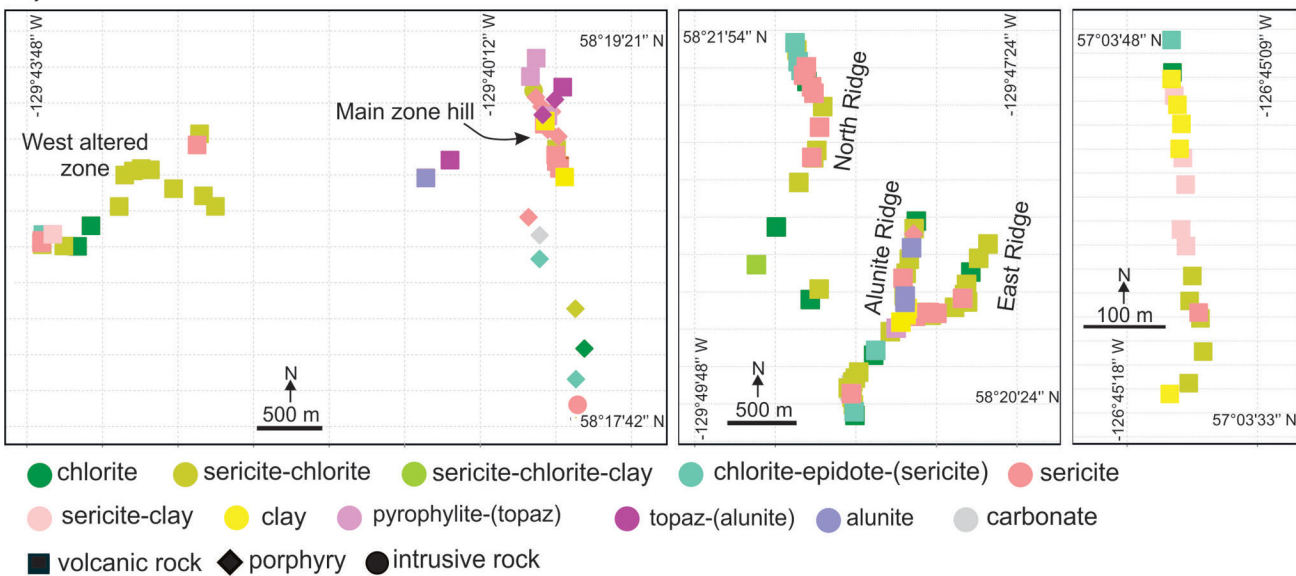


Figure 5. Location of samples from the Tanzilla, Alunite Ridge and Kemess North study areas: **a)** distribution relative to the regional geology (see Figures 2–4 for legend of geological units); **b)** distribution of alteration-mineral assemblages identified by shortwave-infrared analyses.

with alunite, kaolinite, dickite, sericite and locally pyrophyllite. The sericite is typically poorly crystalline illite (Bouzari et al., 2020). This zone is surrounded by an alteration zone of pale green pervasive sericite with weakly altered to intermediate, fine- to medium-grained chlorite and pyrite, which is generally disseminated but also occurs in thin veinlets largely oxidized to jarosite and hematite (Figures 6d, 7b). This alteration gradually transitions to the north and east to darker green alteration of chlorite-sericite and locally epidote occurs more distally (Figure 5b).

Kemess North

The alteration zone exposed at the surface at the north-trending Kemess North ridge is hosted by basaltic flows of the Takla Group and is distinctly zoned from south to north

(Figures 4, 5b). In the southern parts of the ridge, alteration is characterized by green sericite-chlorite and gradually transitions northward to a green-grey sericite (illite) assemblage and then to grey-white sericite-dickite-kaolinite typically with pervasive silicification and quartz veins (Figure 5b). Clay alteration of kaolinite and dickite forms along fractures, and vugs fill with sericite associated with the silicification (Figure 6b). The silicification can reach as much as 30 vol. %, with clay alteration making up the remaining volume. This strongly argillic-altered Takla rock is in fault contact with the chlorite-epidote-altered volcanic rocks of the Toodoggone Formation to the north. Illite crystallinity increases northward (Bouzari et al., 2020). Pyrite is abundant (>2%), occurring as disseminations and stockwork of quartz veins.

Hostrock Composition

Hostrock composition affects the type and intensity of alteration assemblages. Therefore, it is important to characterize hostrocks and their influence on alteration to identify alteration-related vectors. Data from available geological maps as well as field observations have been used to classify rock types. Geochemical trace-element data can also be used to characterize the hostrocks following methods described by Halley (2020). A V versus Sc scatterplot has been used to distinguish volcanic rocks of the Takla Group from those of the Hazelton Group (Figure 8a). Both V^{3+} and Sc^{3+} have similar behaviour and substitute for Fe in amphibole, pyroxene and biotite during crystallization (Li and Lee, 2004; Halley, 2020). All hostrocks show a positive trend of Sc against V (Figure 8a); however, the slope of the trend is slightly different, with the Takla Group showing the least amount of change with increasing V compared to the Toodoggone Formation rocks, which display the highest degree of change. The Horn Mountain Formation rocks plot between the other two units.

A Th versus Sc scatterplot is useful to characterize mafic to felsic composition of the hostrocks. The Th versus Sc diagram (Figure 8b) shows that all rock units have similar Sc, except some Takla samples that display the highest Sc values; higher Sc means lower Si in the rock. There is a weak negative correlation between Sc and Th values, especially for Takla Group and Toodoggone Formation rocks. However, the Th content shows some distinct variations: Takla Group volcanic rocks, relative to Hazelton Group rocks (Toodoggone and Horn Mountain formations), have lower Th concentrations; within the Hazelton Group, the Horn Mountain Formation has the largest degree of scatter relative to high Th values. The Sc concentration corresponds to high-Fe rocks and Th, an incompatible element, stays in the melts and incorporates into late-stage crystalizing mineral phases (Pearce and Norry, 1979). Therefore, the trend from high Sc to high Th reflects a change in composition from more mafic Takla volcanic rocks to mafic-intermediate felsic rocks of the Toodoggone and Horn Mountain formations. A similar diagram of Th versus Sc colour-coded by alteration assemblage (Figure 8c) shows that there is no distinct hostrock influence and that the fluids dictate the distribution of alteration assemblages. Although rocks with higher Th ($>\sim 8$ ppm) do not show signs of chlorite-dominated alteration, they still show biotite and sericite-chlorite alteration. Therefore, it is possible that more felsic rocks of the Hazelton Group have developed weaker chlorite-type alteration, but the available data suggest that this was not

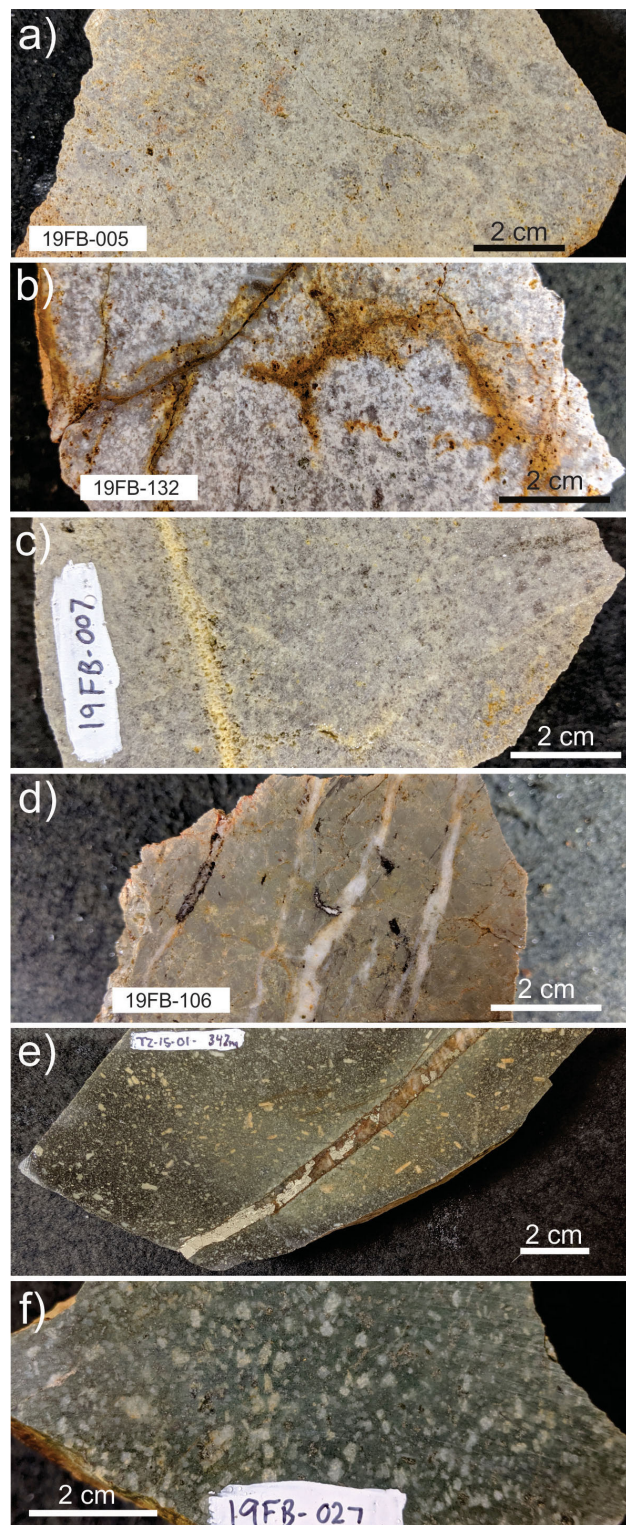


Figure 6. Representative rock samples of alteration assemblages from the study areas: **a)** plagioclase-phyric volcanic rock from Tanzilla with pervasive silification, minor vuggy texture and pale yellow to grey alteration of pyrophyllite and topaz; **b)** Takla Group volcanic rock from Kemess North with strong kaolinite-dickite alteration and silification; **c)** plagioclase-phyric volcanic rock(?) from Tanzilla with pervasive white sericite (muscovite) alteration; **d)** Toodoggone Formation volcanic rock from Alunite Ridge with pervasive pale green sericite alteration and silification cut by quartz veinlets; **e)** plagioclase porphyry from Tanzilla with green sericite-chlorite alteration and remnants of fine-grained disseminated biotite cut by a quartz-pyrite vein; **f)** plagioclase porphyry from the margin of the advanced argillic-alteration zone at Tanzilla, with strong pervasive chlorite-sericite alteration.

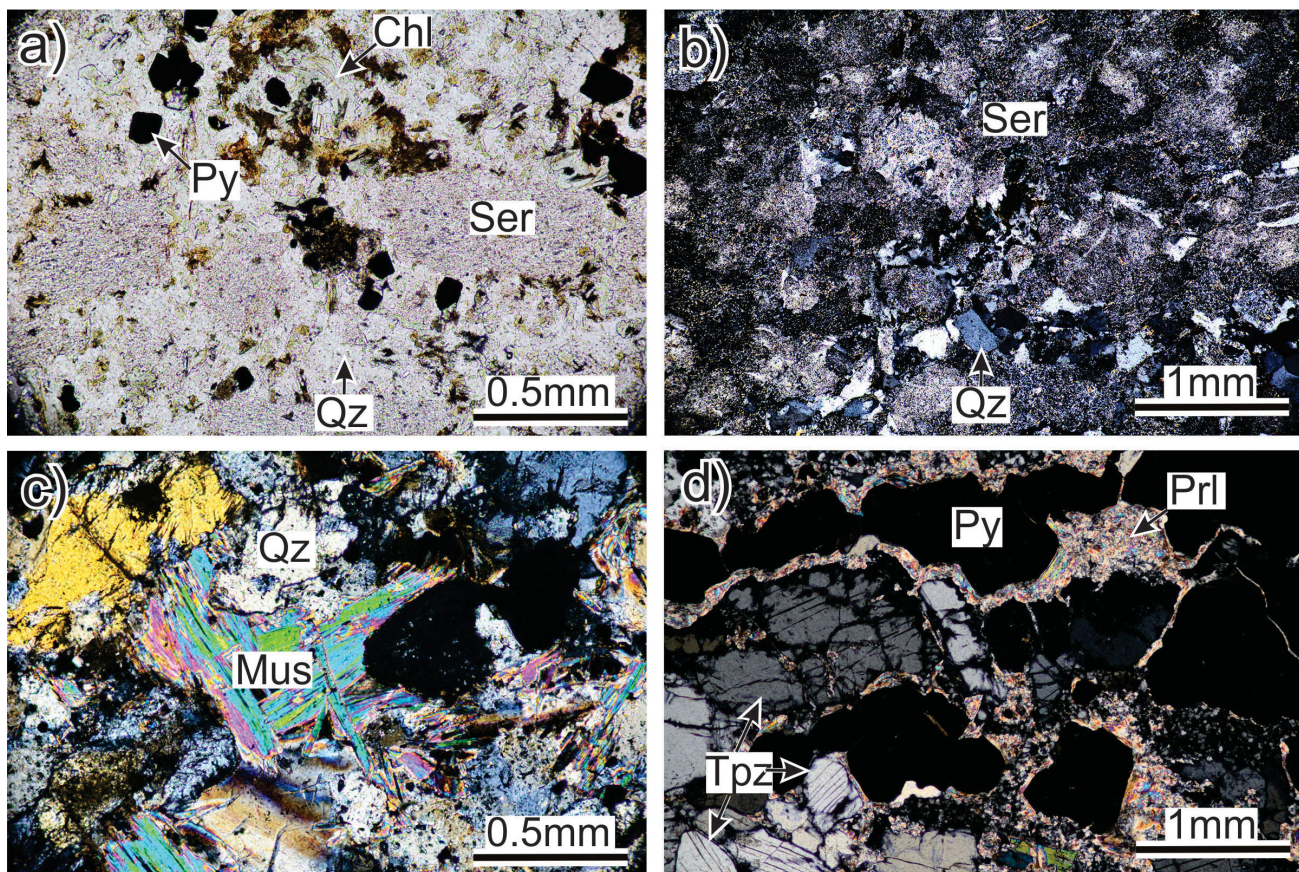


Figure 7. Photomicrographs of selected alteration assemblages from the study areas: **a)** pervasive texturally destructive green sericite-chlorite alteration of groundmass showing chlorite after mafic phases, with remnants of feldspar grains altered to fine-grained sericite (sample from Tanzilla intrusive rock); **b)** pale green sericite alteration showing pervasive fine-grained sericite with quartz, hosted in volcanic rock from Alunite Ridge, and with remnant sulphide and magnetite still present as opaque phases; **c)** white sericite alteration showing coarse muscovite with quartz, hosted in volcanic rock (sample from Tanzilla volcanic breccia); **d)** veinlet-controlled topaz and pyrophyllite alteration with pyrite (sample of felsic crystal tuff from Tanzilla). Mineral abbreviations: Chl, chlorite; Ms, muscovite; Prl, pyrophyllite; Py, pyrite; Qz, quartz; Ser, sericite; Tpz, topaz.

significant and alteration types are scattered throughout various rock units.

A V/Sc versus Sc diagram is also used to discriminate between rock types (Halley, 2020) and to determine this factor's possible influence on alteration intensity. A slight decrease in V/Sc ratios in all rock units is associated with a lower Sc content (Figure 8d), corresponding to higher SiO₂. This decrease is attributed to the crystallization of magnetite, which incorporates V (Halley, 2020). A similar diagram, but colour-coded by intensity of alteration (Figure 8e), shows that hostrocks exercise no distinct control on intensity of alteration (e.g., alteration intensities from weak to very strong occur in all rock units). However, there is an increase in the V/Sc ratio at lower Sc concentration. A high V/Sc ratio has been used to indicate early crystallization of hornblende and clinopyroxene in fertile hydrous magmas (Loucks, 2014). Given the limited number of samples, it is difficult to argue that some of the hostrocks in the study area had originated from more fertile magmas. Comparing the values from Figure 8d with those representing the inten-

sity of alteration (Figure 8e), it appears that in this dataset, the high V/Sc values may have been caused by intense advanced argillic alteration, especially intense silicification. Therefore, it is possible that strong alteration in advanced argillic-altered rocks can increase the V/Sc ratio of the rock.

Geochemical Vectors

Trace-element geochemical data can be used in the advanced argillic-alteration environment to provide vectoring guidance that can assist in indicating proximity to porphyry copper mineralization. Copper is not present in notable concentrations in advanced argillic-altered rocks of the study areas. In fact, Cu seems to have been depleted (<100 ppm) within the zones of strong advanced argillic alteration relative to the rocks associated with distal sericite-chlorite alteration (Figures 5b, 9a). The supergene oxidation may have further contributed to the low copper concentration at near surface. Gold locally shows weak anomalies (~0.1 ppm) in advanced argillic-altered rocks at

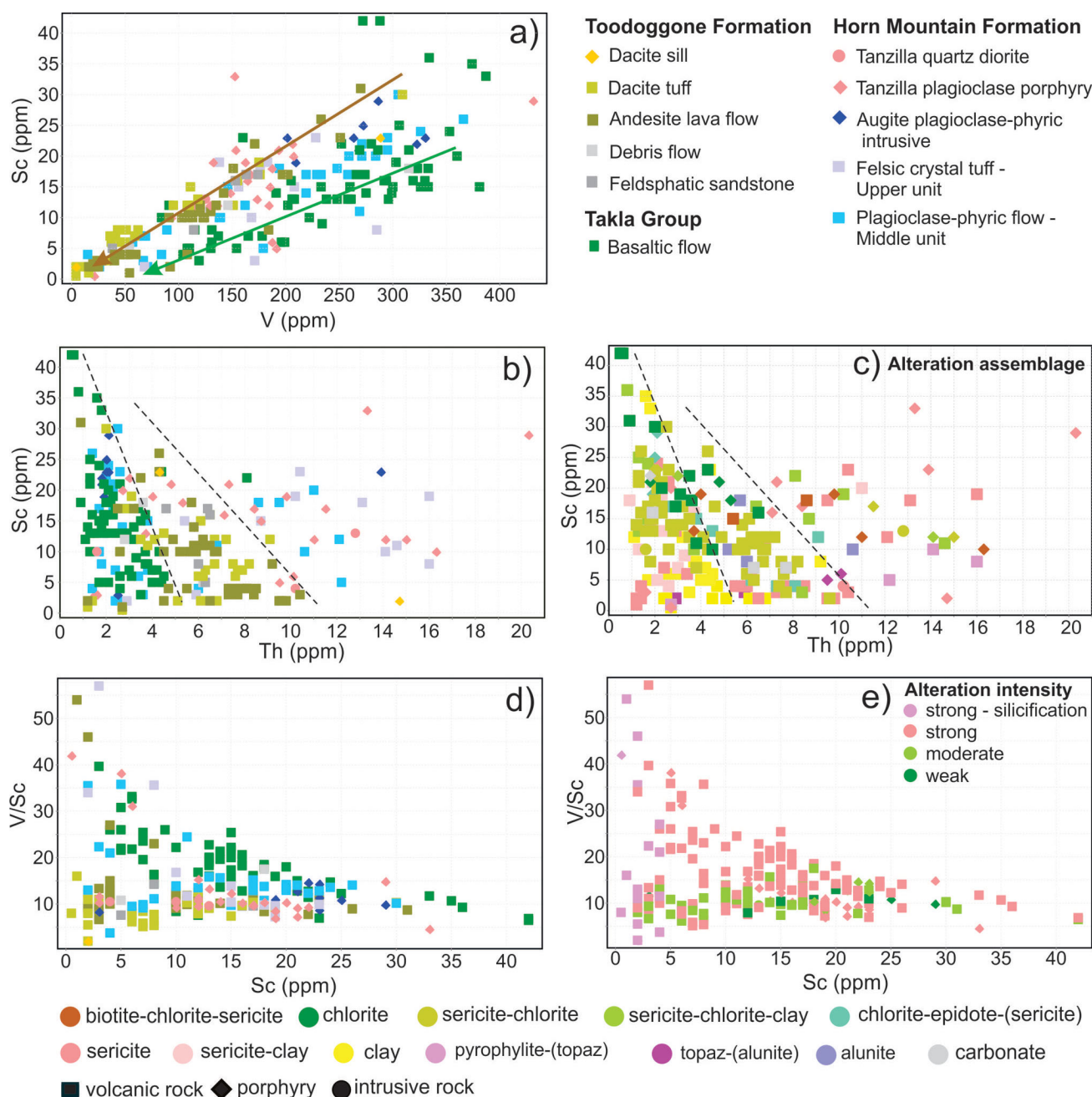


Figure 8. a) Scatterplots used to distinguish rocks of the Takla Group from those of the Hazelton Group in the study areas: **a)** V versus Sc diagram showing hostrock composition (arrowed lines show the main compositional trends); **b)** Th versus Sc scatterplot showing hostrock composition (dashed lines separate the main compositional changes); **c)** same diagram as in (b) but colour-coded by alteration assemblages; **d)** V/Sc versus Sc scatterplot showing hostrock composition; **e)** same diagram as in (d) but colour-coded by alteration intensity.

Tanzilla and Alunite Ridge, but the data do not reveal a clear trend. At Kemess North, there are higher concentrations of Au occurring within the sericite-chlorite-altered rocks in the southern parts of the ridge, whereas Au values are < 0.1 ppm in the sericite-clay-altered rocks on the northern side of the ridge (Figure 9b). Anomalous As concentrations occur with the advanced argillic alteration at Alunite Ridge (23 to 236 ppm) and Tanzilla (14 to 23 ppm),

whereas the As concentration at Kemess North is low (<2 ppm; Figure 9c). This suggests a deeper setting for the alteration at Kemess North relative to Tanzilla and Alunite Ridge, as predicted from the alteration mineralogy (Bouzari et al., 2020). Zinc is largely depleted from the zone of advanced argillic alteration at Tanzilla and from the zone of intense sericite-clay alteration at Kemess North (<30 ppm). At Alunite Ridge, zinc distribution is variable within the

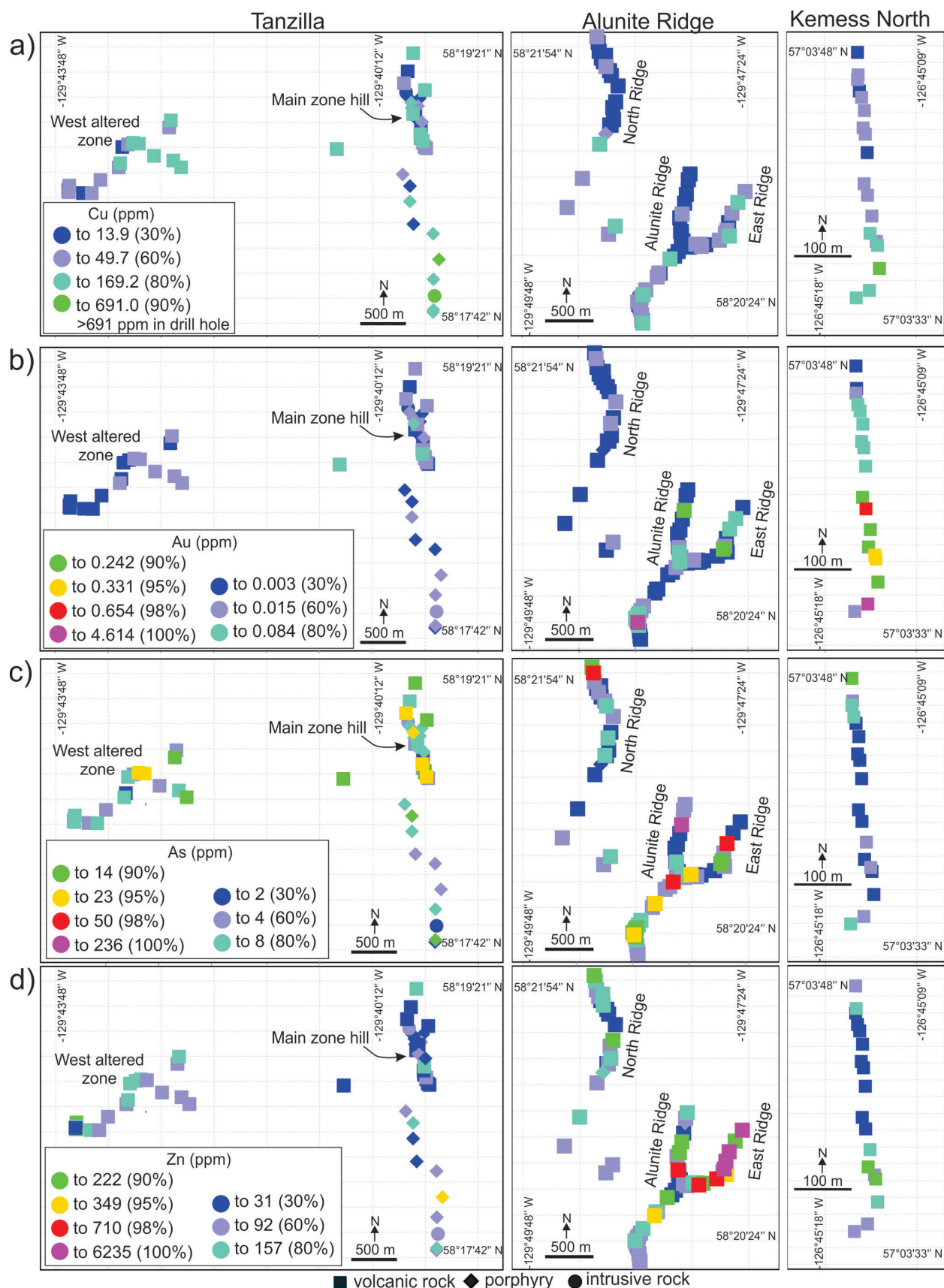


Figure 9. Trace-element distribution in the Tanzilla, Alunite Ridge and Kemess North mineral properties, showing **a)** Cu, **b)** Au, **c)** As, and **d)** Zn.

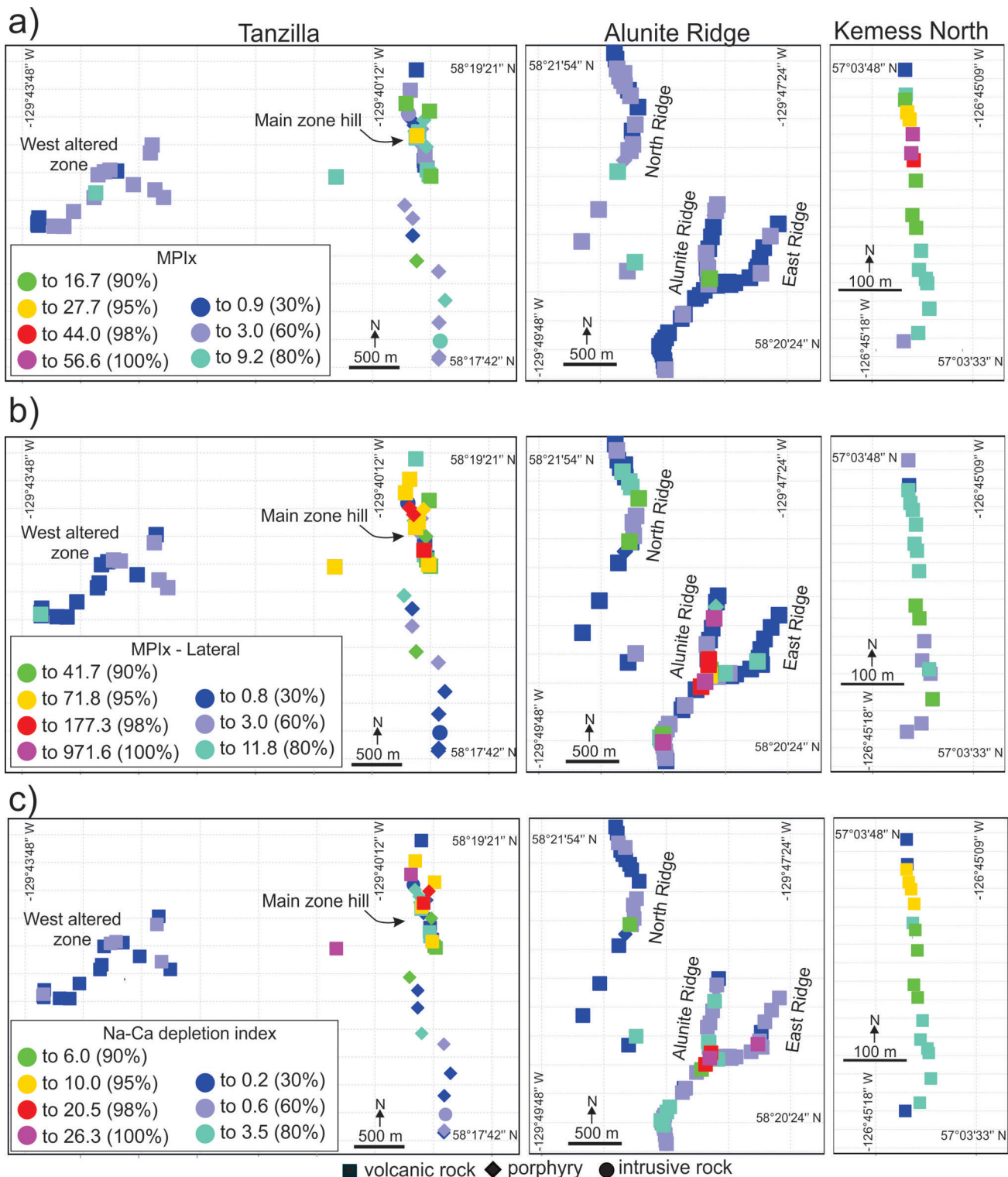


Figure 10. Distribution of relative proportion of elements (samples colour-coded) occurring at various levels of porphyry deposits at the Tanzilla, Alunite Ridge and Kemess North study areas determined using **a)** the MDRU Porphyry Index (MPIx), **b)** the MDRU Porphyry Index-Lateral (MPIx-Lateral), and **c)** the Na-Ca depletion index.

East Ridge, distal to the main area of Alunite Ridge, which shows the highest concentration (>700 ppm; Figure 9d).

MPIx

Whereas the concentration of metals can provide evidence for mineralization, its applicability to vectoring is affected by the intensity of mineralization. Therefore, a ratio of the sum of selected elements provides a more robust vectoring indicator for mineralization. The MDRU Porphyry Index (MPIx; Bouzari et al., 2019) compares the relative proportion of elements occurring at deeper levels of porphyry deposits (Cu, Mo, Sn, W) to those occurring at shallower levels (Sb, As, Ag, Tl, Li). Application of this index to the current study (Figure 10a) shows that, on a vertical profile, Kemess North has the highest MPIx and therefore represents a deeper level of alteration relative to Tanzilla, or to Alunite Ridge that shows the shallowest geochemical signature. The MPIx ratios vector toward the zones of intense central alteration, especially toward the northern side of the ridge at Kemess North and toward the hill in the Tanzilla Main zone. At Alunite Ridge, the MPIx shows the main central parts of the alteration but the vectoring signature is weak and dominated by very low MPIx values.

MPIx-Lateral

The MPIx provides a powerful tool to map the vertical proximity and vector to porphyry copper mineralization. However, at very shallow levels of porphyry copper systems, especially within areas of strong advanced argillic alteration, elements such as Cu, Mo, W and Sn are typically at very low concentrations over much of the altered area and the resulting MPIx value may not provide a lateral vector toward the top-central parts of the porphyry system. To complement the MPIx, the MDRU Porphyry Index-Lateral (MPIx-Lateral) is introduced, which compares metals that are enriched in the shallow parts of a porphyry system (Sb, As, Tl) to those that are more laterally dispersed (Halley et al., 2015) and typically have higher concentrations in more distal parts of the porphyry system (Zn, Mn). Element concentrations are multiplied or divided by an appropriate factor for normalization:

$$\text{MPIx-Lateral} = \frac{(5 \times Sb) + (20 \times Tl) + As}{\frac{Zn}{10} + \frac{Mn}{50}}$$

The MPIx-Lateral (Figure 10b) maps the advanced argillic alteration at the hill in the Tanzilla Main zone, where its footprint shows gradually decreasing values to the east and south. It also shows the Alunite Ridge central zone with decreasing values toward North Ridge. At Kemess North, the MPIx-Lateral values are weaker relative to Tanzilla and Alunite Ridge but still vector toward the more intensely altered parts of the ridge.

Na-Ca Depletion Index

Zones of advanced argillic alteration are characterized by intense removal of many rock-forming elements, particularly Ca and alkali metals such as K and Na, due to leaching of the hostrock by low-pH fluids. Therefore, zones of advanced argillic alteration and areas with the highest intensity of alteration will be characterized by elemental loss. Potassium is usually fixed with the formation of pervasive sericite alteration but Ca and Na depletion, in most cases, correlates with the intensity of advanced argillic alteration. The following elemental ratio is suggested to map the Na-Ca depletion using the sum of the rare-earth elements (REE) as an immobile factor (all values in ppm):

$$\text{Na-Ca depletion index} = \frac{\Sigma \text{REE}}{\text{Ca} + \text{Na}} \times 100$$

The application of the Na-Ca depletion index to the study sites shows that the zones of most intense advanced argillic alteration have the highest level of Na and Ca depletion, with the index gradually decreasing distally (Figure 10c). At Kemess North, where sericite-clay alteration is dominant, the Na and Ca depletion is less intense compared to the advanced argillic alterations at Tanzilla and Alunite Ridge but still vectors, with increasing Na-Ca depletion northward, toward the zone of more intense clay alteration.

Conclusions

Mineralogical and geochemical data and information can all be used individually or integrated to characterize the advanced argillic-alteration environment and to provide tools that identify zoning within the study sites. Variations in alteration assemblages and geochemical signatures suggest that the study sites represent different levels of advanced argillic or shallow-level alteration potentially above a porphyry copper system. Alunite Ridge represents the shallowest levels among the study sites, with abundant silicification, alunite, arsenic, local pyrophyllite and low MPIx ratios. Tanzilla represents slightly deeper levels, with abundant pyrophyllite and topaz alterations, moderate As concentrations and moderate MPIx ratios. Kemess North probably represents a relatively deeper environment, with abundant sericite and dickite alterations and the highest MPIx ratios. High-level lateral zoning is characterized in this paper, in which the following characteristics have been shown to be useful as vectoring tools to identify trends toward the central parts of advanced argillic-alteration zones and potentially the region above the underlying porphyry copper mineralization:

- 1) Regions of advanced argillic alteration are mineralogically zoned. The central parts of the advanced argillic-alteration zone typically contain variable zones of strong silicification. Topaz, andalusite, alunite and pyrophyllite occur within the silicified rocks and vari-

able types of sericite typically occupy the central and most intensely altered parts of advanced argillic-alteration zones. These are zoned outward (distally) to sericite and clay (kaolinite-dickite) mineral assemblages, forming white to grey sericite-(clay) alteration. This alteration is surrounded by a zone of pale green sericite alteration, which transitions outward to zones of green sericite-chlorite alteration. The SWIR data have shown that the sericite composition varies from K-rich to phengitic (Bouzari et al., 2020). More distally, the proportion of the chlorite increases and chlorite-epidote-sericite occurs near the least altered rocks.

- 2) A Na-Ca depletion index was developed to map Ca and alkali depletion within and around zones of advanced argillic alteration. Mapping of various intensities of Na-Ca depletion provides a vector toward zones of high fluid flow and potentially to the more central parts of alteration above a porphyry centre.
- 3) A new tool, the MDRU Porphyry Index-Lateral (MPIx-Lateral) was developed to map the geochemical vectors on a horizontal profile of shallow-level porphyry alteration. This index uses elements that are dispersed distally at shallow levels of porphyry deposits (Zn, Mn) relative to those occurring above a porphyry deposit (Sb, As, Ti) and, therefore, provides a complement to the MPIx as well as being useful for vectoring in the horizontal shallow-level space.

Further characterization of alteration mineralogy, quartz types and chemistry, determination of mineral abundance and mass gain/loss as well as work on the physical properties of the rock samples and mineral chemistry are underway, all of which will contribute to improving the toolbox used in the exploration of advanced argillic-alteration zones in BC.

Acknowledgments

Geoscience BC is thanked for its financial contribution in support of this project. Kaizen Discovery Inc. gave permission to visit the Tanzilla property and sample drillcore. Centerra Gold provided access to Kemess North and drillcore, as well as accommodation at the Kemess mine. The authors thank R. Billingsley for giving them the permission to visit the Alunite Ridge property. Field assistance was provided by Z. Boileau and B. Najafian helped with laboratory work. The authors thank H. Leal-Mejía, of the MDRU-Mineral Deposit Research Unit at The University of British Columbia, and staff members of Geoscience BC for their review of and comments on this paper.

References

- Barresi, T. and Luckman, N. (2016): Diamond drilling report on the Tanzilla property, northwestern British Columbia; BC Ministry of Energy, Mines and Low Carbon Innovation, Assessment Report 36431, 46 p., URL <<https://aris.empr.gov.bc.ca/ARISReports/36431.PDF>> [September 2020]
- Bissig, T. and Cooke, D.R. (2014): Introduction to the special issue devoted to alkalic porphyry Cu-Au and epithermal Au deposits; *Economic Geology*, v. 109, p. 819–825.
- Bouzari, F., Bissig, T., Hart, C.J.R. and Leal-Mejía, H. (2019): An exploration framework for porphyry to epithermal transitions in the Toodoggone mineral district (94E); *Geoscience BC Report 2019-08*, MDRU Publication 424, 101 p., URL <<http://www.geosciencebc.com/wp-content/uploads/2019/11/Geoscience-BC-Report-2019-08.pdf>> [September 2020].
- Bouzari, F., Lee, R.G., Hart, C.J.R. and van Straaten, B.I. (2020): Porphyry vectoring within advanced argillic-altered rocks of British Columbia; in *Geoscience BC Summary of Activities 2019: Minerals*, Geoscience BC, Report 2020-01, p. 115–130, URL <http://www.geosciencebc.com/i/pdf/SummaryofActivities2019/Minerals/Project%202018-022_Minerals_SOA2019.pdf> [September 2020].
- Deyell, C.L., Thompson, J.F.H., Friedman, R.M. and Groat, L.A. (2000): Age and origin of advanced argillic alteration zones and related exotic limonite deposits in the Limonite Creek area, central British Columbia; *Canadian Journal of Earth Sciences*, v. 37, p. 1093–1107.
- Diakow, L.J. (2001): Geology of the southern Toodoggone River and northern McConnell Creek map areas, north-central British Columbia (parts of NTS 94E/2, 94D/15 and 94D16); BC Ministry of Energy, Mines and Low Carbon Innovation, BC Geological Survey, *Geoscience Map 2001-1*, scale 1:50 000, URL <http://cmscontent.nrs.gov.bc.ca/geoscience/PublicationCatalogue/GeoscienceMap/BCGS_GM2001-01.pdf> [September 2020].
- Diakow, L.J., Nixon, G.T., Rhodes, R. and van Bui, P. (2006): Geology of the central Toodoggone River map area, north-central British Columbia (parts of NTS 94E/2, 6, 7, 10 and 11); BC Ministry of Energy, Mines and Low Carbon Innovation, Open file map 2006-6, scale 1:50 000, URL <http://cmscontent.nrs.gov.bc.ca/geoscience/PublicationCatalogue/GeoscienceMap/BCGS_GM2006-06.pdf> [September 2020].
- Diakow, L.J., Panteleyev, A. and Schroeter, T.G. (1991): Jurassic epithermal prospects in the Toodoggone river area, northern British Columbia: examples of well preserved, volcanic-hosted, precious metal mineralization. *Economic Geology*, v. 86, p. 529–554.
- Diakow, L.J., Panteleyev, A. and Schroeter, T.G. (1993): Geology of the early Jurassic Toodoggone Formation and gold-silver deposits in the Toodoggone river map area, northern British Columbia; BC Ministry of Energy, Mines and Low Carbon Innovation, *Bulletin 86*, 72 p., URL <http://cmscontent.nrs.gov.bc.ca/geoscience/PublicationCatalogue/Bulletin/BCGS_B086.pdf> [September 2020].
- Halley, S. W. (2020): Mapping magmatic and hydrothermal processes from routine exploration geochemical analyses; *Economic Geology*. V. 115, p. 489–503.
- Halley, S.W., Dilles, J.H. and Tosdal, R.M. (2015): Footprints: hydrothermal alteration and geochemical dispersion around porphyry copper deposits; *Society of Economic Geologists, Newsletter*, no. 100.
- Hedenquist, J.W. and Taran, Y.A. (2013): Modeling the formation of advanced argillic lithocaps: volcanic vapor condensation above porphyry intrusions; *Economic Geology*, v. 108, p. 1523–1540.

- Hedenquist, J.W., Arribas, A., Jr. and Reynolds, T.J. (1998): Evolution of an intrusion-centered hydrothermal system: Far Southeast-Lepanto porphyry and epithermal Cu-Au deposits, Philippines; *Economic Geology*, v. 93, p. 373–404.
- Heinrich, C.A. (2007): Fluid-fluid interactions in magmatic-hydrothermal ore formation; *Reviews in Mineralogy and Geochemistry*, v. 65, p. 363–387.
- Heinrich, C.A., Driesner, T., Stefánsson, A. and Seward, T.M. (2004): Magmatic vapor contraction and the transport of gold from the porphyry environment to epithermal ore deposits; *Geology*, v. 32, p. 761–764.
- Kuran, D.L. and Barrios, A. (2005): Geological, geochemical and diamond drilling report on the Sickle-BeeGee Claim Group, Toodoggone area; report prepared for Stealth Mineral Limited, BC Ministry of Energy, Mines and Low Carbon Innovation, Assessment Report 27790A, 28 p., URL <<https://aris.empr.gov.bc.ca/ARISReports/27790A.PDF>> [November 2020].
- Li, Z.X.A., and Lee, C.T.A. (2004): The constancy of upper mantle fO_2 through time inferred from V/Sc ratios in basalts; *Earth and Planetary Science Letters*, v. 228, p. 483–493.
- Loucks, R.R. (2014): Distinctive composition of copper-ore-forming arc magmas; *Australian Journal of Earth Sciences*, v. 61, no. 1, p. 5–16.
- McKinley, B.S.M. (2006): Geological characteristics and genesis of the Kemess North porphyry Au-Cu-Mo deposit, Toodoggone district, north-central British Columbia, Canada; M.Sc. thesis, The University of British Columbia, 136 p., URL <[https://open.library.ubc.ca/cIRcle/collecti ons/ubctheses/24/items/1.0052897](https://open.library.ubc.ca/cIRcle/collections/ubctheses/24/items/1.0052897)> [September 2020].
- Meyer, C. and Hemley, J.J. (1967): Wall rock alteration; in *Geochemistry of Hydrothermal Ore Deposits*, H.L. Barnes (ed.), Holt, Reinhart and Winston, Inc., New York, New York, p. 166–235.
- Panteleyev, A. and Koyanagi, V.M. (1994): Advanced argillic alteration in Bonanza volcanic rocks, northern Vancouver Island – lithologic and permeability controls; in *Geological Fieldwork 1993*, BC Ministry of Energy, Mines and Low Carbon Innovation, BC Geological Survey, Paper 1994-1, p. 101–110, URL <<https://www2.gov.bc.ca/gov/content/industry/mineral-exploration-mining/british-columbia-geological-survey/publications/fieldwork>> [September 2020].
- Pearce, J.A. and Norry, M.J. (1979): Petrogenetic implications of Ti, Zr, Y, and Nb variation in volcanic rocks; *Contributions to Mineralogy and Petrology*, v. 69, p. 33–47.
- Sillitoe, R.H. (1993): Epithermal models: genetic types, geometrical controls and shallow features; in *Mineral Deposit Modelling*, R.V. Kirkham, W.D. Sinclair, R.J. Thorpe and J.M. Duke (ed.), Geological Association of Canada, Special Paper 40, p. 403–417.
- Sillitoe, R.H. (2010): Porphyry copper systems; *Economic Geology*, v. 105, p. 3–41.
- Simmons, S.F., White, N.C. and John, D. (2005): Geological characteristics of epithermal precious and base metal deposits; in *Economic Geology One Hundredth Anniversary Volume 1905–2005*, J.W. Hedenquist, J.F.H. Thompson, R.J. Goldfarb and J.P. Richards (ed.), *Economic Geology*, p. 485–522.
- SRK Consulting Inc. (2016): Technical report for the Kemess underground project and Kemess East resource estimate, British Columbia, Canada; report prepared for AuRico Metals Inc., 409 p., URL <https://www.centerragold.com/cg-raw/cg/KemessUG_Updated_Technical-Report_2CA046-004_20160506_FNL.pdf> [September 2020].
- Ulusay, R. and Hudson, J.A. (2007): The Complete ISRM Suggested Methods for Rock Characterization, Testing and Monitoring: 1974–2006; compiled by the ISRM Turkish National Group, International Society for Rock Mechanics, ISRM Commission on Testing Methods, 628 p.
- van Straaten, B.I. and Bouzari, F. (2018): The Middle Jurassic Tanzilla–McBride hydrothermal system: one of the largest lithocaps in BC?; *Mineral Exploration RoundUp*, Vancouver, BC, January 22–25, 2018, poster presentation.
- van Straaten, B.I. and Gibson, R. (2017): Late Early to Middle Jurassic Hazelton Group volcanism and mineral occurrences in the McBride–Tanzilla area, northwest British Columbia; in *Geological Fieldwork 2016*, BC Ministry of Energy, Mines and Low Carbon Innovation, BC Geological Survey, Paper 2017-1, p. 83–115, URL <http://cmscontent.nrs.gov.bc.ca/geoscience/PublicationCatalogue/Paper/BCGS_P2017-01-06_vanStraaten.pdf> [September 2020].
- van Straaten, B.I. and Nelson, J.L. (2016): Syncollisional late Early to early Late Jurassic volcanism, plutonism, and porphyry-style alteration on the northeastern margin of Stikinia; in *Geological Fieldwork 2015*, BC Ministry of Energy, Mines and Low Carbon Innovation, BC Geological Survey, Paper 2016-1, p. 113–143, URL <http://cmscontent.nrs.gov.bc.ca/geoscience/PublicationCatalogue/Paper/BCGS_P2016-01-07_vanStraaten.pdf> [September 2020].
- van Straaten, B.I., Gibson, R. and Nelson, J. (2017): Preliminary bedrock geology of the Tanzilla and McBride area, British Columbia; BC Ministry of Energy, Mines and Low Carbon Innovation, BC Geological Survey, Open File 2017-9, scale 1:50 000, URL <http://cmscontent.nrs.gov.bc.ca/geoscience/PublicationCatalogue/OpenFile/BCGS_OF2017-09.pdf> [September 2020].
- Watanabe, Y. and Hedenquist, J.W. (2001): Mineralogic and stable isotope zonation at the surface over the El Salvador porphyry copper deposit, Chile; *Economic Geology*, v. 96, p. 1755–1797.

Preliminary Zircon Geochemistry of Northern Hogem Batholith, Quesnel Terrane, North-Central British Columbia (Parts of NTS 093M/16, 093N/13, 14, 094C/03–06, 094D/01, 08)

G.O. Jones¹, Department of Earth and Atmospheric Sciences, University of Alberta, Edmonton, Alberta, gojones@ualberta.ca

D.G. Pearson, Department of Earth and Atmospheric Sciences, University of Alberta, Edmonton, Alberta

A. Vezinet, Department of Earth and Atmospheric Sciences, University of Alberta, Edmonton, Alberta

Y. Luo, Department of Earth and Atmospheric Sciences, University of Alberta, Edmonton, Alberta

R.A. Stern, Department of Earth and Atmospheric Sciences, University of Alberta, Edmonton, Alberta

D. Milidragovic, Natural Resources Canada, Geological Survey of Canada–Pacific, Vancouver, British Columbia

L. Ootes, British Columbia Geological Survey, British Columbia Ministry of Energy, Mines and Low Carbon Innovation, Victoria, British Columbia

Jones, G.O., Pearson, D.G., Vezinet, A., Luo, Y., Stern, R.A., Milidragovic, D. and Ootes, L. (2021): Preliminary zircon geochemistry of northern Hogem batholith, Quesnel terrane, north-central British Columbia (parts of NTS 093M/16, 093N/13, 14, 094C/03–06, 094D/01, 08); in Geoscience BC Summary of Activities 2020: Minerals and Mining, Geoscience BC, Report 2021-01, p. 105–120.

Introduction

In 2018, the British Columbia Geological Survey initiated a three-year mapping program after Geoscience BC released the Search III airborne magnetic and radiometric data for the area between the Lorraine and Kemess porphyry deposits (Figures 1, 2; CGG Canada Services Ltd., 2018). The mapping program was initiated to update the bedrock geology in the southern part of the Search III footprint, with a focus on northern Hogem batholith (Figures 1, 2; Ootes et al., 2019, 2020a, b).

This project was initiated as part of the bedrock mapping program to study the details of magma genesis in the Hogem batholith and provide insights into the petrogenesis of plutonic suites that host porphyry style Cu-Au (\pm Mo) mineralization. The Thane Creek suite (ca. 196 Ma) hosts several Cu-Au porphyry occurrences (e.g., Cathedral prospect), while the Duckling Creek suite (ca. 180 Ma) hosts the Lorraine Cu-Au deposit, amongst other prospects and occurrences (Bath et al., 2014;

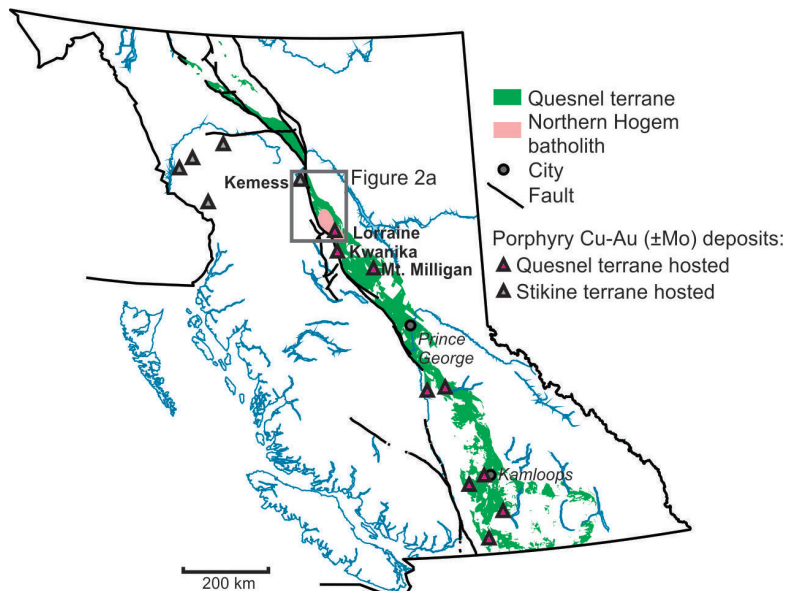


Figure 1. Geographic distribution of the Quesnel terrane (with the Hogem batholith highlighted) and major Triassic–Jurassic porphyry deposits in British Columbia. Porphyry deposits of interest in this study are labelled. The footprint of Figure 2a, which includes the Search III geophysical data, is outlined in grey. The study area is in northern Hogem batholith, which was covered by the southeastern extent of the Search III survey. Geology from BC Geological Survey (2020).

Devine et al., 2014). This paper introduces a multi-isotopic study from these two intrusive suites. Interpretation of crystallization ages has been previously presented (Bath et al., 2014; Devine et al., 2014; Ootes et al., 2020b) and the focus of this contribution is an integrated multi-isotopic and trace-element study of zircon, and the application of

¹The lead author is a 2020 Geoscience BC Scholarship recipient.

This publication is also available, free of charge, as colour digital files in Adobe Acrobat® PDF format from the Geoscience BC website: <http://geosciencebc.com/updates/summary-of-activities/>.

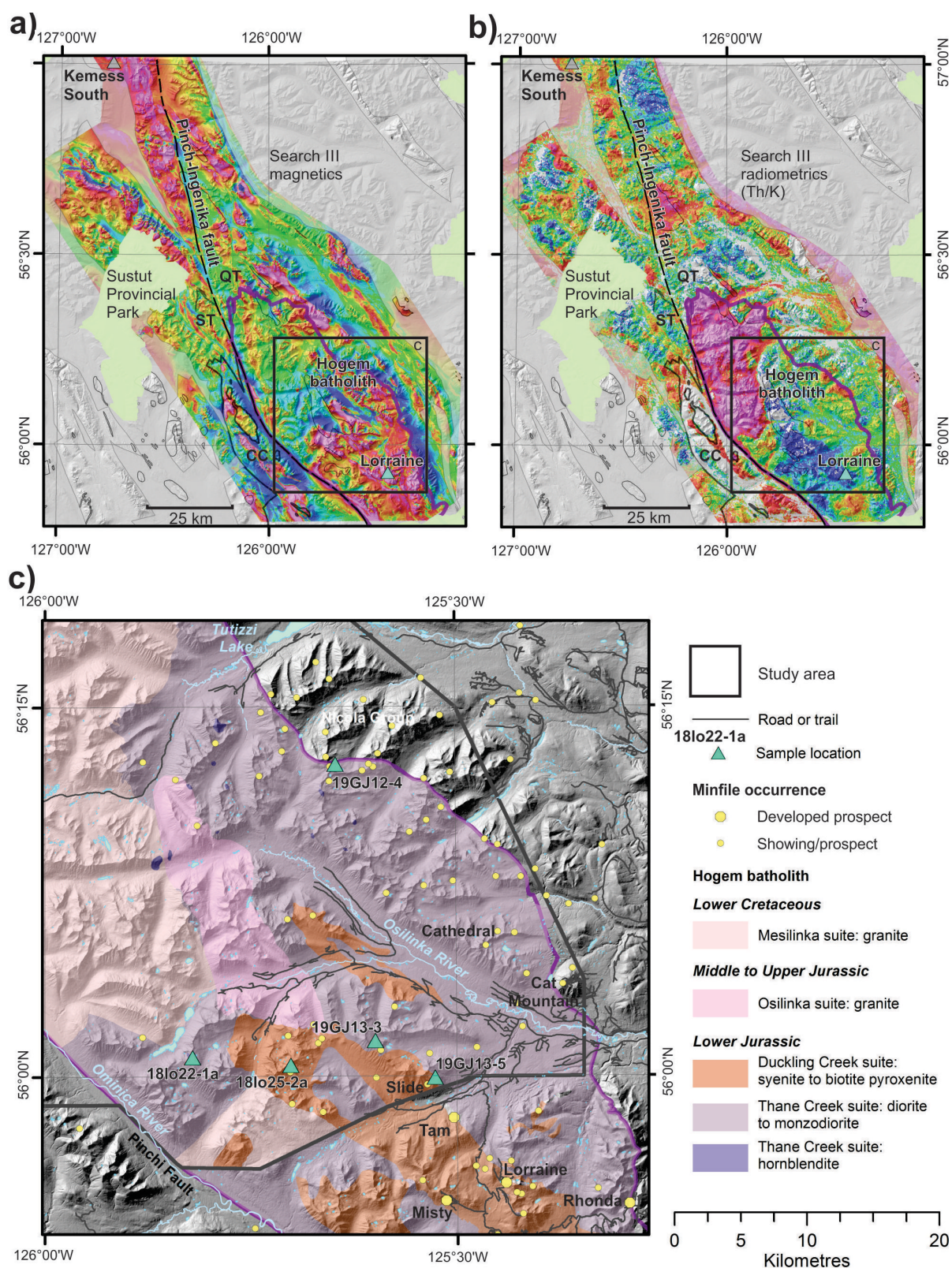


Figure 2. Results from the Search III airborne survey: **a)** radio magnetic indicator (RMI) and **b)** radiometric (Th/K; CGG Canada Services Ltd., 2018). Warm colours correspond to higher magnetism and Th/K values, and cool colours correspond to lower magnetism and Th/K values. The Pinchi-Ingenika fault separates the Quesnel terrane (QT) on the east from the Stikine (ST) and Cache Creek (CC) terranes on the west. The northern part of the Hogem batholith is outlined in purple. The Lorraine and Kemess South porphyry deposits are shown for reference. **c)** Bedrock geology of northern Hogem batholith. The black line depicts the location of the study area and limit of mapping by Ootes et al. (2019, 2020a, b). The geology to the south of the black line is from Devine et al. (2014). Prospects and developed prospects that are labelled are discussed in the text.

these data for understanding magmatic-metal enrichment and carrying capacity in the Hogem batholith.

Porphyry deposits typically have alteration haloes that are produced by chemical and mineralogical alteration of the hostrocks (e.g., Byrne et al., 2016). This paper focuses on magmatic phases that are spatially, genetically and temporally associated with porphyry-style mineralization, and sampling was conducted away from mineralized or heavily altered zones. Such an approach provides a background perspective on igneous petrogenesis and regional, versus deposit scale, insights into the controls on mineralization potential of the magma (i.e., fertility; e.g., Richards, 2013). The data collected for this study are from single zircon crystals and include U-Pb, Lu-Hf and oxygen isotopes, and trace elements. Isotopic U-Pb analysis allows for the determination of crystallization ages; Lu-Hf analysis provides insight into the nature of the parental magma and its source reservoir(s); oxygen isotopes establish if the magmatic source has been recycled following exposure to the hydro-sphere; and the trace-element data allow estimates of temperature and oxidation state during crystallization.

Regional Geology

The northern part of the Hogem batholith was mapped by Armstrong (1946), Lord (1948, 1949), Armstrong and Roots (1948, 1954), Roots (1954), Woodsworth (1976) and Ootes et al. (2019, 2020a, b). The southern part of the Hogem batholith was subdivided by Garnett (1972, 1978). Mapping by Ferri et al. (2001a, b) and Schiarizza and Tan (2005) focused on the Takla Group (referred to herein as the Nicola Group; cf. Ootes et al., 2020b) but left the northern part of the Hogem batholith largely undivided. Nixon and Peatfield (2003), Bath et al. (2014) and Devine et al. (2014) studied the Lorraine porphyry Cu-Au deposit, hosted in the Duckling Creek suite southeast of the study area, and provided isotopic ages and whole-rock geochemistry for mineralization and the hostrocks.

Thane Creek Suite

The eastern and southwestern parts of the study area (Figure 2c) are underlain by diorite to quartz monzodiorite and lesser hornblendite of the Thane Creek suite, the oldest intrusive rocks in northern Hogem batholith (Ootes et al., 2019, 2020a, b). Diorite crosscuts and commingles with the hornblendite. Where commingling is present, the rocks are texturally and compositionally heterogeneous in terms of amphibole, plagioclase and magnetite abundances.

Hornblendite

Black to ‘salt and pepper’, medium-grained to pegmatitic hornblendite forms ≤ 100 m wide plutons scattered through diorite of the Thane Creek suite (Figure 2c); see Ootes et al. (2019) for outcrop photos. Dark green amphibole crystals, with rare corroded clinopyroxene cores, predominate and

range from medium to coarse grained. Plagioclase, where present, is interstitial between amphibole and ranges from fine to coarse grained. Biotite, generally medium grained, is a common accessory mineral in the hornblendites, in concentrations ranging from 0 to 20%. Accessory euhedral titanite and euhedral to subhedral crystals of apatite are also common. Magnetite abundance in hornblendite varies (mostly $\leq 5\%$), and these rocks have a strong magnetic signature (Figure 2a). Epidote is a secondary alteration mineral in the hornblendite and generally forms $\leq 5\%$ of the rock. Trace amounts of disseminated pyrite and chalcopyrite occur and, in a few small outcrops (~ 1 m 2), chalcopyrite constitutes a few percent of the rock. Some of the sulphide-bearing rocks have local malachite or iron-rust staining on weathered surfaces. The hornblendites are entirely within diorite and display both sharp and diffuse contacts, the latter indicating magma commingling. The hornblendites are interpreted as comagmatic with the diorite plutons and represent either crystal cumulates formed from a more primitive parental magma or injections of a hydrous mafic to ultramafic magma into a predominantly dioritic chamber. A sample of plagioclase-bearing pegmatitic hornblendite yielded a chemical-abrasion isotope dilution–thermal ionization mass spectrometry (CA-ID-TIMS) zircon U-Pb crystallization age of 197.55 ± 0.11 Ma (Ootes et al., 2020b).

Diorite to Quartz Monzodiorite

The eastern and southwestern parts of northern Hogem batholith are underlain mostly by green- and white-weathering to black- and white-weathering, equigranular, medium- to coarse-grained diorite that is foliated to locally mylonitic (Figure 2c). Along the eastern and northern margins of northern Hogem batholith, diorite of the Thane Creek suite intruded Nicola Group volcano-sedimentary rocks (Ferri et al., 2001a, b; Schiarizza and Tan, 2005; Ootes et al., 2020a). The diorite consists mostly of plagioclase and hornblende but locally transitions to units with more significant amounts of quartz and K-feldspar (quartz diorite, quartz monzodiorite, monzodiorite, granodiorite) and gabbro. Accessory phases include clinopyroxene (as corroded cores to amphibole), euhedral to subhedral titanite, magnetite and apatite. Epidote is locally common and interpreted as an alteration product. The diorite locally contains biotite, in some cases in much greater abundance than amphibole. The relatively potassic phases contain blotchy pink K-feldspar in the groundmass, which is accompanied by mint-green weathering in outcrop; these zones correspond to biotite- and epidote-rich phases, where plagioclase has been altered to clay minerals, amphibole is rare and titanite locally displays highly corroded grain boundaries. These features may indicate either late magmatic or secondary potassic alteration. The diorite contains variable abundances of magnetite; this variation could be from magmatic fractionation, secondary alteration or both.

The magnetic variation is evident on the airborne magnetic map (Figure 2a) and from magnetic susceptibility measurements (Ootes et al., 2019).

The diorite crosscuts and commingles with the hornblende (Ootes et al., 2019). Where there is commingling, the rocks are texturally and compositionally heterogeneous in terms of amphibole, plagioclase and magnetite concentrations. In some locations, the combined effects of mixing with enclaves, magmatic differentiation and K-alteration resulted in textural and compositional variations that are too small to show at the scale of the map (Ootes et al., 2019, 2020a). The diorite locally contains xenoliths of layered, fine-grained green rock, possibly derived from the Nicola Group. The diorite is locally stained with malachite and rarely contains disseminated chalcopyrite (<1%).

In the southeastern part of northern Hogem batholith, a diorite sample yielded a CA-ID-TIMS zircon U-Pb crystallization age of 196.61 ± 0.19 Ma. This sample was taken ~30 m away from the location of a ca. 197.5 Ma hornblende sample referred to above (Ootes et al., 2020b). The result is comparable to, albeit younger than, a 204.0 ± 0.4 Ma diorite at the Cat Mountain prospect in the eastern Thane Creek suite (Figure 2c; Mortensen et al., 1995) and a 200.9 ± 0.2 Ma gabbro-diorite body at the Rhonda Cu prospect, 20 km south of the study area (Figure 2c; Devine et al., 2014). The Thane Creek diorite sample that yielded the ca. 196.6 Ma age also yielded an $^{40}\text{Ar}/^{39}\text{Ar}$ biotite step-heating age of ca. 124 Ma, interpreted to record postdeformation cooling (Ootes et al., 2020b).

Duckling Creek Suite

The south-southeastern part of the study area is underlain by quartz-undersaturated rocks of the Duckling Creek suite (Figure 2c; Ootes et al., 2019); this was called the ‘Duckling Creek syenite complex’ by Woodsworth (1976), Garnett (1978), Nixon and Peatfield (2003) and Devine et al. (2014). The Duckling Creek suite is mostly syenite to monzonite, with lesser monzodiorite and local zones of biotite pyroxenite. South of the study area, Devine et al. (2014) identified three stages of the Duckling Creek suite and constrained the timing with the following U-Pb zircon ages: 1) biotite pyroxenite (ca. 182–178.5 Ma); 2) predominantly K-feldspar–porphyritic syenite to monzonite (ca. 178.8–178.4 Ma); and 3) massive syenite and pegmatite (ca. 177–175 Ma). All three phases exist in the study area. The biotite pyroxenite is black weathering and locally contains megascopic phenocrysts (up to 0.5 cm) of white-weathering apatite. It is generally preserved at higher elevations and traceable over areas of tens to hundreds of metres, where it is extensively crosscut by syenite to monzonite and lesser monzodiorite. These more intermediate to felsic rocks range from equigranular to porphyritic to pegmatitic. Porphyritic varieties contain tabular, com-

monly zoned, K-feldspar phenocrysts (up to 5 cm long) that are set in a groundmass of equigranular green pyroxene and lesser albite, amphibole, magnetite, titanite and apatite. Rhythmic magmatic layering, defined by varying felsic and mafic mineral ratios and alignment of K-feldspar phenocrysts, is common. The entire unit has moderate to strong magnetism (Figure 2a), with areas of highest magnetism spatially associated with biotite pyroxenite. Biotite pyroxenite zones are locally stained with malachite and contain disseminated chalcopyrite.

Amphibole separated from a K-feldspar porphyritic syenite sample yielded an $^{40}\text{Ar}/^{39}\text{Ar}$ step-heating age of ca. 177.6 Ma (Ootes et al., 2020b). This result overlaps, within uncertainty, with a previously reported $^{40}\text{Ar}/^{39}\text{Ar}$ biotite age of 177.1 ± 0.9 Ma for a similar syenite sample to the south (Devine et al., 2014). These ages are best interpreted as cooling of the pluton through the closure temperature of hornblende (~550°C).

Mineralization

The Hogem batholith and the surrounding Nicola Group host porphyry-style deposits and prospects, including one producer (Mount Milligan; Figure 1). The most significant developed prospect in northern Hogem batholith is the Lorraine Cu-Au deposit, containing 6.42 million tonnes of indicated resource at 0.62% Cu and 0.23 g/t Au, and 28.82 million tonnes of inferred resource at 0.45% Cu and 0.19 g/t Au (Figures 1, 2c; Giroux and Lindinger, 2012). The Lorraine deposit is hosted by the biotite-pyroxenite phase of the Duckling Creek suite (Bath et al., 2014; Devine et al., 2014), which also hosts other developed prospects (Tam, Misty) and prospects/showings (e.g., Slide; Figure 2c).

The Thane Creek suite hosts a number of porphyry Cu-Au prospects and showings (e.g., Cathedral; Figure 2c). The Rhonda developed prospect (Figure 2c) is hosted by Rhonda-Dorothy gabbro (ca. 200 Ma; Devine et al., 2014), which is correlative with the Thane Creek suite. The Cat Mountain prospect is hosted in Nicola Group volcanic rocks that are intruded by dikes of the Thane Creek suite (ca. 204 Ma; Mortensen et al., 1995). A number of other Cu-Au prospects occur throughout the Thane Creek, Duckling Creek and Nicola Group rocks (Figure 2c; Ootes et al., 2019).

Field and Laboratory Work

Zircon U-Pb, Lu-Hf, oxygen-isotope and trace-element geochemistry has become commonly used in igneous-petrogenetic studies (e.g., Lee et al., 2020; Sagan et al., 2020). Zircon geochemistry is a powerful tool, providing insight into the nature and antiquity of the magma source and evolution. This paper presents preliminary data for the

oldest locally mineralized intrusive phases of the Hogem batholith (i.e., the Thane Creek and Duckling Creek suites).

During fieldwork and sampling in 2018 and 2019, five samples were acquired from across the batholith to represent the geochemical heterogeneity of the intrusive suites (Figure 2c). Most samples were collected from areas lacking obvious alteration related to porphyry mineralization. The exception is sample 19GJ13-5a, which was collected next to the Slide prospect (Figure 2c) from outcrop exposures that also contain Cu mineralization. A single grab sample with chalcopyrite, collected 7 m north of 19GJ13-5a, yielded 0.07 wt. % Cu (19GJ13-5b; Ootes et al., 2020b).

Sample preparation was completed at the University of Alberta. Approximately 1 kg of sample was cut into centimetre-size pieces using a diamond-blade rock saw. These pieces were disaggregated using the SELFRAG laboratory electronic-pulse disaggregation system in the Canadian Centre for Isotopic Microanalysis (CCIM) to yield high-quality mineral separates. The mineral separates were sieved and panned to separate fine-grained (<355 µm), high-density minerals. The high-density mineral separates were examined using a stereo microscope to hand-pick clear, euhedral zircon grains. These zircons were set in epoxy mounts and polished to expose the grain midsections. Back-scattered electron (BSE), cathodoluminescence (CL) and secondary electron (SE) images of the zircon crystals were obtained on a scanning electron microscope at CCIM. These images were used to select spots for microanalysis.

For this study, a detailed workflow was designed prior to the analytical work because single zircon grains were to be used for multiple analyses. Acquisition of zircon oxygen-isotope data by secondary-ion mass spectrometry (SIMS) analysis, using a Cameca IMS 1280 multicollector ion microprobe, was completed first according to standard CCIM operating procedures (e.g., Vezinet et al., 2018) because this is the least destructive analytical method and requires precision-polished grain mounts. The SIMS analysis is sensitive to grain-mount topography, as the beam configuration involves focusing a primary $^{133}\text{Cs}^+$ ion beam at an angle onto the sample to produce negative secondary ions ($^{18}\text{O}^-$ and $^{16}\text{O}^-$). After oxygen-isotope data collection by SIMS, zircons were investigated by laser-ablation inductively coupled plasma–mass spectrometry (LA-ICP-MS). Zircon U-Pb data were collected first, followed by trace elements and Lu-Hf. The LA-ICP-MS method involves focusing a RESolution™ 193 nm ArF excimer laser, equipped with a 2-volume Laurin-Technic S-155 ablation cell, on a solid sample to ablate fine particles that are then transported via argon gas to a Thermo Fisher Scientific Element-XR™ (U-Pb and trace elements) or Thermo Fisher Scientific Neptune Plus™ (Lu-Hf) mass spectrometer for analysis. A preliminary subset of the U-Pb and Lu-Hf analyses was carried out simultaneously on a portion of the

same ablated material using the laser-ablation split-stream (LASS) ICP-MS technique (e.g., Fisher et al., 2014) and reduced with the software described in Fisher et al. (2017). The LA-ICP-MS analytical method was used for this study because it is relatively fast and cost effective, can produce large datasets and provides the opportunity to analyze specific within-grain growth zones. However, this method sacrifices precision, compared to more precise solution methods, such as thermal ionization-mass spectrometry (TIMS).

Results

Magmatic-crystallization ages and Lu-Hf and oxygen-isotope results ($\delta^{18}\text{O}$) obtained from zircon analyses are summarized in Table 1. All uncertainties are reported at the 2σ (95%) confidence level. Both single-zircon $^{206}\text{Pb}/^{238}\text{U}$ dates and interpreted magmatic-crystallization ages are plotted on Figures 3 and 4. The magmatic-crystallization ages are from this study, Ootes et al. (2020b) and Devine et al. (2014)

Radiogenic Lu-Hf Isotopes

The results of Lu-Hf analyses are presented as the $^{176}\text{Hf}/^{177}\text{Hf}$ ratio of a sample at the time of crystallization (t) relative to the $^{176}\text{Hf}/^{177}\text{Hf}$ ratio of the chondritic uniform reservoir (CHUR), which is expressed as εHf_t (uncertainty calculated using the Excel template of Ickert, 2013):

$$\varepsilon\text{Hf}_t = \left(\frac{(^{176}\text{Hf}/^{177}\text{Hf}_{\text{SAMPLE}(t)})}{(^{176}\text{Hf}/^{177}\text{Hf}_{\text{CHUR}(t)})} - 1 \right) \times 10000,$$

where $^{176}\text{Hf}/^{177}\text{Hf}_{(t)} = ^{176}\text{Hf}/^{177}\text{Hf}_{(\text{measured})} - ^{176}\text{Lu}/^{177}\text{Hf} \times e^{[(\lambda^{176}\text{Lu} \times t) - 1]}$,

$^{176}\text{Hf}/^{177}\text{Hf}_{\text{CHUR}(\text{measured})} = 0.282785 \pm 1$, $^{176}\text{Lu}/^{177}\text{Hf}_{\text{CHUR}} = 0.0336 \pm 1$ (Bouvier et al., 2008),

and $\lambda^{176}\text{Lu} = 1.867 \times 10^{-11}$ (Söderlund et al., 2004).

When using εHf_t to determine the relative contributions of crust and mantle in the magma source, it is useful to have a comparable end-member rock suite. The estimated Hf isotopic ratio at time of rock formation is commonly compared to the CHUR and the depleted-mantle–evolution curve. Depleted mantle is calculated using the $^{176}\text{Hf}/^{177}\text{Hf}$ ratio through time based on $^{176}\text{Lu}/^{177}\text{Hf}$ and $^{176}\text{Hf}/^{177}\text{Hf}_{\text{measured}}$ values of mid-ocean–ridge basalts (Chauvel and Blichert-Toft, 2001; Figures 3a, b). However, the depleted mantle may not be the best estimate of the composition of the mantle source to the Hogem batholith. The Stuhini Group in Stikine terrane has picritic tuffs that represent mantle-derived melts minimally contaminated by crustal interaction (Milidragovic et al., 2018). The Hogem batholith is part of Quesnel terrane and the Stuhini Group is part of Stikine terrane, but these two terranes have a remarkably similar geological history (e.g., Dostal et al., 1999), making the

Table 1. Summary of secondary-ion mass spectrometry (SIMS) and laser-ablation inductively coupled plasma–mass spectrometry (LA-ICP-MS) results for Thane Creek suite and Duckling Creek suite samples. Uncertainties are reported at the 2σ level. Abbreviation: MSWD, mean square of weighted deviates.

Sample name	19GJ13-5a	18Io25-2a	19GJ13-3	18Io22-1a	19GJ12-4
Suite	Duckling Creek	Duckling Creek	Thane Creek	Thane Creek	Thane Creek
Lithology	Syenite	Syenite	Monzodiorite	Hornblendite	Diorite
Interpreted crystallization age	ca. 175 Ma	ca. 179 Ma	ca. 197 Ma	ca. 198 Ma	ca. 207 Ma
$\delta^{176}\text{Hf}/^{177}\text{Hf}$ range	0.282899±52–0.282979±38	0.282907±30–0.282970±32	0.282928±29–0.282938±31	0.282901±43–0.282984±42	0.282898±74–0.282972±54
$\delta^{176}\text{Hf}/^{177}\text{Hf}$ median	0.282934	0.282933	0.282949	0.282948	0.282948
$\delta^{176}\text{Hf}/^{177}\text{Hf}$ weighted mean	0.282940±7	0.282936±4	0.282954±5	0.282944±6	0.282947±11
No. of analyses	29/29	39/39	40/40	42/42	11
MSWD	0.86	1.15	0.93	1.24	0.48
$\delta^{176}\text{Lu}/^{177}\text{Hf}$ range	0.000560±36–0.002340±390	0.000220±5–0.005789±25	0.000600±120–0.002020±100	0.000105±1–0.002033±42	0.000301±13–0.003630±520
$\delta^{176}\text{Lu}/^{177}\text{Hf}$ median	0.00109	0.001426	0.001227	0.000759	0.001760
ΣHf_t range	7.9±1.9–10.5±1.4	8.2±1.8–10.1±1.0	9.3±1.1–11.5±1.2	8.2±1.6–11.1±1.5	8.4±2.7–11.0±2.0
ΣHf_t Median	9.02	9.11	9.99	9.86	10.1
ΣHf_t weighted mean	9.2±0.3	9.1±0.2	10.1±0.2	9.8±0.2	10.1±0.5
No. of analyses	29/29	38/38	40/40	42/42	11
MSWD	0.8	1.08	0.85	0.98	0.5
$\delta^{18}\text{O}_{\text{VSMOW}}$ (%) range	5.48±0.19–6.50±0.18	6.20±0.22–6.72±0.18	5.22±0.21–6.05±0.18	5.77±0.25–6.30±0.24	4.95±0.19–6.03±0.20
$\delta^{18}\text{O}_{\text{VSMOW}}$ (%) median	6.17	6.57	5.58	6.02	5.54
$\delta^{18}\text{O}_{\text{VSMOW}}$ (%) weighted mean	6.15±0.03	6.57±0.03	5.57±0.03	6.01±0.03	5.53±0.04
No. of analyses	38/39	39/40	53/55	43/43	22/22
MSWD	3.05	1.1	0.65	1.16	1.1

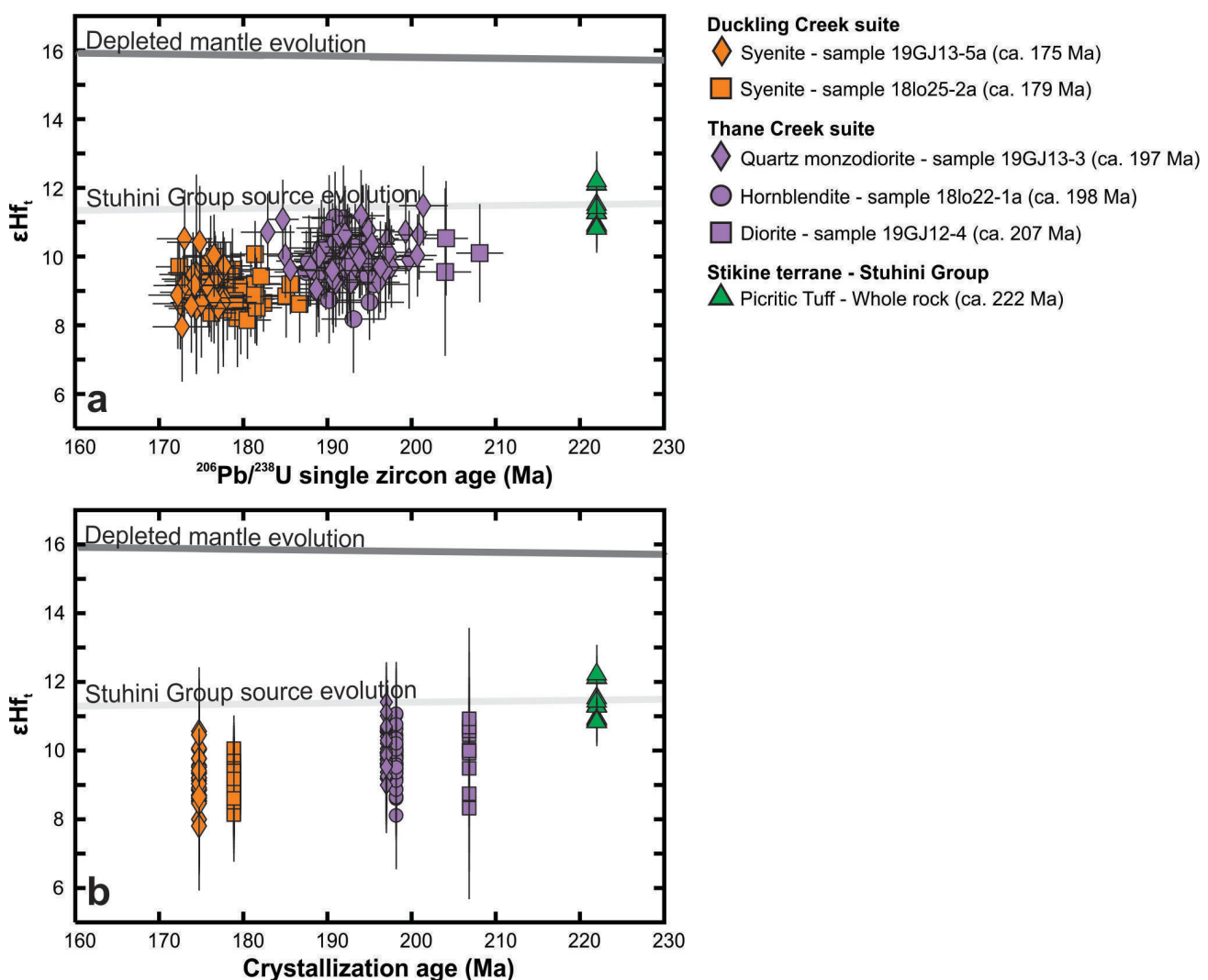


Figure 3. Plot of single-zircon ϵHf_t (calculated at time (t) of crystallization) for multiple Duckling Creek and Thane Creek suite samples across the Hogem batholith plotted versus **a**) laser-ablation inductively coupled plasma–mass spectrometry (LA-ICP-MS) $^{206}\text{Pb}/^{238}\text{U}$ single-zircon date (Ma) and **b**) crystallization U-Pb ages determined by thermal ionization-mass spectrometry (TIMS) for the Thane Creek diorite (ca. 197 Ma) and the Duckling Creek syenite (ca. 178 Ma), which have been previously reported (Devine et al., 2014; Ootes et al., 2020b). Interpreted crystallization ages on Figure 3b include data from G.O. Jones (unpublished data, 2020), Ootes et al. (2020b) and Devine et al. (2014). The depleted mantle (DM) Hf-evolution curve was calculated assuming present $^{176}\text{Hf}/^{177}\text{Hf}_{\text{DM}} = 0.28325$ and $^{176}\text{Lu}/^{177}\text{Hf}_{\text{DM}} = 0.0384$ (Chauvel and Blachert-Toft, 2001). The Stuhini picrite Hf-evolution curve was constructed assuming average present $^{176}\text{Hf}/^{177}\text{Hf} = 0.283086$ and $^{176}\text{Lu}/^{177}\text{Hf} = 0.0279$, calculated from results in Milidragovic et al. (2018).

Stuhini picrite the best estimate of Quesnel terrane mantle. Milidragovic et al. (2018) posited that Late Triassic asthenospheric mantle underlying Stikine terrane, and by extrapolation the Quesnel terrane mantle, was less radiogenic than the depleted mantle at 222 Ma (Figures 3a, b). As such, in Figure 3a and b, the Hogem batholith ϵHf_t values are also compared to Stuhini picrite, with a Hf evolution curve calculated using the average $^{176}\text{Lu}/^{177}\text{Hf}$ and $^{176}\text{Hf}/^{177}\text{Hf}_{\text{measured}}$ values from whole-rock analyses of Milidragovic et al. (2018).

The ϵHf_t values of zircon from the Thane Creek suite generally overlap, but are less radiogenic than, the calculated time-evolved ϵHf_t of the Stuhini Group picrite (Figure 3).

The oldest sample (19GJ12-4), a ca. 207 Ma diorite, has the most juvenile ϵHf_t signature, with a weighted mean of 10.1 ± 0.5 . The ca. 198 Ma hornblendite (18lo22-1a) is more evolved than the diorite, with a weighted mean ϵHf_t of 9.8 ± 0.2 . The ca. 197 Ma monzodiorite (19GJ13-3) has a weighted mean ϵHf_t of 10.1 ± 0.2 , indistinguishable from the older diorite sample.

The oldest Duckling Creek syenite sample (18lo25-2a; ca. 179 Ma) is the most evolved (Figure 3) and has a weighted mean ϵHf_t of 9.1 ± 0.2 . The ca. 175 Ma Duckling Creek syenite (19GJ13-5a) is slightly more juvenile, with a weighted mean of 9.2 ± 0.3 . The ca. 175 Ma syenite ϵHf_t

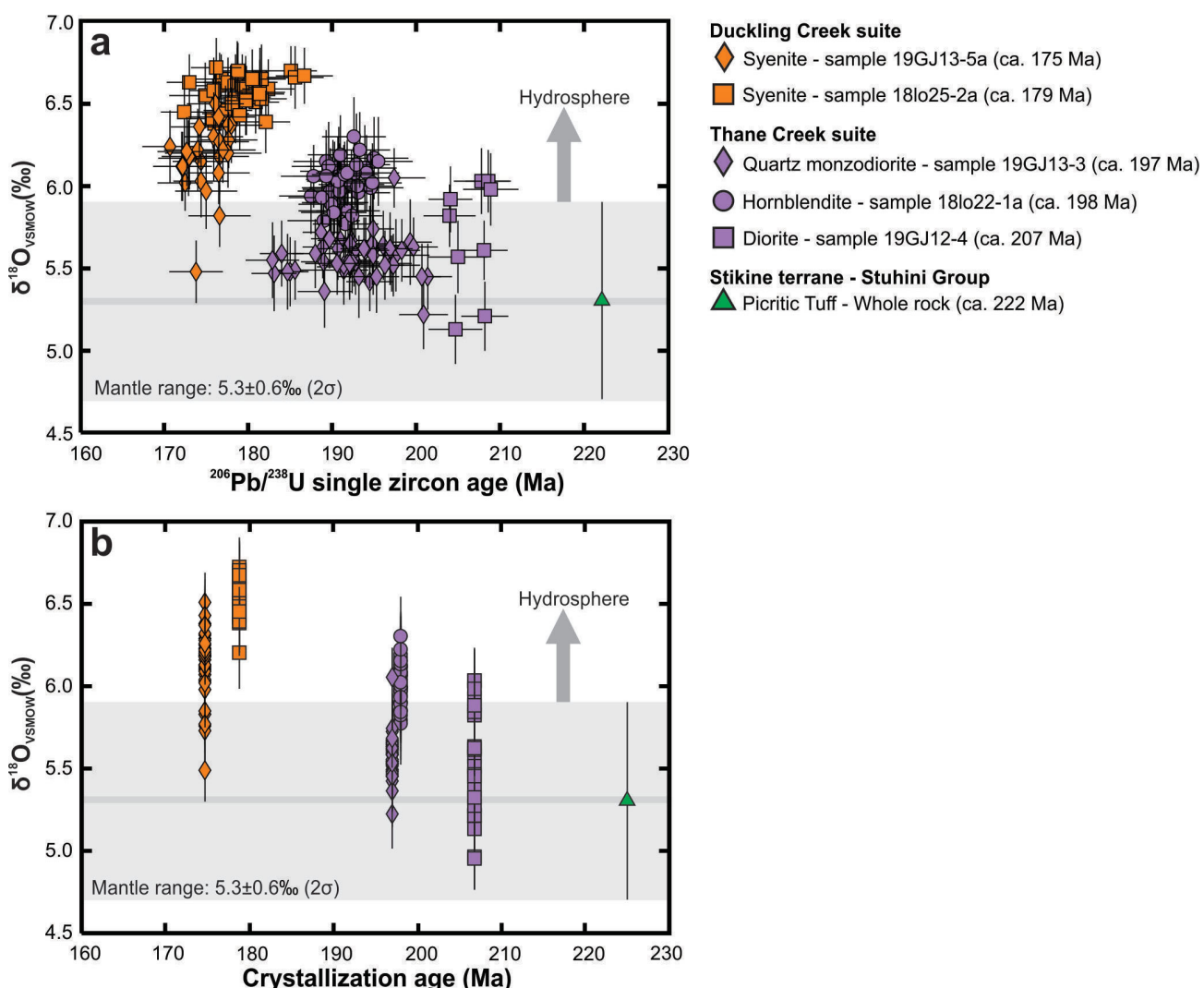


Figure 4. Plot of single-zircon $\delta^{18}\text{O}$ for multiple Duckling Creek and Thane Creek suite samples across the Hogem batholith versus **a)** laser-ablation inductively coupled plasma-mass spectrometry (LA-ICP-MS) $^{206}\text{Pb}/^{238}\text{U}$ single-zircon date (Ma) and **b)** crystallization ages (explained in Figure 3b caption). Mantle zircon $\delta^{18}\text{O}$ from Valley et al. (2005).

overlaps, within uncertainty, the Stuhini picrite, whereas the ca. 179 Ma syenite is slightly more evolved (Figure 3).

Oxygen Isotopes

The results of oxygen-isotope analyses are presented as the $^{18}\text{O}/^{16}\text{O}$ ratio relative to average seawater (VSMOW), which is expressed as $\delta^{18}\text{O}$ in per mille (‰):

$$\delta^{18}\text{O} = \left(\frac{(^{18}\text{O}/^{16}\text{O}_{\text{SAMPLE}})}{(^{18}\text{O}/^{16}\text{O}_{\text{VSMOW}})} - 1 \right) \times 1000,$$

where $^{18}\text{O}/^{16}\text{O}_{\text{VSMOW}} = 0.0020052$ (Baertschi, 1976).

On Figure 4, the Hogem batholith $\delta^{18}\text{O}$ data are compared to the average mantle zircon $\delta^{18}\text{O}$ value of $5.3 \pm 0.6\text{‰}$ (2σ ; Valley et al., 2005), which is invariant through time. The ambient mantle $\delta^{18}\text{O}$ value is assigned to the Stuhini picrite

(Figure 4a, b), as oxygen isotope data are not available for those Stuhini samples (Milidragovic et al., 2018).

The $\delta^{18}\text{O}$ data for the Thane Creek suite are mostly within the mantle range. The ca. 207 Ma diorite has the largest range in $\delta^{18}\text{O}$ and a weighted mean of $5.53 \pm 0.04\text{‰}$. The ca. 198 Ma hornblendite has a higher $\delta^{18}\text{O}$ signature that is slightly above the mantle range, with a weighted mean of $6.01 \pm 0.03\text{‰}$. The ca. 197 Ma monzodiorite is indistinguishable from the older diorite sample, with a weighted mean $\delta^{18}\text{O}$ of $5.57 \pm 0.03\text{‰}$.

Zircon from the ca. 179 Ma Duckling Creek syenite has the highest $\delta^{18}\text{O}$ signature, higher than mantle values, with a weighted mean of $6.57 \pm 0.03\text{‰}$. The ca. 175 Ma Duckling Creek syenite has a larger range in $\delta^{18}\text{O}$ values and a weighted mean of $6.15 \pm 0.03\text{‰}$. This weighted mean is

above the mantle values, with only a few individual analyses overlapping it (Figure 4).

Europium and Titanium Concentrations

Europium concentration data are presented as chondrite-normalized Eu anomalies ($\text{Eu}_N/\text{Eu}_{N^*}$), calculated as follows:

$$\frac{\text{Eu}_{N^*}}{\text{Eu}_N} = \frac{\text{Eu}_N}{\sqrt{(\text{Sm}_N \times \text{Gd}_N)}},$$

where N signifies C1 chondrite normalized. C1 chondrite values are from Sun and McDonough (1989).

The ca. 207 Ma Thane Creek diorite, ca. 197 Ma Thane Creek monzodiorite and ca. 175 Ma Duckling Creek syenite have strong negative Eu anomalies ($\text{Eu}_N/\text{Eu}_{N^*} \sim 0.3\text{--}0.5$; Figure 5). The ca. 198 Ma Thane Creek hornblendite has a moderate to weak negative Eu anomaly ($\text{Eu}_N/\text{Eu}_{N^*} \sim 0.6\text{--}0.8$) and the ca. 179 Ma Duckling Creek syenite has a weak negative to positive Eu anomaly ($\text{Eu}_N/\text{Eu}_{N^*} \sim 0.8\text{--}1.2$; Figure 5).

Titanium concentration data are presented as Ti-in-zircon temperatures, calculated using the zircon crystallization thermometer of Watson et al. (2006), assuming rutile saturation:

$$T(^{\circ}\text{C})_{\text{Zircon}} = \frac{5080 \pm 30}{(6.01 \pm 0.03) - \log(\text{Ti})} - 273,$$

where Ti signifies the measured concentration of Ti in zircon (ppm).

The ca. 207 Ma diorite has the highest concentration and largest range of Ti (~10–22 ppm), resulting in Ti-in-zircon temperatures of ~740–817°C (Figure 6). The ca. 198 Ma hornblendite has lower Ti concentrations and a range of ~2–7 ppm, with Ti-in-zircon temperatures of ~639–711°C. The ca. 197 Ma monzodiorite overlaps the hornblendite Ti range, with concentrations of ~4–9 ppm and Ti-in-zircon temperatures of ~677–729°C (Figure 6).

The ca. 179 Ma Duckling Creek syenite sample has the lowest Ti concentrations, ranging from below the limit of detection to 4 ppm, and Ti-in-zircon temperatures of ~484–669°C. The ca. 175 Ma Duckling Creek syenite has a higher concentration and larger range in Ti (~6–15 ppm) and Ti-in-zircon temperatures (~699–778°C; Figure 6).

Discussion

Zircon oxygen-isotope data are useful for igneous petrogenetic studies because oxygen isotopes are not significantly fractionated in the mantle (Valley et al., 2005). Zircon $\delta^{18}\text{O}$ values higher than the mantle range indicate that ^{18}O is preferentially fractionated relative to ^{16}O , which re-

quires the magmatic source to have experienced low-temperature, near-surface processes (Valley et al., 2005). This would typically occur during interaction with the hydrosphere and implies that the parental magma melted or interacted with crust that was recycled. Enrichment of $\delta^{18}\text{O}$ relative to the average mantle range in some Hogem zircons may reflect the incorporation of crustal material in the magma or magma source (Figures 4, 7). This crustal material may be derived externally (i.e., recycled supracrustal material or assimilation of hostrock) or internally (i.e., remelting of the Hogem batholith that has interacted with the hydrosphere).

The samples from the Thane Creek suite have $\delta^{18}\text{O}$ signatures within the range of the average mantle and εHf_t values that are slightly less radiogenic than the Hf-evolution curve of the Stuhini Group picrite (Figure 3). This implies that the Thane Creek suite crystallized from predominantly juvenile magmas of mantle- or near-mantle composition (Figure 7).

The ca. 179 Ma syenite has $\delta^{18}\text{O}$ values higher than the mantle range and εHf_t values that are less radiogenic than the Stuhini picrite and Thane Creek suite (Figures 3, 4, 7), possibly indicating minor crustal contamination of the magma. The ca. 175 Ma Duckling Creek syenite has mantle-like εHf_t values but elevated $\delta^{18}\text{O}$ (Figures 3, 4, 7), implying the magma was juvenile and with a near-mantle composition, albeit with fractionated oxygen. The ca. 175 Ma syenite sample was obtained close to the previously mentioned Slide showing/prospect (19GJ13-5a; Figure 2c). The results from this sample may have implications for characterizing magmatic-mineralization potential in the Hogem area.

Preliminary $\delta^{18}\text{O}$ and εHf_t results from Hogem S-type granites (Early Cretaceous; G.O. Jones, unpublished data, 2020) are compared to those from the Thane Creek and Duckling Creek suites on Figure 7. The S-type granites have fractionated $\delta^{18}\text{O}$ characteristic of magmas with a source that was recycled through the hydrosphere. The most evolved Duckling Creek and Thane Creek samples have lower $\delta^{18}\text{O}$ and higher εHf_t signatures than the Hogem S-type granite field, indicating these intrusions have more primitive source characteristics.

Samples from both the Thane Creek and Duckling Creek suites do not show a simple temporal trend in Hf-O systematics. The Thane Creek hornblendite and the oldest Duckling Creek syenite have the most evolved Hf-O compositions. The variability in $\delta^{18}\text{O}$ and εHf_t , unrelated to time, indicate variability in the magma sources and/or variability in crustal contamination during magma genesis and evolution.

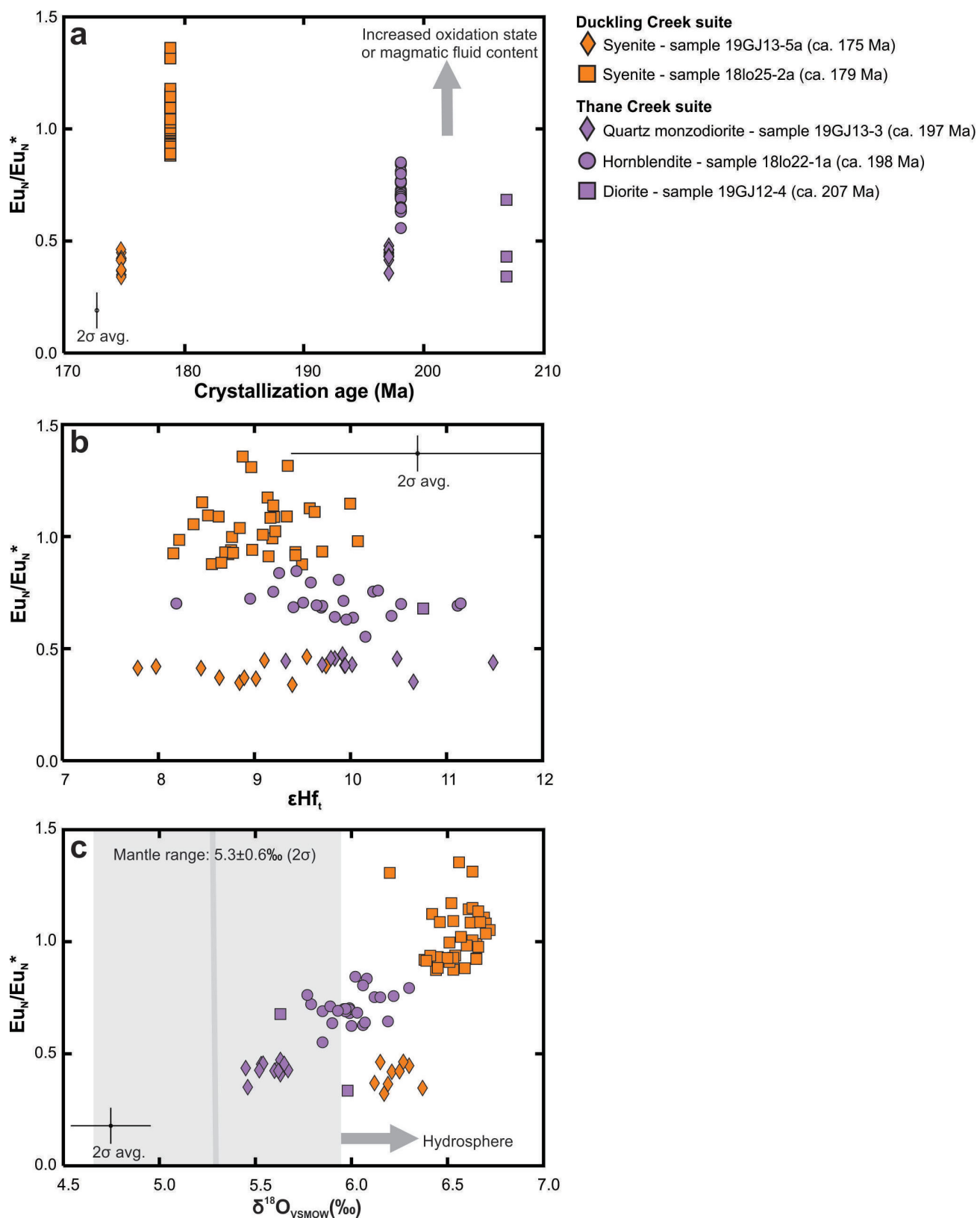


Figure 5. Plot of single-zircon Eu anomaly ($\text{Eu}_N/\text{Eu}_N^*$) for multiple samples of the Duckling Creek and Thane Creek suites across the Hogem batholith versus a) crystallization ages (explained in Figure 3b caption), b) ϵHf_t , and c) $\delta^{18}\text{O}$. The darker grey line in Figure 5c represents the $\delta^{18}\text{O}$ of average mantle zircon ($5.3\text{\textperthousand}$) and the light-grey shading represents the 2σ uncertainty of this value ($0.6\text{\textperthousand}$; Valley et al., 2005).

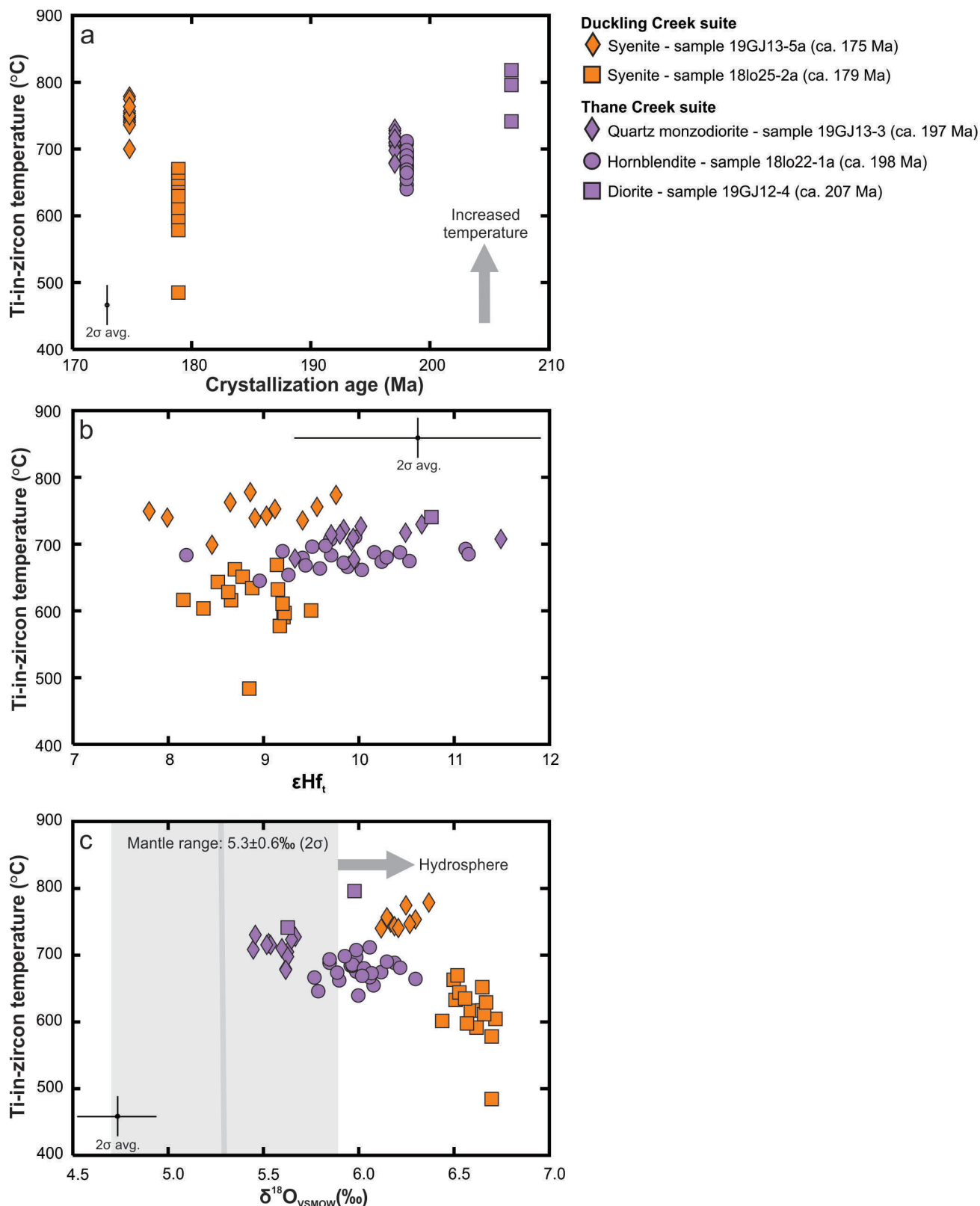


Figure 6. Plot of single Ti-in-zircon temperature for multiple samples of the Duckling Creek and Thane Creek suites across the Hogem batholith versus a) crystallization ages (explained in the caption for Figure 3b), b) ϵHf_t , and c) $\delta^{18}\text{O}$.

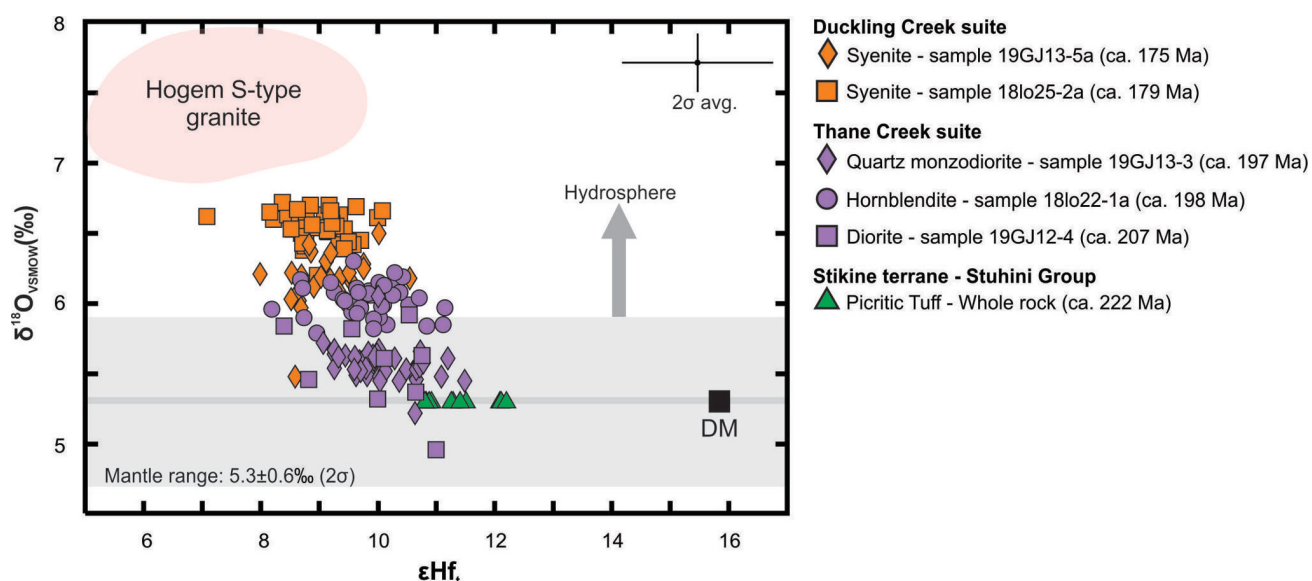


Figure 7. Plot of single-zircon ϵHf_t versus $\delta^{18}\text{O}$. Depleted mantle (DM) Hf data are from Chauvel and Blichert-Toft (2001). Mantle zircon $\delta^{18}\text{O}$ is from Valley et al. (2005). Hogem S-type granite field is from G.O. Jones (unpublished data, 2020).

Europium anomalies in zircon are potential proxies for oxygen fugacity during crystallization in a magma (Shen et al., 2015; Lee et al., 2017; Lee et al., 2020) and/or magmatic-water content (Lu et al., 2016). Elevated magmatic-water content suppresses plagioclase crystallization, which results in increased Eu in the magma and crystallizing zircon (Wilke and Behrens, 1999; Ballard et al., 2002; Lee et al., 2017). In oxidized magmas, Eu^{2+} can be converted to Eu^{3+} , which cannot be substituted into the plagioclase crystal lattice but can be incorporated into zircon (Ballard et al., 2002; Lee et al., 2017). This results in a less negative Eu anomaly in zircon, reflecting relative magmatic-water content and oxidation state (Lee et al., 2017).

Titanium-in-zircon concentrations are used to calculate crystallization temperatures, assuming rutile saturation in the magma (Watson et al., 2006). The assumption of rutile saturation in the magma implies zircon TiO_2 and SiO_2 activities of 1. The Ti-in-zircon temperatures presented here are minimum temperatures, as the TiO_2 activities of these zircons are likely less than 1. A lower zircon TiO_2 activity will result in an increased crystallization-temperature estimate, up to ~70°C higher (Ferry and Watson, 2007). Additionally, these Ti-in-zircon temperatures represent only single temperature points in the overall temperature range of the cooling and crystallizing magmas but are useful for comparisons between intrusive suites. The ca. 207 Ma diorite,

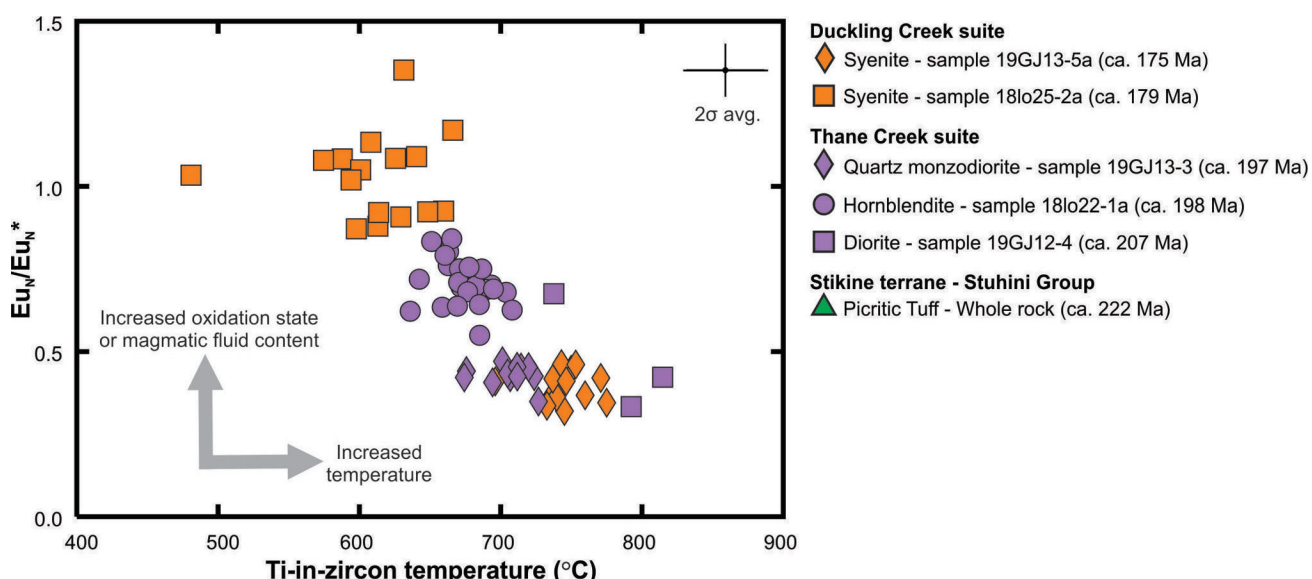


Figure 8. Plot of single titanium-in-zircon temperature versus Eu anomaly ($\text{Eu}_N/\text{Eu}_N^*$).

ca. 197 Ma monzodiorite and ca. 175 Ma syenite have higher Ti-in-zircon temperatures (~677–817°C) and stronger negative Eu anomalies (~0.3–0.5) compared to the ca. 198 Ma hornblendite and ca. 179 Ma syenite (~484–711°C; ~0.6–1.2; Figure 8). Higher Ti concentrations and stronger Eu anomalies imply the zircons crystallized from higher temperature and less oxidized or less hydrous magmas.

The Eu anomaly and Ti data have differing relationships with $\delta^{18}\text{O}$ and εHf_t . The $\text{Eu}_N/\text{Eu}_{N^*}$ and Ti-in-zircon temperature versus $\delta^{18}\text{O}$ show discrete clusters, indicating that Eu anomaly and Ti vary with $\delta^{18}\text{O}$ (Figures 5c, 6c). However, Figures 5b and 6b show significant overlap in individual zircon εHf_t values, despite slight variances in the weighted mean εHf_t between samples. This overlap implies the source of oxygen-isotope fractionation in the magmas may also influence the Eu anomaly and Ti concentration.

Conclusions and Future Work

The porphyry-hosting Thane Creek and Duckling Creek suites have $\delta^{18}\text{O}$, εHf , Ti and $\text{Eu}_N/\text{Eu}_{N^*}$ signatures that are variable through time. These variations indicate changes in the crustal input (crustal recycling in the source or crustal contamination of a magma), temperature, and oxidation state or fluid content of magma sources that formed these intrusive suites. These differences likely had an impact on magma fertility (i.e., the metal-carrying and concentration-capacity of the magmas), as water-rich and oxidized magmas are necessary to increase the metal contents of hydrothermal fluids that contribute to porphyry mineralization (e.g., Sillitoe, 2010).

The zircon geochemistry (U-Pb, Lu-Hf, $\delta^{18}\text{O}$ and trace elements) used in this study will help further characterize the magmas that formed the Hogem batholith, determine differences between intrusive suites and phases within those suites, and assess the impact of these characteristics on magma fertility. Future analytical work includes additional SIMS $\delta^{18}\text{O}$ and LA-ICP-MS Lu-Hf and trace-element analyses. Estimating zircon crystallization temperatures using the Ti-in-zircon thermometer with more accurate zircon TiO_2 and SiO_2 activities, comparing Ce and Eu anomalies, and evaluating the zircon and whole-rock geochemical dataset in relation to porphyry-style mineralization will further characterize the magmatic evolution of northern Hogem batholith.

Acknowledgments

This study is funded by the BC Geological Survey and the Diamond Exploration Research Training School (DERTS). The latter is funded by the Natural Sciences and Engineering Research Council of Canada (NSERC) Collaborative Research and Training Experience (CREATE) Program and the University of Alberta. The principal author grate-

fully acknowledges support from Geoscience BC and NSERC scholarships. The authors thank L. Aspler and D. Thorkelson for constructive reviews of this manuscript.

Natural Resources Canada, Lands and Minerals Sector contribution 20200542

References

- Armstrong, J.E. (1946): Aiken Lake (south half), British Columbia; Geological Survey of Canada, Paper 46-11, 1 map at 1 inch to 2 mile scale, URL <<https://open.library.ubc.ca/cIRcle/collections/ubetheses/831/items/1.0107001>> [September 2020].
- Armstrong, J.E. and Roots, E.F. (1948): Geology and mineral deposits of the Aiken Lake map-area, British Columbia; Geological Survey of Canada, Paper 48-5, 46 p., URL <<https://doi.org/10.4095/101388>>.
- Armstrong, J.E. and Roots, E.F. (1954): Aiken Lake, Cassiar District, British Columbia; Geological Survey of Canada, Map 1030A, scale 1 inch to 4 miles, URL <<https://doi.org/10.4095/106855>>.
- Baertschi, P. (1976): Absolute ^{18}O content of standard mean ocean water; Earth and Planetary Science Letters, v. 31, no. 3, p. 341–344, URL <[https://doi.org/10.1016/0012-821X\(76\)90115-1](https://doi.org/10.1016/0012-821X(76)90115-1)>.
- Ballard, J.R., Palin, J.M. and Campbell, I.H. (2002): Relative oxidation states of magmas inferred from Ce(IV)/Ce(III) in zircon: application to porphyry copper deposits of northern Chile; Contributions to Mineralogy and Petrology, v. 144, p. 347–364, URL <<https://doi.org/10.1007/s00410-002-0402-5>>.
- Bath, A.B., Cooke, D.R., Friedman, R.M., Faure, K., Kamenetsky, V.S., Tosdal, R.M. and Berry, R.F. (2014): Mineralization, U-Pb geochronology, stable isotope geochemistry of the Lower Main Zone of the Lorraine deposit, north-central British Columbia: a replacement-style alkalic Cu-Au porphyry; Economic Geology, v. 109, p. 979–1004, URL <<https://doi.org/10.2113/econgeo.109.4.979>>.
- BC Geological Survey (2020): MapPlace GIS internet mapping system; BC Ministry of Energy, Mines and Low Carbon Innovation, BC Geological Survey, URL <<http://www.MapPlace.ca>> [October 2020].
- Bouvier, A., Vervoort, J.D. and Patchett, P.J. (2008): The Lu-Hf and Sm-Nd isotopic composition of CHUR: constraints from unequilibrated chondrites and implications for the bulk composition of terrestrial planets; Earth and Planetary Science Letters, v. 273, no. 1–2, p. 48–57, URL <<https://doi.org/10.1016/j.epsl.2008.06.010>>.
- Byrne, K., Lesage, G., Gleeson S.A. and Lee, R.G. (2016): Large-scale sodic-calcic alteration around porphyry Cu systems: examples from the Highland Valley Copper district, Guichon batholith, south-central British Columbia; in Geoscience BC Summary of Activities 2016, Report 2017-1, p. 213–222, URL <http://cdn.geosciencebc.com/pdf/SummaryofActivities2016/SoA2016_Byrne.pdf> [September 2020].
- CGG Canada Services Ltd. (2018): Geophysical survey report: MIDAS high resolution magnetic and radiometric survey, Search Project, Phase III; Geoscience BC, Report 2018-02, 72 p., URL <http://cdn.geosciencebc.com/project_data/GBCReport2018-02/GBCR2018-02-Report.pdf> [September 2020].

- Chauvel, C. and Blachert-Toft, J. (2001): A hafnium isotope and trace element perspective on melting of the depleted mantle; *Earth and Planetary Science Letters*, v. 190, p. 137–151, URL <[https://doi.org/10.1016/S0012-821X\(01\)00379-X](https://doi.org/10.1016/S0012-821X(01)00379-X)>.
- Devine, F., Chamberlain, C.M., Davies, A.G.S., Friedman, R. and Baxter, P. (2014): Geology and district-scale setting of tilted alkalic porphyry Cu-Au mineralization at the Lorraine deposit, British Columbia; *Economic Geology*, v. 109, no. 4, p. 939–977, URL <<https://doi.org/10.2113/econgeo.109.4.939>>.
- Dostal, J., Gale, V. and Church, B.N. (1999): Upper Triassic Takla Group volcanic rocks, Stikine terrane, north-central British Columbia: geochemistry, petrogenesis, and tectonic implications; *Canadian Journal of Earth Sciences*, v. 36, p. 1483–1494, URL <<https://doi.org/10.1139/c99-048>>.
- Ferri, F., Dudka, S.F., Rees, C. and Meldrum, D. (2001a): Geology of the Aiken Lake area, north-central British Columbia, NTS 94C/5, 6 and 12; BC Ministry of Energy, Mines and Low Carbon Innovation, BC Geological Survey, Geoscience Map 2001-10, scale 1:50 000, URL <http://cmscontent.nrs.gov.bc.ca/geoscience/PublicationCatalogue/GeoscienceMap/BCGS_GM2001-10.pdf> [September 2020].
- Ferri, F., Dudka, S.F., Rees, C.J., Meldrum, D.G. and Willson, M.J. (2001b): Geology of the Uslika Lake area, north-central British Columbia (NTS 94C/2, 3 and 4); BC Ministry of Energy, Mines and Low Carbon Innovation, BC Geological Survey, Geoscience Map 2001-04, scale 1:50 000, URL <http://cmscontent.nrs.gov.bc.ca/geoscience/PublicationCatalogue/GeoscienceMap/BCGS_GM2001-04.pdf> [September 2020].
- Ferry, J.M. and Watson, E.B. (2007): New thermodynamic models and revised calibrations for the Ti-in-zircon and Zr-in-rutile thermometers; *Contributions to Mineralogy and Petrology*, v. 154, p. 429–437, URL <<https://doi.org/10.1007/s00410-007-0201-0>>.
- Fisher, C.M., Paton, C., Pearson, D.G., Sarkar, C., Tersmette, D.B. and Chacko, T. (2017): Data reduction of laser ablation split-stream (LASS) analyses using newly developed features within Iolite – with applications to Lu-Hf + U-Pb in detrital zircon and Sm-Nd + U-Pb in igneous monazite; *Geochemistry, Geophysics, Geosystems*, v. 18, p. 4604–4622, URL <<https://doi.org/10.1002/2017GC007187>>.
- Fisher, C.M., Vervoort, J.D. and DuFrane, S.A. (2014): Accurate Hf isotope determinations of complex zircons using the ‘laser ablation split stream’ method; *Geochemistry, Geophysics, Geosystems*, v. 15, p. 121–139, URL <<https://doi.org/10.1002/2013GC004962>>.
- Garnett, J.A. (1972): Preliminary geological map of part of Hogem batholith, Duckling Creek area (parts of NTS 93N/13, 14; 94C/3, 4); BC Ministry of Energy, Mines and Low Carbon Innovation, BC Geological Survey, Preliminary Map 09, scale 1:63 360.
- Garnett, J.A. (1978): Geology and mineral occurrences of the southern Hogem batholith; BC Ministry of Energy, Mines and Low Carbon Innovation, BC Geological Survey, Bulletin 70, 75 p., URL <http://cmscontent.nrs.gov.bc.ca/geoscience/PublicationCatalogue/Bulletin/BCGS_B070.pdf> [September 2020].
- Giroux, G. and Lindinger, L.J. (2012): Summary report on the Lorraine-Jajay property, Omenica Mining Division, BC; Report 09-2012 prepared for Lorraine Copper Corp., 122 p., URL <http://www.sedar.com/issuers/issuers_en.htm> [September 2020].
- Ickert, R. (2013): Algorithms for estimating uncertainties in initial radiogenic isotope ratios and model ages; *Chemical Geology*, v. 340, p. 131–138, URL <<https://doi.org/10.1016/j.chemgeo.2013.01.001>>.
- Lee, R.G., Byrne, K., D’Angelo, M., Hart, C.J.R., Hollings, P., Gleeson, S.A. and Alfaro, M. (2020): Using zircon trace element composition to assess porphyry copper potential of the Guichon Creek batholith and Highland Valley Copper deposit, south-central British Columbia; *Mineralium Deposita*, URL <<https://doi.org/10.1007/s00126-020-00961-1>>.
- Lee, R.G., Dilles, J.H., Tosdal, R.M., Wooden, J.L. and Mazdab, F.K. (2017): Magmatic evolution of granodiorite intrusions at the El Salvador porphyry copper deposit, Chile, based on trace element composition and U/Pb age of zircons; *Economic Geology*, v. 112, no. 2, p. 245–273, URL <<https://doi.org/10.2113/econgeo.112.2.245>>.
- Lord, C.S. (1948): McConnel Creek map-area, Cassiar District, British Columbia; Geological Survey of Canada, Memoir 251, 82 p., URL <<https://doi.org/10.4095/101588>>.
- Lord, C.S. (1949): McConnell Creek, Cassiar District, British Columbia; Geological Survey of Canada, Map 962A, scale 1 inch to 4 miles, URL <<https://doi.org/10.4095/106938>>.
- Lu, Y., Loucks, R.R., Fiorentini, M., McCuaig, T.C., Evans, N.J., Yang, Z., Hou, Z., Kirkland, C.L., Parra-Avila, L.A. and Kobussen, A. (2016): Zircon compositions as a pathfinder for porphyry Cu±Mo±Au deposits; Chapter 13 in *Tectonic and Metallogeny of the Tethyan Orogenic Belt*, J.P. Richards (ed.), Society of Economic Geologists, Special Volume 19, p. 329–348, URL <<https://doi.org/10.5382/SP.19.13>>.
- Milidragovic, D., Zagorevski, A., Weis, D., Joyce, N. and Chapman, J.B. (2018): Picrite ‘intelligence’ from the Middle-Late Triassic Stikine arc: composition of mantle wedge asthenosphere; *Lithos*, v. 308–309, p. 446–461, URL <<https://doi.org/10.1016/j.lithos.2018.03.014>>.
- Mortensen, J.K., Ghosh, D.K. and Ferri, F. (1995): U-Pb geochronology of intrusive rocks associated with copper-gold porphyry deposits in the Canadian Cordillera; Canadian Institute of Mining, Metallurgy and Petroleum, Special Volume 46, p. 142–158, URL <<https://store.cim.org/fr/u-pb-geochronology-of-intrusive-rocks-associated-with-copper-gold-porphyry-deposits-in-the-canadian-cordillera>> [October 2020].
- Nixon, G.T. and Peatfield, G.R. (2003): Geological setting of the Lorraine Cu-Au porphyry deposit, Duckling Creek Syenite Complex, north-central British Columbia; BC Geological Survey Open File 2003-4, 24 p., URL <http://cmscontent.nrs.gov.bc.ca/geoscience/PublicationCatalogue/OpenFile/BCGS_OF_2003-04.pdf> [September 2020].
- Ootes, L., Bergen, A.L., Milidragovic, D., Graham, B. and Simmonds, R. (2019): Preliminary geology of northern Hogem batholith, Quesnel terrane, north-central British Columbia; in *Geological Fieldwork 2018*, BC Ministry of Energy, Mines and Low Carbon Innovation, BC Geological Survey, Paper 2019-01, p. 31–53, URL <http://cmscontent.nrs.gov.bc.ca/geoscience/PublicationCatalogue/Paper/BCGS_P2019-01-03_Ootes.pdf> [September 2020].
- Ootes, L., Bergen, A.L., Milidragovic, D. and Jones, G.O. (2020a): Bedrock geology of the northern Hogem batholith and its surroundings, north-central British Columbia; BC Ministry

- of Energy, Mines and Low Carbon Innovation, BC Geological Survey, Open File 2020-02, scale 1:50 000, URL <http://cmscontent.nrs.gov.bc.ca/geoscience/PublicationCatalogue/OpenFile/BCGS_OF2020-02.pdf> [September 2020].
- Ootes, L., Bergen, A.L., Milidragovic, D., Jones, G.O., Camacho, A. and Friedman, R. (2020b): An update on the geology of northern Hogem batholith and its surroundings, north-central British Columbia; *in* Geological Fieldwork 2019, BC Ministry of Energy, Mines and Low Carbon Innovation, BC Geological Survey Paper 2020-01, p. 25–47, URL <http://cmscontent.nrs.gov.bc.ca/geoscience/PublicationCatalogue/Paper/BCGS_P2020-01-03_Ootes.pdf> [September 2020].
- Richards, J.P. (2013): Giant ore deposits formed by optimal alignments and combinations of geological processes; *Nature Geoscience*, v. 6, p. 911–916, URL <<https://doi.org/10.1038/ngeo1920>>.
- Roots, E.F. (1954): Geology and mineral deposits of Aiken Lake map-area, British Columbia; Geological Survey of Canada, Memoir 274, 246 p., URL <<https://doi.org/10.4095/101499>>.
- Sagan, M., Heaman, L.M., Pearson, D.G., Luo, Y. and Stern, R. (2020): Removal of continental lithosphere beneath the Canary archipelago revealed from a U-Pb age and Hf/O isotope study of modern sand detrital zircons; *Lithos*, v. 362–363, 18 p., URL <<https://doi.org/10.1016/j.lithos.2020.105448>>.
- Schiarizza, P. and Tan, S.H. (2005): Geology of the Johanson Lake area, parts of NTS 94D/8 and 9; BC Ministry of Energy, Mines and Low Carbon Innovation, BC Geological Survey Open File 2005-4, scale 1:50 000, URL <http://cmscontent.nrs.gov.bc.ca/geoscience/PublicationCatalogue/OpenFile/BCGS_OF2005-04.pdf> [September 2020].
- Shen, P., Hattori, K., Pan, H., Jackson, S. and Seitmuratova, E. (2015): Oxidation condition and metal fertility of granitic magmas: zircon trace-element data from porphyry Cu deposits in the central Asian orogenic belt; *Economic Geology*, v. 110, no. 7, p. 1861–1878, URL <<https://doi.org/10.2113/econgeo.110.7.1861>>.
- Sillitoe, R.H. (2010): Porphyry copper systems; *Economic Geology*, v. 105, p. 3–41, URL <<http://dx.doi.org/10.2113/gsecongeo.105.1.3>>.
- Söderlund, U., Patchett, P.J., Vervoort, J.D. and Isachsen, C.E. (2004): The ^{176}Lu decay constant determined by Lu-Hf and U-Pb isotope systematics of Precambrian mafic intrusions; *Earth and Planetary Science Letters*, v. 219, no. 3–4, p. 311–324, URL <[https://doi.org/10.1016/S0012-821X\(04\)00012-3](https://doi.org/10.1016/S0012-821X(04)00012-3)>.
- Sun, S. and McDonough, W.F. (1989): Chemical and isotopic systematics of oceanic basalts: implications for mantle composition and processes; *Geological Society of London, Special Publications*, v. 42, p. 313–345, URL <<https://doi.org/10.1144/GSL.SP.1989.042.01.19>>.
- Valley, J.W., Lackey, J.S., Casavie, A.J., Clechenko, C.C., Spicuzza, M.J., Basei, M.A.S., Bindeman, I.N., Ferreira, V.P., Sial, A.N., King, E.M., Peck, W.H., Sinha, A.K. and Wei, C.S. (2005): 4.4 billion years of crustal maturation: oxygen isotope ratios of magmatic zircon; *Contributions to Mineralogy and Petrology*, v. 150, p. 561–580, URL <<https://doi.org/10.1007/s00410-005-0025-8>>.
- Vezinet, A., Pearson, D.G., Thomassot, E., Stern, R.A., Sarkar, C., Luo, Y. and Fisher, C.M. (2018): Hydrothermally-altered mafic crust as source for early Earth TTG: Pb/Hf/O isotope and trace element evidence from TTG of the Eoarchean Saglek Block, N. Labrador (electronic supplementary material); *Earth and Planetary Science Letters*, v. 503, p. 95–107, URL <<https://doi.org/10.1016/j.epsl.2018.09.015>>.
- Watson, E.B., Wark, D.A. and Thomas, J.B. (2006): Crystallization thermometers for zircon and rutile; *Contributions to Mineralogy and Petrology*, v. 151, p. 413–433, URL <<https://doi.org/10.1007/s00410-006-0068-5>>.
- Wilke, M. and Behrens, H. (1999): The dependence of the partitioning of iron and europium between plagioclase and hydrous tonalitic melt on oxygen fugacity; *Contributions to Mineralogy and Petrology*, v. 137, p. 102–114, URL <<https://doi.org/10.1007/s004100050585>>.
- Woodsworth, G.J. (1976): Plutonic rocks of McConnell Creek (94 D west half) and Aiken Lake (94 C east half) map-areas, British Columbia; Geological Survey of Canada, Paper 76-1A, p. 69–73, URL <<https://doi.org/10.4095/104166>>.

Pilot Study Comparing Eddy Covariance and Dynamic Closed-Chamber Methods for Measuring CO₂ Fluxes above the Hydromagnesite-Magnesite Playas near Atlin, Northwestern British Columbia (NTS 105N/12)

A.-M. Doucet¹, The University of British Columbia, Vancouver, British Columbia, amdoucet@eoas.ubc.ca

F.A. Jones, The University of British Columbia, Vancouver, British Columbia

G.M. Dipple, The University of British Columbia, Vancouver, British Columbia

K.U. Mayer, The University of British Columbia, Vancouver, British Columbia

Doucet, A.-M., Jones, F.A., Dipple, G.M. and Mayer, K.U.(2021): Pilot study comparing eddy covariance and dynamic closed-chamber methods for measuring CO₂ fluxes above the hydromagnesite-magnesite playas near Atlin, northwestern British Columbia (NTS 105N/12); *in* Geoscience BC Summary of Activities 2020: Minerals and Mining, Geoscience BC, Report 2021-01, p. 121–128.

Introduction

Carbon dioxide (CO₂) sequestration by carbon mineralization in ultramafic materials has emerged as a promising strategy to reduce net greenhouse-gas emissions (e.g., Seifritz, 1990; Lackner et al., 1995; Wilson et al., 2009; Power et al., 2013). This process incorporates CO₂ gas into inert carbonate minerals (MgCO₃·xH₂O) through the aqueous reaction of bicarbonate anions (HCO₃⁻) and magnesium cations leached from ultramafic rocks. Carbon mineralization can occur passively via chemical-weathering processes at the surface, or actively by CO₂ injection into the subsurface (e.g., mine-tailings storage facilities and/or in deep geological formations).

The current method used to estimate passive carbon capture in ultramafic mine tailings is mineral quantification, by which a CO₂ sequestration rate is calculated from the weight of precipitated carbonate minerals in tailings samples over an area and time of deposition. Estimates from a recent study revealed that some mines passively offset over 10% of their CO₂ emissions through carbonate-mineral precipitation in their tailings material (Wilson et al., 2014). Accurately measuring passive rates of CO₂ uptake using mineral quantification has proven challenging due to the intensive field and laboratory labour it requires and low spatial and temporal resolution it provides. Accurate quantification of carbon-uptake rates is necessary to validate this novel form of carbon capture and storage. Developing protocols involving environmental monitoring methods that measure real-time CO₂ fluxes will aid mining companies in quantifying their carbon uptake.

Eddy covariance (EC) and dynamic closed-chamber (DCC) systems, two widely accepted environmental monitoring technologies used in soil science and ecosystem science, can potentially be employed in a geological context to measure CO₂ fluxes between the atmosphere and mine waste. Eddy covariance measures the time-averaged covariance between the fluctuations in vertical wind velocity and CO₂ concentration to compute the gas fluxes between the ground surface and the atmosphere. The dynamic closed-chamber method measures the CO₂ concentration over time in a closed-chamber system and computes the flux from the change in gas concentration occurring over time at the soil-atmosphere interface. In previous studies in ecosystems and agricultural sciences, EC and DCC methods have been paired to cross-validate measured fluxes (Norman et al., 1997; Riederer et al., 2014; Wang et al., 2017; Lucas-Moffat et al., 2018). The EC and DCC methodologies have only once been paired at an operating mine site to measure CO₂ and water-vapour fluxes from a waste-rock pile undergoing pyrite oxidation in the presence of carbonate minerals (Kabwe et al., 2005). No conclusions were made about acid neutralization and CO₂ emissions because the signal was mixed with a biogenic source. Additionally, EC has been implemented at deep geological CO₂ injection sites to quantify, in real-time, surface leakage of CO₂ into the biosphere (Burba et al., 2013). Pairing EC and DCC methods, to target low carbon emissions at mine sites where the ore is hosted in ultramafic rock, may provide the quantification and verification needed to determine CO₂ sequestration potential; nonetheless, the fact remains that there is a clear lack of studies testing the effectiveness of these methods in this geological setting.

¹The lead author is a 2020 Geoscience BC Scholarship recipient.

This publication is also available, free of charge, as colour digital files in Adobe Acrobat® PDF format from the Geoscience BC website: <http://geosciencebc.com/updates/summary-of-activities/>.

In this study, the EC and DCC methods were employed on the hydromagnesite-magnesite playas of Atlin, British Columbia (BC). These playas have been forming at the Earth's surface since the most recent deglaciation and comprise an assemblage of calcium and magnesium carbonate minerals

(Power et al., 2014). It has been proposed that, due to the high concentration of carbonate in the alkaline groundwater, CO₂ is likely to degas. (Power et al., 2014, 2019). This site is of interest because it provides insights on conditions favourable for ex situ carbon mineralization and presents features similar to deep geological CO₂ injection sites with potential CO₂ leakage.

The objectives of this study are to

- detect and compare fluxes occurring at this site using both EC and DCC methods; and
- identify the source of the CO₂ emitted.

The overarching goal is to establish protocols for validating these methods of measuring in real time CO₂ fluxes associated with both passive and active carbon mineralization in ultramafic mine tailings, leading to the development of carbon capture and storage strategies.

Geological Setting

The study site is located in Atlin, northwestern BC, where unique bedrock geology and postglacial history have led to the formation of hydromagnesite-magnesite alkaline playas. Atlin lies 48 km from the Yukon border (59.5818°N,

133.6885°W, at an elevation of 696 m asl; Figure 1). The bedrock is composed of ultramafic and altered ultramafic materials originating in the upper mantle of the oceanic lithosphere, and contains Mg-rich harzburgite and dunite (Ash and Arksey, 1990; Hansen et al., 2005). The ophiolitic material was obducted onto the Stikine and Cache Creek terranes of BC (Ash and Arksey, 1990). Serpentization occurred via pre- and post-obduction hydrothermal-fluid alteration, followed by a carbonation event resulting from CO₂-rich fluids and forming listwanite (Hansen et al., 2005).

To the east of Atlin are two large playas described as the northern playa and the southern playa. The playas formed via shallow groundwater flow that weathered the rocks in the subsurface, leaching magnesium (Mg²⁺) from the serpentinite and then bicarbonate (HCO₃⁻) from the listwanite, and forming hydromagnesite-magnesite deposits in topographic lows carved by the last glaciation (Power et al., 2014, 2019). Power et al. (2014) proposed a depositional model supported by radiocarbon dates, suggesting that deposition in the playas has been continuous since the retreat of the last glaciation (11 000 BP). Above the glacial till and glaciolacustrine sediments, a layer of calcium-magnesium

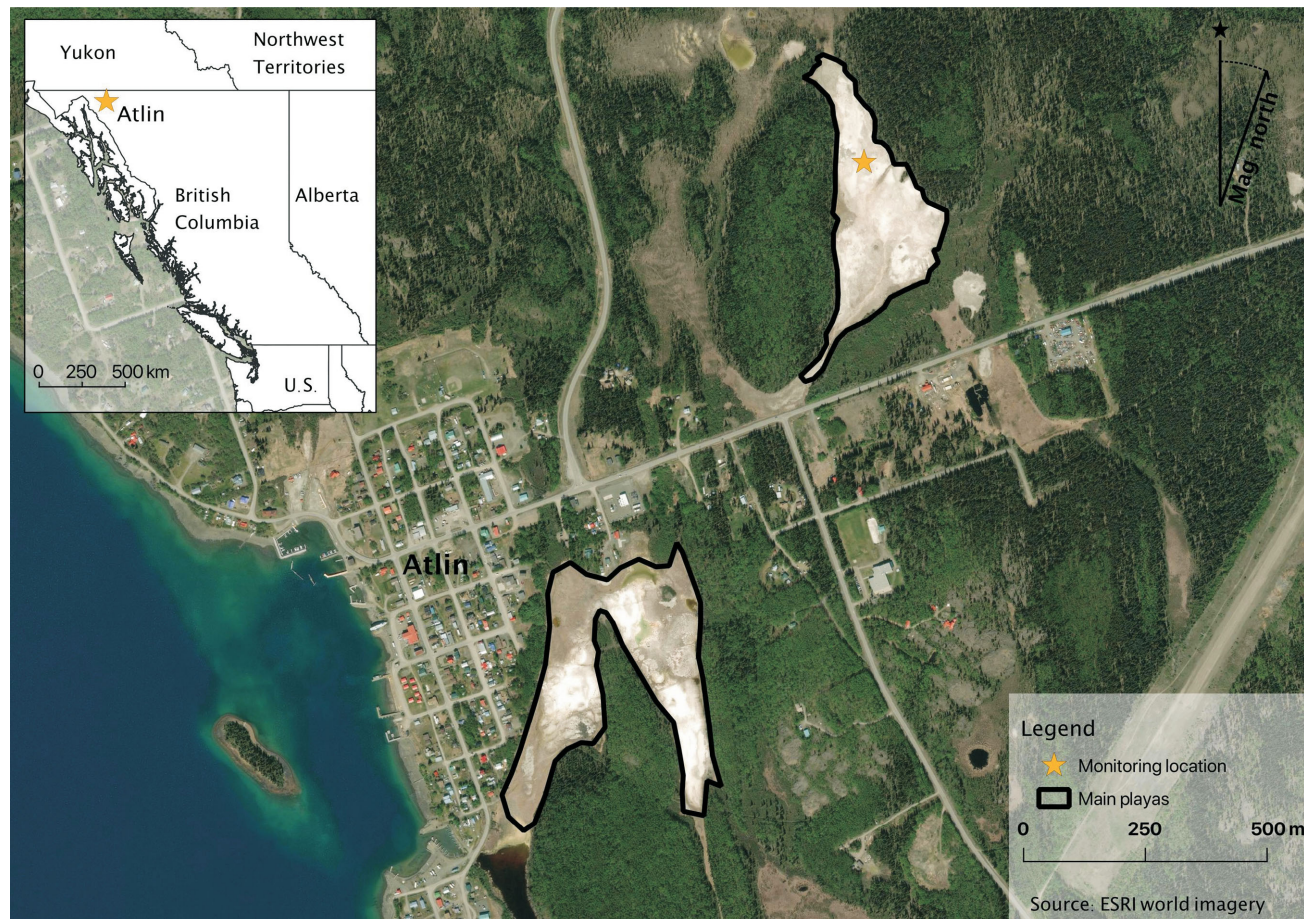


Figure 1. Location of study area in Atlin, northwestern British Columbia (map generated using QGIS V3.14, see <http://qgis.org>).

carbonate was deposited in subaqueous wetland fed by the alkaline groundwater ($\text{pH} \sim 8.6$). At the surface, a layer of magnesium carbonate minerals was formed and expanded in subaerial conditions due to evapoconcentration and degassing processes (Power et al., 2014). The southern playa displays four of the depositional environments (i.e., wetland, grassland, localized mounds and amalgamated mounds) described in Power et al. (2014) and the northern playa primarily displays amalgamated mounds at the surface. During the formation of the hydromagnesite-magnesite mounds, the groundwater reaching atmospheric conditions degassed CO_2 and precipitated carbonate minerals, specifically $\{\text{Mg}_5(\text{CO}_3)_4(\text{OH})_2\cdot 4\text{H}_2\text{O}_{[\text{s}]}\}$, to maintain thermodynamic equilibrium (Power et al., 2014, 2019).

Site Description

The northern playa was selected for long-term monitoring of CO_2 fluxes (Figure 1). This location for pairing the EC and DCC systems was chosen due to the large areal extent of hydromagnesite-magnesite playa, the reduced surface roughness, as well as the absence of grassland influence.

Data were collected over 27 days during August 2020. Long-term DCC were set in pairs at 5 m intervals toward the south of the EC tower (Figures 2, 3) surrounded by a grid of 22 soil collars for survey DCC measurements. Desiccation cracks are common at the surface of the northern playa, extending vertically into the hydromagnesite deposit.

The average air temperature for the month of August, 14°C during daytime and 6°C at nighttime, was comparable to the multiyear averages, 18°C and 5°C , respectively, for the month of August (Environment Canada, 2020). Over the monitoring period, the nighttime temperatures decreased steadily. The rainfall measured by the rain gauge on the EC tower was 38 mm over this period, consistent with the historical average for August (32 \pm 15 mm). Historical wind direction was considered for establishing the EC tower in the best location to capture the desired fetch (i.e., monitoring area of interest). The historical prevailing-wind direction in August was from the southwest. However, during the monitoring period around 50% of the wind was from the southeast. Since the fetch was homogeneous at 180 degrees east

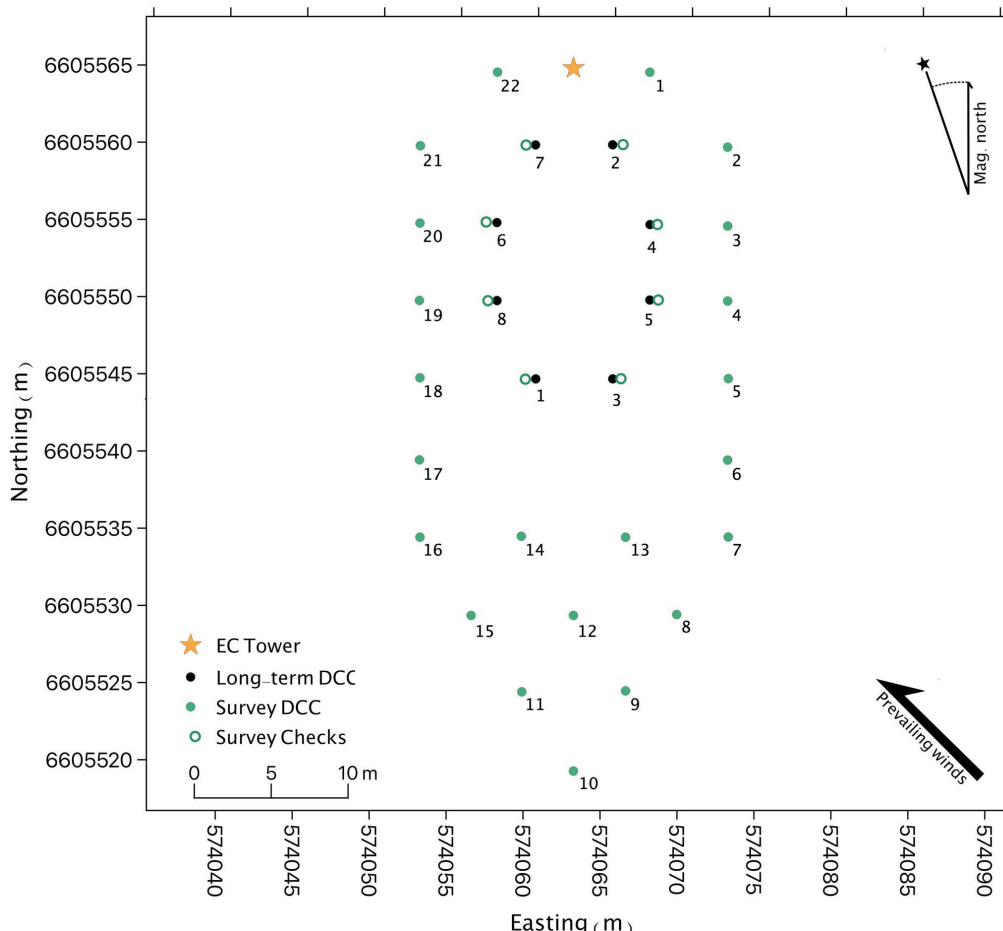


Figure 2. Location of the EC tower relative to the long-term DCC pair system and the DCC survey grid (prevailing-wind arrow for August 2020) in Atlin, northwestern British Columbia. Note that survey DCC co-located with the long-term DCC were used as checks to ground-truth the flux data (grid generated using QGIS V3.14, see <http://qgis.org>). All co-ordinates are in UTM Zone 8N, NAD 83.

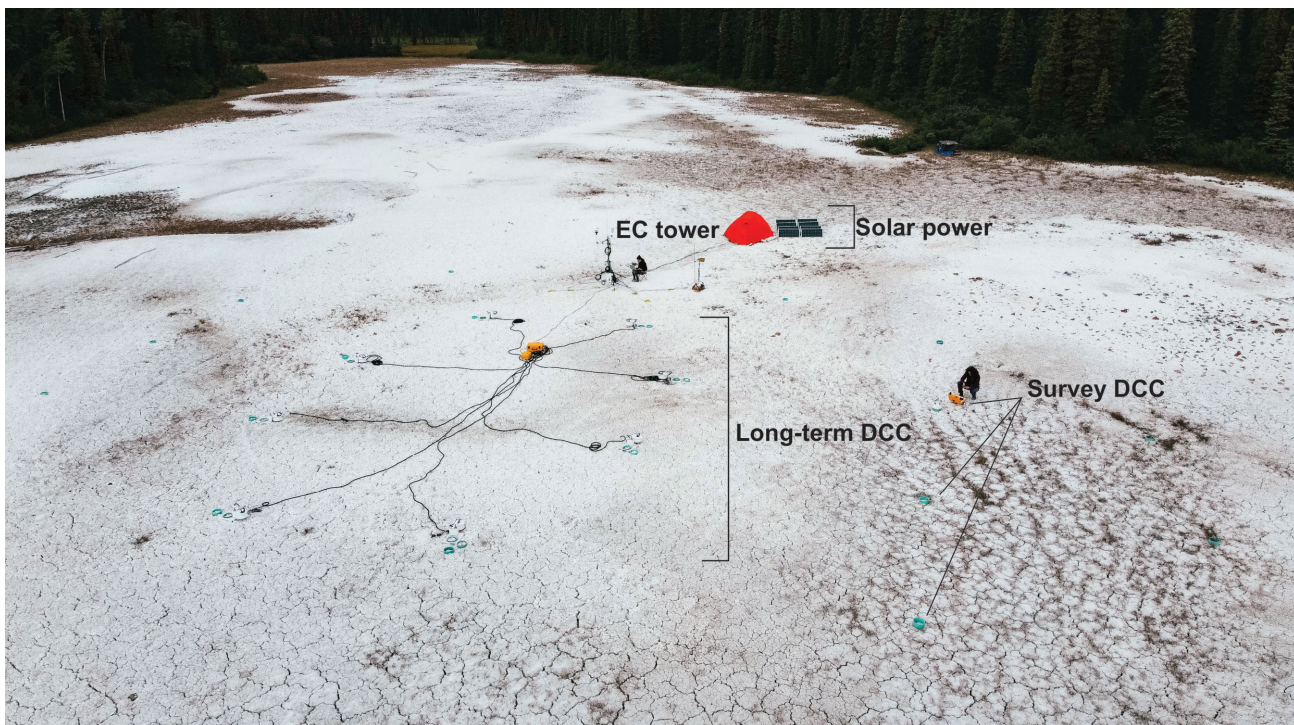


Figure 3. Drone image of the research site facing true north, showing the EC tower near the centre and the long-term DCC system to the left (two researchers for scale) on the northern playa in Atlin, northwestern British Columbia.

to west in the south direction, it was possible to collect valid EC data regardless of the historical wind direction and the choice of tower location.

Materials and Methods

Eddy Covariance

The principles of EC rely on the turbulence created by ground surface roughness, which forms eddies that transport gases, heat and momentum between the Earth's surface and the atmosphere (Baldocchi, 2003). The EC system consisted of a CSAT3B 3-D sonic anemometer manufactured by Campbell Scientific, Inc. (CSI) and a LI-COR Biosciences LI-7200RS enclosed-path CO₂/H₂O gas analyzer (Figure 4). A 7200-101 flow module was installed to maintain a precise air flow through the gas analyzer. Additionally, an analyzer interface unit was installed to integrate the data from the enclosed gas analyzer and the sonic anemometer, then the data was stored and made accessible through the unit's SMARTFlux system. The instruments were set on a tower at a height of 2.1 m above the soil with high-frequency data continuously sampled at 10 Hz for the first two weeks. For the last two weeks, the tower height was lowered to 1.65 m and the sampling frequency increased to 20 Hz to better align the EC-system sampling footprint with the area covered by DCC measurements. The footprint used to compute the area-normalized flux was proportional to the height of the instrument and inversely proportional to

the wind speed, among other minor variables. It was critical that the footprint of the instrumentation not extend beyond the fetch, as it would contribute unwanted fluxes to the final estimate.

The flux from an area of interest (i.e., the footprint) was computed from the covariance using Reynolds averaging of vertical wind speed, scalar CO₂ concentrations in dry air and air density outlined in Baldocchi (2003) using the Webb-Pearman-Leuning correction (Webb et al., 1980) given by the following equation:

$$F_{CO_2} = \rho_a \overline{w' CO_2'}$$

where ρ_a is the dry-air density, $w' CO_2'$ is the time-averaged vector-path covariance of the vertical wind speed and the scalar CO₂ concentration in dry air.

The open-source EddyPro® software, released by LI-COR Biosciences, was used to process the flux data. The high-frequency data were averaged over 30 min intervals. Fluxes computed with a friction velocity (u^*) less than 0.15 were rejected from this dataset, the low values resulting from the wind-speed being too low to create eddies and transport gases near the surface. Data collected from a wind direction between 270 to 90 degrees from the direction behind the anemometer (at 180 degrees) were rejected. Additionally, a water-vapour correction (Webb et al., 1980) and high-frequency corrections were applied in EddyPro®.

Additional soil and meteorological instruments at the EC station included two soil heat-flux plates (Hukseflux thermal sensor models HFP01SC and HFP01) at 5 cm depth and soil moisture probes (CSI model CS650) installed at an average depth of 10 cm, as well as sensors to measure wind speed and direction (CSI Windsonic4-L), air temperature and relative humidity (CSI model HMP 155A), barometric pressure (CSI model CS106) and rainfall (CSI model TE525WS-L). Energy balances were also calculated using incoming and outgoing radiation (CSI CNR4-L radiometer). Soil and meteorological data were averaged over 30 min intervals from 1 s measurements and were stored on a CSI CR1000X datalogger. All these components were used to measure the weather patterns and ground-truth the EC anemometer data.

Routine tests and diagnostic checks were conducted twice daily to ensure the proper functioning of the components on the flux tower. Processing, data filtering and corrections are ongoing.

Dynamic Closed Chambers

The dynamic closed chambers (DCC) in long-term and survey modes (using LI-COR Biosciences system models LI8100A with the LI-8150 and LI-8100A, respectively) were used to measure the flux from the change in concentration of CO₂ and water vapour (H₂O_(g)) in the chamber headspace over time. Eight dynamic long-term DCC were set in a grid in the direction of the prevailing winds south of the EC tower, as shown in Figures 2 and 3. The long-term chamber system consisted of eight automatic opaque chamber domes on rectangular platforms, an infrared gas analyzer unit (IRGA) and a LI-8150 multiplexer (Figure 5a). Each chamber recorded observations every 30 min, providing time-series data for fluxes directly across the ground surface. Additionally, a survey grid was set around the long-term DCC consisting of 22 soil collars permanently embedded in the ground, as shown in Figure 2. There were also 12 soil collars emplaced at selected locations, including on the forest floor, in the transition zone between grassland and carbonate materials and in excavations with a depth of 20 cm. A total of 25 observations were made at each survey collar in the grid and a further 12 at the strategically located survey collars. The survey system consisted of a portable opaque chamber dome, polyvinyl chloride (PVC) collars and an IRGA unit (Figure 5b).

The automated chamber, controlled by the analyzer unit, was placed on a collar embedded in the ground, temporarily creating a closed environment to measure accumulation of CO₂ over time in the chamber headspace. Air was circulated between the chamber and the IRGA with an internal pump, creating small-scale eddies to ensure well-mixed conditions in the system. The IRGA measured the concentration of CO₂ and H₂O_(g) over time and subsequently cor-

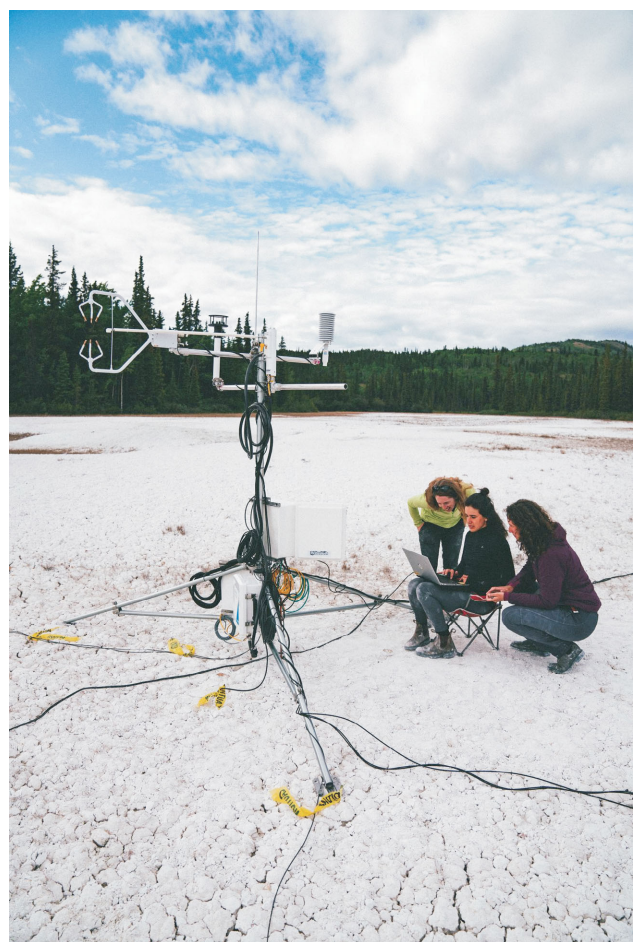


Figure 4. Eddy covariance flux tower in Atlin, northwestern British Columbia (radiometer, rain gauge and soil heat-flux plates are not shown).

rected the concentration of CO₂ for the influence of H₂O_(g) (i.e., dry-air CO₂ or mixing ratio). Additionally, the chamber was vented to the atmosphere to prevent a pressure gradient from affecting the flux measurement.

Based on qualitative-data analysis, the length of each observation was 120 s during the period of chamber closure. The linear-regression method was used to fit the data points between 5 and 45 s to obtain the rate of change of water-corrected CO₂ over time (see Figure 6). To compute CO₂ fluxes across the ground surface, the temporal CO₂ gradient was then substituted into the following equation:

$$F_{CO_2} = \frac{10VP_0(1 - \frac{W_0}{1000}) \partial C'}{RS(T_0 - 273.15) \partial t}$$

where, F_{CO_2} is the gas flux ($\mu\text{mol}/\text{m}^2/\text{s}$), P_0 is the initial pressure measured inside the chamber (kPa), W_0 is the initial water-vapour mole fraction (mmol/mol), $\partial C'/\partial t$ is the rate of change in the water-corrected CO₂ mole fraction ($\mu\text{mol}/\text{mol}/\text{s}$), S is the soil surface area over which the flux occurs (cm^2), V is the total volume of the system (the sum of the volume of the chamber headspace, the volume of the

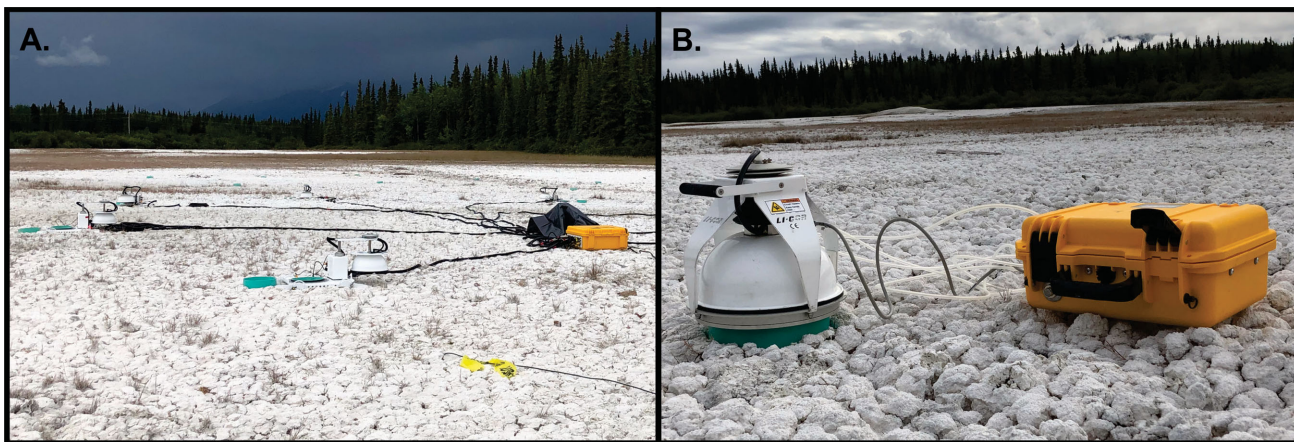


Figure 5. Study area in Atlin, northwestern British Columbia, showing **a)** a long-term chamber system, and **b)** a survey chamber system with infrared gas analyzer unit. Both are used to make gas-flux measurements and can be seen here with their associated soil collars (constructed from green polyvinyl chloride pipe sections).

collar above the ground surface and associated connection tubing and the internal analyzer volume in cm^3), R is the ideal gas constant ($8.314 \text{ kPa}\cdot\text{m}^3/\text{K/mol}$) and T_0 is the initial air temperature ($^\circ\text{C}$).

Additionally, data and diagnostic checks were conducted five times during the observation period to ensure the proper functioning of both chamber modes. On four separate days, survey-mode observations were made alongside the long-term chambers as checks, to ground-truth the fluxes and assess the heterogeneity of the sampling. Processing, data filtering and corrections are ongoing.

Gas Sampling for Isotopic and Radiocarbon Analysis

The source of CO_2 from the subsurface and air can be distinguished based on their stable isotopes and radiocarbon composition. Carbon-dioxide gas composition will be determined via stable isotopes of carbon and oxygen, and age will be estimated using radiocarbon analysis. Following

recommendations, a static chamber method was chosen for gas-sample collection and sampling from the playas (A. Wozney, I.D. Clark and K.U. Mayer, work in progress). The static chambers, consisting of a section of PVC pipe 10 cm across and 30 cm in length, were embedded 20 cm into the carbonate soil and fitted with a PVC cap equipped with a septum for sample extraction. To gain insight on the discrete and spatial variation in gas composition at depth, the static chambers were placed in excavations dug to three depths (5 cm, 40 cm and 65 cm below ground surface) at two locations on the northern playa. The static chambers were left undisturbed for a week before initial sampling.

Gas was collected from the septum with a 25 mL gas-tight syringe and 20 mL of sample was inserted into a 12 mL Labco Limited pre-evacuated Exetainer® to be analyzed for stable isotopes of CO_2 , C^{13} and O^{18} . Samples for radiocarbon required a large volume of pore gas and air due to low CO_2 concentrations, ranging approximately from 400 to 1000 ppm. The method used for ^{14}C sample collection was

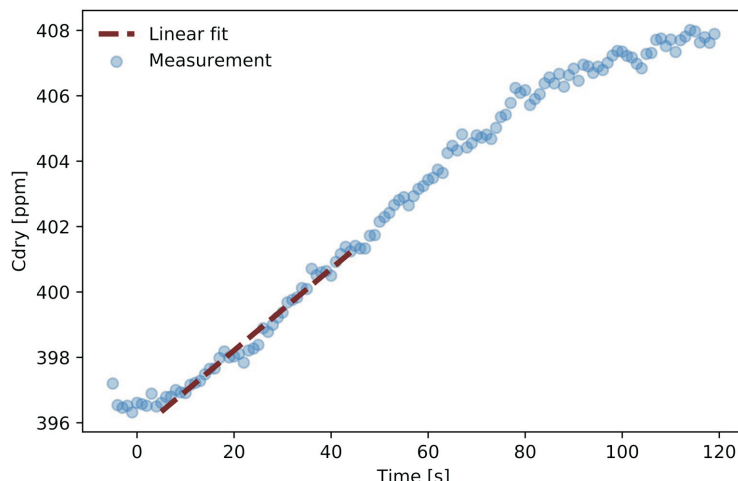


Figure 6. Determination over time of the rate of change in dry-air CO_2 (Cdry) with a linear fit (in red) for CO_2 -flux calculation.

recently developed at the A.E Lalonde AMS Laboratory (Ottawa, ON). Using this method, the gas sample is bubbled through a 0.4 mL solution of barium hydroxide $\{\text{Ba}(\text{OH})_2\}$, leading to the sequestration of CO_2 as a barium carbonate precipitate (Reynolds, 2019). Twenty-five samples for stable-isotope analysis were taken over three days and nine (six static chamber and three atmospheric) samples were collected for radiocarbon analysis.

Work in Progress and Expected Outcomes

Data analysis is in progress to compare the CO_2 fluxes from the EC and DCC methods. A correlation analysis of the EC and DCC data will be conducted. Additional weather correlation plots will be prepared to observe any climatic phenomena influencing the fluxes. Finally, the associated errors and limitations of both methods will be evaluated. For example, the desiccation cracks at the surface of the playas are expected to add a level of spatial variability to the DCC method. The EC method is well suited to quantify average fluxes over an area with desiccation cracks; however, the DCC method requires the headspace be closed to the atmosphere to record a valid observation. Cracks and leaks around the collars during installation were kept to a minimum in this study, but a careful inspection of the data will be needed to assess potential impact on data quality and interpretation due to the presence of cracks. The desiccation-crack problem and other potential limitations can be transposed to mine tailings with mudcracks; therefore, insights from the outcomes of this pilot study will be reflected in the application of this method to mine sites. The deployment of the technologies in the field and a preliminary review of the data suggest that these methods show promise for application at an active mine site where the ore is hosted in ultramafic rock to measure real-time CO_2 sequestration in mine tailings.

Carbon dioxide stable isotopes and radiocarbon in CO_2 from pore and atmospheric gas samples are currently being analyzed. These results will provide a better understanding of the origin of the CO_2 given the age and composition of the gas. If the CO_2 is from a deep geological source, there is an option to further study the Atlin playas as a natural analogue for scenarios for the leakage of CO_2 following injection and, also, to develop a better understanding of these unique geological features. Studying the mechanism and kinetics of carbonate precipitation as a mean for scrubbing the CO_2 as it is emitted at this site could be warranted.

Conclusions

This study on the hydromagnesite-magnesite playas in Atlin, BC has shown that EC and DCC methods show promise as a means of measuring CO_2 fluxes in a geological environment to characterize CO_2 exchange with the atmosphere. As suggested in the literature, passive CO_2 fluxes in

mine tailings containing ultramafic minerals are significant and can substantially impact the carbon budget of the mine facility. The eddy covariance method may provide an efficient and continuous real-time approach to quantifying rates of CO_2 capture. The dynamic closed-chamber method is useful in cross-validating fluxes from EC measurements to corroborate the validity of the findings. The overarching goal of this project was to inform verification protocols for use by mining companies to secure carbon credits, not only in BC but also in other localities in the world where ultramafic deposits have the potential to passively capture atmospheric CO_2 . These protocols would need to be recognized by the provincial and federal governments and, eventually, these environmental monitoring technologies would aid mine operators in proving reductions in their carbon footprint, which in turn could be traded for carbon credits and to market low-carbon metals at a premium.

Acknowledgments

The authors thank Geoscience BC, the Natural Science and Engineering Research Council, the Canada Foundation for Innovation and the Clean Growth Program of Natural Resources Canada for financial support of this project. Special thanks to R. Beckie from the department of Earth, Ocean and Atmospheric Sciences of The University of British Columbia for reviewing this manuscript and providing valuable insights.

References

- Ash, C.H. and Arksey, R.L. (1990): The Atlin ultramafic allochthon: ophiolitic basement within the Cache Creek terrane; tectonic and metallogenic significance (104N/12); in Geological Fieldwork 1989, BC Ministry of Energy, Mines and Low Carbon Innovation, BC Geological Survey, Paper 1990-1, p. 365–374, URL <<http://citeserx.ist.psu.edu/view/doc/download?doi=10.1.1.176.4956&rep=rep1&type=pdf>> [September 2020].
- Baldocchi, D.D. (2003): Assessing the eddy covariance technique for evaluating the carbon balance of ecosystems; Global Change Biology, v. 9, p. 1–41, URL <<https://doi.org/10.1046/j.1365-2486.2003.00629.x>>.
- Burba, G., Madsen, R. and Feese, K. (2013): Eddy covariance method for CO_2 emission measurements in CCUS applications: principles, instrumentation and software; Energy Procedia, v. 40, p. 29–336, URL <<https://doi.org/10.1016/j.egypro.2013.08.038>>.
- Environment Canada. (2020): Historical climate data; Environment Canada, URL <https://climate.weather.gc.ca/index_e.html> [September 2020].
- Hansen, L.D., Dipple, G.M., Gordon, T.M. and Kellett, D.A. (2005): Carbonated serpentinite (listwanite) at Atlin, British Columbia: a geological analogue to carbon dioxide sequestration; Canadian Mineralogist, v. 43, p. 225–239, URL <<https://doi.org/10.2113/gscanmin.43.1.225>>.
- Kabwe, L.K., Farrell, R.E., Carey, S.K., Hendry, M.J. and Wilson, G.W. (2005): Characterizing spatial and temporal variations in CO_2 fluxes from ground surface using three complementary measurement techniques; Journal of Hydrology, v. 311,

- p. 80–90, URL <<https://doi.org/10.1016/j.jhydrol.2004.12.015>>.
- Lackner, K.S., Wendt, C.H., Butt, D.P., Joyce, E.L. and Sharp, D.H. (1995): Carbon dioxide disposal in carbonate minerals; *Energy*, v. 20, p. 1153–1170, URL <[https://doi.org/10.1016/0360-5442\(95\)00071-N](https://doi.org/10.1016/0360-5442(95)00071-N)>.
- Lucas-Moffat, A.M., Huth, V., Augustin, J., Brümmer, C., Herbst, M. and Kutsch, W.L. (2018): Towards pairing plot and field scale measurements in managed ecosystems: using eddy covariance to cross-validate CO₂ fluxes modeled from manual chamber campaigns; *Agricultural and Forest Meteorology*, v. 256–257, p. 362–378, URL <<https://doi.org/10.1016/j.agrformet.2018.01.023>>.
- Norman, J.M., Kucharik, C.J., Gower, S.T., Baldocchi, D.D., Crill, P.M., Rayment, M., Savage, K. and Striegl, R.G. (1997): A comparison of six methods for measuring soil-surface carbon dioxide fluxes; *Journal of Geophysical Research Atmospheres*; v. 102, p. 28771–28777, URL <<https://doi.org/10.1029/97JD01440>>.
- Power, I.M., Harrison, A.L., Dipple, G.M., Wilson, S.A., Barker, S.L.L. and Fallon, S.J. (2019): Magnesite formation in playa environments near Atlin, British Columbia, Canada; *Geochimica et Cosmochimica Acta*, v. 255, p. 1–24, URL <<https://doi.org/10.1016/j.gca.2019.04.008>>.
- Power, I.M., Harrison, A.L., Dipple, G.M., Wilson, S.A., Kelemen, P.B., Hitch, M. and Southam, G. (2013): Carbon mineralization: from natural analogues to engineered systems; *Reviews in Mineralogy and Geochemistry*, v. 77, p. 305–360, URL <<https://doi.org/10.2138/rmg.2013.77.9>>.
- Power, I.M., Wilson, S.A., Harrison, A.L., Dipple, G.M., McCutcheon, J., Southam, G. and Kenward, P.A. (2014): A depositional model for hydromagnesite-magnesite playas near Atlin, British Columbia, Canada; *Sedimentology*, v. 61, p. 1701–1733, URL <<https://doi.org/10.1111/sed.12124>>.
- Reynolds, L. (2019): Soil ¹⁴CO₂ source apportionment for biodegradation in contaminated soils in permafrost cli-
mates: a novel technique for rapid sample collection by barium carbonate precipitation; M.Sc. thesis, University of Ottawa, 86 p.
- Riederer, M., Serafimovich, A. and Foken, T. (2014): Net ecosystem CO₂ exchange measurements by the closed chamber method and the eddy covariance technique and their dependence on atmospheric conditions; *Atmospheric Measurement Techniques*, v. 7, p. 1057–1064, <<https://amt.copernicus.org/articles/7/1057/2014/>> [December 2020].
- Seifritz, W. (1990): CO₂ disposal by means of silicates; *Nature*, v. 345, p. 486, URL <<https://doi.org/10.1038/345486b0>>.
- Wang, X., Wang, C. and Bond-Lamberty, B. (2017): Quantifying and reducing the differences in forest CO₂-fluxes estimated by eddy covariance, biometric and chamber methods: a global synthesis; *Agricultural and Forest Meteorology*, v. 247, p. 93–103, URL <<https://doi.org/10.1016/j.agrformet.2017.07.023>>.
- Webb, E.K., Pearman, G.I. and Leuning, R. (1980): Correction of flux measurements for density effects; *Quarterly Journal of the Royal Meteorological Society*, v. 106, p. 85–100, URL <<https://doi.org/10.1002/qj.49710644707>>.
- Wilson, S.A., Dipple, G.M., Power, I.M., Thom, J.M., Anderson, R.G., Raudsepp, M., Gabites, J.E. and Southam, G. (2009): Carbon dioxide fixation within mine wastes of ultramafic-hosted ore deposits: examples from the Clinton Creek and Cassiar Chrysotile deposits, Canada; *Economic Geology*, v. 104, p. 95–112, URL <<https://doi.org/10.2113/gsecongeo.104.1.95>>.
- Wilson, S.A., Harrison, A.L., Dipple, G.M., Power, I.M., Barker, S.L.L., Mayer, K.U., Fallon, S.J., Raudsepp, M. and Southam, G. (2014): Offsetting of CO₂ emissions by air capture in mine tailings at the Mount Keith Nickel Mine, Western Australia: rates, controls and prospects for carbon neutral mining; *International Journal of Greenhouse Gas Control*, v. 25, p. 121–140, URL <<https://doi.org/10.1016/j.ijggc.2014.04.002>>.

Invertebrate Response to Mine Reclamation in South-Central British Columbia (NTS 092I): Effects of Reclamation Age on Arthropod Assemblages at the Highland Valley Copper and New Afton Mines

C.A. Gervan, Department of Natural Resource Science, Thompson Rivers University, Kamloops, British Columbia, chantallegervan@hotmail.com

W.C. Gardner, Department of Natural Resource Science, Thompson Rivers University, Kamloops, British Columbia

E.M. Bottos, Department of Biological Sciences, Thompson Rivers University, Kamloops, British Columbia

J.D. Van Hamme, Department of Biological Sciences, Thompson Rivers University, Kamloops, British Columbia

R.J. Higgins, Department of Biological Sciences, Thompson Rivers University, Kamloops, British Columbia

L.H. Fraser, Department of Natural Resource Science, Thompson Rivers University, Kamloops, British Columbia

Gervan, C.A., Gardner, W.C., Bottos, E.M., Van Hamme, J.D., Higgins, R.J. and Fraser, L.H. (2021): Invertebrate response to mine reclamation in south-central British Columbia (NTS 092I): effects of reclamation age on arthropod assemblages at the Highland Valley Copper and New Afton mines; *in* Geoscience BC Summary of Activities 2020: Minerals and Mining, Geoscience BC, Report 2021-01, p. 129–136.

Introduction

Resources extracted from mines are used in the making of many items used in everyday life; clearly, there are vast social and economic benefits associated with mining operations. In 2017, for example, mining in British Columbia (BC) was responsible for generating \$11.7 billion in gross revenue and creating more than 10 000 jobs for British Columbians (Mining Association of British Columbia, 2019). However, mining activity significantly alters the landscape and surrounding native ecosystems.

In Canada, planning for mine closure must occur before mining operations can begin (Mining Association of Canada, 2019). Therefore, areas (terrestrial, aquatic and cultural resources) altered by mining activities must be returned to self-sustaining ecosystems (Government of British Columbia, 2019) through a process called ecosystem reclamation. The aim of research on postmining ecosystem reclamation is to reduce knowledge gaps and further understanding of the reclamation trajectory, thus leading to improved reclamation practices.

Postmining areas naturally undergo a process of secondary succession. It should be noted that natural succession occurs without human intervention; however, since the timescale needed for natural succession to occur may not be acceptable for the public or industry, use of reclamation

practices is required. A knowledge gap currently exists concerning long-term postmining reclamation outcomes and trajectory (Buchori et al., 2018); this knowledge gap is particularly notable with regard to invertebrate-community recovery. To be fully functional, an ecosystem must comprise both biotic and abiotic components. One measure of biotic health is biodiversity. Biodiversity refers to the variety of life in a given area with regard to taxonomy, trophic levels and genetic variance (Gaston and Spicer, 2004). Therefore, biodiversity can be used as a measure of ecological health.

Invertebrates work well as indicators of environmental change because they have short generation times and produce large numbers of offspring; they also have mobility, which allows them to efficiently relocate in response to change (Samways et al., 2010). Similarly, invertebrates act as a good subject for species richness (alpha diversity). Invertebrates such as arthropods make up a significant portion of species biodiversity and support vital ecosystem services (McGeoch et al., 2011). Invertebrates encourage nutrient turnover, litter breakup and decomposition (Majer et al., 2002). In addition, many invertebrates are herbivorous, thus potentially contributing to plant-species composition by changing competitive dynamics within the plant community (Yu et al., 2012; Barnett and Facey, 2016). Invertebrates are affected by plant-community composition through a bottom-up effect (Barnett and Facey, 2016). Re-establishment of diverse invertebrate assemblages in postmining reclamation areas, particularly species

This publication is also available, free of charge, as colour digital files in Adobe Acrobat® PDF format from the Geoscience BC website: <http://geosciencebc.com/updates/summary-of-activities/>.

correlated with ecosystem functions, is encouraged (Majer et al., 2002).

Objectives

Arthropods have seldom been used as a measure of examining reclamation success because of the difficulties associated with identifying them morphologically. Recent progress in molecular identification techniques (deoxyribonucleic acid or DNA metabarcoding) has helped to overcome challenges in taxonomic identification of arthropods and other invertebrates. In this study, invertebrate-assemblage response to mine reclamation is assessed, using DNA metabarcoding to identify collected invertebrates. The research questions this study aims to address are based on the use of parallel sequencing of invertebrate DNA metabarcodes as a novel method for assessing reclamation trajectory. The first step entails examining whether changes in invertebrate assemblages can be identified across reclamation sites of different age as a result of ongoing succession characterized by changes in biotic assemblages. Secondly, careful examination will reveal whether specific taxa indicate the age of reclamation. Thirdly, species richness (alpha diversity, i.e., average species diversity within a site) among different age sites will be measured.

Methodology

In 2017, sampling was conducted at four sites: the Teck Resource Highland Valley Copper mine, the New Gold Inc. New Afton mine, the Imperial Metals Corporation Mount Polley mine and the Avino Silver & Gold Mines Ltd. Bralorne Gold mine (Figure 1). However, the Highland Valley Copper and New Afton mines are the focus of this paper. At each mine, two reclamation treatments were sampled: one site reclaimed within the last eight years ('new') and one

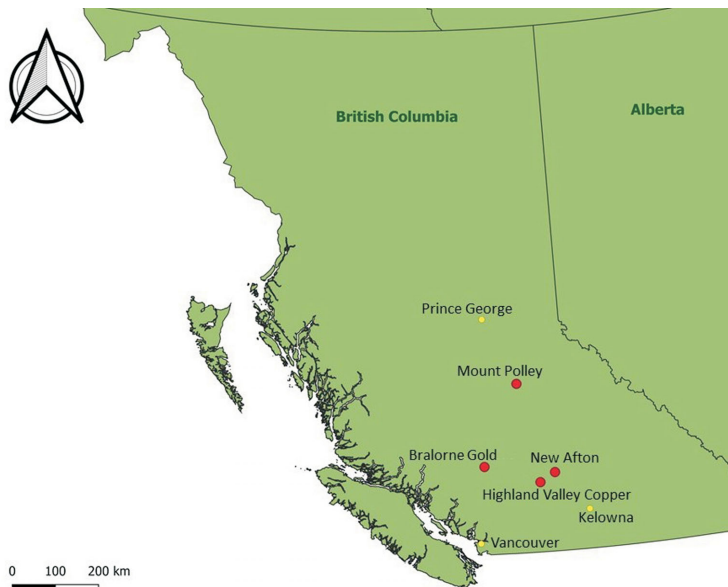


Figure 1. Location of mines in the study area sampled in July and August of 2017 and 2018 for vegetation and invertebrate data. Data from Highland Valley Copper (Teck Resource) and New Afton (New Gold Inc.) mines are the focus of this paper.

site that was reclaimed more than eighteen years ago ('old'). A grassland 'control' site was also sampled at the Highland Valley Copper mine. 'Control' sites were also sampled at the New Afton mine but were not processed for this paper. Site descriptions of the sampled areas (including the year of reclamation, reclaimed materials and the methods used to conduct reclamation) can be seen in Table 1.

Both vegetation data and invertebrate samples were collected from the Highland Valley Copper and New Afton sites in 2017. Vegetation was measured using canopy cover by species with 0.5 by 0.5 m quadrats. Invertebrate samples were collected using two types of traps: pitfall traps (Figure 2) and Malaise traps (Figure 3). Pitfall traps were used to collect primarily ground-dwelling invertebrates (Bassett and Fraser, 2015). At each site, a 100 m transect was laid

Table 1. Site description (years since reclamation from 2020, reclaimed materials and reclamation methods) of two mines (Teck Resource's Highland Valley Copper and New Gold Inc.'s New Afton) sampled for invertebrates and vegetation data in the summer of 2017.

Mine	Site	Year reclaimed	Years since reclamation	Reclaimed material	Reclamation method
Highland Valley Copper	New	2014	6	Waste rock and overburden	Biosolids, seeded
	Old	2000	20	Waste rock and overburden	Seeded (crested wheatgrass)
New Afton	Control	n/a	n/a	n/a	n/a
	New	n/a	n/a	Tailings	n/a
	Old	2001	19	Tailings	Fertilizer and cattle manure, seeded

Abbreviation: n/a, not available



Figure 2. Sampling of epigaeal invertebrates at the Imperial Metals Corporation Mount Polley mine in 2017 using a pitfall trap consisting of **a**) a 450 g container placed flush with ground level; and **b**) a plastic plate over the top to reduce ethanol evaporation.

out and pitfall traps were placed every 10 m. Pitfall traps were constructed using a 450 g container (Solo® cup) placed flush with ground level. The pitfall traps were filled with ethanol and a plastic plate, held up by nails, was placed over them to reduce the amount of ethanol evaporation. Malaise traps are tent-like structures with bottles of ethanol attached to them and are used to collect primarily flying invertebrates (Thomas, 2016). One Malaise trap was placed at each site. The invertebrate traps were left on site for five days once over the summer. After collection, the samples were stored at -20 °C until laboratory processing.

Laboratory Methods

Identification of the collected invertebrates was conducted using high-throughput DNA metabarcoding. This was done by homogenizing invertebrate tissue in liquid nitrogen using mortar and pestle (Beng et al., 2016). The DNA was extracted from the homogenized tissue using a Mag Bind® Blood and Tissue Kit (Omega Bio-tek, Inc., Norcross, GA). A 450 base-pair region of the mitochondrial cytochrome c oxidase sub-unit 1 gene was amplified in two rounds of polymerase chain reaction (PCR) using the universal PCR primer pair MHemF and dghCO2198 (Beng et al., 2016). The amplicons were sequenced on an Ion S5™ sequencing platform (Thermo Fisher Scientific, Waltham, MA) using an Ion 520™ and Ion 530™ Chip Kit. The bioinformatic pipeline AMPtk was used to cluster sequences into operational taxonomic units (OTUs) at an identity threshold of 97% (Palmer et al., 2018); one OTU represented the sequence of one species (Ji et al. 2013). Taxonomies were assigned to each OTU using the Barcode

of Life Data system (BOLD) downloaded at the time of analysis (Yu et al., 2012).

Statistical Analysis

Four methods of statistical analysis were used to analyze the 2017 Highland Valley Copper and New Afton data: principal co-ordinate analysis (PCoA), permutational multivariate analysis of variance using distance matrices (adonis), and random-forest regression and linear mixed-effects models. Data used in the PCoA, adonis and random-forest model analyses were rarified to 10 000 reads and converted into presence-absence data. The PCoA plot was calculated using Euclidean distances and compared five sites (Highland Valley Copper ‘control’, ‘old’ and ‘new’, and New Afton ‘old’ and ‘new’). Calculations car-



Figure 3. Malaise trap set up at the Imperial Metals Corporation Mount Polley mine in 2017 to capture flying invertebrates.

ried out using adonis were also based on Euclidean distance. The random-forest regression model uses the OTU as a predictor value to describe the most change relative to reclamation treatment. The linear mixed-effects model was used to compare species richness between the sites. Data residuals from the linear mixed model were tested for normality using the Shapiro-Wilk test. A log transformation was performed on the data. There was a gap in the New Afton ‘old’ data as a result of samples still being processed for sequencing; therefore, the mean of five sites was calculated and applied to the sixth sample to create the linear mixed-effects model measuring species richness. All the statistical analyses were conducted in RStudio, a free, open-source integrated development environment for the R software system for statistical computing (RStudio, 2015).

Results

The multivariate analysis methods PCoA and adonis were used to examine invertebrate assemblages by reclamation age group ('old', 'new', 'control') and mine location. Figure 4 illustrates that the difference in mine locations and

their respective reclamation ages explain 35.1% of the variation in the invertebrate assemblages collected. The PCoA diagram shows that sites (classified by reclamation age and mine location) located closer to each other in ordination space are more similar. There are three distinct groupings, depicted in the top right, bottom right and bottom left (Figure 4). The group in the top right consists exclusively of ‘old’ sites, the small group into the left consists of ‘old’ and ‘control’ sites, and the largest grouping is made up of a combination of reclamation ages. It should be noted that PCoA works to preserve the calculated distances.

The statistical analysis using the adonis function, highlighted in Table 2, gives an R^2 value that represents the correlation between the treatments and invertebrate assemblages. The ‘mine’ (location) factor explains 13.8% of the variation, the (reclamation) ‘age’ factor explains 8.6% of variation and mine location combined with reclamation age ('mine: age') explains 4.4%. The p-value shows if the R^2 value is likely a result of chance; in this case, the p-values for mine location and reclamation age are 0.002, respec-

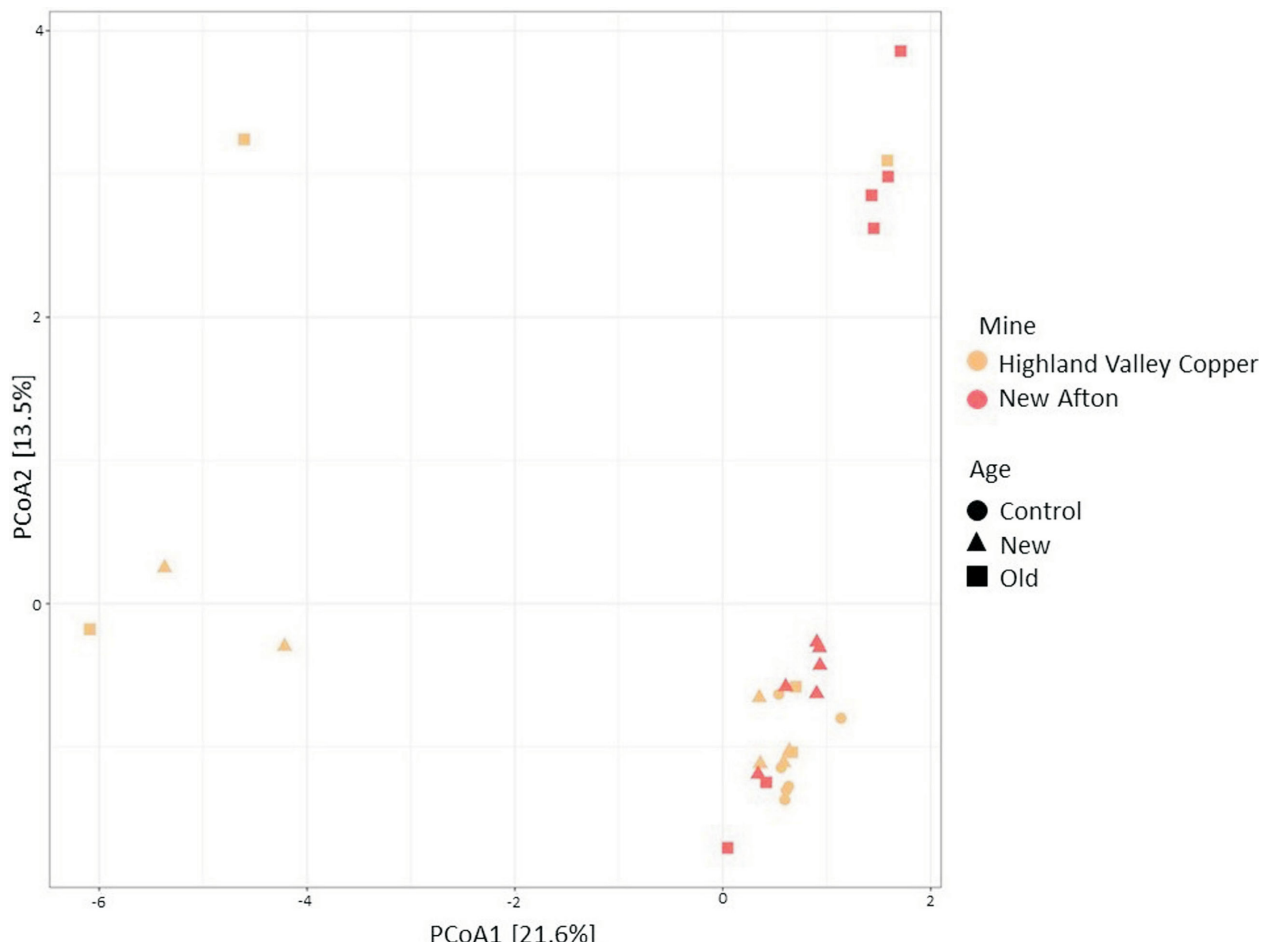


Figure 4. PCoA diagram created using Euclidean distance, illustrating invertebrate assemblages of different reclamation ages ('new', 'old', 'control') between 2017 sample sites at the Highland Valley Copper (Teck Resources) and New Afton (New Gold Inc.) mines. In this method, uncorrelated (orthogonal) axes measure the variability within data and an eigenvalue is determined, which indicates the influence of each axis.

tively, well below a 0.05 significance level, indicating that the results are not likely caused by chance.

To assess if specific taxa indicate the age of reclamation, a random-forest regression model was used to plot the top 20 OTUs that account for the observed change in invertebrate assemblages between reclamation age sites (Figure 5). As the measure of mean decrease of accuracy reduces, the more influential the variable. Thus, OTUs with a larger mean decrease in accuracy are more meaningful for classification of data. In other words, variable accuracy describes how useful the variables are for explaining the change. As a result, OTU 4 (*Nabicula nigrovittata*), OTU 69 (*Phloeostiba lapponica*) and OTU 52 (*Trichoptera*) appear most valuable in classifying this dataset (Figure 5; Table 3).

Table 4 shows the random effects (mine location) in the linear mixed-effects model. The standard deviation column measures the variability of the random effects. The variance of the ‘mine’ location variable is smaller than that of the ‘residual’ variable. A low standard deviation in the random effect indicates the contributing values are near the mean. The ‘residual’ indicates the variability that is not a result of the ‘mine’ location factor.

Table 5 displays the fixed effects (reclamation age) analyzed in the linear mixed-effects model. The coefficient ‘AgeNew’ is the slope (standard error of the estimate) for the effect of species richness between the ‘control’ and ‘new’ sites. The standard error of the estimate for

Table 2. Permutational analysis of variance calculated using Euclidean distance (adonis), where ‘f’ represents the ratio of the two mean-square values and ‘p’ is the probability of finding the obtained results given that the null hypothesis is true; the R^2 value represents the correlation between the treatments and invertebrate assemblages, where the degrees of freedom represent the number of ways the values are able to vary and where the sum of squares is the measure of the data points from the mean.

Factor	Degrees of freedom	Sum of squares	Mean square	f-value	R^2	p-value
Mine	2	1.3835	0.69173	2.22823	0.13884	0.002
Age	1	0.8659	0.86589	2.8569	0.0869	0.002
Mine:Age	1	0.4412	0.44124	1.45558	0.04424	0.133
Residuals	24	7.2742	0.30309		0.72999	
Total	28	9.9648				1

Table 3. Top three operational taxonomic units (OTU), and their corresponding taxonomy, that account for the change in invertebrate presence between the New Afton (New Gold Inc.) ‘new’ and Highland Valley Copper (Teck Resource) ‘control’ sites, as determined by a random-forest regression model using Euclidean distance.

OTU	Taxonomy
OTU 4	<i>Nabicula nigrovittata</i>
OTU 69	<i>Phloeostiba lapponica</i>
OTU 52	<i>Trichoptera</i>

‘AgeNew’ highlights the change in species richness from Highland Valley Copper to New Afton and indicates that the ‘new’ sites have fewer species (inverse log 0.003849) accounted for than the ‘control’ site. The ‘AgeOld’ stan-

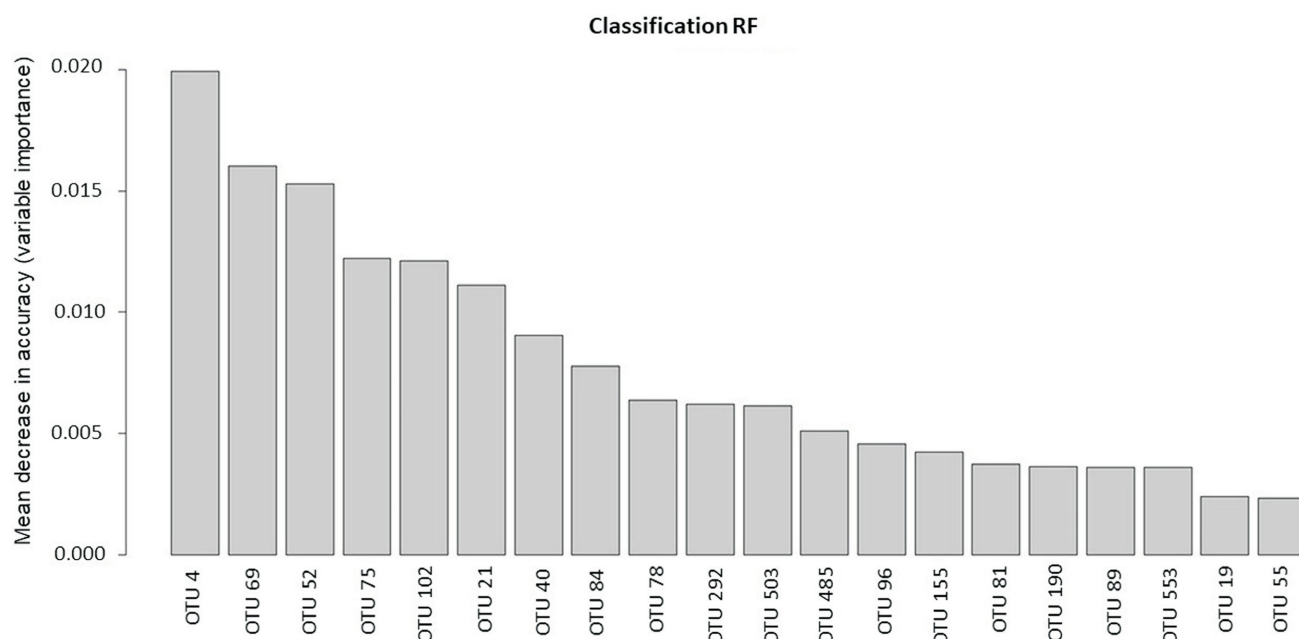


Figure 5. Top 20 operational taxonomic units (OTU) explaining the change in invertebrate presence between different reclamation ages ('new', 'old', 'control') of the 2017 sample sites at the Highland Valley Copper (Teck Resources) and New Afton (New Gold Inc.) mines, where a larger mean decrease in accuracy is the more meaningful variable for classification of data. Abbreviation: RF, random forest.

dard deviation indicates that the ‘old’ sites have more species (inverse log 0.15214; Table 5) accounted for than the ‘control’ site. It should be noted that both the ‘new and ‘old’ reclamation age categories are not statistically significant ($p>0.05$).

Discussion

The effects of postmining reclamation on recovering invertebrate assemblages were examined at four sites in BC using vegetation and invertebrate surveys over two years. For invertebrates, DNA metabarcoding techniques were used and few differences in invertebrate-community composition between mine sites and different reclamation-age plots were detected.

As a first step, invertebrate-assemblage similarity of different age plots (‘new’, ‘old’ and ‘control’) between 2017 sample sites at the Highland Valley Copper and New Afton mines was measured using PCoA and adonis. Understanding the reclamation trajectory of invertebrate assemblage postmining reclamation is an important objective on the road to achieving successful end land use. The PCoA used in this study shows visible separation between ‘old’, ‘new’ and ‘control’ age sites (Figure 4). The PCoA explains 35.1% of the variability seen within these assemblages, with three distinct groupings. Most notably, there is a cluster of ‘old’ sites; however, the largest group consists of a variety of reclamation age treatments and mine locations, indicating that the variables (reclamation age, mine location) analyzed in this paper fail to explain the variation in invertebrate assemblage. Likewise, adonis analysis (Table 2) confirms that the correlation between the reclamation age and mine location variables does not account for the invertebrate variation seen between the plots. This is a result of low R^2 values for mine location (13.8%), reclamation age (8.6%) and a combination of mine location and reclamation age (4.4%). It should be noted that the Highland Valley Copper ‘old’ and ‘new’ sites are located on wasterock and overburden, whereas the ‘control’ site is located within a fenced enclosure near the highway. New Afton ‘old’ and ‘new’ sites occur on a historical tailings facility.

Secondly, a measure of influence of invertebrate taxa characterizing reclamation age and mine sites was examined. Site assemblage-species profiles can be generated using DNA metabarcoding. In this study, the focus was put on recognizing the change in invertebrate taxa between sites. The taxon that accounts for the greatest observed change in assemblage was *Nabicula nigrovittata*, a predatory insect that belongs to the order *Hemiptera* (Lattin, 1989). In this case, *Nabicula nigrovittata* was primarily found on the Highland Valley Copper and New Afton ‘old’ sites, whereas it was absent on the ‘new’ and ‘control’ sites. Another species that accounted for the disparity between sites was OTU 69, *Phloeostiba lapponica*, which is a member of

Table 4. Linear mixed-effects model residual and random output (mine location), comparing species richness defined by the number of operational taxonomic units between each of the five study sites: Highland Valley Copper (Tech Resource) ‘new’, ‘old’ and ‘control’, and New Afton (New Gold Inc.) ‘new’ and ‘old’.

Factor	Name	Variance	Std
Mine	Intercept	<0.0001	<0.001
Residual		0.07967	0.2823

Abbreviation: Std, standard deviation

Table 5. Linear mixed-effects model fixed output (reclamation age), comparing species richness defined by the number of operational taxonomic units between each of the five study sites: Highland Valley Copper (Tech Resource) ‘new’, ‘old’ and ‘control’, and New Afton (New Gold Inc.) ‘new’ and ‘old’.

Coefficient	Estimate	Std	Error	d.f.	t-value	p-value
Intercept	1.25966	0.11523	27	10.932	2.03E-11	
AgeNew	-0.003849	0.14113	27	0.273	0.787	
AgeOld	0.15214	0.14113	27	1.078	0.291	

Abbreviations: d.f., degrees of freedom; Std, standard deviation

the *Staphylinidae* family (rove beetle). In the random-forest model, *Phloeostiba lapponica* was identified at the Highland Valley Copper ‘new’ and ‘old’ sites. A final species, OTU 52 (*Trichoptera*) contributed to site differences; this genus belongs to the order that includes caddisflies. Trichopteran taxa were identified in both the Highland Valley Copper and New Afton ‘old’ sites. The presence of *Trichoptera* can be used as a positive bioindicator for good water quality (Pereira et al., 2012).

Lastly, alpha diversity characterizing reclamation age plots was measured between the sampled sites. The linear mixed-effects model demonstrated no significant difference in species richness between the sampled sites; this is potentially a result of large variation between the replicates.

Conclusions and Ongoing Work

The above results and correlations are based on data from 2017; additional analyses are underway as the remaining 2017 samples are currently being sequenced. The 2018 samples are also being sequenced and future papers will address the effects of biosolids as a soil amendment. However, it should be noted that the COVID-19 pandemic has affected the sequencing timeline of the remaining 2017 and 2018 samples.

The results of this study should aid in reducing the knowledge gap regarding postmining reclamation outcomes. Using novel methods (high-throughput DNA metabarcoding), this project will contribute to the improvement of planning and management practices, leading to more effective postmining ecosystem-reclamation outcomes. This in turn

will assist in the development of further advancements in the field of mine reclamation as they relate to the sustainable health of ecosystems, which are vital to the continued growth of BC's communities and economy. Future studies, determining which environmental variables are associated with invertebrate recovery, may help land managers facilitate restoration through simulation of the relevant conditions.

Acknowledgments

Funding for this project is provided through Geoscience BC as well as through the Natural Sciences and Engineering Research Council of Canada Industrial Research Chair in Ecosystem Reclamation with industry partners: Genome BC, Arrow Transportation Systems Inc., the Real Estate Foundation of BC, New Gold's New Afton mine, Teck Resource's Highland Valley Copper mine, Trans Mountain Corporation, Metro Vancouver and the BC Cattlemen's Association. Special thanks to the individuals who helped in the field and laboratory: M. Coghill, J. Foster, B. McAmmond, J. Paulson, J. Singh C. Stephens and S. Vogel. The authors also thank A. Fischer, who peer reviewed this submission.

References

- Barnett, K.L. and Facey, S.L. (2016): Grasslands, invertebrates, and precipitation: a review of the effects of climate change; *in* Grassland-Invertebrate Interactions: Plant Productivity Resilience and Community Dynamics, I. Hiltbold and M. Rostás (ed.), Frontiers in Plant Science, v. 7, art. 1196, p. 67–74, URL <<https://doi.org/10.3389/fpls.2016.01196>>.
- Bassett, E. and Fraser, L. (2015): Effects of cattle on the abundance and composition of carabid beetles in temperate grasslands; Agricultural Studies, v. 3, no. 1, p. 36–47, URL <<https://doi.org/10.5296/jas.v3i1.6731>>.
- Beng, K.C., Tomlison, K.W., Shen, X.H., Surget-Groba, Y., Hughes, A.C., Corlett, R.T. and Slik, J.W.F. (2016): The utility of DNA metabarcoding for studying the response of arthropod diversity and composition to land-use change in the tropics; *Scientific Reports* 6, art. 24965, URL <<https://doi.org/10.1038/srep24965>>.
- Buchori, D., Rizali, A., Rahayu, G.A. and Mansur, I. (2018): Insect diversity in post-mining areas: investigating their potential role as bioindicator of reclamation success; *Biodiversitas*, v. 19, p. 1696–1702, URL <<https://doi.org/10.13057/biodiv/d190515>>.
- Gaston, K.J. and Spicer, J.I. (2004): Biodiversity: an Introduction (2nd edition), Blackwell, Oxford, United Kingdom, 191 p.
- Government of British Columbia (2019): Reclamation & closure; Government of British Columbia, URL <<https://www2.gov.bc.ca/gov/content/industry/mineral-exploration-mining/permitting/reclamation-closure>> [November 2020].
- Ji, Y., Ashton, L., Pedley, S.M., Edwards, D.P., Tang, Y., Nakamura, A., Kitching, R., Dolman, P.M., Woodcock, P., Edwards, F.A., Larsen, T.H., Hsu, W.W., Bendick, S., Hamer, K.C., Wilcove, D., Bruce, C., Wang, X., Levi, T., Lott, M., Emerson, B.C. and Yu, D.W. (2013): Reliable, verifiable and efficient monitoring of biodiversity via metabarcoding; *Ecology Letters*, v. 16, p. 1245–1257.
- Lattin, J. (1989): Bionomics of the Nabidae; *Entomology*, v. 34, p. 383–400.
- Majer, J.D., Brennan, E. and Lubomir, B. (2002): Terrestrial invertebrates; *in* Handbook of Ecological Restoration, Volume 1 Principles of Restoration, M.R. Perro and A.J. Davy (ed.), Cambridge University Press, Cambridge, p. 279–294.
- McGeoch, M.A., Sithole, H., Samways, M.J., Simaika, J.P., Pryke, J.S., Picker, M., Uys, C., Armstrong, A.J., Dippenaar-Schoeman, A.S., Engelbrecht, I.A., Braschler, B. and Hamer, M. (2011): Conservation and monitoring of invertebrates in terrestrial protected areas; *Koedoe*, v. 53, p. 1–13.
- Mining Association of Canada (2019): Reclamation; Mining Association of Canada, URL <<http://mining.ca/resources/canadian-mining-stories/reclamation>> [February 2019].
- Mining Association of British Columbia (2019): Mining in BC – Economic impact; Mining Association of British Columbia, URL <<https://www.mining.bc.ca/economic-impact>> [February 2019].
- Palmer, J.M., Jusino, M.A., Banik, M.T. and Lindner, D.L. (2018): Non-biological synthetic spike-in controls and the AMPtk software pipeline improve mycobiome data; *PeerJ*, v. 6, art. e4925, URL <<https://doi.org/10.7717/peerj.4925>>.
- Pereira, L.R., Cabette, H.S.R. and Juen, L. (2012): Trichoptera as bioindicators of habitat integrity in the Pindaiba river basin, Mato Grosso (Central Brazil); *International Journal of Limnology*, v. 48, no. 3, p. 295–302.
- RStudio (2015): RStudio: Integrated development for R; RStudio, Inc., Boston, Massachusetts, URL <<http://www.rstudio.com/>> [November 2020].
- Samways, M.J., McGeoch, M.A. and New, T.R. (2010): Insect Conservation: a Handbook of Approaches and Methods; Oxford University Press, Oxford, p. 312–313.
- Thomas, M. (2016): Malaise trap and insect sampling; *Research Trend*, v. 2, no. 2, p. 25–40.
- Yu, D.W., Ji, Y., Emerson, B.C., Wang, X., Ye, C., Yang, C. and Ding, Z. (2012): Biodiversity soup: metabarcoding of arthropods for rapid biodiversity assessment and biomonitoring; *Methods in Ecology and Evolution*, v. 3, p. 613–623.

Post-Mining Restoration in South-Central British Columbia: Modelling Microbial and Geochemical Changes in Topsoil Stockpiles (NTS 092I/09, 093A/12)

A.M. Fischer, Department of Natural Resource Science and Department of Biological Science, Thompson Rivers University, Kamloops, British Columbia, granta18@mytru.ca

J.D. Van Hamme, Department of Biological Science, Thompson Rivers University, Kamloops, British Columbia

E.M. Bottos, Department of Biological Science, Thompson Rivers University, Kamloops, British Columbia

W.C. Gardner, Department of Natural Resource Science, Thompson Rivers University, Kamloops, British Columbia

L.H. Fraser, Department of Natural Resource Science, Thompson Rivers University, Kamloops, British Columbia

Fischer, A.M., Van Hamme, J.D., Bottos, E.M., Gardner, W.C. and Fraser, L.H. (2021) Post-mining restoration in south-central British Columbia: modelling microbial and geochemical changes in topsoil stockpiles (NTS 092I/09, 093A/12); *in* Geoscience BC Summary of Activities 2020: Minerals, Geoscience BC, Report 2021-01, p. 137–142.

Introduction

The mining industry in Canada is an essential source of resources and a key contributor to the economy. In 2018, mining contributed \$69.5 billion dollars to real GDP and provided approximately 626 000 jobs. In British Columbia, the gross mining revenue amounted to 12.3 billion in 2018 (Mining Association of British Columbia, 2019). Federal and provincial regulations ensure that the restoration or reclamation of landscapes is conducted at minesites to repair disturbances and return the land to a sustainable ecosystem with a historical level of productivity. Research to understand and optimize restoration practices is crucial because needs and response vary greatly from site to site and from ecosystem to ecosystem. Mining is particularly damaging to ecosystems because soils are stripped from landscapes and require reconstruction, which would take hundreds or thousands of years if left to natural processes (Bradshaw, 1997).

To preserve valuable topsoil in mining operations, it is common practice to store stripped topsoil on site as a topsoil stockpile for ecosystem rehabilitation. Stockpiled topsoil can be used post mining to provide nutrients, structure and seeds, and to amend waste materials on site. However, it is known that microbial composition and functions degrade significantly over time, likely depending on factors such as stockpile depth, exposure to sun, weather, temperature, and chemical and microbial interactions (Abdulkareem and McRae, 1984; Stahl et al., 2002; Ghose and Kundu, 2004). Stockpiles are highly variable between sites,

can reach up to 30 m in height and may sit for the entire duration of mine operation, which could be decades. In addition to possible negative impacts from stockpile height and age, the proper segregation of topsoil from the underlying subsoil is often not possible, resulting in dilution of the topsoil.

The inability to preserve topsoil is one of the basic hindrances to restoration of mining operations. A major question is, “do long-term large topsoil stockpiles remain viable?” In order to address this question, characterization of topsoil-stockpile viability must be carried out by sampling profiles of large stockpiles, and strategies must be developed to increase the viability of stored stockpiles.

Despite the rising demand for restoration management, there is limited research on environmental restoration and there are few dedicated university postgraduate training programs in Canada to address the complexities of ecosystem reclamation. There is a critical need to work with the mining and oil-and-gas industries, in partnership with government agencies, to develop better management practices for successful ecosystem restoration.

Research Objectives

This project investigates factors that affect changes to soil health in topsoil stored in stockpiles by evaluating the stockpiles at two gold operations in BC (Figure 1) The aim is to model changes in factors affecting soil health and function with depth, including geochemical properties and microbial communities. By characterizing these stockpile profiles, the study will improve understanding of the impacts of severe disturbance on soil properties and ecology, and highlight the role of bacteria and fungi in restoration.

This publication is also available, free of charge, as colour digital files in Adobe Acrobat® PDF format from the Geoscience BC website: <http://geosciencebc.com/updates/summary-of-activities/>.

The working hypothesis is that the topsoil-stockpiling practices at the New Afton mine (Figure 2) and QR mill (Figure 3) have had adverse effects on soil properties. Consequently, it is predicted that there will be significant differences in soil composition between depths within the topsoil stockpiles.

Methods

Study Sites and Soil Sampling

New Afton Mine (New Gold Inc.)

The New Afton copper-gold mine of New Gold Inc. is located approximately 10 km west of Kamloops in BC's southern interior. It comprises underground workings, historical support facilities, a historical open pit, a concentrator and a tailings facility. The end land-use objective is to return the ecosystem to native grasslands that support wildlife and traditional hunting opportunities for First Nations (New Gold Inc., 2018). New Afton is located within the traditional territories of the Tk'emplúps te Secwépemc and Skeetchestn bands. These bands are part of the larger cultural group known as the Secwépemc or Shuswap First Nation. Additionally, New Afton is in the Bunchgrass (BGxw1) biogeoclimatic zone at 330–1000 m in elevation. The BGxw1 is commonly known as the 'middle grasslands' and is dominated by bluebunch wheatgrass, junegrass, big sagebrush and rabbit brush (Lloyd et al., 1990).



Figure 1. Sample sites at the New Afton mine (New Gold Inc.) and QR Mill (Barkerville Gold Mines Ltd.), located in British Columbia's southern interior. Map generated in QGIS® with Bing VirtualEarth background.

New Afton has a 7-year-old topsoil stockpile that is 25 m deep and contains approximately 250 600 m³ of topsoil materials. The removal and stockpiling process resulted in some mixing of A, B and C horizons. Sampling of the topsoil stockpile of interest occurred on September 26 and 27 of 2018. Four soil cores were extracted via solid stem auger drilling by Geotech Drilling Services Ltd., the drillholes being approximately 3 m apart. The stockpile was sampled



Figure 2. Aerial image of the New Afton minesite, including a close-up of the topsoil stockpile of interest that shows the locations of soil samples. Map generated in QGIS® with Bing VirtualEarth background.

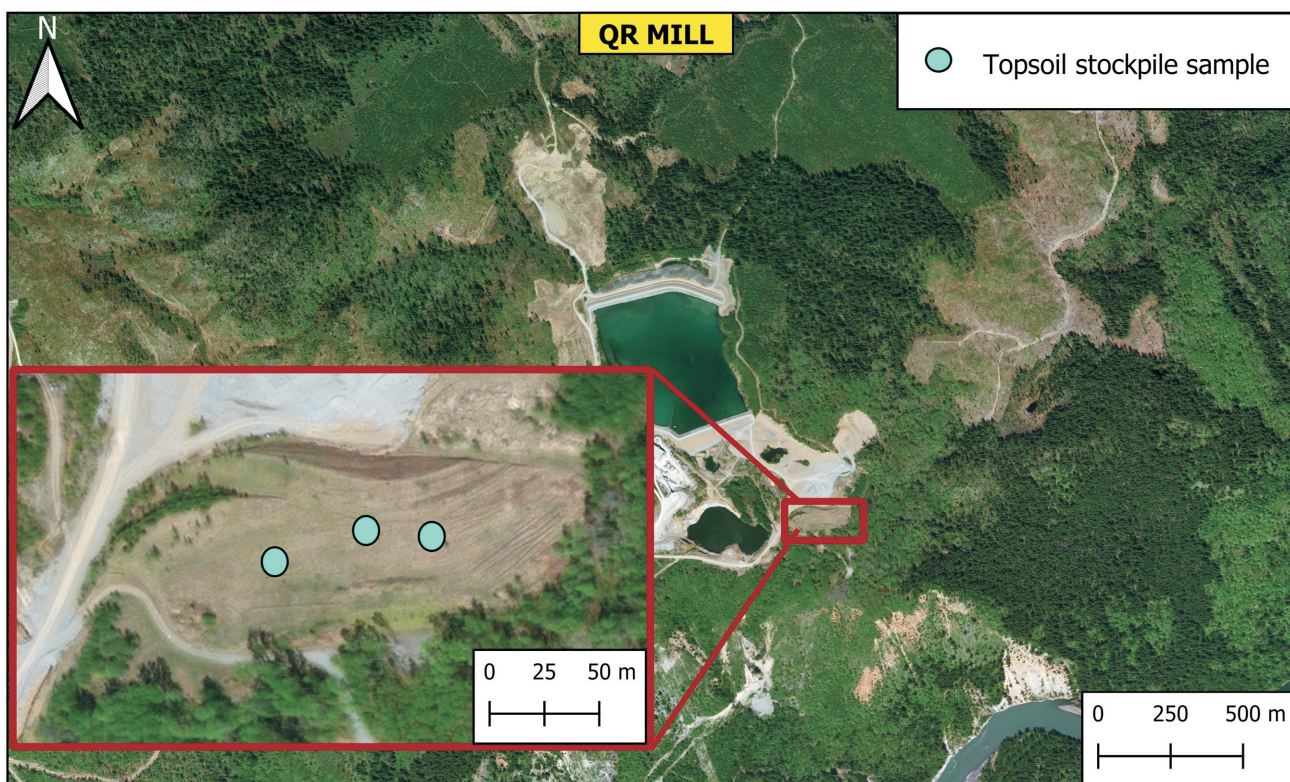


Figure 3. Aerial image of the QR mill, including a close-up of the topsoil stockpile of interest that shows the locations of soil samples. Map generated in QGIS® with Bing VirtualEarth background.

in 0.3 m intervals until the bottom of the stockpile was reached at 13.7 m. The outer 1 cm of the soil core was discarded from each sample to ensure that collected soil was not contaminated by upper layers. Soil samples were originally collected from the thirteen different intervals and then combined into four intervals (0.0–0.6 m, 0.6–1.5 m, 1.5–6.1 m and 6.1–13.7 m) for testing. The interval size increased with depth because the most activity and differences with depth were expected closer to the surface of the pile. A reference soil sample of approximately 16 kg was collected from the top 10 cm at a nearby grassland site.

QR Mill (Barkerville Gold Mines Ltd.)

The Quesnel River (QR) mill of Barkerville Gold Mines Ltd. is located approximately 80 km east of the city of Quesnel in the Cariboo district of BC's southern interior. Ore and concentrate from the Bonanza Ledge mine and Cariboo Gold mine are transported and processed in the QR mill. The mill is also used as a tailings-storage facility. It is situated in the traditional territories of the Secwépemc or Shuswap First Nation and lies within the Engelmann Spruce–Subalpine Fir (ESSF) biogeoclimatic zone at 1200–1500 m elevation. The ESSF is the wettest zone of the Cariboo Forest Region (mean annual precipitation 1044 mm) and is dominated by oak fern, foamflower, rose twisted-stalk, feathermosses, Engelmann spruce and subalpine fir. The current reclamation goal set for the QR mill is

to restore the landscape so that it does not require further human intervention (Barkerville Gold Mines Ltd, 2019).

The QR mill has a 20-year-old topsoil stockpile that is 6 m deep. It is a combination of organic soil and general till soil stripped from the surface. The stockpile is intended to be re-spread during post-mining reclamation. Sampling at the QR mill was completed in May 2019. Three holes, approximately 100 m apart, were dug using an excavator to access various layers of the stockpile: 0–10 cm, 10–20 cm, 60–120 cm, 200–260 cm, 350–390 cm and 500–575 cm. A corresponding reference soil sample was collected from the top 10 cm in an undisturbed forest site adjacent to the mill.

Experiment Design

The variation of all measured soil properties with depth was summarized using principal component analysis (PCA) on scaled geochemical variables (ggfortify in R). To test for significant differences in centroids between different depths, permutational multivariate analysis of variance (PERMANOVA) was measured using the adonis function from the vegan package in R. All errors are reported as standard error. To visualize differences in bacterial and fungal communities between stockpile depths, a non-metric multidimensional scaling (NMDS) plot was calculated for each sample site.

Characterizing Soil Geochemical Properties

The major-element composition of the soil samples is being measured at the analytical laboratory of the Ministry of Environment and Climate Change Strategy in Victoria, BC. The samples were prepared by heating soil samples at 70°C for 24 hours, followed by sieving through a 2 mm pan. The report will include a complete profile of all major elements; Al, B, Ca, Cu, Fe, Mg, Mn, P, K, S and Zn by acid and microwave digestion; available P by Bray P-1 extraction and UV analysis; and available NH_4^+ and NO_3^- by KCl extraction.

In the Thompson Rivers University (TRU) greenhouse lab, organic matter and moisture content were measured using loss-on-ignition (LOI), and pH and electrical conductivity (EC) were determined using a Palintest® 800 meter. The loss-on-ignition was calculated by weighing approximately 1.5 g from each sample of soil into a tin and then heating it at 105°C for 12 hours and then 500°C for 5 hours. The dried soil was weighed to calculate its water content and organic content.

Lastly, total C, S and N were measured with a Thermo-Scientific CHNS Elemental Analyzer. These samples were prepared for analysis by drying in an oven at 70°C for 24 hours, followed by sieving through a 2 mm pan and grinding with a mortar and pestle in the greenhouse lab.

Metabarcoding Soil Microbial Communities

The microbial-community composition of soil samples was characterized in the Applied Genomics Laboratory at TRU (TRUGen, Rockville, Maryland). The DNA from the soil samples was extracted using a MagAttract PowerSoil DNA Kit (QIAGEN, Hilden, Germany) and a portion of the bacterial 16S rRNA gene was amplified by Polymerase Chain Reaction (PCR) using primers 341F and 806R. For fungi, the primers ITS86F and ITS4R were used to amplify the second internal transcribed spacer of the nuclear ribosomal DNA (ITS2) region between the 5.86S rRNA and 28S rRNA genes. Amplicon libraries were prepared for sequencing during a second round of PCR with indexed primers, and purified with AgenCourt AMPure (Beckman Coulter Inc., Brea, California) magnetic beads to remove DNA under 100 base pairs in length. Sequencing was carried out using 400 base-pair chemistry on an Ion Torrent S5 XL platform (Thermo Fisher Scientific, Waltham, Massachusetts). Filtered sequencing reads were rarefied as outlined in McKnight et al. (2019). Operational taxonomic units (OTU) clustering and taxonomy assignment were carried out using the bioinformatic pipeline AMPtk (Palmer et al., 2018).

Preliminary Results

Changes in Geochemical Properties with Stockpile Depth

Principal component analysis (PCA) suggests that changes with depth led to changes in soil properties. The first principal component (PC1) explains 41.09% of variation and the second principal component (PC2) explains 18.47% of variation seen between samples (Figure 4). Running PERMANOVA on the New Afton ($p = 0.022$, $R^2 = 0.29$) and QR mill ($p = 0.038$, $R^2 = 0.27$) samples shows a significant difference in geochemical properties with stockpile depth (Figure 4). There is relatively little spread within the New Afton samples, but a relatively high amount of spread is observed in the QR mill samples. Here, the depths represent a rough gradient, with the top intervals being close together at the top right and the bottom depth intervals being the most distant. Additionally, the stockpile samples from both New Afton and QR mill are highly separated from their corresponding reference soil samples.

Changes in Soil Microbial Communities with Stockpile Depth

Preliminary non-metric multidimensional scaling (NMDS) plots illustrate that bacterial and fungal communities in reference soils are separated from their corresponding stockpile soils (Figure 5). Additionally, results indicate that there are significant differences in bacterial communities with depth in QR mill soil ($p = 0.001$, $R^2 = 0.55$) but not New Afton soil ($p = 0.08$, $R^2 = 0.19$). Furthermore, there are sig-

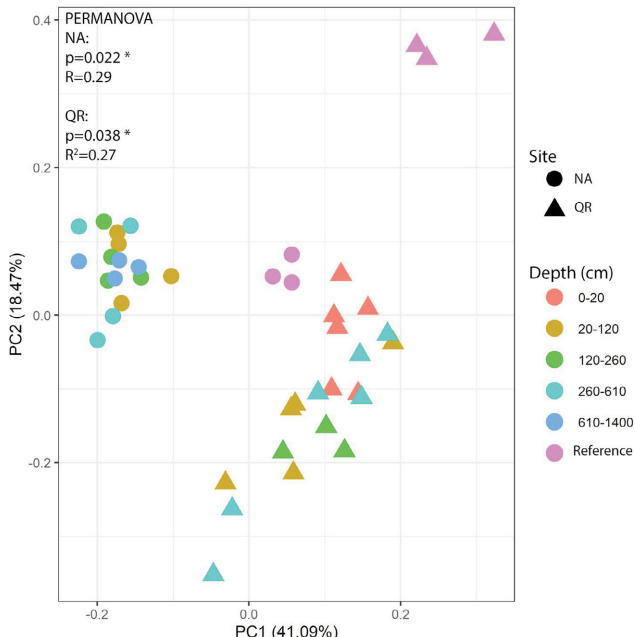


Figure 4. Principal component analysis (PCA) plots showing differences in soil chemical properties with changing stockpile depths at New Afton (NA) and QR mill (QR). Significance level represented by **.

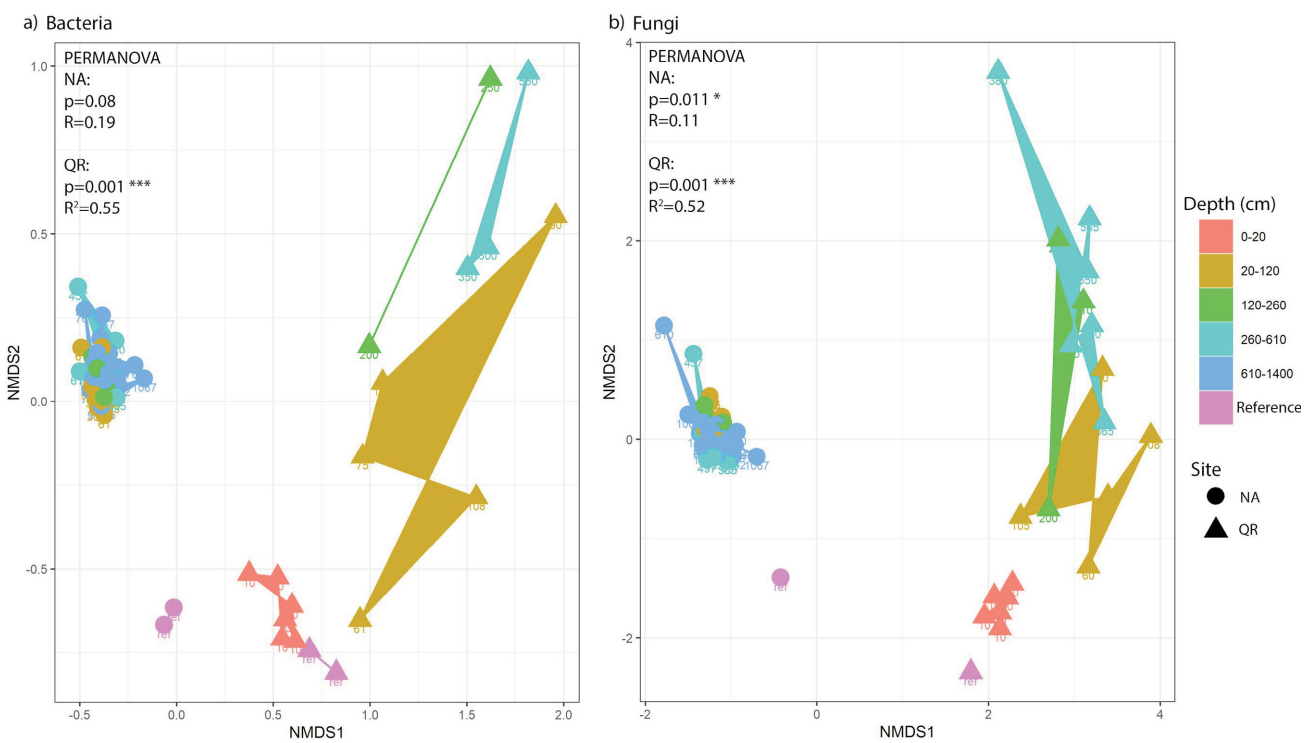


Figure 5. Non-metric multidimensional scaling (NMDS) plots showing differences in bacterial communities (a) and fungal communities (b) with changing depths in the New Afton (NA) and QR mill (QR) topsoil stockpiles. Significance level represented by '*'.

nificant differences in fungal communities with depth in the New Afton ($p=0.011$, $R^2=0.11$) and QR mill stockpiles ($p = 0.001$, $R^2 = 0.52$). Bacterial and fungal communities are relatively less similar between depth intervals in the QR mill stockpile than in the New Afton stockpile. This pattern matches what is observed with the PCA of geochemical properties (Figure 4).

Discussion

These results are preliminary and therefore subject to modification as research continues. The vertical position within the topsoil stockpile impacts the geochemical and microbial characteristics of the soil profile. However, the changes with depth observed in the New Afton stockpile were relatively smaller than those observed in the QR mill stockpile (Figures 4, 5). Interestingly, bacterial communities changed significantly with depth in only the QR mill stockpile, whereas fungal communities changed significantly with depth in both the New Afton and QR mill stockpiles. The smaller changes with stockpile depth observed at New Afton compared to QR mill may be a product of various site-specific influences, such as the difference in stockpile age or the addition of fresh topsoil.

Additionally, these preliminary results indicate that the geochemical properties in reference soils are notably distinct from those of the corresponding stockpile soils. The NMDS ordination plots show that bacterial and fungal communities in the reference soils are also noticeably dif-

ferent than those in the corresponding stockpile soils. The bacterial and fungal communities found in the deepest soil interval (260–610 cm) of the stockpile are farthest from, and those in the top soil interval (0–20 cm) closest to, the reference soil samples at QR mill. This indicates that increasing stockpile height may drive communities in the deeper soils farther away from their historical state, creating a greater barrier to restoration. Not surprisingly, this shows that long-term storage of topsoil can cause significant chemical and microbial alteration. These findings are supported by a study by Harris et al. (1989), which found that when soil was stockpiled in piles that were more than a metre deep, chemical effects such as accumulation of ammonium and establishment of anaerobic conditions occurred in the topsoil at the base of the pile. Additionally, Mummmey et al. (2002) showed that reapplying stockpiled topsoil to overburden materials post mining had long-lasting detrimental effects on plant diversity, soil microbial populations and soil organic-matter content compared to undisturbed sites, even 20 years after seeding of the reclaimed sites.

Conclusions

This project addresses knowledge gaps in the industry by exploring the compositional nature of topsoil stockpiles and their ability to facilitate post-mining revegetation. Specifically, these results highlight the important influence of topsoil-stockpile height on the geochemical properties and microbial communities in the soil, which ultimately influ-

ences the success of restoration. Optimized reclamation methods that allow for a more harmonious coexistence between industry and environment are needed. This need can be met, in part, by research focused on understanding and mastering ecosystem-reclamation processes.

Acknowledgments

This project is funded by Geoscience BC and through an NSERC Industrial Research Chair in Ecosystem Reclamation, with the following industry partners: Metro Vancouver, New Afton mine (New Gold Inc.), Highland Valley Copper mine (Teck Resources Limited), Genome BC, Arrow Transportation, the Real Estate Foundation of BC, Trans Mountain Corporation and the BC Cattlemen's Association. Thanks go to C. Gervan, who peer-reviewed this submission. Additional thanks go to all the researchers who helped in the field and the lab: B. McAmmond, S. Vogel, M. Coghill and S. Kega.

References

- Abdul-Kareem, A.W. and McRae, S.G. (1984): The effects on topsoil of long-term storage in stockpiles; *Plant and Soil*, v. 76, URL <<https://link.springer.com/article/10.1007/BF02205593>> [September 2020].
- Bradshaw, A. (1997): Restoration of mined lands – using natural processes; *Ecological Engineering*, v. 8, p. 255–269, URL <<https://doi.org/10.1023/A:1005177815154>>.
- Barkerville Gold Mines Ltd. (2019): Cariboo Gold project, Wells, BC; Barkerville Gold Mines Ltd., URL <<https://projects.eao.gov.bc.ca/>> [September 2020].
- Ghose, M.K. and Kundu, N.K. (2004): Deterioration of soil quality due to stockpiling in coal mining areas; *International Journal of Environmental Studies*, v. 61, no. 3, p. 327–335, URL <<https://doi.org/10.1080/0020723032000093991>>.
- Harris, J.A., Birch, P. and Short, K.C. (1989): Changes in the microbial community and physico-chemical characteristics of topsoils stockpiled during opencast mining; *Soil Use and Management*, v. 5, no. 4, p. 161–168, URL <<https://doi.org/10.1111/j.1475-2743.1989.tb00778.x>>.
- Lloyd, D.A., Angove, K., Hope, G.D. and Thompson, C. (1990): A guide to site identification and interpretation for the Kamloops Forest Region; Ministry of Forests, Lands, Natural Resource Operations and Rural Development, Land Management Handbook 23, URL <<https://www.for.gov.bc.ca/hfd/pubs/docs/lmh/lmh23.htm>> [September 2020].
- Mining Association of British Columbia (2019): Facts & figures 2019; Mining Association of British Columbia, URL <<https://www.mining.bc.ca/>> [September 2020].
- Mummey, D.L., Stahl, P.D. and Buyer, J.S. (2002): Soil microbiological properties 20 years after surface mine reclamation: spatial analysis of reclaimed and undisturbed sites; *Soil Biology and Biochemistry*, v. 34, no. 11, p. 1717–1725, URL <[https://doi.org/10.1016/S0038-0717\(02\)00158-X](https://doi.org/10.1016/S0038-0717(02)00158-X)>.
- McKnight, D.T., Huerlimann, R., Bower, D.S., Schwarzkopf, L., Alford, R.A. and Zenger, K.R. (2019): Methods for normalizing microbiome data: an ecological perspective; *Methods in Ecology and Evolution*, v. 10, no. 3, p. 389–400, URL <<https://doi.org/10.1111/2041-210X.13115>>.
- New Gold Inc. (2018): New Afton: 2017 annual reclamation report, Kamloops, BC; New Gold Inc., URL <<https://www.newgold.com>> [September 2020].
- Palmer, J.M., Jusino, M.A., Banik, M.T. and Lindner D.L. (2018): Non-biological synthetic spike-in controls and the AMPtk software pipeline improve mycobiome data; *PeerJ* 6:e4925, URL <<https://doi.org/10.7717/peerj.4925>>.
- Stahl, P.D., Perryman, B.L., Sharmasarkar, S. and Munn, L.C. (2002): Topsoil stockpiling versus exposure to traffic: a case study on in situ uranium wellfields; *Restoration Ecology*, v. 10, no. 1, p. 129–137, URL <<https://doi.org/10.1046/j.1526-100X.2002.10114.x>>.

Progress Report on Smithers Exploration Group's Rock Room and Getting Creative During COVID (Northwestern British Columbia)

A. Ledwon, Smithers Exploration Group, Smithers, British Columbia, rockroom@smithersexplorationgroup.com

C. Ogryzlo, Smithers Exploration Group, Smithers, British Columbia

Ledwon, A. and Ogryzlo, C. (2021): Progress report on Smithers Exploration Group's Rock Room and getting creative during COVID; in Geoscience BC Summary of Activities 2020: Minerals, Geoscience BC, Report 2021-01, p. 143–146.

Introduction

Smithers Exploration Group (SEG) was founded in the early 1970s and has enjoyed successful growth and community involvement over the decades. From co-creating the School of Exploration and Mining with Northwest Community College (now Coast Mountain College) to organizing a myriad of public-education projects, SEG has been an active part of Smithers, the northwestern region of British Columbia (BC) and BC as a whole through its advocacy for the mining and exploration industry. During this time, SEG had amassed an extensive rock collection that, through a grant and some very hard work, was sorted into what is now the SEG Rock Room. Located in Smithers, the collection has attracted much attention at recent conferences and has become the focus of many hopes and plans for the future. Thanks to a Geoscience BC grant, SEG has been able to move forward with many of these projects.

When SEG presented their Geoscience BC (GBC) progress report in November 2019, no one could have foreseen the changes that would affect the world in 2020. With most of SEG's funding from GBC earmarked for educational programs and conference presentations related to improvements to the SEG Rock Room and updating of its extensive rock collection, COVID-19 forced SEG to get creative and present some alternatives to the original project deliverables. An exciting—albeit masked—spring and summer followed, with focus on taking the hands-on aspects digital and in-person teaching virtual.

Project Updates

Completion of Collection

An enormous collection received from the BC Ministry of Energy, Mines and Low Carbon Innovation office in Prince George (described in Ledwon and Ogryzlo, 2020) has been sorted and catalogued, with many rocks being used for future teaching collections. Retiring geologists have continued to send their rock collections (Figure 1) to Smithers,

and SEG has been grateful to receive some stunning samples. The catalogue has been digitized and is available through the SEG website at <http://smithersexplorationgroup.com/rock-room/>.

Partnering with Below BC

3-D Photography Project and Online Interactive Map

SEG's work in 2019 with the non-profit society 'Below BC', another recipient of Geoscience BC funding, came to fruition at Roundup 2020 with the launch of a joint interactive map and website. In July 2020, Below BC visited Smithers to continue photographing the collection, this time focusing on rock samples to support the additional education posters that were produced for future prospecting



Figure 1. One example of rock samples submitted to the SEG collection. Many of these rocks will be used as teaching samples in the future. Always fun to unpack though!

This publication is also available, free of charge, as colour digital files in Adobe Acrobat® PDF format from the Geoscience BC website: <http://geosciencebc.com/updates/summary-of-activities/>.

and outreach programs. SEG's entire rock collection is now digitally catalogued, the catalogue hosted on Below BC servers and searchable on their interactive web map (<https://bbcga.com/bc-interactive-map/>). SEG also redirected some funding to support Below BC and their Gigapan technology to add SEG's Hazelton Arc field trip to the educational website (Figure 2; https://bbcga.com/hazelton_geotour/). With additional time and funding, SEG hopes to eventually have all of the rocks available via the map, for 360° viewing.

Training for Regional Rockhounds

As in-person gatherings were cancelled, SEG had to develop other training options. In conjunction with Below BC and the Centre for Training Excellence in Mining (CTEM), SEG put together numerous webpages on the Below BC site in anticipation of moving the prospector course, the rockhounding course and potential university-level geology lab courses to online formats. This is one of the most exciting things to be involved with this year, after many years of advocating for online access to geology training for students and professionals alike.

Presentations

SEG Rock Talk Workshop

Rock Talk 2020, held February 19 and 20, was a success, with numerous geologists from across BC and the Yukon attending the two-day event (Figure 3). Presentations were top notch and current, with a variety of talks focusing on early- to late-stage exploration. The rock collection was once again front and centre, allowing participants a chance to see and handle samples from the deposits being discussed upstairs.

The educational posters that were created for the 2019 Rock Talk have been digitized and printed. They were so well received and useful, for geologists and the general public alike, that SEG has invested additional funding in creating more posters. These will be used to teach future prospecting courses and be incorporated into the Below BC educational interactive website, where they will be combined with the digital photographs of the Rock Room collection.

Poster and Regional Table Presentations at AME Roundup

With the support of SEG, Peter Ogryzlo presented an exciting new poster display (Figure 4) at the 2020 Association for Mineral Exploration (AME) Roundup conference in Vancouver in January. A regional table display (Figure 4), a booth at BC Night, and rock specimens showcased at various other booths on the Trade Show floor rounded out SEG's presence at the event.



Figure 2. J. Moffat of Below BC using Gigapan technology to photograph Brian Boru volcanics, part of SEG's geological field trip.



Figure 3. Rock Talk 2020 participants enjoying a variety of talks.



Figure 4. SEG's new regional table display at Roundup 2020.

Acknowledgments

The Smithers Exploration Group would like to thank J. Nelson, H. Tremblay, H. Smit and T. Richards for their ongoing support and championing of the Rock Room project. Many others have been instrumental in bringing the Rock Room to its current state, and SEG thanks them all.

Reference

- Ledwon, A. and Ogryzlo, C. (2020): Progress report on the Smithers Exploration Group's Rock Room (northwestern British Columbia); *in* Geoscience BC Summary of Activities 2019: Minerals, Geoscience BC, Report 2020-01, p. 155–158, URL <http://www.geosciencebc.com/i/pdf/SummaryofActivities2019/Minerals/Project%202018-012_Minerals_SOA2019.pdf> December 2020].



t: 604 662 4147
e: info@geosciencebc.com

**SUITE 1101–750 WEST PENDER ST
VANCOUVER, BC V6C 2T7 CANADA**

www.geosciencebc.com